UNIVERSIDADE ESTADUAL DE CAMPINAS

Faculdade de Engenharia Química

FERNANDA PALUDETTO PELAQUIM

SOLUBILIDADE DE GASES LEVES EM *DEEP EUTECTIC SOLVENTS* A ALTAS PRESSÕES

LIGHT GAS SOLUBILITY IN DEEP EUTECTIC SOLVENTS UNDER HIGH PRESSURE

CAMPINAS

2023

FERNANDA PALUDETTO PELAQUIM

SOLUBILIDADE DE GASES LEVES EM *DEEP EUTECTIC SOLVENTS* A ALTAS PRESSÕES

LIGHT GAS SOLUBILITY IN DEEP EUTECTIC SOLVENTS UNDER HIGH PRESSURE (*)

Tese apresentada à Faculdade de Engenharia Química da Universidade Estadual de Campinas como parte dos requisitos exigidos para a obtenção do título de Doutor em Engenharia Química

Thesis presented to the Faculty of Chemical Engineering of the University of Campinas as partial fulfillment of the requirements for the degree of phD, in Thermodynamics

Orientador: Profa. Dra. Mariana Conceição da Costa

Coorientador: Profa. Dra. Irede Angela Lucini Dalmolin

ESTE TRABALHO CORRESPONDE À VERSÃO FINAL DA DISSERTAÇÃO/TESE DEFENDIDA PELA ALUNA FERNANDA PALUDETTO PELAQUIM, E ORIENTADA PELA PROFA. DRA. MARIANA CONCEIÇÃO DA COSTA

CAMPINAS

2023

Ficha catalográfica
Universidade Estadual de Campinas
Biblioteca da Área de Engenharia e Arquitetura
Rose Meire da Silva - CRB 8/5974

P361s

Pelaquim, Fernanda Paludetto, 1991-
Solubilidade de gases leves em Deep Eutectic Solvents a altas pressões / Fernanda Paludetto Pelaquim. – Campinas, SP : [s.n.], 2023.

Orientador: Mariana Conceição da Costa.
Coorientador: Irede Angela Lucini Dalmolin.
Tese (doutorado) – Universidade Estadual de Campinas, Faculdade de Engenharia Química.

1. Solubilidade. 2. Solvente eutético profundo. 3. Dióxido de carbono. I. Costa, Mariana Conceição da, 1977-. II. Dalmolin, Irede Angela Lucini, 1984-. III. Universidade Estadual de Campinas. Faculdade de Engenharia Química. IV. Título.

Informações Complementares

Título em outro idioma: Light gas solubility in Deep Eutectic Solvents under high pressure
Palavras-chave em inglês:
Solubility
Deep eutectic solvents
Carbon dioxide
Área de concentração: Engenharia Química
Titulação: Doutora em Engenharia Química
Banca examinadora:
Mariana Conceição da Costa [Orientador]
Marcelo Lanza
Evertan Antonio Rebelatto
Klicia Araújo Sampaio
Rafael Mengotti Charin
Data de defesa: 24-02-2023
Programa de Pós-Graduação: Engenharia Química

Identificação e informações acadêmicas do(a) aluno(a)
- ORCID do autor: https://orcid.org/0000-0002-9418-3041
- Currículo Lattes do autor: http://lattes.cnpq.br/6794467017216093

Folha de Aprovação da Defesa de Tese de Doutorado defendida por **FERNANDA PALUDETTO PELAQUIM** e aprovada em 24 de fevereiro de 2023 pela Comissão Examinadora constituída pelos doutores:

Profa. Dra. Mariana Conceição da Costa

Presidente e Orientadora

FEQ / UNICAMP

Videoconferência

Dr. Rafael Mengotti Charin

Escola Politécnica Universidade Federal do Rio de Janeiro – POLI/UFRJ

Videoconferência

Dr. Evertan Antonio Rebelatto

Universidade Federal de Santa Catarina – UFSC

Videoconferência

Profa. Dra. Klicia Araújo Sampaio

Universidade Estadual de Campinas – FEA/UNICAMP

Dr. Marcelo Lanza

Universidade Federal de Santa Catarina - UFSC

Videoconferência

A Ata da defesa com as respectivas assinaturas dos membros encontra-se no SIGA/Sistema de Fluxo de Dissertação/Tese e na Secretaria do Programa da Unidade.

Dedico esse trabalho aos meus pais, Rosana e Donizeti, pelo amor, educação e incentivo que sempre me proporcionaram.

Aos meus avós, Benedita, José, Helena e Paulo (à memória de), por terem me amado de forma incondicional.

Ao meu marido Yghor, pela paciência, compreensão, amor e carinho ao longo dessa jornada.

“Se caíste, ergue-te e anda.
Caminha para frente.
Regressa aos teus deveres e esforça-te a cumpri-los.
Ora, pedindo a Deus mais força para a marcha.
Muitas vezes a queda é uma lição de vida.
Quem cai sente do valor do perdão aos caídos.
O futuro te espera...” (Chico Xavier)

AGRADECIMENTOS

Primeiramente, gostaria de agradecer a Deus e todos os anjos que me guiam e me intuem, por todas as bênçãos a mim concedidas todos os dias da minha vida, e principalmente por me dar forças para continuar na carreira acadêmica com muita saúde, vida essa que possui desafios diários de empenho, força de vontade, resignação e receios pelo futuro desconhecido.

À minha família, principalmente minha mãe Rosana, meu pai Donizeti e meu tio José Nivaldo, que foi a minha inspiração e meu principal incentivador no início da jornada acadêmica. Agradeço por todo carinho, o entendimento da minha escolha de profissão e todo o amor dado ao longo dessa caminhada. Nós sabíamos que seria difícil, que muitos não entenderiam, mas vocês acolheram a minha decisão e até hoje lutam por ela comigo.

Ao meu amado esposo Yghor, aquele que a dez anos me faz uma pessoa mais feliz, mais amada, mais evoluída, mais atenciosa, amiga e melhor. Obrigada por ter me acompanhado ao longo desses anos, entendendo minhas necessidades, troca de carreira, me incentivando e me mostrando que a jornada é longa, mas bonita e os frutos serão colhidos a longo prazo. Você foi a minha âncora, meu aconselhador, me deu broncas, mas também me acolheu em seu peito quando viu que o fardo estava pesado demais para eu carregar sozinha.

À Profa. Dra. Mariana Conceição da Costa por toda a parceria, de muito sucesso, ao longo desses mais de cinco anos. Obrigada por toda a orientação, suporte, dedicação, confiança no meu trabalho e esforço para concluir esta pesquisa. Agradeço por ter me amparado nos momentos difíceis, principalmente na pandemia, me entendendo e encontrando soluções para que nosso trabalho prosperasse. Espero que essa parceria se perpetue pelos anos.

À Profa. Dra. Irede Angela Lucini Dalmolin pela coorientação do meu doutorado, mesmo de longe, sempre com tanto empenho e carinho. Obrigada por todos os ensinamentos profissionais e também de vida, por ter enfrentado horas de ônibus de Beltrão a Campinas para me ajudar, sempre feliz, por ter se tornado minha amiga, conselheira, companheira de casa e de experimentos em Aracaju, que aguentava meus mau-humores, meus dias difíceis, minha negatividade. Se não fosse por você, com certeza esse doutorado não teria sido concluído. Obrigada por ter me

ensinado a ver a vida como pequenas vitórias e assim também a minha carreira acadêmica. E também ao professor Antonio Marinho Barbosa Neto, que esteve comigo nos momentos difíceis ao longo da pandemia, com muita paciência, auxiliando na minha jornada pela modelagem termodinâmica, ensinando conceitos, corrigindo artigos e realizando infinitas reuniões.

Aos professores Claudio Dariva, Gustavo Rodrigues Borges e Elton Franceschi da Universidade Tiradentes, e a todos do laboratório NUESC por terem me recebido com tanto carinho ao longo de três meses. Agradeço por todos os ensinamentos, por toda a liberdade em utilizar os equipamentos do laboratório e pela parceria edificante.

À Faculdade de Engenharia Química da UNICAMP e ao Departamento de Desenvolvimento de Processos e Produtos, pela oportunidade, e auxílio para a minha entrada e estadia no mundo científico.

Aos membros da banca examinadora, pela disponibilidade, sugestões e correções do trabalho.

Aos amigos do Laboratório de Equilíbrio de Fases, Rafael, Débora, Filipe e Sérgio, e aqueles amigos que a FEQ me proporcionou, Thiago, Mariana, e Nilza por todos os momentos felizes que vivemos juntos, por cada almoço, sobremesa pós almoço, todos os trabalhos em conjunto, os artigos lidos e corrigidos, as ajudas nos experimentos e a amizade que se perpetuará pelos anos. Aos amigos recém-feitos na UNIT: Klebson, o super técnico de laboratório que me auxiliou nas montagens da célula, que chegava às 6h da manhã comigo, me salvava dos momentos de desespero e aflição, Fagne que se tornou meu companheiro de aventuras, de comilança, de passeios ao shopping todo final de semana, meu amigo do coração que estava sempre ali comigo na bancada, interessado pela minha pesquisa e vida, e também a Monique, Denis, Elvio, Tamires, Thauane, Any, Aninha, Manu, Havila, Iago, Ayslan e Arley. Obrigada por terem feito meus três meses em Aracaju muito bem aproveitados.

Aos amigos que a vida me proporcionou, principalmente, Thais, Thatyane, Tais, Karen, Rodrigo, Abel e o grupo Sem Chance, por sempre me apoiarem e estarem comigo em todos os momentos, inclusive os mais difíceis.

À Fundação de Amparo à Pesquisa do Estado de São Paulo (FAPESP) - Processo 2018/19198-9 pelo financiamento do projeto de pesquisa, tornando possível a produção desta tese.

RESUMO

Os crescentes níveis globais dos gases do efeito estufa, especialmente as emissões de dióxido de carbono (CO_2), causam danos ambientais e problemas que afetam a humanidade e o ecossistema. O CO_2 é o gás do efeito estufa que mais contribui para esses problemas devido à combustão de carvão, petróleo e gás natural, transporte, e outros processos industriais. A captura e armazenamento de carbono (CCS) tem se mostrado um método eficaz para reduzir a emissão de CO_2. A absorção, por sua vez, é a tecnologia mais utilizada para capturar o CO_2 pré e pós-combustão. A monoetanolamina (MEA) tem provado ser o solvente químico mais eficiente. No entanto, a MEA é ambientalmente nociva. O processo comercial Selexol, que usa o éter dimetílico de polietilenoglicol como solvente físico também é amplamente usado na captura do CO_2, porém sua alta viscosidade aumenta os custos operacionais. Dessa maneira, há a necessidade de desenvolver solventes mais ecologicamente corretos para a captura de CO_2, tais como os solventes eutéticos profundos (DESs) e os solventes eutéticos (ESs). Os DESs ou ESs são formados por meio da mistura de até três componentes de alta pureza e baixo custo, que, devido as forças atrativas, formam uma mistura eutética. Eles podem ser produzidos em larga escala e além disso, são biodegradáveis e vêm sendo apontados, em diversos estudos, como substitutos dos solventes orgânicos na absorção de gases, como o CO_2, entretanto apenas a pressão atmosférica. Assim, este projeto de doutorado teve como principais objetivos: (I) determinar dados de equilíbrio de fases de seis tipos de ESs puros a altas pressões, até 250 bar; (II) obter dados de solubilidade de CO_2 em seis ESs a altas pressões, a fim de verificar qual ES é o melhor absorvente dos gases; (III) estudar a influência da temperatura e pressão no processo de absorção; (IV) fazer a modelagem termodinâmica utilizando equações de estado e o COSMO-RS na solubilidade de gases leves em ESs encontrados na literatura. Os dados foram modelados usando as Equações de Estado (EoS) de Peng-Robinson e *Cubic Plus Association* (CPA) para predizer o comportamento das fases e suas propriedades em função da pressão e temperatura.

ABSTRACT

Increasing global levels of greenhouse gases (GHGs), especially CO_2 emissions, cause environmental damage and problems that affect humanity and the ecosystem. Carbon dioxide (CO_2) is the GHG that most contributes to these problems due to the combustion of coal, oil and natural gas, transportation, and other industrial processes. Carbon capture and storage (CCS) is an effective method for reducing CO_2 emissions. Absorption is the most used technology to capture pre- and post-combustion CO_2. Monoethanolamine (MEA) has proven to be the most efficient chemical solvent. However, MEA is environmentally harmful. The commercial Selexol process, which uses polyethylene glycol dimethyl ether as the physical solvent, is also widely used for CO_2 capture, but its high viscosity increases operating costs. Thus, it is necessary to develop more environmentally friendly solvents for CO_2 captures, such as Deep Eutectic Solvents (DESs) and eutectic solvents (ESs). DESs or ESs are formed by mixing up to three components of high purity and usually low cost, which, due to attractive forces, form a eutectic mixture. They can be produced on large scale, are biodegradable, and have been suggested in several studies as substitutes for organic solvents in the absorption of gases such as CO_2, but only at atmospheric pressure. Thus, this Ph.D. project had as main objectives: (I) to determine the phase equilibrium diagram of six types of pure ESs at high pressures, up to 250 bar; (II) to obtain the CO_2 solubility data in six ESs at high pressures, to verify which ES is the best gas absorber; (III) to study the influence of temperature and pressure on the absorption process; (IV) to perform thermodynamic modeling using equations of state and COSMO-RS for the solubility of light gases in ESs found in the literature. The data were modeled using Peng- Robinson and Cubic Plus Association (CPA) Equations of State (EoS) to predict the behavior of the phases and their properties as a function of pressure and temperature.

SUMÁRIO

CAPÍTULO 1

INTRODUÇÃO GERAL, JUSTIFICATIVA, OBJETIVOS E ESTRUTURA DA TESE

1. Introdução

O clima global tem testemunhado mudanças severas na última década, principalmente devido aos gases de efeito estufa liberados pela combustão de carvão, petróleo e gás natural (GN) (ALDAWSARI et al., 2020). Dentre eles, o CO_2 é o principal gás de efeito estufa contribuindo significativamente para o aquecimento global e as alterações climáticas (DAVIS; CALDEIRA; MATTHEWS, 2010). Nos últimos anos, a concentração de CO_2 na atmosfera, principalmente a partir da combustão de combustíveis fósseis, aumentou drasticamente, sendo 149% superior aos níveis anteriores à industrialização (VALENCIA-MARQUEZ; FLORES-TLACUAHUAC; VASQUEZ-MEDRANO, 2017). Apesar do declínio em 2020 devido a uma menor procura de energia durante a pandemia, as emissões globais de CO_2 foram de 31,5 Gt; maior concentração anual média na atmosfera, atingindo 412,5 ppm (INTERNATIONAL ENERGY AGENCY, 2022) – cerca de 50% maior que no início da revolução industrial. Por conseguinte, é vital utilizar tecnologias de captura para reduzir as emissões de CO_2 e minimizar o seu impacto nas alterações climáticas.

Diferentes abordagens são consideradas e adotadas por vários países para reduzir as suas emissões de CO_2, incluindo: melhorar a eficiência energética e promover a conservação de energia; aumentar a utilização de combustíveis com baixo teor de carbono, entre eles o gás natural, hidrogênio ou energia nuclear; utilizar energias renováveis, tais como solar, eólica, hidroelétrica e bioenergia; aplicar abordagens de geoengenharia, por exemplo, arborização e reflorestamento; e captura e armazenamento de CO_2 (CCS).

A CCS é um dos métodos mais eficazes para evitar a liberação de grandes quantidades de CO_2 para a atmosfera. Ela consiste na separação, transporte e armazenamento do CO_2 produzido industrialmente num local seguro para ser utilizado em substâncias ou produtos mais valiosos (SCHMELZ; HOCHMAN; MILLER, 2020). Existem três sistemas principais de captura de CO_2 associados a diferentes processos de combustão: pós-combustão, pré-combustão e oxy-combustão.

A pré e pós-combustão são as mais utilizadas entre elas e possuem três principais tecnologias de separação – absorção, adsorção, e separação por membranas – em que a absorção é a mais utilizada, inclusive para a remoção do CO_2 do gás natural, no processo conhecido como “adoçamento do gás” (do inglês, *gas*

sweetening), que consiste na separação do CO_2 do gás de combustão através de um solvente líquido regenerável (BHOWN; FREEMAN, 2011; ALDAWSARI et al., 2020).

Os solventes químicos tipicamente utilizados na pós-combustão incluem a monoetanolamina (MEA), a dietanolamina (DEA) e o carbonato de potássio. Aroonwilas e Veawab (2004) descobriram que a MEA é o composto mais eficiente para a absorção de CO_2, com eficiência superior a 90%. Entretanto, esses compostos possuem um potencial para a degradação da amina, resultando na perda de solventes, corrosão do equipamento e geração de compostos voláteis de degradação (ROCHELLE, 2012; FREDRIKSEN; JENS, 2013). Além disso, as emissões de aminas podem degradar-se em nitrosaminas e nitraminas, que são potencialmente nocivas para a saúde humana e o ambiente.

Uma das tecnologias de geração de energia, onde a captura de pré-combustão é implementada é a estação de geração de energia de ciclo combinado de gaseificação integrado (do inglês *integrated gasification combined cycle,* IGCC). As centrais eléctricas IGCC possuem alta eficiência, alta flexibilidade na alimentação de entrada, possibilidade de cogeração, facilidade de captura e cogeração de CO_2. A elevada pressão parcial de CO_2 no gás combustível na captura pré-combustão torna a absorção física favorável para as centrais eléctricas IGCC. O CO_2 é absorvido em solventes físicos devido à sua maior solubilidade em certos solventes orgânicos. O Selexol é um dos vários processos comerciais, que utiliza éter dimetílico de polietilenoglicol (DEPG) como solvente físico. Ele apresenta baixa pressão de vapor, alta solubilidade de CO_2, estabilidade química e térmica, natureza não corrosiva e não tóxica. Porém, o solvente DEPG tem alta viscosidade, o que leva a um aumento do custo de bombeamento (Ramzan et al., 2022)

Dessa maneira, torna-se importante encontrar alternativas mais viáveis para evitar esses problemas, como por exemplo a utilização dos solventes eutéticos profundos (do inglês, *Deep eutectic solvents,* DESs) e dos solventes eutéticos (do inglês, *eutectic solvents,* ESs) como absorventes físicos.

A captura de gases, como por exemplo, o CO_2 pelos DESs e/ou ESs vêm sendo muito estudada apenas à pressão atmosférica, com a finalidade de remover o CO_2 que está em excesso no ambiente, e têm apresentado resultados promissores, porém inferiores ao MEA e ao Selexol (HAIDER; KUMAR, 2020; HAGHBAKHSH et

al., 2021; PISHRO et al., 2021; RABHI; MUTELET; SIFAOUI, 2021; LIU et al., 2022). Os DESs são uma mistura de 2 ou 3 componentes puros para os quais a temperatura do ponto eutético está abaixo da temperatura do ponto eutético esperado para uma mistura líquida ideal. Caso a mistura não obedeça a essa definição, ela pode ser intitulada simplesmente como ESs (MARTINS; PINHO; COUTINHO, 2018). Na literatura poucas misturas foram classificadas como DESs, e, portanto, nesse trabalho, todas serão chamadas de ESs. Após sua mistura, os componentes dos ESs e/ou DESs normalmente têm um ponto de fusão, na composição eutética muito menor que o de qualquer um de seus componentes individuais, um receptor (HBA) e um doador de ligação de hidrogênio (HBD) (DAI et al., 2013). Também são considerados solventes verdes, produzidos de maneira simples, com alta pureza e custo relativamente baixo, e que podem ser produzidos em larga escala. Entretanto, essas propriedades dependem de quais componentes serão utilizados na mistura (ABBOTT et al., 2003; GORKE; SRIENC; KAZLAUSKAS, 2010).

Embora muitos trabalhos estudem a solubilidade do CO_2 nos ESs, a sua definição indica que a solubilidade física destas misturas não é atrativa. Isto ocorre devido à elevada viscosidade dos ESs, que reduz a dissolução do gás, e a transferência de massa causando a lenta difusão do CO_2. Além disso, a maioria dos ESs estudados (especialmente os baseados em ChCl) apresentam desvios negativos da idealidade (ou seja, coeficientes de atividade inferior a um), diminuindo o volume livre, e consequentemente a solubilidade (Martins et al., 2020).

Entretanto, informações sobre equilíbrio de fases a altas pressões dos ESs são essenciais para muitos processos químicos e operações de separação que são realizadas sob pressões mais altas, além de preencherem uma lacuna da literatura, uma vez que os dados de equilíbrio sólido-líquido (ESL) dessas misturas eutéticas existem apenas em pressão ambiente (CRESPO et al., 2017, 2018; PONTES et al., 2017; SILVA et al., 2020). Em relação a absorção do CO_2 em ESs, o equilíbrio de fases a altas pressões é um indicativo de quais são as melhores condições de trabalho para que esse gás seja eliminado do gás natural e/ou da atmosfera, e se essa absorção ocorre em quantidade significativa para o processo como um todo. Soma-se a isso o preenchimento de lacunas na literatura, uma vez que dados de solubilidade existem apenas até 100 bar (LERON; LI, 2013a, 2013b).

Além de dados experimentais, a modelagem termodinâmica é crucial para ajudar a compreender o comportamento do sistema. Entretanto artigos contendo dados de modelagem são uma parcela ainda menor da literatura neste tópico. Alguns estudos modelaram solubilidade de CO_2 nos ESs, a maioria dos quais utilizou a Teoria da Associação Estatística de Fluidos em Cadeia Perturbada (do inglês, *Perturbed Chain-Statistical Associating Fluid Theory*, PC-SAFT) (ZUBEIR et al., 2016; DIETZ et al., 2017; RABHI; MUTELET; SIFAOUI, 2021) ou a equação de estado de Peng-Robinson (ALI et al., 2014; MIRZA et al., 2015; HAIDER et al., 2018, 2020; HAIDER; KUMAR, 2020). Contudo, esses estudos e a diversidade de equações de estado utilizadas ainda são escassos na literatura, de modo que os resultados obtidos pelos modelos (por exemplo, parâmetros de interação binária, k_{ij}) não podem ser utilizados para prever a solubilidade de CO_2 em qualquer tipo de ES.

Nesse contexto, este projeto de doutorado teve como objetivo a determinação do equilíbrio sólido-líquido de seis ESs em diversas frações molares, e em pressões até 250 bar (cloreto de colina + glicerol, + etileno glicol, + 1,3 propanodiol, + ácido malônico, + ácido lático e + ácido glicólico); determinação de dados do equilíbrio de fases em altas pressões do dióxido de carbono com os mesmos seis ESs já utilizados, mas na fração molar do ponto eutético, a fim de analisar a absorção desse gás pelos ESs; determinação da densidade de quatro ESs (cloreto de colina + glicerol, + etileno glicol, + 1,3 propanodiol e + ácido glicólico) em pressões até 500 bar. Além disso, no trabalho foi feita a modelagem termodinâmica de dados experimentais de solubilidade de gases leves em ESs encontrados na literatura e também da densidade a altas pressões. Para essa última etapa foram utilizando os *softwares* Multiflash e COSMO-RS.

2. Justificativa

Este trabalho de doutorado se justificou pelos seguintes motivos:

1. Necessidade de estudar novas alternativas para reduzir a emissão de CO_2 na atmosfera e remoção do CO_2 das correntes de gás natural para melhora do meio ambiente;
2. Buscar solventes que absorvam o CO_2 de maneira eficiente, cuja produção seja viável em larga escala e com baixo preço, uma vez que o MEA pode ser degradado resultando na perda de solventes, corrosão do equipamento e geração de compostos voláteis e o Selexol apresenta altos custos operacionais;
3. Utilizar os ESs como absorvedores por serem solventes normalmente verdes e de fácil manipulação, o que torna o processo mais seguro, já que não oferecem riscos aos seres humanos e ao meio ambiente;
4. Determinar dados de equilíbrio de fases de diferentes ESs puros à altas pressões, devido à diminuta literatura nessas condições, e como análise prévia do seu desempenho frente aos gases leves;
5. Determinação de dados de solubilidade de misturas de CO_2 e ESs à altas pressões, devido à escassez de dados na literatura e para verificar a absorção do gás pelos ESs.

3. Objetivos

3.1. Objetivo geral

Este projeto de doutorado teve por objetivo a determinação de dados de equilíbrio de fases de seis ESs diferentes à altas pressões (cloreto de colina + glicerol, + etileno glicol, + 1,3 propanodiol, + ácido malônico, + ácido lático e + ácido glicólico), além da determinação de dados de solubilidade de CO_2 nesses ESs nas mesmas condições de pressão anteriormente citadas e em quatro temperaturas (298,15, 303,15, 318,15 e 333,15 K).

3.2. Objetivos específicos

Para alcançar o objetivo geral, os seguintes objetivos específicos foram delineados:

1. Síntese de seis ESs e caracterização dos mesmos por meio dos experimentos de densidade a baixas e altas pressões, viscosidade, índice de refração e condutividade elétrica;
2. Determinação de dados de equilíbrio de fases dos seis ESs usando uma célula de alta pressão e a construção dos respectivos diagramas de fases;
3. Determinação de dados de solubilidade do dióxido de carbono (CO_2) nos seis ESs usando uma célula de equilíbrio à altas pressões e construção dos respectivos diagramas de fases;
4. Avaliação da influência da pressão, da temperatura e do ESs (quanto ao HBD) na solubilidade do CO_2 para determinar as melhores condições de absorção do gás pelo ES;
5. Modelagem termodinâmica do equilíbrio de fases dos ESs a altas e baixas pressões e das densidades a altas pressões.

4. Estrutura da tese

Essa tese está dividida em oito capítulos que abordam os seguintes tópicos:

- **Capítulo 1** – **Introdução, Justificativa, Objetivos gerais e específicos da tese de doutorado e sua estrutura**
- **Capítulo 2** – ***Gas Solubility Using Deep Eutectic Solvents: Review and Analysis***, artigo de revisão publicado na revista *Industrial & Engineering Chemistry Research* que aborda a solubilidade de gases leves em DESs. Para escrever esse trabalho, artigos científicos foram pesquisados nas bases de dados Google Scholar, Web of Science, Elsevier, e Springer Link usando como palavras chaves "*carbon dioxide solubility*," "*deep eutectic solvents*," e "*liquid absorption of carbon dioxide*". Do total de artigos encontrados, após uma criteriosa seleção, 25 foram usados totalizando mais de mais de 40 DESs que foram analisados quanto (i) as diferenças entre DESs e ILs com relação a capacidade de absorção, (ii) as diferentes técnicas utilizadas para medir a solubilidade de CO_2 em DESs, (iii) a influência da razão molar dos DESs na solubilidade do gás, observando as interações moleculares, (iv) o impacto da mudança do HBD na solubilidade do gás, (v) o efeito da mudança do HBA na solubilidade, (v) as diferenças entre DESs hidrofílicos e hidrofóbicos, e (vi) a solubilidade de diferentes gases em DESs.
- **Capítulo 3** – **Materiais e Métodos**, em que são abordados os materiais que foram utilizados para a determinação dos dados experimentais, o aparato experimental e o procedimento para determinação dos mesmos. Conta também as metodologias dos *softwares* Multiflash – e as respectivas equações de estado (EoSs) utilizadas – e COSMO-RS, além das metodologias experimentais de determinação de dados de equilíbrio de fases a altas pressões e densidade a altas pressões.
- **Capítulo 4** – ***Carbon Dioxide Solubility in Deep Eutectic Solvents: Modelling using Cubic Plus Association and Peng-Robinson Equations of State***, artigo publicado na revista *Process Safety and Environmental Protection.* Neste artigo modelou-se a solubilidade de CO_2 em treze DESs em uma ampla faixa de temperatura (303,15 a 343,15 K) e pressão (0,06 a 12 MPa), usando as equações de estado CPA e Peng-Robinson. Os DESs foram

considerados pseudo-componentes em uma primeira abordagem e, em seguida, foram considerados os HBAs e HBDs individualmente. Essa abordagem foi nomeada como abordagem de componente individual. O objetivo, com essas duas abordagens, foi comparar os resultados de ambas para verificar se, ao se seguir a definição de DES - segunda abordagem, os resultados obtidos teriam valores próximos, o que não justificaria o seu uso uma vez que essa é mais trabalhosa. Além disso, o trabalho comparou as predições da solubilidade do CO_2 nos DESs utilizando as duas equações de estado, a utilização ou não do parâmetro de interação binária e três diferentes esquemas associativos para o CO_2.

- **Capítulo 5** – ***Prediction of greenhouse gas solubility in Eutectic Solvents using COSMO-RS***, artigo em fase de correção e submissão. Neste artigo foi utilizado o COSMO-RS como ferramenta para prever as solubilidades dos gases CO_2, CH_4 e H_2S em 17 solventes eutéticos à base de cloreto de colina (ChCl) encontrados na literatura a 298,15 K ou 313,15 K e em pressões entre 1 e 125 bar. Foi analisada a influência das razões molares de HBA:HBD 1:2, 1:3 e 1:4 para a solubilidade do CO_2 e 1:1 para a solubilidade do CH_4 nos ESs, e também a comparação dos resultados do COSMO-RS com os dados da literatura, e com diferentes equações de estado como CPA e Peng-Robinson. Além disso, inferiu-se o efeito de três razões molares diferentes (1:1,5; 1:2 e 1:2,5) do ES composto por ChCl:ureia na solubilidade do CO_2, CH_4 e H_2S.
- **Capítulo 6** – ***Characterization by SLE phase diagrams and density of Eutectic Solvents based on ChCl, alcohols and acids at high pressures***, artigo em fase de correção e submissão. No artigo foram determinados os diagramas de fase do equilíbrio sólido-líquido de seis solventes eutéticos (cloreto de colina como HBA, etilenoglicol, glicerol, 1,3 propanodiol, ácido glicólico, ácido lático e ácido malônico como HBDs) em altas pressões (6, 10, 14, 20 e 25 MPa) utilizando uma célula de alta pressão com volume variável. Os diagramas de fases foram comparados com os encontrados na literatura a pressão atmosférica. Além disso, foram determinadas as densidades de quatro ESs em suas composições eutéticas (cloreto de colina e etilenoglicol, glicerol, 1,3 propanodiol e ácido glicólico) em pressões entre 1 e 50 MPa e temperaturas variando de 293,15 a 353,15 K. Os dados foram correlacionados

com a equação modificada de Tammann-Tait e modelados utilizando a equação de estado CPA considerando os ESs como componentes individuais.

- **Capítulo 7** – ***Phase behavior and thermodynamic modeling of Deep eutectic solvents and carbon dioxide at high pressures***, artigo em fase de correção e submissão. Nesse artigo foi determinada a solubilidade do CO_2 em seis ESs (cloreto de colina como HBA, etilenoglicol, glicerol, 1,3 propanodiol, ácido glicólico, ácido lático e ácido malônico como HBDs) nas temperaturas de 298,15, 303,15, 318,15 e 333,15 K e pressões variando de 0,1 a 26 MPa, utilizando uma célula de alta pressão com volume variável. Além disso, os valores da constante de Henry e as energias livre de Gibbs, foram calculados nas pressões e temperaturas estudadas para todos os ESs.
- **Capítulo 8** – **Conclusões Gerais**, são apresentadas as conclusões obtidas a partir do trabalho desenvolvido e são dadas sugestões para trabalhos futuros nos temas aqui desenvolvidos.

Referências bibliográficas

ABBOTT, A. P. et al. Novel solvent properties of choline chloride / urea mixtures. **The Royal Society of Chemistry**, v. 1, p. 70–71, 2003.

ALDAWSARI, J. N. et al. Polyethylene glycol-based deep eutectic solvents as a novel agent for natural gas sweetening. **PLoS ONE**, v. 15, p. 1–22, 2020. Disponível em: <http://dx.doi.org/10.1371/journal.pone.0239493>.

ALI, E. et al. Solubility of CO2 in deep eutectic solvents: Experiments and modelling using the Peng-Robinson equation of state. **Chemical Engineering Research and Design**, v. 92, n. 10, p. 1898–1906, 2014.

AROONWILAS, A.; VEAWAB, A. Characterization and Comparison of the CO 2 Absorption Performance into Single and Blended Alkanolamines in a Packed Column. **Industrial & Engineering Chemistry Research**, v. 43, n. 9, p. 2228–2237, 1 abr. 2004. Disponível em: <https://pubs.acs.org/doi/10.1021/ie0306067>.

BHOWN, A. S.; FREEMAN, B. C. Analysis and status of post-combustion carbon dioxide capture technologies. **Environmental Science and Technology**, v. 45, p. 8624–8632, 2011.

CRESPO, E. A. et al. Characterization and Modeling of the Liquid Phase of Deep Eutectic Solvents Based on Fatty Acids/Alcohols and Choline Chloride. **Industrial & Engineering Chemistry Research**, v. 56, n. 42, p. 12192–12202, 2017. Disponível em: <http://pubs.acs.org/doi/abs/10.1021/acs.iecr.7b02382>.

CRESPO, E. A. et al. The Role of Polyfunctionality in the Formation of [Ch]Cl-Carboxylic Acid-Based Deep Eutectic Solvents. **Industrial and Engineering Chemistry Research**, v. 57, n. 32, p. 11195–11209, 2018.

DAI, Y. et al. Natural deep eutectic solvents as new potential media for green technology. **Analytica Chimica Acta**, v. 766, p. 61–68, 2013. Disponível em: <http://dx.doi.org/10.1016/j.aca.2012.12.019>.

DAVIS, S. J.; CALDEIRA, K.; MATTHEWS, H. D. Future CO2 Emissions and Climate Change from Existing Energy Infrastructure. **Science**, v. 329, n. 5997, p. 1330–1333, 10 set. 2010. Disponível em: <https://www.science.org/doi/10.1126/science.1188566>.

DIETZ, C. H. J. T. et al. PC-SAFT modeling of CO2 solubilities in hydrophobic deep eutectic solvents. **Fluid Phase Equilibria**, v. 448, p. 94–98, 2017. Disponível em: <http://dx.doi.org/10.1016/j.fluid.2017.03.028>.

FREDRIKSEN, S. B.; JENS, K.-J. Oxidative Degradation of Aqueous Amine Solutions of MEA, AMP, MDEA, Pz: A Review. **Energy Procedia**, v. 37, p. 1770–1777, 2013. Disponível em: <https://linkinghub.elsevier.com/retrieve/pii/S1876610213002968>.

GORKE, J. T.; SRIENC, F.; KAZLAUSKAS, R. J. Deep Eutectic Solvents for Candida antarctica Lipase B-Catalyzed Reactions. In: **Ionic Liquid Applications: Pharmaceuticals, Therapeutics, and Biotechnology**. Washington, D.C: American Chemical Society, 2010.

HAGHBAKHSH, R. et al. Experimental investigation of carbon dioxide solubility in the deep eutectic solvent (1 ChCl + 3 triethylene glycol) and modeling by the CPA EoS. **Journal of Molecular Liquids**, v. 330, p. 1–12, 2021. Disponível em: <https://doi.org/10.1016/j.molliq.2021.115647>.

HAIDER, M. B. et al. Thermodynamic and Kinetic Studies of CO2 Capture by Glycol and Amine-Based Deep Eutectic Solvents. **Journal of Chemical and Engineering Data**, v. 63, p. 2671–2680, 2018.

HAIDER, M. B. et al. Ternary hydrophobic deep eutectic solvents for carbon dioxide absorption. **International Journal of Greenhouse Gas Control**, v. 92, n. September 2019, p. 102839, 2020. Disponível em: <https://doi.org/10.1016/j.ijggc.2019.102839>.

HAIDER, M. B.; KUMAR, R. Solubility of CO2 and CH4 in sterically hindered amine-based deep eutectic solvents. **Separation and Purification Technology**, v. 248, p. 117055, 2020. Disponível em: <https://doi.org/10.1016/j.seppur.2020.117055>.

INTERNATIONAL ENERGY AGENCY. **Global Energy Review: CO2 Emissions in 2021 Global emissions rebound sharply to highest ever levelIEA**. [s.l: s.n.]. Disponível em: <https://iea.blob.core.windows.net/assets/c3086240-732b-4f6a-89d7-db01be018f5e/GlobalEnergyReviewCO2Emissionsin2021.pdf>.

LERON, R. B.; LI, M. H. Solubility of carbon dioxide in a eutectic mixture of choline chloride and glycerol at moderate pressures. **Journal of Chemical Thermodynamics**, v. 57, p. 131–136, 2013a. Disponível em: <http://dx.doi.org/10.1016/j.jct.2012.08.025>.

LERON, R. B.; LI, M. H. Solubility of carbon dioxide in a choline chloride-ethylene glycol based deep eutectic solvent. **Thermochimica Acta**, v. 551, p. 14–19, 2013b. Disponível em: <http://dx.doi.org/10.1016/j.tca.2012.09.041>.

LIU, X. et al. CO2capture by alcohol ammonia based deep eutectic solvents with different water content. **Materials Research Express**, v. 9, n. 1, 2022.

MARTINS, M. A. R.; PINHO, S. P.; COUTINHO, J. A. P. Insights into the Nature of Eutectic and Deep Eutectic Mixtures. **Journal of Solution Chemistry**, p. 1–3, 2018.

MIRZA, N. R. et al. Experiments and Thermodynamic Modeling of the Solubility of Carbon Dioxide in Three Different Deep Eutectic Solvents (DESs). **Journal of Chemical and Engineering Data**, v. 60, p. 3246–3252, 2015.

PISHRO, K. A. et al. Carbon dioxide solubility in amine-based deep eutectic solvents: Experimental and theoretical investigation. **Journal of Molecular Liquids**, v. 325, p. 115133, 2021. Disponível em: <https://doi.org/10.1016/j.molliq.2020.115133>.

PONTES, P. V. A. et al. Measurement and PC-SAFT modeling of solid-liquid equilibrium of deep eutectic solvents of quaternary ammonium chlorides and carboxylic acids. **Fluid Phase Equilibria**, v. 448, p. 69–80, 2017.

RABHI, F.; MUTELET, F.; SIFAOUI, H. Solubility of Carbon Dioxide in Carboxylic Acid-Based Deep Eutectic Solvents. **Journal of Chemical and Engineering Data**, v. 66, p. 702–711, 2021.

RAMZAN, N. et al. Pre-combustion carbon dioxide capture: A thermo-economic comparison for dual-stage Selexol process and combined Sulfinol-Selexol process. **International Journal of Energy Research**, 2022.

ROCHELLE, G. T. Thermal degradation of amines for CO2 capture. **Current Opinion in Chemical Engineering**, v. 1, p. 183–190, 2012. Disponível em: <http://dx.doi.org/10.1016/j.coche.2012.02.004>.

SCHMELZ, W. J.; HOCHMAN, G.; MILLER, K. G. Total cost of carbon capture and storage implemented at a regional scale: northeastern and midwestern United States. **Interface Focus**, v. 10, p. 1–15, 2020.

SILVA, L. P. et al. Eutectic Mixtures Based on Polyalcohols as Sustainable Solvents: Screening and Characterization. **ACS Sustainable Chemistry and Engineering**, v. 8, p. 15317–15326, 2020.

VALENCIA-MARQUEZ, D.; FLORES-TLACUAHUAC, A.; VASQUEZ-MEDRANO, R. An optimization approach for CO2 capture using ionic liquids. **Journal of Cleaner Production**, v. 168, p. 1652–1667, dez. 2017. Disponível em: <https://linkinghub.elsevier.com/retrieve/pii/S0959652616319035>.

ZUBEIR, L. F. et al. PC-SAFT Modeling of CO2 Solubilities in Deep Eutectic Solvents. **The Journal of Physical Chemistry B**, v. 120, p. 2300–2310, 2016. Disponível em: <http://pubs.acs.org/doi/10.1021/acs.jpcb.5b07888>.

CAPÍTULO 2

Gas solubility using Deep Eutectic Solvents: Review and analysis

(Artigo publicado na *Industrial & Engineering Chemistry Research*
DOI: 10.1021/acs.iecr.1c00947)

Fernanda Paludetto Pelaquim[a], Antonio Marinho Barbosa Neto[b], Irede Angela Lucini Dalmolin[c], Mariana Conceição da Costa[a1*].

[a] School of Chemical Engineering, University of Campinas – UNICAMP, 500 Albert Einstein Avenue, zip code 13083-852, Campinas, SP, Brazil

[b] Petroleum Engineering Department, State University of Santa Catarina – UDESC, Lourival Cesário Pereira Avenue, zip code 88336-275, Balneário Camboriú, SC, Brazil

[c] Academic Department of Engineering, Federal Technological University of Paraná (UTFPR), Linha Santa Bárbara, zip code 85601-970, Francisco Beltrão, PR, Brazil

1 * Corresponding author.

E-mail address: mcdcosta@unicamp.br (M.C. Costa)

phone number: +551935213962.

Abstract

The increasing global levels of anthropogenic greenhouse gases (GHGs), especially CO_2 emissions, have caused environmental problems that impact the humanity and ecosystems. Therefore, gas capture and storage are a feasible solution to this global issue; some aqueous amine solutions, such as monoethanolamine (MEA), have been used to capture GHGs, but they are not environment friendly. Research on greener solvents for this task led to deep eutectic solvents (DESs) as a novel option. This review explores the applications of different DESs; compares the differences between gas solubility methodologies; and studies the interference of the DESs' molar ratio, the influence of HBA and HBD, and the differences between the solubility of some gases in these solvents. More than 40 DESs have been analyzed; however, some gaps need to be filled, such as data for gas solubility under higher pressures and thermodynamic modeling of experimental data.

1. Introduction

The increase in anthropogenic greenhouse gases (GHGs) emission, especially carbon dioxide (CO_2), that started in the pre-industrial era is very likely to be the main cause of recent atypical changes in the global climate system. The increased global temperature, sea levels, floods, droughts, rainfall pattern changes, and infectious diseases can be observed. The continuous GHGs emissions and long-lasting climate changes are estimated to lead to risk of severe and irreversible impacts on the humanity and ecosystems, increasing surface temperature up to 5 °C by the end of this century [1–3]. According to the Intergovernmental Panel on Climate Change (IPCC), fossil fuels and minerals used for power generation contribute to almost 80% of the total CO_2 emissions [4].

CO_2 emissions are produced from combustion of fossil fuels, transportation, and other industrial process such as cement manufacturing, natural gas processing, iron smelters, and ammonia production. In 2019, global energy-related CO_2 emissions remained at around 33 gigatonnes (Gt), following two years of increases, and the global CO_2 emissions from coal decreased by almost 200 million tonnes (Mt), or 1.3%, from the 2018 level. In 2020, due to the pandemic, the global energy demand decreased by 3.8% relative to the first quarter of 2019. In October 14, 2020, CO_2 emissions reached 33.1 Gt and the atmospheric concentration reached values around 411.10 ppm [5–7]. This increase was due to the higher energy consumption from a global economy, as well as to the weather conditions in countries, which led to increased energy demand for heating and cooling [6,8,9]. Therefore, CO_2 capture and storage (CCS) has become one of the effective methods to prevent the release of large quantities of CO_2 into the atmosphere.

CCS comprises three steps: CO_2 waste capture, CO_2 transportation into a storage location, and CO_2 storage in a safe place. However, due to the high cost of separating gas in CCS, approximately US$ 60 per ton of CO_2, several efforts have been made to develop efficient technologies to capture and separate CO_2 from combustion gas, atmospheric air, and synthesis gas. The main technologies for CO_2 capture include post-combustion, pre-combustion, oxy-fuel combustion, and electrochemical separation [9–12].

Post-combustion capture is the most straightforward technology among the available technologies. It is used to remove CO_2 from the flue gases produced by a process using a fossil fuel. According to Figure 1, which shows the post combustion process, it is necessary remove CO_2 from other gases and then capture it using absorption, adsorption and membrane separation for example, and then CO_2 can be stored or utilized [13].

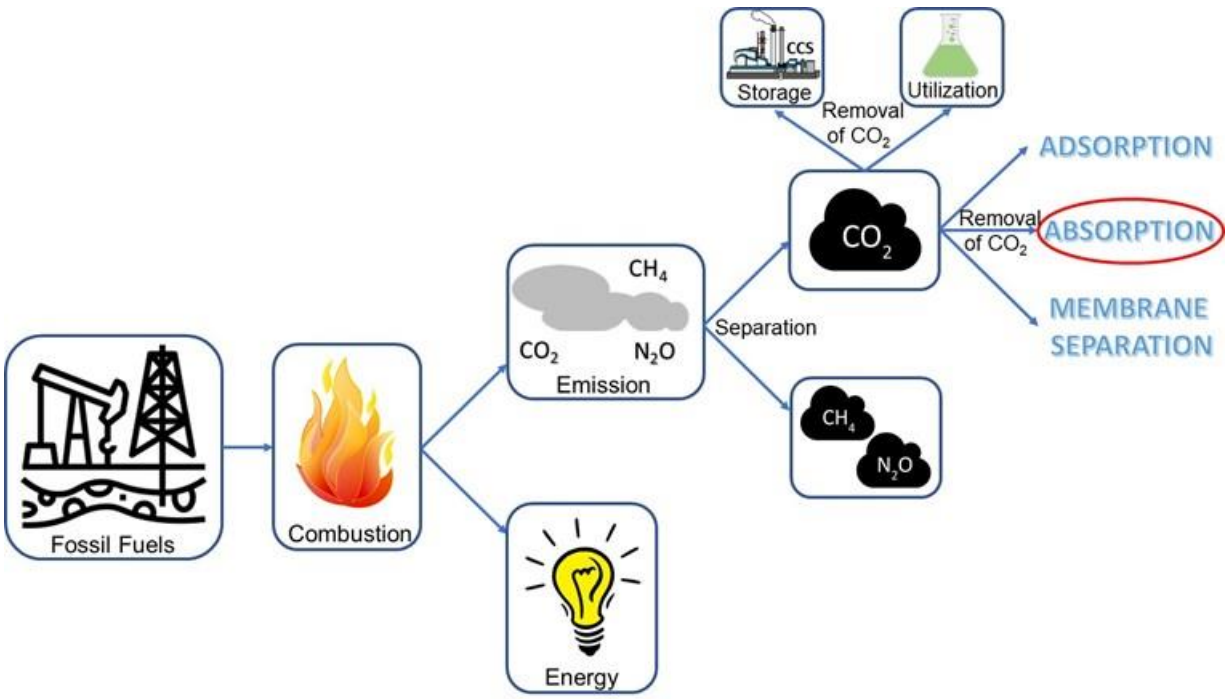

Figure 1. Post-combustion CO_2 capture process.

In the absorption, the focus of this work, in which atoms, molecules or ions are dissolved in a bulk phase, the CO_2-rich solution of the absorber is transferred to the regenerator to release CO_2, which increases temperature and/or decreases pressure. There are two types of absorption: physical absorption, in which CO_2 is physically absorbed in the solvent and removed in the absorber column, and chemical absorption, in which chemical reagents capture CO_2 by a reversible chemical reaction, and loosely bound intermediates are formed [9]. However, absorption has some drawbacks, such as the limited number of cycles (absorption and desorption), equipment corrosion, high energy consumption required by solvent regeneration, solvent loss by evaporation, and solvent degradation in oxygen-rich atmosphere [10].

Among the several technologies for CO_2 capture from flue gases, aqueous amine solutions, such as monoethanolamine (MEA), methyldiethanolamine (MDEA) and 2-amino-2-methyl-1-propanol (AMP) have traditionally been used as chemical solvents to capture CO_2 by chemical absorption [14–19]. They exhibit excellent absorption capacity, high reactivity, high selectivity, and low price [2]. However, they are not environment friendly due to their toxicity, partial degradation, high vapor pressure, corrosive byproduct formation, intensive energy consumption, and high uptake costs. Thus, scientists and engineers have developed economic absorbers or CO_2 capture technology [2,3,20,21]. Among the several possibilities, ionic liquids (ILs) and deep eutectic solvents (DESs) have attracted much attention for replacing aqueous amine solutions [22–31].

ILs have been proposed for CO_2 capture due to their low vapor pressure, which results in low energy consumption for regeneration and CO_2 stripping, high thermal and chemical stability, the possibility of adjusting their properties and, therefore, their affinity for CO_2 molecules, through the selection of suitable ions [8,30,32,33]. However, ILs

need to be synthesized, which involves a series of chemical reaction and purification steps that add cost to the solvent. In addition, some of ILs could be toxic and can be present poor biodegradability. Moreover, their high viscosities usually limit a large-scale application when compared with traditional solvents [8,21,34]. These disadvantages can be enhanced depending on the precursor materials chosen to prepare the ILs.

To overcome these disadvantages, DESs have drawn attention as novel solvents for capturing CO_2 [11,20,35,36]. They have very similar properties to ILs, such as high stability to heat and chemical attack, task specificity, non-flammability, and negligible vapor pressures. Moreover, DESs have advantages, such as low cost, good biodegradability, simple preparation process without further purification step, the possibility of synthesis from biodegradable components, very little byproduct generation, and low toxicity [13,36–38]. DESs are composed of two or more pure compounds, including hydrogen bond acceptors (HBAs) and hydrogen bond donors (HBDs), in which the eutectic point temperature is below the temperature of an ideal liquid mixture [39,40].

Over the years, several studies have been carried out to determine the solubility of carbon dioxide [2,20,23,25,35,41–43], and few studies have evaluated the solubility of other gases, such as methane and sulfur dioxide [11,44–48]. Therefore, this study explores the applications of different DESs in CO_2 capture technology, compares the different techniques, and studies the interference of the DESs' molar ratio, the influence of HBA and HBD on gas solubility, and the differences between the solubility of CO_2, H_2S, CH_4 and SO_2 in DESs.

The HBAs used as precursors to DESs preparation in the revised literature are choline chloride (ChCl), benzyltriphenylphosphonium chloride (BTPC), n-butyltriphenylphosphonium bromide (BTPB), methyltriphenylphosphonium bromide

(MTPB), tetra-N-Butyl ammoniumbromide (TBAB)., N,N,N-trimethyl-methanaminium chloride (TMAC), N, N, N-triethyl-ethanaminium chloride (TEAC), acetylcholine chloride (ACC), tetraethylammonium bromide (TEAB), tetrabutylammonium chloride (TBAC), diethylamine hydrochloride (DH), allyltriphenylphosphonium bromide (ATPPB), alanine, betaine, 1-hydroxyethyl-1,4-dimethyl-piperazinium bromide (PPZBr), 1-ethyl-3-methylimidazolium chloride (EmimCl), 1-butyl-3-methylimidazolium chloride (BmimCl), methyltrioctylammonium chloride (N_{8881}−Cl), methyltrioctylammonium bromide (N_{8881}−Br), tetraoctylammonium chloride (N_{8888}−Cl), tetraoctylammonium bromide (N_{8888}−Br), triethylenetetramine chloride ([TETA]Cl-), tetraethylenepentamine chloride ([TEPA]Cl-) and L-arginine. While the HBDs are urea, dimethylurea, N-methylurea, ethylenurea, thiourea, ethylene glycol, triethylene glycol, glycerol, ethanol amine, methyldiethanol amine, diethanol amine, triethanol amine, thioacetamide, dicyandiamide, 1,4-butanediol, 2,3-butanediol, 1,2-propanediol, phenol, guaiacol, cardanol, thymol, furfuryl alcohol, piperazine, aminoethylpiperazine, imidazole, 1,2,4-triazole, 4-methylimidazole, levulinic acid, lactic acid, malonic acid, phenylacetic acid, octanoic acid, decanoic acid, dodecanoic acid, caprolactam, 2-methylaminoethanol (MAE) and 2-Ethylaminoethanol (EAE).

Pertinent scientific journals were thoroughly researched to select findings relevant to the content of this review. Google Scholar, Web of Science, Elsevier, and Springer Link were searched using the terms: “carbon dioxide solubility,” “deep eutectic solvents,” “liquid absorption of carbon dioxide.”

2. Gas solubility in DESs – Measurements

Studies have been conducted to determine the solubility of gases in DESs, as well as the properties related to gas solubility, such as Henry’s law constant and gas

selectivity. The first reported article addressing CO_2 solubility was carried out by Li et al. (2008) [49], who determined the solubility of CO_2 in the DES composed of choline chloride (ChCl) and urea at temperatures ranging from 313.15 to 333.15 K and pressures between 10 and 130 bar. It was found that CO_2 solubility in DESs depends on three factors: (i) CO_2 pressure (CO_2 solubility increased with increasing pressure); (ii) temperature (CO_2 solubility decreased with increasing temperature); and (iii) the ChCl:urea molar ratio also has a significant effect on CO_2 values [49]. For the 2009–2012 period, no publications were returned in the aforementioned databases used in this study. Subsequently, significant research results were returned for several groups from 2013 to 2020, as shown in Figure 2.

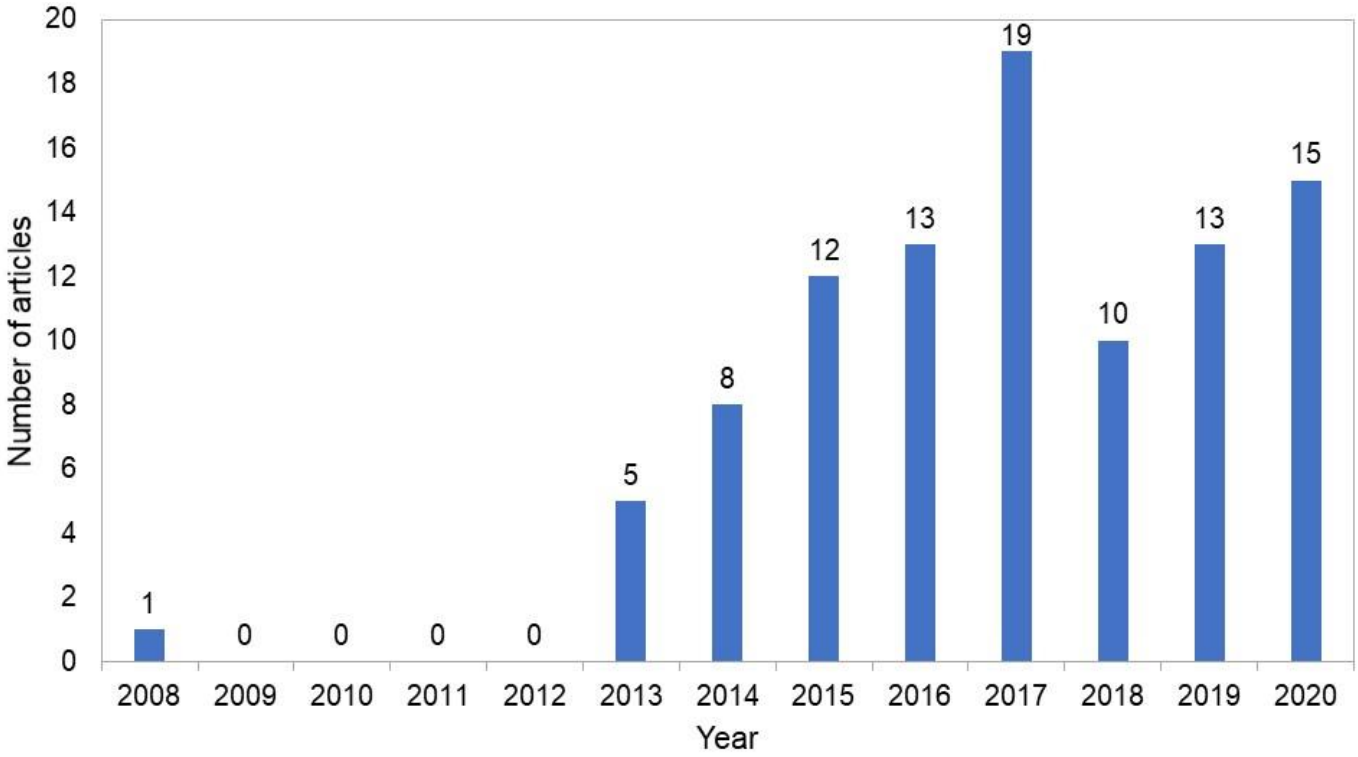

Figure 2. Number of articles investigating CO_2 capture using DESs from 2008 to 2020 – Google Scholar, Web of Science, Elsevier, and Springer Link were the databases used in the search.

Gas solubility is one of the most important properties for gas separation [36]. The solubility of some gases in DESs and their aqueous solutions and the Henry's constant were evaluated and presented in the Supporting Information in Tables S1 and S2.

Table S1 and Table S2 show pressure and temperature ranges between 0.10–133 bar and 293.15–353.15 K, respectively. This review presents 40 different DESs studied for CO_2 solubility, and 21 DESs for the solubility of the other gases. In addition, 25 different articles were analyzed to compile Table S1 and Table S2. It is observed that, in all studies, solubility increases with increasing pressure and decreases with increasing temperature, as expected. Therefore, the best results are always obtained at the highest pressure and lowest temperature.

2.1. Comparison between gas solubility in ILs and DESs

Gases solubility in ILs has been explored since 2001 [26,50–56] as well as determination of gases solubility in DESs has initiated in 2008 [49]. It was proved that gases solubility in ILs occurs by either chemical or physical absorption depending on their functional groups and it has been usually higher than organic solvents [26,57].

The low melting point and low volatility of ILs make them promise candidates as carbon capture solvents [58]. Unfortunately, ILs normally present high viscosity and this property can increase even more due to intermolecular hydrogen bond formation between ILs and CO_2, which can result in the formation of a gel that harms CO_2 absorption. However, the increase of viscosity during the CO_2 capture can be circumvented by design ILs to avoid intermolecular hydrogen bond formation between ILs and CO_2. It is desirable to design ILs in which hydrogen bond formation turns to be preferable intramolecular [59,60].

DESs are a new class of solvents, generally more environmentally friend than the usual solvents. They have been suggested as an alternative to ILs in many processes such as extraction and separation of metals and removal of alkali and transition metal ion from water. Besides, they can also be used for CO_2 capture [61–63], a process that also occurs by physical and chemical absorption. Dissolution enthalpy and entropy of CO_2 in DESs are always negative, which indicate that the process is exothermic but not spontaneous [37]. DESs present melting temperature lower than the melting points of their respective precursors. Thus, for gas solubility those DESs in which the melting points are close to ambient temperature are preferred, in order to reduce energy requirements. Regarding density, they usually present densities in the range of 1–1.35 g/cm^3, but it changes according to their functional groups and the HBA:HBD molar ratio [64,65]. As ILs, DESs present high viscosity that makes difficult mass and heat transfer. Although the viscosity can be diminished with the addition of water, both water and CO_2 molecules can compete each other by DESs [66]. Sarmad et al. (2017) [9] studied the solubility of CO_2 in various DESs and ILs between 293.15 – 313.15 K and 5 – 125 bar, and they observed that choline chloride based DESs is better CO_2 solubilizer than similar ILs counterparts.

Alkhatib et al. (2020) [67] applied the soft statistical associating fluid theory equation of state (soft-SAFT EoS) for screening ILs and DESs for CO_2 capture at industrially relevant conditions and through engineering calculations. They have evaluated the potentiality of these solvents using cyclic working capacity, heat of regeneration, viscosity, diffusivity, and solvent consumption. The solubility was evaluated at 298 K and in the pressure range of 0.001 – 25 bar. They observed that the majority of studied ILs had a higher CO_2 absorption (between x_{CO2} = 0.05 and 0.50) than all the studied DESs (between x_{CO2} = 0.025 and 0.15), which are different results

from those ones observed by Sarmad et al. (2017) [9]. Regarding the cyclic working capacity evaluated at 298 K and at 10 and 25 bar, Alkhatib et al. (2020) [67] observed that pressure increase from 10 to 25 bar increases the cyclic working capacity of all solvents examined, but it was higher for ILs than DESs (ranging from 19% to 51% for ILs and 28% to 43% for DESs). Both DESs and ILs present negligible effect on the viscosity as they are incompressible fluids, and the CO_2 diffusion coefficient increased as pressure raises from 10 to 25 bar, which enhances the mass transfer of CO_2 and its absorption. In this study the ILs present a better performance than DESs in terms of working capacity.

2.2. Techniques used to measure gas solubility

Several techniques have been used to measure gas solubility in DESs. These techniques were compared in order to understand which one could be the best to be used. To exemplify, we will analyze techniques that measure CO_2 solubility in ChCl:urea DES at molar ratio of 1:2. All the details of each technique is described in Supporting Information.

Unfortunately, it is difficult to classify the best technique, since each one has its limitation of pressure and temperature and its advantages and disadvantages, as shown in Table 1. Although the CO_2 solubility values of the studies of Li et al. (2008) [49] and Leron, Caparanga and Li (2013) [41] are close, the second uses a lower pressure, which promotes less energy expenditure, for example.

Table 1. Advantages and disadvantages of CO_2 solubility in DES apparatus.

Reference	Points		
	Techniques	**Positive**	**Negative**
Li et al. (2008) [68]	• CO_2 cylinder • Syringe pump • Constant-temperature water bath • Pressure gauge • Volume-variable view cell • Sample bomb	• Good temperature and pressure control	• With sampling
Liu et al. (2019) [69]	• Isothermal water bath • Balance of absorption, • Two chambers to stores and isolates CO_2	• No sampling. • Small sample amount	• Temperature values with low precision
Ali et al. (2014) [43]	• Variable-volume high-pressure equilibrium cell	• Computational data recording	• With sampling
Mirza et al. (2015) [70]	• Buffer tank • Incubation heater • Static stainless steel equilibrium vessel	• No sampling	• Temperature values with low precision • Long time to achieve equilibrium
Leron et al. (2013) [41]	• Thermogravimetric pressure scale	• Computational data recording • No sampling • Small sample amount	• Temperature values with low precision

2.3. DESs molar ratio in gas solubility

An important factor that affects gas solubility, usually increasing it, is the molar ratio between HBA and HBD donors of DESs. The first study concerning CO_2 solubility compares the difference in solubility between 1:1.5, 1:2, and 1:2.5 molar ratios of choline chloride and urea [49]. In this study, the highest CO_2 solubility was found when the ChCl:urea molar ratio was 1:2 with the value of 0.309. This occurs probably because the DES is really formed at 1:2 molar ratio; therefore, its melting point is the lowest and the molecular interaction favors the dissolution of the gas [68,71,72]. Liu et al. (2019) [69] also studied CO_2 solubility in DES composed of choline chloride and urea at

the same molar ratios as the previous study. They analyzed Henry's constant and the lowest value was also found at 1:2 molar ratio, indicating higher solubility than those at 1:1.5 and 1:2.5 molar ratios, which is consistent with the literature [69]. Figure 3 shows the behavior previously explained.

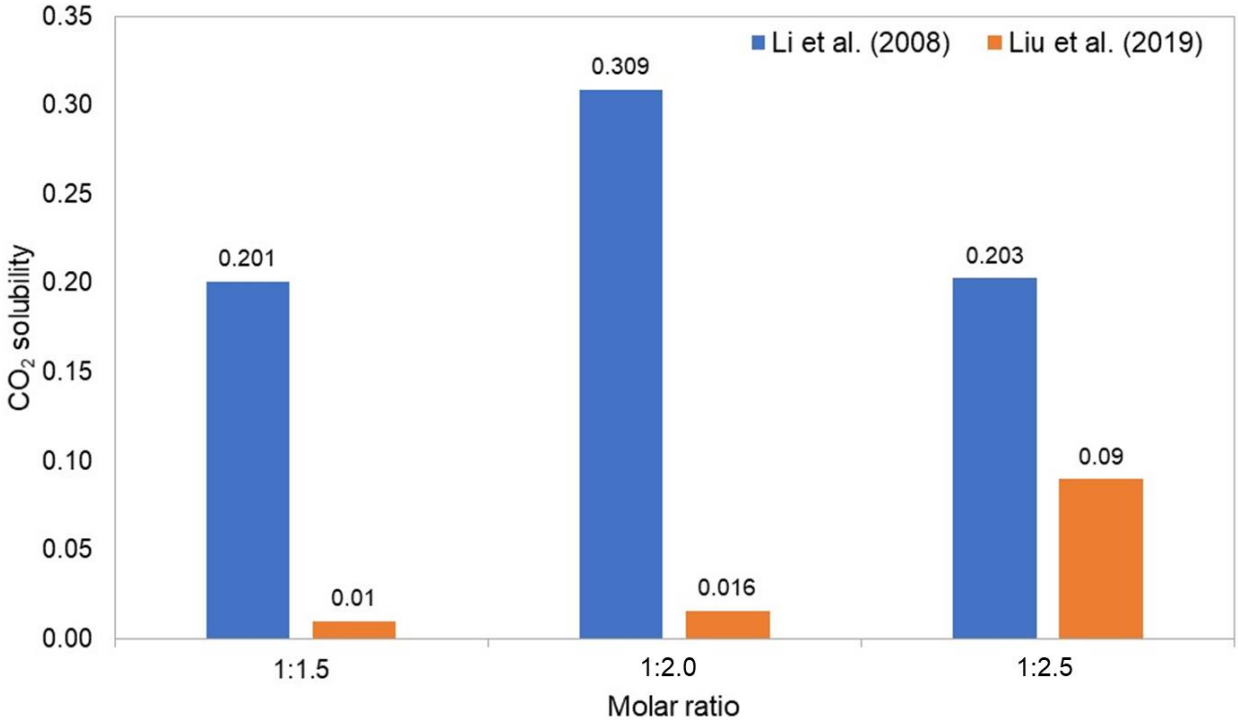

Figure 3. Influence of molar ratio on CO_2 solubility for ChCl:urea.

Liu et al. (2017) [20] studied CO_2 solubility in DESs composed of ChCl:guaiacol, DH:guaiacol, and ACC:guaiacol, at 1:2, 1:3, and 1:4 molar ratios. They found that CO_2 solubility in the same kind of DES increased with increasing molar ratio of guaiacol. This indicates that guaiacol has an important role in CO_2 dissolution into DES probably because of its hydroxyl group [73]. Another study comparing CO_2 solubility and DESs molar ratios was conducted by Haider et al. (2018) [21]. They compared ChCl:diethylene glycol at 1:3 and 1:4 molar ratios, ChCl:methyldiethanol amine at 1:6 and 1:7 molar ratios, TBAB:ethylene glycol and TBAB:diethylene glycol at 1:2, 1:3 and 1:4 molar ratios, and TBAB:methyldiethanol amine at 1:3 and 1:4 molar ratios. In all cases, it was found that increasing HBD:HBA molar ratio increases CO_2 solubility in DESs. In the

case of glycols, this increase occurs due to the strength of hydrogen bond that decreases in DESs. And the increasing solubility when increasing amines composition was reflected due to amine affinity toward CO_2 [21]. The same behavior previously discussed in this paragraph also occurs with ChCl:levulinic acid and ChCl:fufuryl alcohol at 1:3, 1:4, and 1:5 molar ratios [23]. It is important to clarify that, in the cases described in this paragraph, the exact molar ratio at which DES is really formed, according to Martins, Pinho and Coutinho (2018) [40] is unknown; therefore, the discussion only concerned molecular interactions in which an increase in molar ratio leads to increased solubility, which is not necessarily true. The behavior previously explained that solubility increases with increasing molar ratio, is shown in Figure 4.

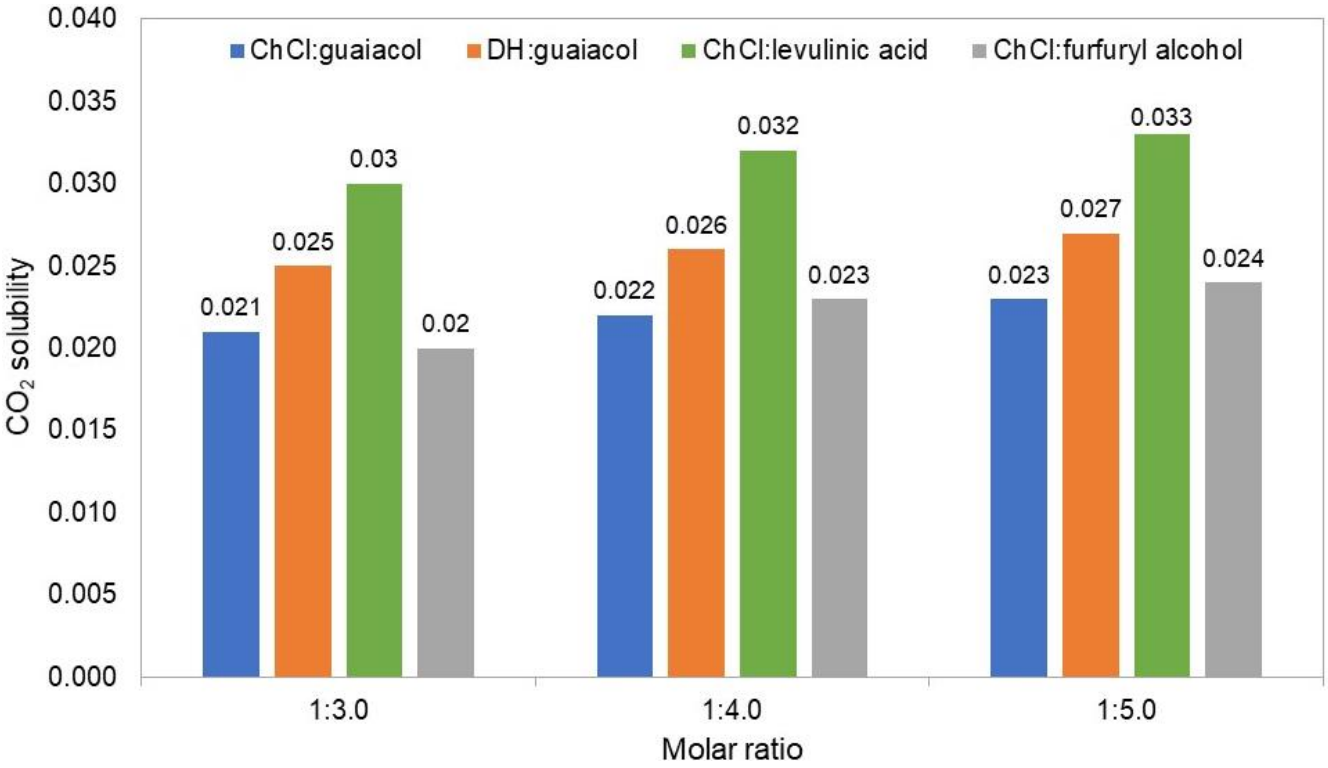

Figure 4. Influence of molar ratio on CO_2 solubility.

Ali et al. (2014) [43] studied CO_2 solubility in ChCl:glycerol at 1:3 and 1:8 molar ratios, and MTPB:ethanolamine at 1:6, 1:7, and 1:8 molar ratios. In both cases, solubility decreased with increasing HBD. This result indicates that physical behavior of these DESs cannot be predicted considering only the contribution effect of its

components' molar ratio [43]. The MTPB:ethanolamine mixture has no solid-liquid equilibrium study to confirm the exact molar ratio at which DES is formed; however, ChCl:glycerol mixture is formed at 1:2 molar ratio, where probably occurs the highest CO_2 solubility [22,74].

2.4. Influence of HBD on gas solubility

The hydrogen bond donor is an important factor that must be considered in gas solubility because it directly interferes with absorption capacity. Leron et al. (2013, 2013[1], 2013[2]) [22,41,42] studied CO_2 solubility in ChCl:urea, ChCl:ethylene glycol, and ChCl:glycerol DESs at 1:2 molar ratio and at moderate pressures. It is possible to observe that ChCl:glycerol (0.398) > ChCl:urea (0.308) > ChCl:ethylene glycol (0.275), which was expected since glycerol has a larger alkyl chain and three hydroxyl groups that can bond more powerfully with CO_2. Urea has two amine groups and ethylene glycol has only two hydroxyl groups bonding less powerfully to CO_2 (Table 2) [22,41,42]. Mirza et al. (2015) [70] also measured CO_2 solubility in ChCl:urea and ChCl:ethylene glycol at 1:2 molar ratio and found a different result from Leron et al., which means that the DES composed of urea has lower solubility than the DES composed of ethylene glycol. According to the study, CO_2 presents better affinity toward basic solvents than acidic ones during carbon absorption. In nonaqueous fluids, acidity and basicity are represented by pK_a. Therefore, lower pK_a represents acidic species and higher pK_a represents basic species. Analyzing the pK_a of the HBDs, the ethylene glycol pK_a is equal to 14.22 [75], and the urea pK_a is equal to 13.82 [76]. Since ethylene glycol has the highest pK_a value, it is capable of solubilizing the highest CO_2 amount [70,77,78].

Table 2. Chemical structures of HBDs discussed in topic 2.3.

HBDs chemical structures		
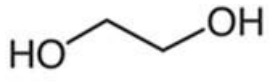 Ethylene glycol	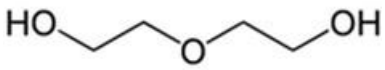 Diethylene glycol	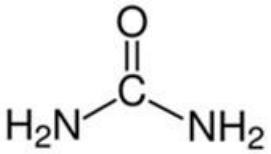 Urea
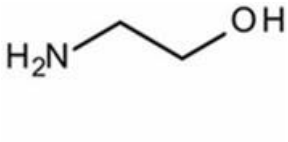 MEA	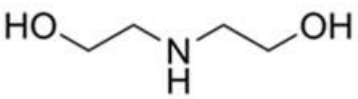 DEA	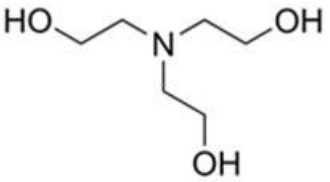 TEA
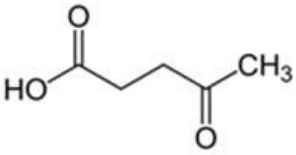 Levulinic acid	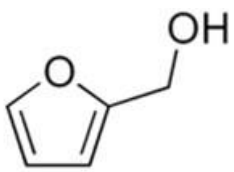 Furfuryl alcohol	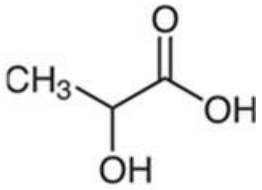 Lactic acid
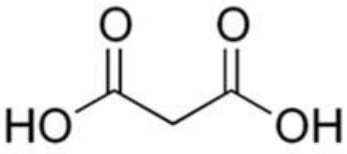 Malonic acid	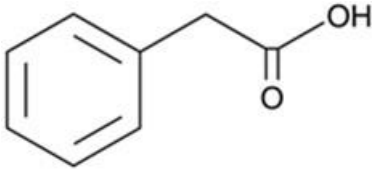 Phenylacetic acid	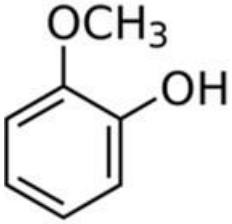 Guaiacol
	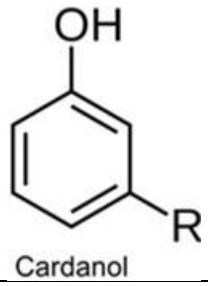 Cardanol	

In 2014, Ali et al. (2014) [43] studied CO_2 solubility in 17 DESs, containing amines and alcohols as HBD. Comparing ChCl:ethylene glycol and ChCl:triethylene glycol, the latter has twice the absorption capacity than ChCl:ethylene glycol due to the larger

alkyl chain, increasing the free volume [24,43,79]. They also observed that the use of ethanol amine as HBD improved the solubility substantially; thus, they investigated the effect of monoethanol amine (MEA), diethanol amine (DEA) and triethanol amine (TEA) as HBD with tetra butyl ammonium bromide as HBA. MEA presented the highest CO_2 solubility, which was not expected since TEA presents the largest alkyl chain, which increases the steric hindrance (Table 2) [43]. Li et al. (2014) [80] also studied CO_2 solubility in ChCl:ethylene glycol and ChCl:triethylene glycol and obtained results similar to those of Ali et al. (2014) [43], which means ChCl:triethylene glycol > ChCl:ethylene glycol. They also measured the solubility in ChCl:phenol, but the results were not higher than for triethylene glycol.

Another interesting study was conducted by Lu et al. (2015) [23], in which CO_2 solubility was measured in ChCl:levulinic acid and ChCl:furfuryl alcohol at 1:5 molar ratio. At the same temperature, it was observed that CO_2 solubility in levulinic acid-based DESs is higher than that of furfuryl alcohol-based DESs. This is probably because the carbonyl group of levulinic acid establishes stronger bonds with CO_2 than the hydroxyl group of furfuryl alcohol (Table 2) [23,80].

Altamash et al. (2019) [44] studied CH_4 solubility in ChCl:lactic acid, ChCl:malonic acid at 1:1 molar ratio and ChCl:phenylacetic acid at 1:2 molar ratio. The CH_4 absorption performance was: ChCl:lactic acid > ChCl:phenylacetic acid > ChCl:malonic acid. CH_4 solubility in ChCl:lactic acid has the highest value due to the C−OH···CH_4 or C=O···CH_4 interactions (Table 2) [44].

In 2018, Liu et al. (2018) [81] studied SO_2 solubility in DESs containing ChCl:guaiacol and ChCl:cardanol at 1:3 molar ratio. The results showed that the absorption capacity of ChCl:guaiacol was higher than those of ChCl:cardanol, probably

due to the structural difference of guaiacol and cardanol [82]. In the literature, studies prove that the ether group in guaiacol is helpful for binding acidic SO_2 (Table 2) [73,81,83].

2.5. Influence of HBA on gas solubility

Hydrogen bond acceptors play an important role in gas solubility because they can influence the solubility more than the HBDs [82]. In 2016, Ji et al. (2016) [84] compared the CO_2 solubility in DESs composed of phenol as HBD and ChCl, TMAC and TEAC as HBA at 1:3 molar ratio. They found that CO_2 solubility decreases in the following order: ChCl:phenol > TMAC:phenol > TEAC:phenol. The authors suppose that this result is due to the molecular interaction between ChCl – which has one hydroxyl group – and CO_2 being stronger than the interaction between TMAC or TEAC and CO_2 (Table 3) [84].

Table 3. Chemical structures of HBAs discussed in topic 2.4.

HBAs chemical structures		
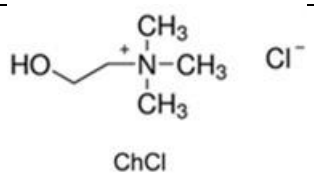 ChCl	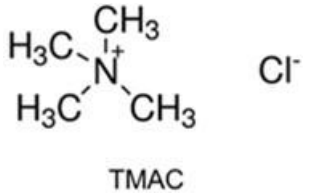 TMAC	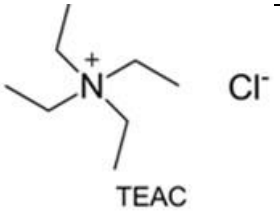 TEAC
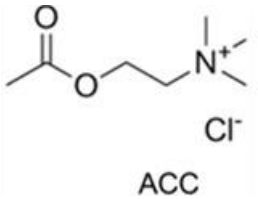 ACC	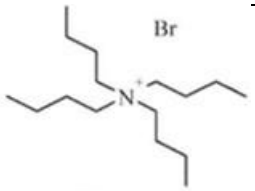 TBAB	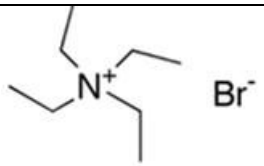 TEAB
	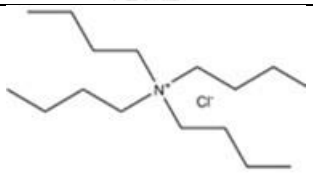 TBAC	

Deng et al. (2016, 2015) [11,25] investigated CO_2 and SO_2 solubilities in DESs composed of levulinic acid as HBD and ChCl, ACC, TEAC, TEAB, TBAC, and TBAB as HBA at 1:3 molar ratio. For CO_2 solubility, at the same temperature, TEAB:levulinic acid presented the lowest CO_2 absorption capacity, and TBAC:levulinic acid the highest one. With these results, it is observed that the influence of quaternary ammonium salts on CO_2 absorption is related with the structure of cations rather than of anions. Table 3 shows that the largest the cation, the highest the CO_2 solubility, except for ACC:levulinic acid DES, due to the additional acetyl ester group decreasing the absorption capacity. For SO_2, however, the performance of anions defined the absorption capacity. The relatively largest bromide ion binds more to SO_2 than the chloride ion, as the tetrabutylammonium salt had higher absorption capacity than the tetraethylammonium salt. For the ChCl and ACC HBAs, when the hydroxyl group was replaced with acetyl ester the absorption capacity was enhanced. Therefore, the performance of the ester group is more effective than the hydroxyl group for SO_2 solubility [11,80,85].

Haider et al. (2018) [21] studied CO_2 solubility in ChCl:ethylene glycol, ChCl:diethylene glycol, ChCl:methyldiethanol amine, ChCl:diethanol amine, TBAB:ethylene glycol, TBAB:diethylene glycol, TBAB:methyldiethanol amine, and TBAB:diethanol amine. It was observed that CO_2 solubility increased in TBAB-based DESs. This is probably due to the larger alkyl chain length of TBAB, increasing the free volume and consequently the absorption capacity when compared to ChCl [21,80].

So far, the authors used the alkyl chain length and the functional groups to determine the best HBA to absorb CO_2. Wang et al. (2019) [86] studied experimentally and using molecular dynamics the CO_2 solubility in TBPB:phenol and ATPPB:phenol at 1:4 molar ratio. In order to analyze the effect of HBA type, the site-to-site radial

distribution function (RFD) and spatial distribution function (SDF) of $TBP^+ - CO_2$ and $ATPP^+ - CO_2$ were compared. A sharp and intense peak of CD·HB (CD symbolizes the atom of CO_2 and HB means H atoms in the benzene rings) was observed for the $ATPP^+ - CO_2$ pair, while, for the $TBP^+ - CO_2$ pair, broader and weaker peaks (CD···H3/H5/H7) were observed. This difference implies stronger interactions between $ATPP^+$ and CO_2 than between TBP^+ and CO_2, explaining the higher CO_2 solubility in ATPPB:phenol DES [86].

2.6. Comparison between hydrophobic and hydrophilic DESs in CO_2 solubility

Studies concerning CO_2 solubility in hydrophilic DESs are extensive and it is the main focus of this review. Although hydrophilic DESs have been showed to be an interesting solvent to gases capture, they can absorb an amount of water during the absorption process, which reduces their mass absorption capacity as well as lead to high energy consumption in the CO_2 desorption process [87]. Hydrophobic DESs seem to be an alternative to such disadvantage. They were discovered in 2015 and have been used for removal of fatty acids, biomolecules and metal ions from water [62,88,89]. However, the first study concerning CO_2 solubility in these DESs was done only in 2018 [90] and showed promising results.

Zubeir et al. (2018) [90] determined the CO_2 solubility in TBAB:decanoic acid, N_{8881}−Cl:decanoic acid, N_{8881}−Br:decanoic acid, N_{8888}−Cl:decanoic acid and N_{8888}−Br:decanoic acid between 298.15 – 323.15 K and 0.90 – 19 bar. They observed that the hydrophobic DESs investigated present the highest solubility of CO_2 (values between 0.239 – 0.284 mol CO_2/mol DES) when compared to other DESs from literature until that date. These DESs were even better than some fluorinated ILs.

Gu et al. (2020) [87] measured the CO_2 solubility in [TETA]Cl:thymol and [TEPA]Cl:thymol at 313.15 K and 1 bar. The values observed were equal to 1.298 and 1.355 mol CO_2/mol DES, respectively. These values are much higher than those observed for several ILs and DESs found in literature (Table S1). The authors noted that during the CO_2 absorption process there was no change of water amount in DESs, which was expected to happen once the flue gases always have an amount of water. Another interesting result presented in this study was the formation of a new chemical bond between DES and CO_2 that are stronger than physical interaction but not suppress it. Even though with the new chemical bonds, both DESs remains hydrophobic during CO_2 absorption.

Despite the literature presents only these two studies about gas absorption using hydrophobic DESs, they seem to be a promise solvent to CO_2 capture according to the results presented above and expands the research needs in the topic.

2.7. Comparison of CO_2, CH_4, H_2S, and SO_2 absorption capacity

CO_2 is the most studied gas when it comes to its solubility in DES. Although SO_2, H_2S and CH_4 are important GHGs, few studies were found in the literature concerning the solubility of these gases in DESs. Liu et al. (2019) [69] studied CO_2, H_2S and CH_4 absorption in ChCl:urea. Comparing the solubilities at 313.15 K, 2 bar and 1:2 molar ratio, it was observed that the scale in decreasing order of absorption is: H_2S (0.0464) > CO_2 (0.016) > CH_4 (0.0008). The authors used Grand-canonical Monte Carlo (GCMC) to calculate the site-to-site RDFs of ChCl:urea:gas systems. It was observed that hydrogen bonds were formed between ChCl:urea and H_2S, especially between Cl of ChCl and H of H_2S. The RDF profiles of ChCl:urea and CO_2 are similar to those of ChCl:urea and H_2S, but in small quantity. This result suggests hydrogen

bonds formation between ChCl:urea and CO_2. Cl of ChCl is again the major site for binding with CO_2. CH_4 is a rigid and inert molecule, and the RDF profiles of ChCl:urea and CH_4 are flat and noisy, meaning that van der Waals interactions are weak [69]. Sun et al. (2015) [47] studied SO_2 absorption in ChCl:urea at the same conditions mentioned above and obtained a solubility of 1.17, an indication that the interaction between the DES and SO_2 is stronger than that with CO_2, H_2S and CH_4 [47].

Deng et al. (2015, 2016) [11,25] studied CO_2 and SO_2 solubilities in TBAC:levulinic acid DES at 1:3 molar ratio, 303.15 K, and 6 bar. These gases are the major acid gases that coexist in real flue gas and efforts to separate SO_2 from CO_2 are made [91] and are necessary. For that reason, it is important to compare the potential of the DESs to solubilize these gases. For SO_2, the solubility was equal to 1.052 and, for CO_2, the solubility was equal to 0.04, proving that SO_2 has much higher solubility than CO_2, approximately 25 times higher [11,25]. Similar results were obtained by Liu et al. (2017, 2018) [20,81], who studied CO_2 and SO_2 solubilities in ChCl:guaiacol at 1:3 molar ratio, 293.15 K and 1 bar. For SO_2, the solubility was equal to 1.056 and, for CO_2, it was equal to 0.006, showing that SO_2 has the highest solubility when compared with other gases, such as CO_2, H_2S and CH_4 [20,81], as shown in Figure 5.

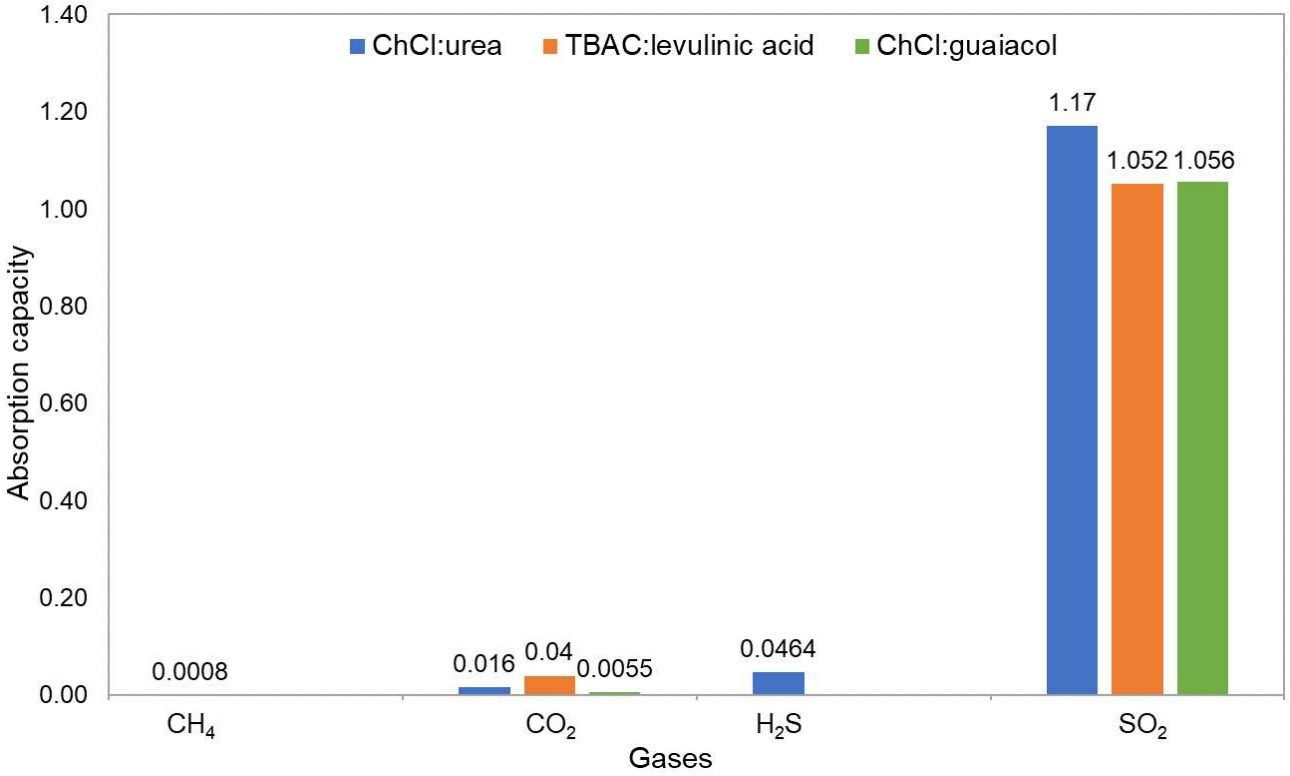

Figure 5. Comparison of the solubility of the gases.

Malik et al. (2021) [92] did ab initio molecular dynamics (AIMD) simulations to understand the local solvation structure around CO_2 and SO_2 in ChCl:urea and ChCl:ethylene glycol DESs. They observed that Cl^- and $N_{[Ch]+}$ interacts strongly with C_{CO2} while $O_{[Ch]+}$ is more associated with O_{CO2} for atomic distribution around CO_2 and ChCl:urea. Therefore, the ammonium group of $[Ch]^+$ is closer to C_{CO2} than the hydroxyl group, and the hydroxyl group of $[Ch]^+$ is closer to O_{CO2} than the ammonium group. Concerning the atomic distribution around SO_2 and ChCl:urea, they observed a strong association between Cl^- and S_{SO2}, and N_{urea} and O_{SO2}, while $N_{[Ch]+}$ has a strong association with both S_{SO2} and O_{SO2}.Thus, the number of $N_{[Ch]+}$ molecules surrounding SO_2 in the solvation is relatively greater than that of $O_{[Ch]+}$. This means that choline cations approach to SO_2 from their ammonium group side.

The authors [92] also studied the spatial distribution functions (SDFs) of CO_2 and SO_2 in both DESs, ChCl:urea and ChCl:ethylene glycol. They observed a similar isosurface for both DESs, in which the isosurface of Cl^- and HBD species are around

the C_{CO2} and the isosurface of $[Ch]^+$ are symmetrically in both sides of O_{CO2} as it can be seen in Figure 6. The same SDFs is not observed for SO_2, the Cl^- isosurface is near to S_{SO2} molecule differently from the circular solvation around CO_2 molecule. This difference is probably due to the shapes of the two molecules, because CO_2 is linear and SO_2 is bent. Additionally, Malik et al. (2021) [92] analyzed the total Hirshfeld [93] and Mulliken [94] charges to enhance the charge distribution on $[Ch]^+$, Cl^-, HBD, and solute species. In all four systems, CO_2, SO_2 and HBD species of both DESs are not neutral such that a charge transfer is possible between chloride to choline and chloride to HBD and solute species. Hirshfeld (Mulliken) CO_2 charge distributions have peaks at −0.135*e* (−0.015*e*) and −0.175*e* (−0.03*e*) indicating perceptible charge transfer from Cl^- to CO_2. The charge transfer from Cl^- to SO_2 is more pronounced because Hirshfeld (Mulliken) charge is observed around −0.6*e* (−0.3*e*). These observations indicated that Cl^- and SO_2 molecules has a strong interaction, which leads to a better SO_2 absorption.

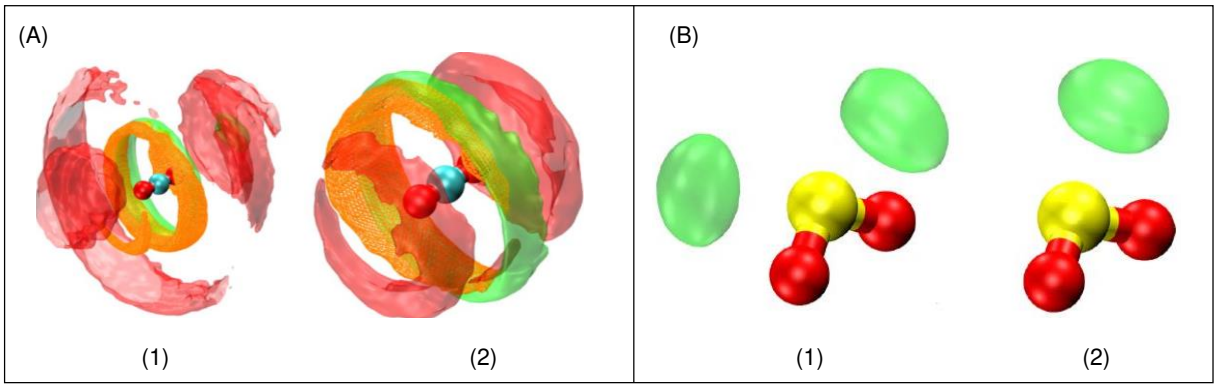

Figure 6. Spatial distribution functions around the central CO_2 (A) and SO_2 (B) molecules in (1) ChCl:urea and (2) ChCl:ethylene glycol at 333 K. The transparent green, orange, and red isosurfaces represent Cl^-, HBD, and $[Ch]^+$ molecules, respectively. Reproduced with permission from [92]. Copyright (2021) American Chemical Society.

3. Gas solubility in DES – Thermodynamic Modelling

Some of the returned articles from our search, in addition to experimental measurements, also studied the thermodynamic modelling to predict gas solubility in DESs. The models used were Peng-Robinson (PR), Perturbed-Chain Statistical Associating Fluid Theory (PC-SAFT), Cubic Plus association (CPA), Non-random two-liquid (NRTL), Conductor like Screening Model (COSMO), Redlich-Kwong (RK) and Monte Carlo simulation. Other authors chose to study only the aspects of thermodynamic modelling to evaluate gas solubility in DESs using data published in literature. Table 4 shows both scenarios.

Table 4. Modelling used in different papers.

Reference	Experimental data	PR	PC-SAFT	CPA	NRTL	COSMO	RK	Monte Carlo
Alioui et al. (2020) [95]						✓		
Sarmad et al. (2020) [37]	✓						✓	
Mirza et al. (2015) [70]	✓	✓						
Haghbakhsh; Raeissi (2018) [96]				✓				
Haider et al. (2019) [97]	✓	✓						
Zubeir et al. (2016) [98]			✓					
Dietz et al. (2017) [99]			✓					
Kamgar et al. (2017) [100]					✓	✓		
Haider; Kumar (2020) [45]	✓	✓			✓			
Ali et al. (2014) [43]	✓	✓						
Salehi et al. (2020) [101]								✓

Alioui et al. (2020) [95] calculated CO_2 solubility in seven DESs composed of ChCl and urea, ethylene glycol, or glycerol at 1:2 molar ratio, ChCl:2-aminothan-1-ol at 1:6 molar ratio, and ATPPB and ethylene glycol or triethylene glycol at 1:4 molar ratio, and MTPPB:levulinic acid at 1:4 molar ratio using COSMO-RS method. In this study, it is observed that the calculated solubility is consistent with experimental values but always higher (between 9 and 63%), as shown in Figure 7.

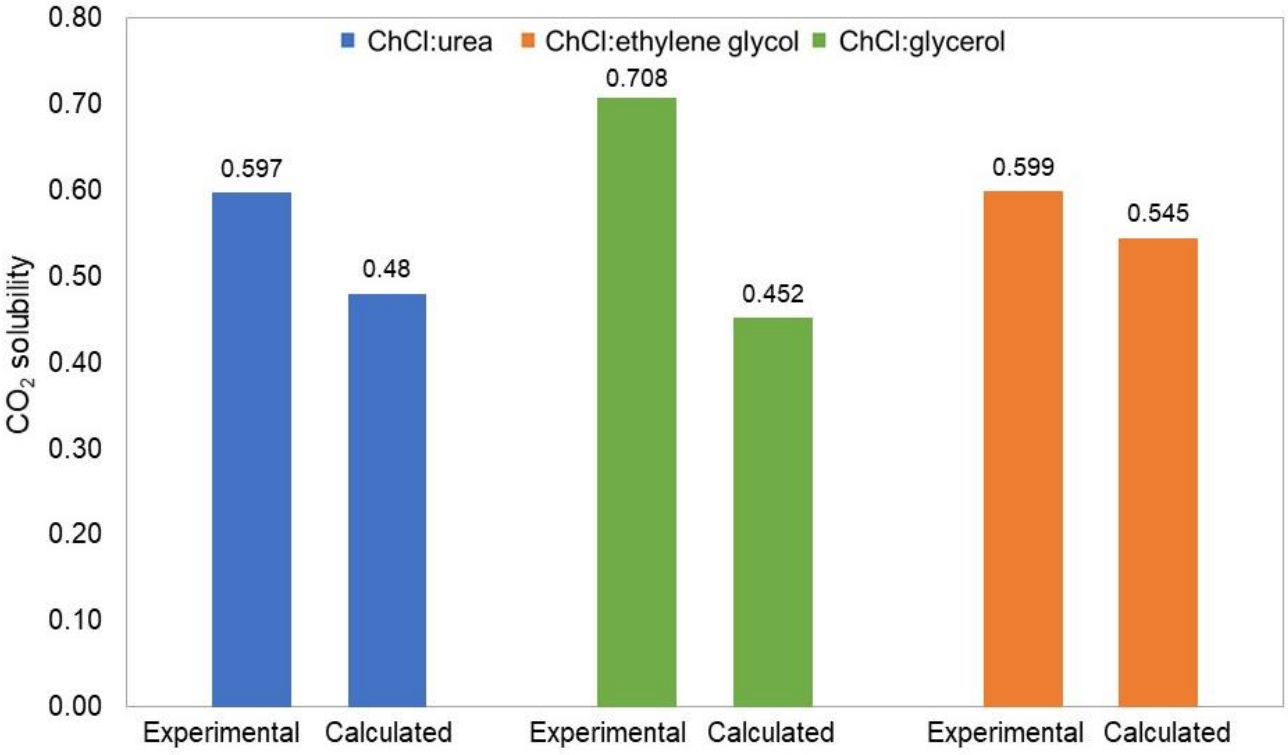

Figure 7. Comparison between calculated (COSMO-RS) and experimental CO_2 solubility in different DESs.

Kamgar et al. (2017) [100] also predicted CO_2 solubility in ChCl:urea at 1:1.5, 1:2 and 1:2.5 molar ratio using COSMO-RS and NRTL, but they found different results from Aliouli et al. (2020) [95]. COSMO-RS model provided acceptable results for CO_2 solubility only at low pressures and high temperatures, where the gas could be assumed ideal. With the increase in pressure and decrease in temperature, the difference between predictions and experimental data becomes larger. COSMO-RS

overpredicts CO_2 solubility in DESs, while for other gases it underpredicts the solubility data, and it did not work for N_2 data. NRTL shows better accuracy than COSMO-RS, probably because COSMO-RS is a totally predictive model, without functional and adjustable parameters [100].

Zubeir et al. (2016) [102] modelled CO_2 solubility in three DESs composed of TMAC:lactic acid, TEAC:lactic acid, and TBAC:lactic acid at 1:2 molar ratio using PC-SAFT equation of state. In a first approach, the authors considered DESs as a pseudo-pure compound and its parameters were obtained by fitting to DESs density data. When pure predictions were carried out (k_{ij} = 0), a large difference was observed between calculated and experimental data. Subsequently, the binary interaction parameter was considered temperature-independent and also different from zero, and then, the modelling results were in good agreement with the experimental data. In the second approach, DESs were considered as two individual components (HBA and HBD), and the pure-component parameters of the HBA and HBD were obtained by fitting to the density of aqueous solutions containing only the individual compounds of the DESs. For this case, the relative deviations AARD (%) between PC-SAFT results and the experimental data were between 12.9% and 6.1%, describing the solubility correctly [98]. Dietz et al. (2017) [99] also applied PC-SAFT pseudo-pure approach for modelling CO_2 solubilities in TBAC:lactic acid at 1:2 and 1:3 molar ratios. The data were predicted without adjusting any binary interaction parameter and shows the AARD (%) between 2.27 and 12.01%, proving that PC-SAFT can be used to model CO_2 solubility in these DESs [99].

Just two papers modelled CO_2 solubility in DESs using the Cubic Plus Association Equation of State (CPA) [96,103]. In Haghbakhsh; Raeissi (2018) [96] study, DESs were considered as a pseudo component with different possible association

schemes: two (2B), three (3B), four (4B) association sites, solvation and inert. It was observed that the carbon dioxide association schemes of 2B, 3B, and 4C have no significant advantage over the inert or solvation association schemes. Using the CPA model by the inert association scheme (binary interaction coefficient), the study shows a good agreement with the experimental data, presenting AARD of 6.2%. With the commonly used association scheme of solvation (cross association volume), AARD is a little higher, 7.1%, but also in good agreement with the experimental data [96].

Several papers modelled CO_2 solubility in DESs using Peng-Robinson equation of state (PR EoS) [21,43,45,70,97]. In all cases, PR EoS presented excellent agreement between model results and experimental data. However, this is only possible because the temperature-dependent interaction parameters (k_{ij}) were determined. Ali et al. (2014) [43] showed a large deviation between the calculated and experimental values when PR EoS was used without the binary interaction parameter, setting k_{ij} equals to zero [43]. Haider et al. (2018, 2020) [21,45] also modelled CO_2 solubility in TBAB:2-Methylaminoethanol, BTEACl:2-Methylaminoethanol, TBAB:2-Ethylaminoethanol, BTEACl:2-Ethylaminoethanol, ChCl:ethylene glycol, ChCl:diethylene glycol, ChCl:methyldiethanol, ChCl:diethanol amine, TBAB:ethylene glycol, TBAB:diethylene glycol, TBAB:methyldiethanol, and TBAB:diethanol amine using NRTL, and observed that the NRTL model has a better fit than PR EoS, showing lower standard deviations [21,45].

All presented models have their own suitability and limitations. When COSMO-RS is used to predict CO_2 solubility in DESs, the DESs representation is a crucial step, because a single DES is composed of more than one molecule. Therefore, it is used the electroneutral approach in which ions are treated as two different compounds in an equimolar mixture, i.e, DESs are represented according to the mole

composition of their constituents, HBA (formed by the salt cation and the salt anion) and the HBD [104]. For example, for a [cation][anion]:HBD (*m:n*) DES, the COSMO-RS input is *m* mol of cations, *m* mol of anions, and *n* mols of the HBD; all of them contribute to the total mols number, that differ from the experimental definition (*m* mol of HBA and *n* mol of HBD) [38]. Unfortunately, COSMO-RS does not predict well equilibrium data under high pressure and low temperatures, as mentioned before. This occurs because the model is completely predictive, with no adjustable parameters [100].

NRTL model could provide trustworthy results for partial and complete miscible systems even under high pressure according to articles cited [45,100]. In NRTL equation, α is related to the non-randomness in the mixture and its value changes between 0.20 and 0.47 [100]. For gas solubility in DESs, Kamgar et al. (2017) reported that NRTL was capable to describe the experimental solubility data of CH_4, N_2 and CO_2 in ChCl:urea DES with good accuracy even under 120 bar. COSMO-RS does not present the same performance as discussed before. The other study presented by Haider and Kumar (2020) concerning the solubility of CH_4 and CO_2 in TBAB:MAE, BTEACl:MAE, TBAB:EAE and BTEACl:EAE shows the NRTL ability to describe the experimental data up to 15 bar in comparison to PR EoS. According to the authors, NRTL shows better results than PR EoS due to the high deviation from the ideal behavior caused by hydrogen bond in DESs.

PC-SAFT is based on the perturbation theory of Barker and Henderson with hard-chain as the reference fluid. One limitation to PC-SAFT use to model gas solubility in DESs is the necessity of pure compounds parameters which are not easily found in the literature. To overcome this problem, the pseudo-pure component or the individual-component approaches can be used. In the first one, DESs are considered as a pseudo-pure component with an average molar mass based on composition and must

be assigned two association sites to DESs. The density of the DESs and binary vapor−liquid equilibrium (VLE) data are fitted to obtain the pure-component parameters and the binary interaction parameter (k_{ij}). Induced association between DESs and CO_2 is considered as an attractive interaction. On the second strategy, the density of aqueous solutions of DESs individual compounds are fitted to obtain pure-component parameters. On this strategy, self-association, cross-association and induced association between DESs components and CO_2 are considered. An important step is to determine the k_{ij} parameter that is done by fitting DES:CO_2 VLE data. The k_{ij} parameter is essential to get a good description of experimental data because it is related to interaction between the gas molecules and DESs, which are particularly different concerning shape and size of these molecules. Both strategies can be applied as they are able to model DESs density and the VLE data accurately [102].

CPA EoS requires three physical parameters (a_0, b, and c_1) and two associative parameters related to the volume (β) and energy (ε). All of them are not easily found in the literature for DESs. One strategy to determine these parameters is based on liquid density data along with the pseudo-pure component approach with two association sites (2B) for DESs. Although many gas solubility data on DESs are available in literature, there is a restriction to model all of them using CPA EoS due to the lack of density data of pure DESs, that is, the CPA parameters cannot be defined. Although the previous studies about CPA EoS mention the need of choosing CO_2 association scheme (inert, solvation, 2B, 3B and 4C), Haghbakhsh and Raeissi (2018)[96] stated the association schemes of 2B, 3B, and 4C for CO_2 have no significant advantage over the inert or solvation association schemes if k_{ij} parameter of cubic equation of CPA is considered.

The PR EoS is used to estimate VLE data, and it is appropriate for systems that contains hydrocarbons, water, CO_2, air and combustion gases[43]. PR EoS also requires the values of the mixture critical properties to be successfully used to model the gas solubility, but such data are unknown. Lydersen–Joback–Reid mixing rule method [105,106] must be used to predict such properties. It is worthy to mention again that k_{ij} parameter has an important role in the results and it is linearly dependent of temperature[43].

Monte Carlo simulations was used only once to predict gases solubility in DESs. Although molecular simulations have already being used to compute some properties of pure DESs, Monte Carlo simulations use is limited due to DESs high viscosity, which is caused by strong intermolecular interactions. These intermolecular interactions make difficult the molecule insertion inside the simulation box, which results an inefficient sampling of phase-space [101]. Salehi et al. (2020) [101] used Monte Carlo simulations to compute the solubilities of CO_2, H_2S, CH_4, CO, H_2, and N_2 in ChCl:urea and ChCl:ethylene glycol in terms of Henry constant at infinite dilution. The authors used Optimized Potentials for Liquid Simulations force field (OPLS) and Generalized Amber force field (GAFF), which return better density results than the first. Despite of GAFF seems to be more adequate for compute gas solubility in DESs, the authors conclude that the force field parameters used for the DESs probably are not suitable for the solubility calculations due to the discrepancy between the calculated and experimental values.

Concerning the distribution of the thermodynamic models used to predict CO_2 solubility in DESs it was observed that Peng-Robinson is the most used EoS; it was used in 33% of the papers included in this review. This is due to its simplicity compared to the other models. The least used models were CPA and Redlich-Kong EoS; they

were used in only 8% of the papers. CPA is more complex, being logical that it is not used frequently, since Peng-Robinson EoS works very well.

4. Final Discussion

Concerning the distribution between the 25 articles found in the literature, comparing how many papers have only experimental data, experimental data and modeling, or only modeling it was observed that 59% of the articles present only experimental data. In addition, articles containing modeling are still the minority, representing 23%, and articles with only modelling representing 18%. These distribution lead us to find a gap as to CO_2 solubility in DESs, which would be the lack of articles containing experimental data and modeling in the same study, and also the lack of studies containing thermodynamic modeling with several equations of state.

Another possible approach is comparing the number of papers and the range of pressure used in each one (Figure 8). Most papers present data for CO_2 solubility in DESs in a pressure range between 1 and 20 bar. This is probably due to the ease and security of working at relatively low pressures. At pressures above 60 bar, the number of papers decreases abruptly, which also represents a gap in this field. These missing data could be used to study, for example, the behavior in offshore oil platforms.

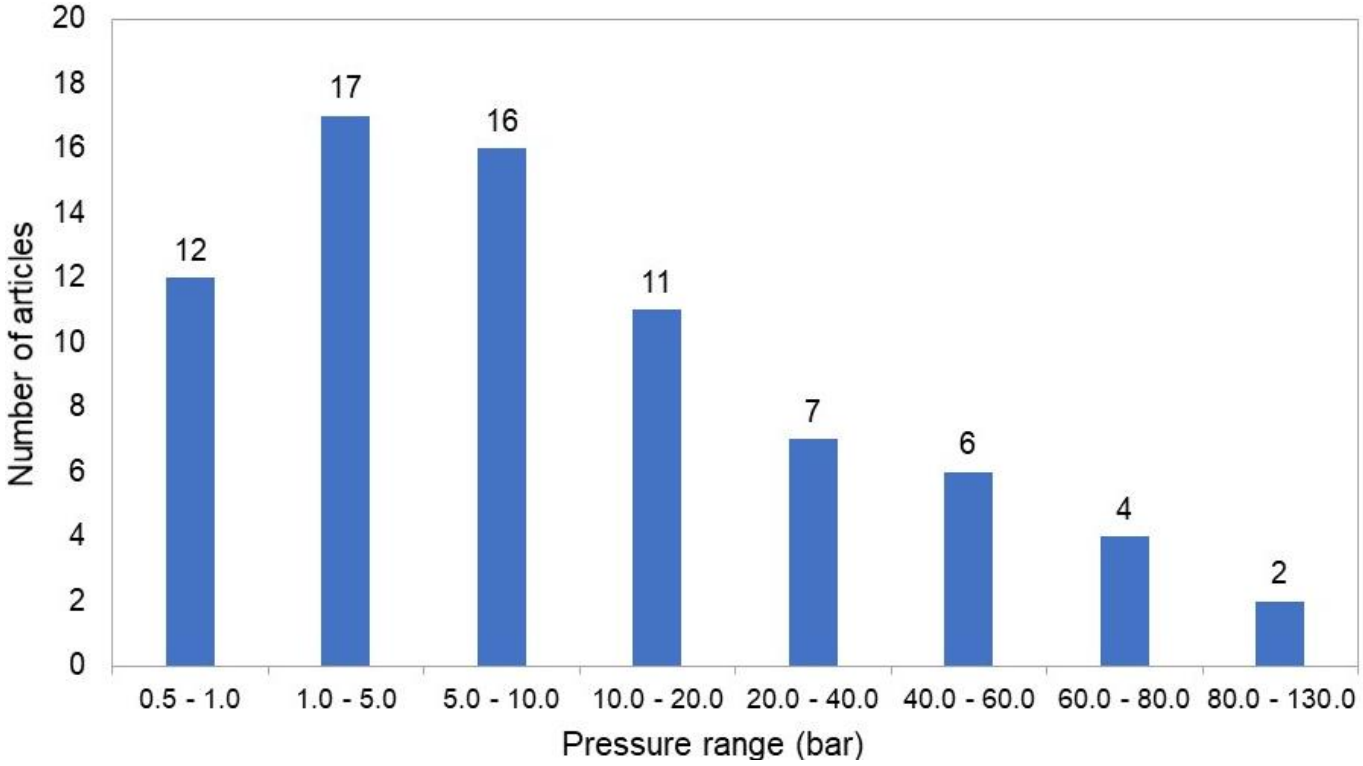

Figure 8. Distribution of the number of articles according to pressure range.

Regarding the distribution of papers that studied the solubility of different gases in DESs, a total of 67% of the papers measure CO_2 solubility, followed by SO_2 solubility, which is measured in 22% of the papers. Thus, there is a lack of studies on the solubility of other GHGs; they are also harmful to the environment and sometimes more dangerous than CO_2.

This review shows that more experimental data of gas solubility in DESs under pressure are needed, even for CO_2 and SO_2 gases. As mentioned before, gas solubility experimental data determined above 40 bar are really scarce. The importance of such data is justified by its necessity to EoS parameters adjustment, which are necessary in process simulation evolving gas solubility and also to help us to understand the chemical interactions between the different molecules during the gas absorption under high pressure. Remember that there are an incredible number of DESs which can be designed and even small traces about molecules interaction can be helpful on the

DESs design process. Note that new DESs can be able to solubilize a great amount of gas, for instance, it is possible to cite the hydrophobic DESs, which are able to solubilize more CO_2 than any other DESs tested before. Moreover, it is necessary the determination of pure DESs thermodynamic properties such as density and molar heat capacity that are suitable in the modelling solubility data process with any cubic EoS.

Although the environmental purpose is really noble to study gas solubility in DESs, this topic can go beyond for looking for new possibilities, new applications for such data. For example, is it economical and environmentally safe to use DESs in oil and gas extraction processes? To answer such question, experimental data are needed. If DESs can be usable in oil and gas extraction processes, new approaches about offshore platforms can be found and new challenges will come to be solved.

5. Conclusions and prospects

Anthropogenic GHGs pollution increases the global average temperature and undesired health effects. Technologies to capture CO_2 and other gases using MEA, MDEA and AMP are commonly applied, exhibiting excellent absorption capacity. However, they are not environmentally friendly due to their toxicity, partial degradation, and high vapor pressure. Therefore, green solvents have gained momentum in carbon capture applications due to their environment-friendly characteristics.

DESs have been investigated as novel solvents for capturing GHGs, especially CO_2 and SO_2, in order to overcome these disadvantages. DESs have high stability, negligible vapor pressures, low cost, good biodegradability, and simple preparation process, among other interesting characteristics. This review explored the applications of different types of DESs in gas capture technology.

In this review, more than 40 DESs were analyzed regarding: (i) the differences between DESs and ILs about their absorption capacity; (ii) the different techniques used to measure CO_2 solubility in DESs; (iii) the influence of DESs molar ratio on gas solubility by observing molecular interactions; (iv) the impact of HBD change on gas solubility; (v) the effect of HBA change on solubility; (vi) the differences between hydrophilic and hydrophobic DESs; and (vii) the solubility of different gases.

Although there are studies on the solubility of gases in DESs, they are still scarce in general, and even more scarce for higher pressures, for instance above 50 bar. It is also scarce the solubility of other gases such as SO_2, CH_4 in DESs. Moreover, few experimental data were modeled among the returned articles and they were not much diversified related to the thermodynamics models used; therefore, it is important to model the solubility data, and to use different thermodynamic models.

Acknowledgement

The authors acknowledge the Coordenação de Aperfeiçoamento de Pessoal de Nível Superior - Brasil (CAPES) - Finance Code 001, FAPESP (2014/21252-0 and 2018/19198-9), CNPq (306666/2020-0), and FAEPEX/UNICAMP for the financial support. The authors are grateful to the Human Resources Program of the National Agency of Petroleum, Natural Gas and Biofuels - PRH-ANP; Espaço da Escrita – Pró-Reitoria de Pesquisa - UNICAMP – for the language services provided.

References

(1) Jiang, J.; Ye, B.; Liu, J. Research on the Peak of CO2 Emissions in the Developing World: Current Progress and Future Prospect. *Appl. Energy* **2019**, *235*, 186–203.

(2) Li, G.; Deng, D.; Chen, Y.; Shan, H.; Ai, N. Solubilities and Thermodynamic Properties of CO2 in Choline-Chloride Based Deep Eutectic Solvents. *J. Chem. Thermodyn.* **2014**, *75*, 58–62.

(3) Ghaedi, H.; Zhao, M.; Clough, P. T.; Anthony, E. J.; Fennell, P. S. High CO2 Absorption in New Amine Based-Transition-Temperature Mixtures (Deep Eutectic Analogues) and Reporting Thermal Stability, Viscosity and Surface Tension: Response Surface Methodology (RSM). *J. Mol. Liq.* **2020**, *316*, 1–11.

(4) IPCC. *IPCC Special Report on Carbon Dioxide Capture and Storage. Prepared by Working Group III of the Intergovernmental Panel on Climate Change*; 2005.

(5) Concentration of CO2 https://scripps.ucsd.edu/programs/keelingcurve/ (2020) (accessed Oct 14, 2020).

(6) IEA. *Global Energy & CO2 Status Report 2019*; Paris, 2019.

(7) IEA. *Global Energy and CO2 Emissions in 2020*; Paris, 2020.

(8) Zhang, Y.; Ji, X.; Lu, X. Choline-Based Deep Eutectic Solvents for CO2 Separation: Review and Thermodynamic Analysis. *Renew. Sustain. Energy Rev.* **2018**, *97*, 436–455.

(9) Sarmad, S.; Mikkola, J. P.; Ji, X. Carbon Dioxide Capture with Ionic Liquids and Deep Eutectic Solvents: A New Generation of Sorbents. *ChemSusChem* **2017**, *10*, 324–352.

(10) Pires, J. C. M.; Martins, F. G.; Alvim-Ferraz, M. C. M.; Simões, M. Recent Developments on Carbon Capture and Storage: An Overview. *Chem. Eng. Res. Des.*

2011, *89*, 1446–1460.

(11) Deng, D.; Han, G.; Jiang, Y. Investigation of a Deep Eutectic Solvent Formed by Levulinic Acid with Quaternary Ammonium Salt as an Efficient SO2 Absorbent. *New J. Chem.* **2015**, *39*, 8158–8164.

(12) Schmelz, W. J.; Hochman, G.; Miller, K. G. Total Cost of Carbon Capture and Storage Implemented at a Regional Scale: Northeastern and Midwestern United States. *Interface Focus* **2020**, *10*, 1–15.

(13) Krishnan, A.; Gopinath, K. P.; Vo, D. V. N.; Malolan, R.; Nagarajan, V. M.; Arun, J. Ionic Liquids, Deep Eutectic Solvents and Liquid Polymers as Green Solvents in Carbon Capture Technologies: A Review. *Environ. Chem. Lett.* **2020**.

(14) Shunji, K.; Xizhou, S.; Wenze, Y. Investigation of CO2 Desorption Kinetics in MDEA and MDEA+DEA Rich Amine Solutions with Thermo-Gravimetric Analysis Method. *Int. J. Greenh. Gas Control* **2020**, *95*, 1–10.

(15) Nozaeim, A. A.; Tavasoli, A.; Mortaheb, H. R.; Mafi, M. CO2 Absorption/Desorption in Aqueous DEEA/MDEA and Their Hybrid Solutions with Sulfolane. *J. Nat. Gas Sci. Eng.* **2020**, *76*, 1–10.

(16) Skylogianni, E.; Perinu, C.; Cervantes Gameros, B. Y.; Knuutila, H. K. Carbon Dioxide Solubility in Mixtures of Methyldiethanolamine with Monoethylene Glycol, Monoethylene Glycol–Water, Water and Triethylene Glycol. *J. Chem. Thermodyn.* **2020**, *151*, 1–10.

(17) Pandey, D.; Mondal, M. K. Equilibrium CO2 Solubility in the Aqueous Mixture of MAE and AEEA: Experimental Study and Development of Modified Thermodynamic Model. *Fluid Phase Equilib.* **2020**, *522*, 1–11.

(18) Ayittey, F. K.; Saptoro, A.; Kumar, P.; Wong, M. K. Energy-Saving Process Configurations for Monoethanolamine-Based CO2 Capture System. *Asia-Pacific J.*

Chem. Eng. **2020**, No. February, 1–15.

(19) Hartono, A.; Ahmad, R.; Usman, M.; Asif, N.; Svendsen, H. F. Solubility of CO2 in 0.1M, 1M and 3M of 2-Amino-2-Methyl-1-Propanol (AMP) from 313 to 393K and Model Representation Using the ENRTL Framework. *Fluid Phase Equilib.* **2020**, *511, 1*–53.

(20) Liu, X.; Gao, B.; Jiang, Y.; Ai, N.; Deng, D. Solubilities and Thermodynamic Properties of Carbon Dioxide in Guaiacol-Based Deep Eutectic Solvents. *J. Chem. Eng. Data* **2017**, *62*, 1448–1455.

(21) Haider, M. B.; Jha, D.; Marriyappan Sivagnanam, B.; Kumar, R. Thermodynamic and Kinetic Studies of CO2 Capture by Glycol and Amine-Based Deep Eutectic Solvents. *J. Chem. Eng. Data* **2018**, *63*, 2671–2680.

(22) Leron, R. B.; Li, M. H. Solubility of Carbon Dioxide in a Eutectic Mixture of Choline Chloride and Glycerol at Moderate Pressures. *J. Chem. Thermodyn.* **2013**, *57*, 131–136.

(23) Lu, M.; Han, G.; Jiang, Y.; Zhang, X.; Deng, D.; Ai, N. Solubilities of Carbon Dioxide in the Eutectic Mixture of Levulinic Acid (or Furfuryl Alcohol) and Choline Chloride. *J. Chem. Thermodyn.* **2015**, *88*, 72–77.

(24) Zubeir, L. F.; Lacroix, M. H. M.; Kroon, M. C. Low Transition Temperature Mixtures as Innovative and Sustainable CO2 Capture Solvents. *J. Phys. Chem. B* **2014**, *118* (49), 14429–14441.

(25) Deng, D.; Jiang, Y.; Liu, X.; Zhang, Z.; Ai, N. Investigation of Solubilities of Carbon Dioxide in Five Levulinic Acid-Based Deep Eutectic Solvents and Their Thermodynamic Properties. *J. Chem. Thermodyn.* **2016**, *103*, 212–217.

(26) Jacquemin, J.; Costa Gomes, M. F.; Husson, P.; Majer, V. Solubility of Carbon Dioxide, Ethane, Methane, Oxygen, Nitrogen, Hydrogen, Argon, and Carbon Monoxide

in 1-Butyl-3-Methylimidazolium Tetrafluoroborate between Temperatures 283 K and 343 K and at Pressures Close to Atmospheric. *J. Chem. Thermodyn.* **2006**, *38*, 490–502.

(27) Jacquemin, J.; Husson, P.; Majer, V.; Gomes, M. F. C. Low-Pressure Solubilities and Thermodynamics of Solvation of Eight Gases in 1-Butyl-3-Methylimidazolium Hexafluorophosphate. *Fluid Phase Equilib.* **2006**, *240*, 87–95.

(28) Martins, M. A. R.; Sharma, G.; Pinho, S. P.; Gardas, R. L.; Coutinho, J. A. P.; Carvalho, P. J. Selection and Characterization of Non-Ideal Ionic Liquids Mixtures to Be Used in CO2 Capture. *Fluid Phase Equilib.* **2020**, *518, 1*–13.

(29) Yim, J. H.; Oh, B. K.; Lim, J. S. Solubility Measurement and Correlation of CO2in Bis(Pentafluoroethylsulfonyl)Imide ([BETI]) Anion-Based Ionic Liquids: [EMIM][BETI], [BMIM][BETI], [HMIM][BETI]. *J. Chem. Eng. Data* **2020**, *65*, 4378–4386.

(30) Sohaib, Q.; Vadillo, J. M.; Gómez-Coma, L.; Albo, J.; Druon-Bocquet, S.; Irabien, A.; Sanchez-Marcano, J. CO2 Capture with Room Temperature Ionic Liquids; Coupled Absorption/Desorption and Single Module Absorption in Membrane Contactor. *Chem. Eng. Sci.* **2020**, *223*, 1–11.

(31) Aghaie, M.; Zendehboudi, S. Estimation of CO2 Solubility in Ionic Liquids Using Connectionist Tools Based on Thermodynamic and Structural Characteristics. *Fuel* **2020**, *279*, 1–11.

(32) Ramdin, M.; De Loos, T. W.; Vlugt, T. J. H. State-of-the-Art of CO 2 Capture with Ionic Liquids. *Ind. Eng. Chem. Res.* **2012**, *51* (24), 8149–8177.

(33) Bates, E. D.; Mayton, R. D.; Ntai, I.; Davis, J. H. CO2 Capture by a Task-Specific Ionic Liquid. *J. Am. Chem. Soc.* **2002**, *124* (6), 926–927.

(34) Ullah, R.; Atilhan, M.; Anaya, B.; Khraisheh, M.; García, G.; Elkhattat, A.; Tariq, M.; Aparicio, S. A Detailed Study of Cholinium Chloride and Levulinic Acid Deep

Eutectic Solvent System for CO2capture via Experimental and Molecular Simulation Approaches. *Phys. Chem. Chem. Phys.* **2015**, *17*, 20941–20960.

(35) Chen, Y.; Ai, N.; Li, G.; Shan, H.; Cui, Y.; Deng, D. Solubilities of Carbon Dioxide in Eutectic Mixtures of Choline Chloride and Dihydric Alcohols. *J. Chem. Eng. Data* **2014**, *59*, 1247–1253.

(36) Hansen, B. B.; Spittle, S.; Chen, B.; Poe, D.; Zhang, Y.; Klein, J. M.; Horton, A.; Adhikari, L.; Zelovich, T.; Doherty, B. W.; Gurkan, B.; Maginn, E. J.; Ragauskas, A.; Dadmun, M.; Zawodzinski, T. A.; Baker, G. A.; Tuckerman, M. E.; Savinell, R. F.; Sangoro, J. R. Deep Eutectic Solvents: A Review of Fundamentals and Applications. *Chem. Rev.* **2021**, *121*, 1232–1285.

(37) Sarmad, S.; Nikjoo, D.; Mikkola, J. P. Amine Functionalized Deep Eutectic Solvent for CO2 Capture: Measurements and Modeling. *J. Mol. Liq.* **2020**, *309*, 1–11.

(38) Song, Z.; Song, Z.; Hu, X.; Wu, H.; Mei, M.; Linke, S.; Zhou, T.; Zhou, T.; Qi, Z.; Sundmacher, K.; Sundmacher, K. Systematic Screening of Deep Eutectic Solvents as Sustainable Separation Media Exemplified by the CO2 Capture Process. *ACS Sustain. Chem. Eng.* **2020**, *8*, 8741–8751.

(39) Smith, E. L.; Abbott, A. P.; Ryder, K. S. Deep Eutectic Solvents (DESs) and Their Applications. *Chem. Rev.* **2014**, *114*, 11060–11082.

(40) Martins, M. A. R.; Pinho, S. P.; Coutinho, J. A. P. Insights into the Nature of Eutectic and Deep Eutectic Mixtures. *J. Solution Chem.* **2018**, 1–3.

(41) Leron, R. B.; Caparanga, A.; Li, M. H. Carbon Dioxide Solubility in a Deep Eutectic Solvent Based on Choline Chloride and Urea at T = 303.15-343.15K and Moderate Pressures. *J. Taiwan Inst. Chem. Eng.* **2013**, *44*, 879–885.

(42) Leron, R. B.; Li, M. H. Solubility of Carbon Dioxide in a Choline Chloride-Ethylene Glycol Based Deep Eutectic Solvent. *Thermochim. Acta* **2013**, *551*, 14–19.

(43) Ali, E.; Hadj-Kali, M. K.; Mulyono, S.; Alnashef, I.; Fakeeha, A.; Mjalli, F.; Hayyan, A. Solubility of CO2 in Deep Eutectic Solvents: Experiments and Modelling Using the Peng-Robinson Equation of State. *Chem. Eng. Res. Des.* **2014**, *92*, 1898–1906.

(44) Altamash, T.; Amhamed, A. I.; Aparicio, S.; Atilhan, M. Combined Experimental and Theoretical Study on High Pressure Methane Solubility in Natural Deep Eutectic Solvents. *Ind. Eng. Chem. Res.* **2019**, *58*, 8097–8111.

(45) Haider, M. B.; Kumar, R. Solubility of CO2 and CH4 in Sterically Hindered Amine-Based Deep Eutectic Solvents. *Sep. Purif. Technol.* **2020**, *248*, 1–11.

(46) Yang, D.; Hou, M.; Ning, H.; Zhang, J.; Ma, J.; Yang, G.; Han, B. Efficient SO2 Absorption by Renewable Choline Chloride–Glycerol Deep Eutectic Solvents. *Green Chem.* **2013**, *15*, 2261–2265.

(47) Sun, S.; Niu, Y.; Xu, Q.; Sun, Z.; Wei, X. Efficient SO2 Absorptions by Four Kinds of Deep Eutectic Solvents Based on Choline Chloride. *Ind. Eng. Chem. Res.* **2015**, *54*, 8019–8024.

(48) Chen, Y.; Jiang, B.; Dou, H.; Zhang, L.; Tantai, X.; Sun, Y. Highly Efficient and Reversible Capture of Low Partial Pressure SO2 by Functional Deep Eutectic Solvents. *Energy & Fuels* **2018**, *32*, 10737–10744.

(49) Li, X.; Hou, M.; Han, B.; Wang, X.; Zou, L. Solubility of CO2 in a Choline Chloride + Urea Eutectic Mixture. *J. Chem. Eng. Data* **2008**, *53*, 548–550.

(50) Anthony, J. L.; Maginn, E. J.; Brennecke, J. F. Gas Solubilities in 1-n-Butyl-3-Methylimidazolium Hexafluorophosphate. *Am. Chem. Soc.* **2002**, *818*, 260–269.

(51) Ramdin, M.; Balaji, S. P.; Vicent-Luna, J. M.; Gutiérrez-Sevillano, J. J.; Calero, S.; De Loos, T. W.; Vlugt, T. J. H. Solubility of the Precombustion Gases CO2, CH4, CO, H2, N2, and H2S in the Ionic Liquid [Bmim][Tf2N] from Monte Carlo Simulations.

J. Phys. Chem. C **2014**, *118*, 23599–23604.

(52) Zubeir, L. F.; Romanos, G. E.; Weggemans, W. M. A.; Iliev, B.; Schubert, T. J. S.; Kroon, M. C. Solubility and Diffusivity of CO2 in the Ionic Liquid 1-Butyl-3-Methylimidazolium Tricyanomethanide within a Large Pressure Range (0.01 MPa to 10 MPa). *J. Chem. Eng. Data* **2015**, *60*, 1544–1562.

(53) Zhang, S.; Chen, Y.; Ren, R. X. F.; Zhang, Y.; Zhang, J.; Zhang, X. Solubility of CO2 in Sulfonate Ionic Liquids at High Pressure. *J. Chem. Eng. Data* **2005**, *50*, 230–233.

(54) Althuluth, M.; Kroon, M. C.; Peters, C. J. High Pressure Solubility of Methane in the Ionic Liquid 1-Hexyl-3-Methylimidazolium Tricyanomethanide. *J. Supercrit. Fluids* **2017**, *128*, 145–148.

(55) Stevanovic, S.; Costa Gomes, M. F. Solubility of Carbon Dioxide, Nitrous Oxide, Ethane, and Nitrogen in 1-Butyl-1-Methylpyrrolidinium and Trihexyl(Tetradecyl)Phosphonium Tris(Pentafluoroethyl)Trifluorophosphate (EFAP) Ionic Liquids. *J. Chem. Thermodyn.* **2013**, *59*, 65–71.

(56) Soriano, A. N.; Doma, B. T.; Li, M. H. Solubility of Carbon Dioxide in 1-Ethyl-3-Methylimidazolium Tetrafluoroborate. *J. Chem. Eng. Data* **2008**, *53*, 2550–2555.

(57) Feng, Z.; Jing-Wen, M.; Zheng, Z.; You-Ting, W.; Zhi-Bing, Z. Study on the Absorption of Carbon Dioxide in High Concentrated MDEA and ILs Solutions. *Chem. Eng. J.* **2012**, *181–182*, 222–228.

(58) Jacquemin, J.; Husson, P.; Padua, A. A. H.; Majer, V. Density and Viscosity of Several Pure and Water-Saturated Ionic Liquids. *Green Chem.* **2006**, *8*, 172–180.

(59) Gurkan, B. E.; Fuente, J. C. De; Mindrup, E. M.; Ficke, L. E.; Goodrich, B. F.; Price, E. A.; Schneider, W. F.; Brennecke, J. F. Equimolar CO2 Absorption by Anion-Functionalized Ionic Liquids. *J. Am. Chem. Soc.* **2010**, *132*, 2116–2117.

(60) Luo, X. Y.; Fan, X.; Shi, G. L.; Li, H. R.; Wang, C. M. Decreasing the Viscosity in CO2 Capture by Amino-Functionalized Ionic Liquids through the Formation of Intramolecular Hydrogen Bond. *J. Phys. Chem. B* **2016**, *120*, 2807–2813.

(61) Schaeffer, N.; Martins, M. A. R.; Neves, C. M. S. S.; Pinho, S. P.; Coutinho, J. A. P. Sustainable Hydrophobic Terpene-Based Eutectic Solvents for the Extraction and Separation of Metals. *Chem. Commun.* **2018**, *54*, 8104–8107.

(62) Van Osch, D. J. G. P.; Parmentier, D.; Dietz, C. H. J. T.; Van Den Bruinhorst, A.; Tuinier, R.; Kroon, M. C. Removal of Alkali and Transition Metal Ions from Water with Hydrophobic Deep Eutectic Solvents. *Chem. Commun.* **2016**, *52*, 11987–11990.

(63) Wojeicchowski, J. P.; Marques, C.; Igarashi-Mafra, L.; Coutinho, J. A. P.; Mafra, M. R. Extraction of Phenolic Compounds from Rosemary Using Choline Chloride – Based Deep Eutectic Solvents. *Sep. Purif. Technol.* **2021**, *258*, 1–8.

(64) Shahbaz, K.; Baroutian, S.; Mjalli, F. S.; Hashim, M. A.; Alnashef, I. M. Densities of Ammonium and Phosphonium Based Deep Eutectic Solvents: Prediction Using Artificial Intelligence and Group Contribution Techniques. *Thermochim. Acta* **2012**, *527*, 59–66.

(65) Lin, C. M.; Leron, R. B.; Caparanga, A. R.; Li, M. H. Henry's Constant of Carbon Dioxide-Aqueous Deep Eutectic Solvent (Choline Chloride/Ethylene Glycol, Choline Chloride/Glycerol, Choline Chloride/Malonic Acid) Systems. *J. Chem. Thermodyn.* **2014**, *68*, 216–220.

(66) Luo, X.; Guo, Y.; Ding, F.; Zhao, H.; Cui, G.; Li, H.; Wang, C. Significant Improvements in CO2 Capture by Pyridine-Containing Anion-Functionalized Ionic Liquids through Multiple-Site Cooperative Interactions. *Angew. Chemie - Int. Ed.* **2014**, *53*, 7053–7057.

(67) Alkhatib, I. I. I.; Ferreira, M. L.; Alba, C. G.; Bahamon, D.; Llovell, F.; Pereiro, A.

B.; Araújo, J. M. M.; Abu-Zahra, M. R. M.; Vega, L. F. Screening of Ionic Liquids and Deep Eutectic Solvents for Physical CO2 Absorption by Soft-SAFT Using Key Performance Indicators. *J. Chem. Eng. Data* **2020**, *65*, 5844–5861.

(68) Li, X.; Hou, M.; Han, B.; Wang, X.; Zou, L. Solubility of CO2 in a Choline Chloride + Urea Eutectic Mixture. *J. Chem. Eng. Data* **2008**, *53*, 548–550.

(69) Liu, F.; Chen, W.; Mi, J.; Zhang, J. Y.; Kan, X.; Zhong, F. Y.; Huang, K.; Zheng, A. M.; Jiang, L. Thermodynamic and Molecular Insights into the Absorption of H2S, CO2 , and CH4 in Choline Chloride plus Urea Mixtures. *AIChE J.* **2019**, *65*, 1–10.

(70) Mirza, N. R.; Nicholas, N. J.; Wu, Y.; Mumford, K. A.; Kentish, S. E.; Stevens, G. W. Experiments and Thermodynamic Modeling of the Solubility of Carbon Dioxide in Three Different Deep Eutectic Solvents (DESs). *J. Chem. Eng. Data* **2015**, *60*, 3246–3252.

(71) Martins, M. A. R.; Pinho, S. P.; Coutinho, J. A. P. Insights into the Nature of Eutectic and Deep Eutectic Mixtures. *J. Solution Chem.* **2018**, 1–21.

(72) Abbott, A. P.; Capper, G.; Davies, D. L.; Rasheed, R. K.; Tambyrajah, V. Novel Solvent Properties of Choline Chloride / Urea Mixtures. *R. Soc. Chem.* **2003**, *1*, 70–71.

(73) Li, X.; Kersten, S. R. A.; Schuur, B. Extraction of Guaiacol from Model Pyrolytic Sugar Stream with Ionic Liquids. *Ind. Eng. Chem. Res.* **2016**, *55*, 4703–4710.

(74) Silva, L. P.; Martins, M. A. R.; Conceição, J. H. F.; Pinho, S. P.; Coutinho, J. A. P. Eutectic Mixtures Based on Polyalcohols as Sustainable Solvents: Screening and Characterization. *ACS Sustain. Chem. Eng.* **2020**, 15317-15326.

(75) Dawson, R. M. C. .; Elliott, D. C. .; Elliott, W. H. .; Jones, K. M. *Data for Biochemical Research*; Oxford University Press: Oxford, 1986.

(76) Hodgman, C. .; Lange, N. *Handbook of Chemistry and Physics*; Chemical

Rubber Publishing Company: Cleveland, 1951.

(77) Keyes, D. B. Handbook of Chemistry and Physics. Twelfth Edition (Hodgman, Charles D.; Lange, Norbert A.). *J. Chem. Educ.* **1928**, *5*, 241.

(78) Wood, E. Data for Biochemical Research (Third Edition). *Biochem. Educ.* **1987**, *15*, 97.

(79) Anderson, J. L.; Dixon, J. K.; Brennecke, J. F. Solubility of CO2, CH4, C2H6, C2H4, O2, and N2 in 1-Hexyl-3-Methylpyridinium Bis(Trifluoromethylsulfonyl)Imide: Comparison to Other Ionic Liquids. *Acc. Chem. Res.* **2007**, *40*, 1208–1216.

(80) Li, Y.; Huang, W.; Zheng, D.; Mi, Y.; Dong, L. Solubilities of CO2 Capture Absorbents 2-Ethoxyethyl Ether, 2-Butoxyethyl Acetate and 2-(2-Ethoxyethoxy)Ethyl Acetate. *Fluid Phase Equilib.* **2014**, *370*, 1–7.

(81) Liu, X.; Gao, B.; Deng, D. SO2 Absorption/Desorption Performance of Renewable Phenol-Based Deep Eutectic Solvents. *Sep. Sci. Technol.* **2018**, *53*, 2150–2158.

(82) Shukla, S. K.; Mikkola, J. P. Intermolecular Interactions upon Carbon Dioxide Capture in Deep-Eutectic Solvents. *Phys. Chem. Chem. Phys.* **2018**, *20*, 24591–24601.

(83) Kumar, P. P.; Paramashivappa, R.; Vithayathil, P. J.; Rao, P. V. S.; Rao, A. S. Process for Isolation of Cardanol from Technical Cashew (Anacardium Occidentale l.) Nut Shell Liquid. *J. Agric. Food Chem.* **2002**, *50*, 4705–4708.

(84) Ji, Y.; Hou, Y.; Ren, S.; Yao, C.; Wu, W. Phase Equilibria of High Pressure CO2 and Deep Eutectic Solvents Formed by Quaternary Ammonium Salts and Phenol. *Fluid Phase Equilib.* **2016**, *429*, 14–20.

(85) Deng, D.; Jiang, Y.; Liu, X.; Zhang, Z.; Ai, N. Investigation of Solubilities of Carbon Dioxide in Five Levulinic Acid-Based Deep Eutectic Solvents and Their

Thermodynamic Properties. *J. Chem. Thermodyn.* **2016**, *103*, 212–217.

(86) Wang, J.; Cheng, H.; Song, Z.; Chen, L.; Deng, L.; Qi, Z. Carbon Dioxide Solubility in Phosphonium-Based Deep Eutectic Solvents: An Experimental and Molecular Dynamics Study. *Ind. Eng. Chem. Res.* **2019**, *58*, 17514–17523.

(87) Gu, Y.; Hou, Y.; Ren, S.; Sun, Y.; Wu, W. Hydrophobic Functional Deep Eutectic Solvents Used for Efficient and Reversible Capture of CO2. *ACS Omega* **2020**, *5*, 6809–6816.

(88) Van Osch, D. J. G. P.; Zubeir, L. F.; Van Den Bruinhorst, A.; Rocha, M. A. A.; Kroon, M. C. Hydrophobic Deep Eutectic Solvents as Water-Immiscible Extractants. *Green Chem.* **2015**, *17*, 4518–4521.

(89) Ribeiro, B. D.; Florindo, C.; Iff, L. C.; Coelho, M. A. Z.; Marrucho, I. M. Menthol-Based Eutectic Mixtures: Hydrophobic Low Viscosity Solvents. *ACS Sustain. Chem. Eng.* **2015**, *3*, 2469–2477.

(90) Zubeir, L. F.; Van Osch, D. J. G. P.; Rocha, M. A. A.; Banat, F.; Kroon, M. C. Carbon Dioxide Solubilities in Decanoic Acid-Based Hydrophobic Deep Eutectic Solvents. *J. Chem. Eng. Data* **2018**, *63*, 913–919.

(91) Sun, C.; Wang, S.; Zhou, S.; Chen, C. SO2 Effect on Monoethanolamine Oxidative Degradation in CO2 Capture Process. *Int. J. Greenh. Gas Control* **2014**, *23*, 98–104.

(92) Malik, A.; Dhattarwal, H. S.; Kashyap, H. K. Distinct Solvation Structures of CO2and SO2 in Reline and Ethaline Deep Eutectic Solvents Revealed by AIMD Simulations. *J. Phys. Chem. B* **2021**, *125*, 1852–1860.

(93) Hirshfeld, F. L. Bonded-Atom Fragments for Describing Molecular Charge Densities. *Theor. Chim. Acta* **1977**, *44*, 129–138.

(94) R. S. Mulliken. Electronic Population Analysis on LCAO-MO Molecular Wave

Functions. I. *J. Chem. Phys* **1955**, *23*, 1833–1840.

(95) Alioui, O.; Benguerba, Y.; Alnashef, I. M. Investigation of the CO2-Solubility in Deep Eutectic Solvents Using COSMO-RS and Molecular Dynamics Methods. *J. Mol. Liq.* **2020**, *307*, 1–9.

(96) Haghbakhsh, R.; Raeissi, S. Modeling the Phase Behavior of Carbon Dioxide Solubility in Deep Eutectic Solvents with the Cubic Plus Association Equation of State. *J. Chem. Eng. Data* **2018**, *63*, 897–906.

(97) Haider, M. B.; Jha, D.; Marriyappan Sivagnanam, B.; Kumar, R. Modelling and Simulation of CO2 Removal from Shale Gas Using Deep Eutectic Solvents. *J. Environ. Chem. Eng.* **2019**, *7*, 1–9.

(98) Zubeir, L. F.; Held, C.; Sadowski, G.; Kroon, M. C. PC-SAFT Modeling of CO2 Solubilities in Deep Eutectic Solvents. *J. Phys. Chem. B* **2016**, *120*, 2300–2310.

(99) Dietz, C. H. J. T.; van Osch, D. J. G. P.; Kroon, M. C.; Sadowski, G.; van Sint Annaland, M.; Gallucci, F.; Zubeir, L. F.; Held, C. PC-SAFT Modeling of CO2 Solubilities in Hydrophobic Deep Eutectic Solvents. *Fluid Phase Equilib.* **2017**, *448*, 94–98.

(100) Kamgar, A.; Mohsenpour, S.; Esmaeilzadeh, F. Solubility Prediction of CO2, CH4, H2, CO and N2 in Choline Chloride/Urea as a Eutectic Solvent Using NRTL and COSMO-RS Models. *J. Mol. Liq.* **2017**, *247*, 70–74.

(101) Salehi, H. S.; Hens, R.; Moultos, O. A.; Vlugt, T. J. H. Computation of Gas Solubilities in Choline Chloride Urea and Choline Chloride Ethylene Glycol Deep Eutectic Solvents Using Monte Carlo Simulations. *J. Mol. Liq.* **2020**, *316*, 1–10.

(102) Zubeir, L. F.; Held, C.; Sadowski, G.; Kroon, M. C. PC-SAFT Modeling of CO2 Solubilities in Deep Eutectic Solvents. *J. Phys. Chem. B* **2016**, *120*, 2300–2310.

(103) Haghbakhsh, R.; Keshtkar, M.; Shariati, A.; Raeissi, S. Experimental

Investigation of Carbon Dioxide Solubility in the Deep Eutectic Solvent (1 ChCl + 3 Triethylene Glycol) and Modeling by the CPA EoS. *J. Mol. Liq.* **2021**, *330*, 1–12.

(104) Salleh, Z.; Wazeer, I.; Mulyono, S.; El-blidi, L.; Hashim, M. A.; Hadj-Kali, M. K. Efficient Removal of Benzene from Cyclohexane-Benzene Mixtures Using Deep Eutectic Solvents – COSMO-RS Screening and Experimental Validation. *J. Chem. Thermodyn.* **2017**, *104*, 33–44.

(105) Lydersen, A. L. *Estimation of Critical Properties of Organic Compounds by the Method of Group Contibutions*; Madison, 1955.

(106) Joback, K. G.; Reid, R. C. Estimation of Pure-Component Properties from Group-Contributions. *Chem. Eng. Commun.* **1987**, *57*, 233–243.

Supporting Information

1. Gas solubility in DESs – Measurements

Table S1. CO_2 solubility in several DESs found in the literature from 2008 to 2021.

HBA	HBD	Molar ratio	Solubility (x_1^*)	T (K)	P(bar)	Henry's constant (MPa)	Reference
ChCl	Urea	1:1.5	0.033 – 0.201	313.15 – 333.15	8.50 – 125.20	18.50 – 28.70	Li et al. (2008) [1]
ChCl	Urea	1:2	0.051 – 0.309	313.15 – 333.15	10.00 – 127.30	12.30 – 18.20	Li et al. (2008) [1]
ChCl	Urea	1:2.5	0.032 – 0.203	313.15 – 333.15	10.60 – 125.50	22.40 – 29.00	Li et al. (2008) [1]
ChCl	Urea	1:2	0.013 – 0.308	303.15 – 343.15	2.99 – 59.11	1.05 – 2.34	Leron et al. (2013) [2]
ChCl	Ethylene glycol	1:2	0.006 – 0.275	303.15 – 343.15	2.36 – 63.23	2.14 – 5.28	Leron; Li (2013a) [3]
ChCl	Glycerol	1:2	0.006 – 0.398	303.15 – 343.15	1.87 – 63.47	1.30 – 3.72	Leron; Li (2013b) [4]
ChCl	Tri Ethylene Glycol	1:4	0.042	298.15	10.00	23.81	Ali et al. (2014) [5]
ChCl	Ethylene glycol	1:4	0.023	298.15	10.00	43.48	Ali et al. (2014) [5]
ChCl	Ethylene glycol	1:8	0.026	298.15	10.00	38.46	Ali et al. (2014) [5]
ChCl	Urea	1:4	0.024	298.15	10.00	41.67	Ali et al. (2014) [5]
ChCl	Urea	1:2.5	0.021	298.15	10.00	47.62	Ali et al. (2014) [5]
ChCl	Glycerol	1:3	0.045	298.15	10.00	22.22	Ali et al. (2014) [5]
ChCl	Glycerol	1:8	0.031	298.15	10.00	32.26	Ali et al. (2014) [5]
ChCl	Ethanol Amine	1:6	0.109	298.15	10.00	9.17	Ali et al. (2014) [5]
ChCl	Diethanol Amine	1:6	0.092	298.15	10.00	10.87	Ali et al. (2014) [5]
BTPC	Glycerol	1:12	0.051	298.15	10.00	19.61	Ali et al. (2014) [5]
BTPB	Ethylene glycol	1:12	0.050	298.15	10.00	20.00	Ali et al. (2014) [5]
MTPB	Ethanol amine	1:6	0.144	298.15	10.00	6.94	Ali et al. (2014) [5]
MTPB	Ethanol amine	1:7	0.125	298.15	10.00	8.00	Ali et al. (2014) [5]
MTPB	Ethanol amine	1:8	0.119	298.15	10.00	8.40	Ali et al. (2014) [5]
TBAB	Ethanol amine	1:6	0.117	298.15	10.00	8.55	Ali et al. (2014) [5]
TBAB	Diethanol amine	1:6	0.104	298.15	10.00	9.62	Ali et al. (2014) [5]
TBAB	Triethanol amine	1:3	0.083	298.15	10.00	12.05	Ali et al. (2014) [5]

HBA	HBD	Molar ratio	Solubility (x_1^*)	T (K)	P(bar)	Henry's constant (MPa)	Reference
ChCl	1,4-butanediol	1:3	0.002 – 0.016	293.15 – 323.15	1.11 – 5.26	30.49 – 49.81	Chen et al. (2014) [6]
ChCl	1,4-butanediol	1:4	0.002 – 0.015	293.15 – 323.15	1.06 – 5.19	32.82 – 51.84	Chen et al. (2014) [6]
ChCl	2,3-butanediol	1:3	0.003 – 0.015	293.15 – 323.15	1.07 – 5.29	33.22 – 44.30	Chen et al. (2014) [6]
ChCl	2,3-butanediol	1:4	0.003 – 0.019	293.15 – 323.15	1.07 – 5.12	26.84 – 39.19	Chen et al. (2014) [6]
ChCl	1,2-propanediol	1:3	0.002 – 0.016	293.15 – 323.15	1.08 – 5.24	30.68 – 55.08	Chen et al. (2014) [6]
ChCl	1,2-propanediol	1:4	0.002 – 0.016	293.15 – 323.15	1.04 – 5.26	30.59 – 59.42	Chen et al. (2014) [6]
ChCl	Phenol	1:2	0.002 – 0.021	293.15 – 323.15	0.99 – 5.20	2.59 – 4.96	Li et al. (2014) [7]
ChCl	Phenol	1:3	0.003 – 0.021	293.15 – 323.15	1.01 – 5.14	2.51 – 4.10	Li et al. (2014) [7]
ChCl	Phenol	1:4	0.003 – 0.021	293.15 – 323.15	1.08 – 5.29	2.48 – 4.09	Li et al. (2014) [7]
ChCl	Diethylene Glycol	1:3	0.003 – 0.019	293.15 – 323.15	1.13 – 5.18	3.12 – 5.18	Li et al. (2014) [7]
ChCl	Diethylene Glycol	1:4	0.002 – 0.021	293.15 – 323.15	1.10 – 5.27	2.80 – 4.96	Li et al. (2014) [7]
ChCl	Triethylene Glycol	1:3	0.003 – 0.027	293.15 – 323.15	1.09 – 5.16	2.71 – 4.70	Li et al. (2014) [7]
ChCl	Triethylene Glycol	1:4	0.003 – 0.028	293.15 – 323.15	1.09 – 5.20	2.69 – 4.64	Li et al. (2014) [7]
ChCl	Levulinic Acid	1:3	0.002 – 0.030	303.15 – 333.15	0.79 – 5.83	2.20 – 3.74	Lu et al. (2015) [8]
ChCl	Levulinic Acid	1:4	0.002 – 0.032	303.15 – 333.15	0.72 – 5.87	2.09 – 3.67	Lu et al. (2015) [8]
ChCl	Levulinic Acid	1:5	0.003 – 0.033	303.15 – 333.15	0.72 – 5.81	1.93 – 3.36	Lu et al. (2015) [8]
ChCl	Furfuryl Alcohol	1:3	0.002 – 0.020	303.15 – 333.15	0.81 – 5.86	3.05 – 4.79	Lu et al. (2015) [8]
ChCl	Furfuryl Alcohol	1:4	0.002 – 0.023	303.15 – 333.15	0.82 – 5.85	2.58 – 4.15	Lu et al. (2015) [8]
ChCl	Furfuryl Alcohol	1:5	0.002 – 0.023	303.15 – 333.15	0.77 – 5.77	2.50 – 3.81	Lu et al. (2015) [8]
ChCl	Urea	1:2	0.0009 – 0.004	309 - 329	0.40 – 1.53	38.25 – 44.44	Mirza et al. (2015) [9]
ChCl	Ethylene Glycol	1:2	0.0007 – 0.003	309 - 329	0.47 – 1.54	51.33 – 67.14	Mirza et al. (2015) [9]
ChCl	Phenol	1:2	0.070 – 0.275	313.15 – 333.15	17.10 – 133.00	24.42 – 48.36	Ji et al. (2016) [10]
ChCl	Phenol	1:3	0.086 – 0.274	313.15	19.10 – 118.20	43.78	Ji et al. (2016) [10]
ChCl	Phenol	1:4	0.087 – 0.293	313.15	21.00 – 121.70	41.54	Ji et al. (2016) [10]
TMAC	Phenol	1:3	0.094 – 0.262	313.15	23.60 – 121.70	46.45	Ji et al. (2016) [10]

HBA	HBD	Molar ratio	Solubility (x_1^*)	T (K)	P(bar)	Henry's constant (MPa)	Reference
TEAC	Phenol	1:3	0.075 – 0.233	313.15	21.20 – 111.70	47.94	Ji et al. (2016) [10]
ACC	Levulinic Acid	1:3	0.003 – 0.031	303.15 – 333.15	0.66 – 5.72	13.92 – 27.72	Deng et al. (2016) [11]
TEAC	Levulinic Acid	1:3	0.004 – 0.028	303.15 – 333.15	0.66 – 5.83	16.30 – 27.17	Deng et al. (2016) [11]
TEAB	Levulinic Acid	1:3	0.033 – 0.028	303.15 – 333.15	0.69 – 5.88	17.35 – 28.66	Deng et al. (2016) [11]
TBAC	Levulinic Acid	1:3	0.005 – 0.040	303.15 – 333.15	0.63 – 5.90	12.30 – 20.96	Deng et al. (2016) [11]
TBAB	Levulinic Acid	1:3	0.006 – 0.037	303.15 – 333.15	0.70 – 5.86	13.00 – 21.19	Deng et al. (2016) [11]
ChCl	Guaiacol	1:3	0.001 – 0.021	293.15 – 323.15	0.51 – 5.36	24.94 – 41.60	Liu et al. (2017) [12]
ChCl	Guaiacol	1:4	0.001 – 0.022	293.15 – 323.15	0.52 – 5 43	23.90 – 37.66	Liu et al. (2017) [12]
ChCl	Guaiacol	1:5	0.001 – 0.023	293.15 – 323.15	0.53 – 5.39	22.71 – 35.88	Liu et al. (2017) [12]
DH	Guaiacol	1:3	0.002 – 0.025	293.15 – 323.15	0.45 – 5.29	20.79 – 31.18	Liu et al. (2017) [12]
DH	Guaiacol	1:4	0.002 – 0.026	293.15 – 323.15	0.49 – 5.51	20.07 – 29.97	Liu et al. (2017) [12]
DH	Guaiacol	1:5	0.002 – 0.027	293.15 – 323.15	0.54 – 5.35	18.69 – 28.34	Liu et al. (2017) [12]
ACC	Guaiacol	1:3	0.002 – 0.026	293.15 – 323.15	0.54 – 5.35	20.75 – 32.44	Liu et al. (2017) [12]
ACC	Guaiacol	1:4	0.002 – 0.025	293.15 – 323.15	0.55 – 5.59	20.69 – 31.04	Liu et al. (2017) [12]
ACC	Guaiacol	1:5	0.002 – 0.026	293.15 – 323.15	0.49 – 5.36	20.43 – 30.09	Liu et al. (2017) [12]
ChCl	Ethylene Glycol	1:2	0.026 – 0.052	303.15	6.44 – 12.46	24.77	Haider et al. (2018) [13]
ChCl	Diethylene Glycol	1:3	0.018 – 0.035	303.15	5.64 – 11.12	31.77	Haider et al. (2018) [13]
ChCl	Diethylene Glycol	1:4	0.017 – 0.036	303.15	5.24 – 11.20	31.11	Haider et al. (2018) [13]
ChCl	Methyldiethanol Amine	1:6	0.106 – 0.156	303.15	4.46 – 10.96	7.03	Haider et al. (2018) [13]
ChCl	Methyldiethanol Amine	1:7	0.119 – 0.199	303.15	5.94 – 10.34	5.20	Haider et al. (2018) [13]
ChCl	Diethanol Amine	1:6	0.032 – 0.090	303.15	6.64 – 9.71	20.75	Haider et al. (2018) [13]
TBAB	Ethylene Glycol	1:2	0.015 – 0.054	303.15	4.12 – 12.79	27.47	Haider et al. (2018) [13]
TBAB	Ethylene Glycol	1:3	0.017 – 0.052	303.15	5.02 – 12.49	29.53	Haider et al. (2018) [13]
TBAB	Ethylene Glycol	1:4	0.019 – 0.050	303.15	5.43 – 13.74	28.58	Haider et al. (2018) [13]
TBAB	Diethylene Glycol	1:2	0.034 – 0.099	303.15	7.21 – 13.92	21.21	Haider et al. (2018) [13]

HBA	HBD	Molar ratio	Solubility (x_1^*)	T (K)	P(bar)	Henry's constant (MPa)	Reference
TBAB	Diethylene Glycol	1:3	0.038 – 0.088	303.15	6.88 – 12.05	18.11	Haider et al. (2018) [13]
TBAB	Diethylene Glycol	1:4	0.047 – 0.090	303.15	5.90 – 10.48	12.55	Haider et al. (2018) [13]
TBAB	Methyldiethanol Amine	1:3	0.086 – 0.204	303.15	4.23 – 10.00	4.92	Haider et al. (2018) [13]
TBAB	Methyldiethanol Amine	1:4	0.110 – 0.225	303.15	5.02 – 10.21	4.56	Haider et al. (2018) [13]
TBAB	Diethanol Amine	1:6	0.046 – 0.102	303.15	6.10 – 10.11	13.26	Haider et al. (2018) [13]
TBPB	Phenol	1:4	0.018 – 0.205	313,15 – 333.15	1.64 – 15.78	7.90 – 9.43	Wang et al. (2019) [14]
TBPB	Diethylene Glycol	1:4	0.017 – 0.212	313,15 – 333.15	0.94 – 13.98	6.72 – 8.29	Wang et al. (2019) [14]
ATPPB	Phenol	1:4	0.020 – 0.213	313,15 – 333.15	1.83 – 13.45	6.46 – 8.24	Wang et al. (2019) [14]
ATPPB	Phenol	1:6	0.021 – 0.195	313,15 – 333.15	1.83 – 13.87	6.99 – 8.65	Wang et al. (2019) [14]
ChCl	Ethanol Amine	1:7	0.056 – 0.286	298.15	1.82 – 20.15	2.02 – 3.25	Sarmad et al. (2020) [15]
ChCl	Ethanol Amine + Diethanol Amine	1:7:1	0.031 – 0.225	298.15	1.05 – 20.11	2.01 – 3.39	Sarmad et al. (2020) [15]
ChCl	Ethanol Amine + Methyldiethanol amine	1:7:1	0.052 – 0.259	298.15	1.78 – 20.09	2.01 – 3.42	Sarmad et al. (2020) [15]
ChCl	Ethanol Amine + Methyldiethanol amine	1:7:5	0.040 – 0.250	298.15	1.41 – 20.11	2.01 – 3.53	Sarmad et al. (2020) [15]
ChCl	Ethanol Amine + Amino ethyl piperazine	1:7:1	0.043 – 0.269	298.15	1.38 – 20.05	2.01 – 3.21	Sarmad et al. (2020) [15]
ChCl	Ethanol Amine + piperazine	1:7:1	0.065 – 0.360	298.15	1.57 – 22.37	2.24 – 2.42	Sarmad et al. (2020) [15]
ChCl	Urea	1:1.5	0.0004 – 0.010	313.15 – 353.15	0.10 – 2.04	19.50 – 40.20	Liu et al. (2019) [16]
ChCl	Urea	1:2	0.0004 – 0.016	313.15 – 353.15	0.11 – 2.02	12.30 – 25.20	Liu et al. (2019) [16]
ChCl	Urea	1:2.5	0.0003 – 0.009	313.15 – 353.15	0.10 – 2.03	21.00 – 40.20	Liu et al. (2019) [16]
ATPPB	Diethylene Glycol	1:4	0.035 – 0.541	303.15	1.60 – 19.46	4.54	Ghaedi et al. (2017) [17]
ATPPB	Diethylene Glycol	1:10	0.028 – 0.432	303.15	1.56 – 19.54	5.56	Ghaedi et al. (2017) [17]
ATPPB	Diethylene Glycol	1:16	0.024 – 0.391	303.15	1.66 – 19.54	7.13	Ghaedi et al. (2017) [17]
ATPPB	Triethylene Glycol	1:4	0.036 – 0.558	303.15	1.42 – 19.50	3.95	Ghaedi et al. (2017) [17]
ATPPB	Triethylene Glycol	1:10	0.030 – 0.450	303.15	1.49 – 19.53	5.11	Ghaedi et al. (2017) [17]

HBA	HBD	Molar ratio	Solubility (x_1*)	T (K)	P(bar)	Henry's constant (MPa)	Reference
ATPPB	Triethylene Glycol	1:16	0.023 – 0.413	303.15	1.46 – 19.57	6.48	Ghaedi et al. (2017) [17]
ACC	Imidazole	2:3	0.001 – 0.025	303.15 – 333.15	0.30 – 5.94	22.38 – 39.77	Li et al. (2018) [18]
ACC	Imidazole	1:2	0.0009 – 0.027	303.15 – 333.15	0.27 – 5.90	20.91 – 38.24	Li et al. (2018) [18]
ACC	Imidazole	1:3	0.0008 – 0.028	303.15 – 333.15	0.26 – 5.92	20.27 – 38.76	Li et al. (2018) [18]
ACC	1,2,4-triazole	1:1	0.002 – 0.027	303.15 – 333.15	0.56 – 5.93	21.69 – 37.14	Li et al. (2018) [18]
TBAB	Octanoic acid	1:2	0.352	313.15	40.00	11.36	Rabhi et al. (2021) [19]
TBAB	Decanoic acid	1:2	0.406	313.15	40.00	9.85	Rabhi et al. (2021) [19]
DL-menthol	Dodecanoic acid	2:1	0.345	313.15	40.00	11.59	Rabhi et al. (2021) [19]
TBAC	Decanoic acid	1:2	0.0086 – 0.239	298.15 – 323.15	0.90 – 19.00	7.55 – 10.71	Zubeir et al. (2018) [20]
N_{8881}−Cl	Decanoic acid	1:2	0.0112 – 0.252	298.15 – 308.15	0.90 – 19.00	7.18 – 8.27	Zubeir et al. (2018) [20]
N_{8888}−Cl	Decanoic acid	1:2	0.0117 – 0.284	298.15 – 323.15	0.90 – 19.00	6.17 – 8.42	Zubeir et al. (2018) [20]
N_{8888}−Br	Decanoic acid	1:2	0.0114 – 0.284	298.15 – 323.15	0.90 – 19.00	6.26 – 8.49	Zubeir et al. (2018) [20]
N_{8881}−Br	Decanoic acid	1:2	0.0107 – 0.257	298.15 – 323.15	0.90 – 19.00	7.15 – 9.43	Zubeir et al. (2018) [20]
[TETA]Cl-	Thymol	1:3	1.298	313.15	1.00	0.077	Gu et al. (2020) [21]
[TEPA]Cl-	Thymol	1:3	1.355	313.15	1.00	0.074	Gu et al. (2020) [21]
L-arginine	Glycerol	1:5	0.403	353.15	1.00	0.248	Ren et al. (2018) [22]
L-arginine	Glycerol	1:6	0.457	353.15	1.00	0.219	Ren et al. (2018) [22]
L-arginine	Glycerol	1:7	0.451	353.15	1.00	0.222	Ren et al. (2018) [22]
TBAB	Lauric acid + Capric acid	4:5	0.011 – 0.197	298.15 – 318.15	2.04 – 16.21	8.23 – 18.55	Haider et al. (2020) [23]
TBAB	Oleic acid + Capric acid	1:2	0.034 – 0.285	298.15 – 318.15	5.00 – 16.52	5.80 – 14.71	Haider et al. (2020) [23]
[TETA]Cl-	Ethylene Glycol	1:3	1.46	353.15	1.00	0.068	Zhang et al. (2018) [24]
[TETA]Cl-	Diethylene Glycol	1:2	1.42	353.15	1.00	0.070	Zhang et al. (2018) [24]

*$\boldsymbol{x_i}$ = molar fraction = $\frac{\frac{m_i}{MM_i}}{\frac{m_i}{MM_i}+\frac{m_j}{MM_j}}$, in which x_i is the molar ratio of component *i*, m_i is the mass of component *i*, MM_i is the molar mass of component *i*, m_j is the mass of component *j* and MM_j is the molar mass of component *j*.

Table S2. Solubility of other gases in several DESs found in the literature from 2013 to 2021.

HBA	HBD	Gas	Molar ratio	Solubility (x_1)	T (K)	P(bar)	Henry's constant (MPa)	Reference
Alanine	Lactic Acid	CH_4	1:1	0.010 – 0.372	298.15	1.00 – 50.00	13.44	Altamash et al. (2019) [25]
Betaine	Lactic Acid	CH_4	1:1	0.009 – 0.348	298.15	1.00 – 50.00	14.37	Altamash et al. (2019) [25]
ChCl	Lactic Acid	CH_4	1:1	0.011 – 0.403	298.15	1.00 – 50.00	12.41	Altamash et al. (2019) [25]
ChCl	Malonic Acid	CH_4	1:1	0.010 – 0.309	298.15	1.00 – 50.00	16.18	Altamash et al. (2019) [25]
ChCl	Phenylacetic Acid	CH_4	1:1	0.012 – 0.476	298.15	1.00 – 50.00	10.50	Altamash et al. (2019) [25]
ChCl	Urea	CH_4	1:1.5	0.00006 – 0.0008	313.15 – 353.15	0.10 – 2.03	0.22 – 0.37	Liu et al. (2019) [16]
ChCl	Urea	CH_4	1:2	0.00007 – 0.0008	313.15 – 353.15	0.13 – 2.03	0.19 – 0.31	Liu et al. (2019) [16]
ChCl	Urea	CH_4	1:2.5	0.00004 – 0.0009	313.15 – 353.15	0.11 – 2.03	0.21 – 0.34	Liu et al. (2019) [16]
ChCl	Urea	H_2S	1:1.5	0.0014 – 0.0554	313.15 – 353.15	0.10 – 2.02	3.57 – 8.58	Liu et al. (2019) [16]
ChCl	Urea	H_2S	1:2	0.0016 – 0.0464	313.15 – 353.15	0.10 – 2.02	4.28 – 8.84	Liu et al. (2019) [16]
ChCl	Urea	H_2S	1:2.5	0.0014 – 0.0351	313.15 – 353.15	0.12 – 2.01	5.57 – 11.00	Liu et al. (2019) [16]
PPZBr	Glycerol	SO_2	1:6	0.990 – 4.280	293.15	0.01 – 1.00	0.023	Cui et al. (2019) [26]
PPZBr	Glycerol	SO_2	1:5	0.960 – 4.100	293.15	0.01 – 1.00	0.024	Cui et al. (2019) [26]
PPZBr	Glycerol	SO_2	1:4	0.980 – 3.970	293.15	0.01 – 1.00	0.025	Cui et al. (2019) [26]
ChCl	Levulinc acid	SO_2	1:3	0.197 – 0.891	293.15 – 343.15	1.00	0.11 – 0.51	Deng et al. (2015) [27]
ACC	Levulinc acid	SO_2	1:3	0.256 – 0.999	293.15 – 343.15	1.00	0.10 – 0.39	Deng et al. (2015) [27]
TEAC	Levulinc acid	SO_2	1:3	0.334 – 1.215	293.15 – 343.15	1.00	0.08 – 0.30	Deng et al. (2015) [27]
TEAB	Levulinc acid	SO_2	1:3	0.345 – 1.166	293.15 – 343.15	1.00	0.09 – 0.29	Deng et al. (2015) [27]
TBAC	Levulinc acid	SO_2	1:3	0.226 – 1.052	293.15 – 343.15	1.00	0.10 – 0.44	Deng et al. (2015) [27]
TBAB	Levulinc acid	SO_2	1:3	0.391 – 1.265	293.15 – 343.15	1.00	0.08 – 0.26	Deng et al. (2015) [27]
ChCl	Ethylene Glycol	SO_2	1:2	0.980 – 2.880	293.15 – 333.15	1.00	0.035 – 0.10	Sun et al. (2015) [28]
ChCl	Malonic Acid	SO_2	1:1	0.640 – 1.880	293.15 – 333.15	1.00	0.053 – 0.16	Sun et al. (2015) [28]
ChCl	Urea	SO_2	1:2	0.690 – 1.410	293.15 – 333.15	1.00	0.071 – 0.15	Sun et al. (2015) [28]
ChCl	Thiourea	SO_2	1:1	1.320 – 2.960	293.15 – 333.15	1.00	0.034 – 0.08	Sun et al. (2015) [28]

HBA	HBD	Gas	Molar ratio	Solubility (x_1)	T (K)	P(bar)	Henry's constant (MPa)	Reference
ChCl	Glycerol	SO_2	1:1	0.288 – 1.226	293.15 – 353.15	1.00	0.082 – 0.35	Yang et al. (2013) [29]
ChCl	Glycerol	SO_2	1:2	0.155 – 0.819	293.15 – 353.15	1.00	0.12 – 0.65	Yang et al. (2013) [29]
ChCl	Glycerol	SO_2	1:3	0.107 – 0.618	293.15 – 353.15	1.00	0.16 – 0.94	Yang et al. (2013) [29]
ChCl	Glycerol	SO_2	1:4	0.087 – 0.508	293.15 – 353.15	1.00	0.20 – 1.15	Yang et al. (2013) [29]
ChCl	Guaiacol	SO_2	1:4	0.994	293.15	1.00	0.101	Liu et al. (2018) [30]
ChCl	Guaiacol	SO_2	1:5	0.948	293.15	1.00	0.105	Liu et al. (2018) [30]
ChCl	Cardanol	SO_2	1:3	0.866	293.15	1.00	0.115	Liu et al. (2018) [30]
ChCl	Cardanol	SO_2	1:4	0.776	293.15	1.00	0.129	Liu et al. (2018) [30]
ChCl	Cardanol	SO_2	1:5	0.695	293.15	1.00	0.144	Liu et al. (2018) [30]
ACC	Imidazole	SO_2	1:1.5	0.631	303.15	1.00	0.157	Deng et al. (2017) [31]
ACC	Imidazole	SO_2	1:2	0.628 – 1.629	303.15	0.10 – 1.00	0.061	Deng et al. (2017) [31]
ACC	Imidazole	SO_2	1:3	0.587	303.15	1.00	0.170	Deng et al. (2017) [31]
ACC	1,2,4-triazole	SO_2	1:1	0.444	303.15	1.00	0.225	Deng et al. (2017) [31]
EmimCl	dimethylurea	SO_2	2:1	2.50 – 7.26	293.15	0.10 – 1.00	0.014	Yang et al. (2020) [32]
EmimCl	*N*-methylurea	SO_2	2:1	2.06 – 6.25	293.15	0.10 – 1.00	0.016	Yang et al. (2020) [32]
EmimCl	thioacetamide	SO_2	2:1	2.13 – 6.79	293.15	0.10 – 1.00	0.015	Yang et al. (2020) [32]
EmimCl	caprolactam	SO_2	2:1	2.86 – 8.00	293.15	0.10 – 1.00	0.013	Yang et al. (2020) [32]
BmimCl	4-methylimidazole	SO_2	1:1	1.42	293.15	1.00	0.070	Hou et al. (2020) [33]
BmimCl	4-methylimidazole	SO_2	2:1	1.37	293.15	1.00	0.073	Hou et al. (2020) [33]
BmimCl	4-methylimidazole + Ethylenurea	SO_2	1:1:1	1.58	293.15	1.00	0.063	Hou et al. (2020) [33]
BmimCl	4-methylimidazole + Ethylenurea	SO_2	2:1:1	1.54	293.15	1.00	0.065	Hou et al. (2020) [33]
BmimCl	4-methylimidazole + Ethylenurea	SO_2	1:2:1	2.29	293.15	1.00	0.044	Hou et al. (2020) [33]
BmimCl	4-methylimidazole + Ethylenurea	SO_2	1:1:2	2.07	293.15	1.00	0.048	Hou et al. (2020) [33]
EmimCl	Dicyandiamide	SO_2	1:3	0.062 – 1.652	292.20 – 353.20	0.006 – 1.02	0.009 – 0.06	Wu et al. (2021)[34]
EmimCl	N-Formylmorpholine	SO_2	1:1	0.276 – 0.876	293.15 – 313.15	0.01 – 0.10	0.004 – 0.01	Deng et al. (2020) [35]
TBAB	caprolactam	SO_2	1:1	2.54	293.15	1.00	0.039	Zhang et al. (2020) [36]

HBA	HBD	Gas	Molar ratio	Solubility (x_1)	T (K)	P(bar)	Henry's constant (MPa)	Reference
TBAB	caprolactam	SO_2	1:2	2.18	293.15	1.00	0.045	Zhang et al. (2020) [36]
TBAB	caprolactam	SO_2	1:3	1.86	293.15	1.00	0.054	Zhang et al. (2020) [36]
TBAB	caprolactam	SO_2	1:4	1.68	293.15	1.00	0.059	Zhang et al. (2020) [36]

2. Techniques used to measure gas solubility

Several techniques have been used to measure gas solubility in DESs. To exemplify we will analyze techniques that measure CO_2 solubility in ChCl:urea DES at molar ratio of 1:2.

Li et al. (2008) [1] used an apparatus described by Zhang et al. (2004) [37], composed of a CO_2 cylinder, a computer-controlled metering syringe pump, a constant-temperature water bath, a pressure gauge, a volume-variable view cell, a sample bomb, and a magnetic stirrer. In an experiment, an amount of DES is inserted in the view cell, the cell is positioned in the constant-temperature water bath, and CO_2 is injected into the system until an appropriate pressure is reached. The system achieved equilibrium when the pressure remains constant over 5 h. The solubility is found by using the masses of the liquid and the CO_2 in the sample. To measure CO_2 solubility, the sampling valve of the lower liquid phase was slowly opened to collect the sample from the phase. At the same time, cell volume was adjusted to keep the pressure unchanged during the process. The valve was closed when enough sample was obtained. Using a similar procedure, samples from the intermediate and upper phases were collected. The highest solubility value at molar ratio of this paper was 0.309 for CO_2 in ChCl:urea DES (1:2) at 125 bar and 313.15 K [1], which are the highest pressure and lowest temperature studied by the authors.

Liu et al. (2019) [16] used an apparatus described by Wang et al. (2011) [38] in which the entire device consists of an isothermal water bath, balance of absorption, and sections for receiving data. This device has two chambers, the largest chamber stores and isolates CO_2 before encountering the samples in the smaller chamber, which is equipped with a magnetic stirrer (the equilibrium cell). A known mass of DES was placed in the smaller chamber with a magnetic bar. Vacuum (<10 Pa) was then applied to degas the entire device for at least 2 h. Then, the two chambers were separated by a needle valve. The larger chamber received known amounts of CO_2, measured by a pressure gauge (P_1). The needle valve between the two chambers was opened to allow CO_2 to be introduced into the sample in the smaller chamber. A pressure drop was observed in the larger chamber (P_1'). Absorption equilibrium was obtained when the pressures of the two chambers (P_1' and P_2) remained constant for at least 1 h. Their best solubility was 0.016 at 2.202 bar and 313.15 K [16]. CO_2 absorption, *n*, was calculated using Equation 1:

$$n = \rho_1 V_1 - \rho_1' V_1 - \rho_2 \left(V_2 - \frac{m}{\rho_0} \right) \quad (1)$$

where ρ_1 is the density in mol/mL of CO_2 in P_1 represented in bar, ρ_1' is the density of gas in P_1', ρ_2 is the density of gas in P_2, ρ_0 is the density of DES, and V_1 and V_2 represent the volumes in mL of the two chambers, respectively. Thus, gas solubility in DESs (x which is defined as the molar fraction of the gas in the liquid phase) was calculated using Equation (2):

$$x = \frac{n}{n + \frac{m(a+b)}{aM_a + bM_b}} \quad (2)$$

where a and b are the molar ratio of ChCl:urea in DES, M_a is the molar mass of ChCl and M_b is the molar mass of urea, both in g/mol.

Ali et al. (2014) [5] used a variable-volume high-pressure equilibrium cell to conduct their experiments. This cell is equipped with a stirrer, three sapphire windows and a heating jacket enabling operation at a constant temperature. It is also connected to a high-performance liquid chromatography (HPLC) pump, and a piston with nitrogen. Before each experiment, the equilibrium cell was cleaned, evacuated using a vacuum pump, and maintained at a fixed temperature using a circulating water bath. Thus, a known amount of DES was inserted in the cell using the HPLC pump. Then, CO_2 was injected into the cell at a defined pressure and the mixture was stirred until equilibrium was achieved. Constant pressure is reached by changing the volume of the cell by moving its piston. This volume change is recorded, and the mass of the dissolved CO_2 is calculated using the Benedict–Webb–Rubin equation of state. The best solubility result of this experiment was 0.021 at 10 bar and 298.15 K [5].

Mirza et al. (2015) [9] used a static vapor-liquid equilibrium (VLE) rig to quantify CO_2 solubility, which consisted of a buffer tank with a top-mounted pressure gauge, incubation heater, a static stainless steel equilibrium vessel fitted with a pressure gauge and valves on the inlet and outlet of the vessel to control gas flow. Initially, a known amount of DES is loaded into the equilibrium vessel in which nitrogen gas is inserted for 2 h at a constant temperature and constant stirrer. Then, CO_2 is introduced into the vessel through the buffer tank and the system is stirred for more than 20 hours. Equilibrium is reached when the pressure reading of the vessel remained constant for 4 hours. The best result using this technique was 0.004 at 1.53 bar and 329 K. Due to the low vapor pressures of the DESs at operating temperatures, it was assumed that the vapor phase consisted only of pure CO_2. Based on this assumption, using the initial

and final pressure readings of the equilibrium vessel, the initial and final CO_2 concentrations were calculated using Equation 3 [9]:

$$\Delta n_{CO_2} = \frac{\Delta P \cdot V}{RT} \quad (3)$$

where Δn_{CO_2} is the amount of CO_2 absorbed in DES (mol), ΔP is the change in pressure from the initial value to the equilibrium pressure in kPa, V is the volume of the equilibrium cell in m^3, T is the temperature in K, and R is the universal gas constant (8.314 $J.mol^{-1}.K^{-1}$).

Leron, Caparanga and Li (2013) [2] used a thermogravimetric pressure scale with a control system that controls weight, pressure, and temperature of the system to conduct the experimental measurements, according to the methodology described by Soriano et al. (2008) [39]. The equipment consists of a recording balance designed to operate at any pressure and a pressure vessel machined. Static operation consists in introducing gas at the top of the balance and then the recipient is closed. A small volume of the DES is loaded into the microbalance pan, then the reactor vessel is closed. The sample is dried and degassed by applying vacuum in the sample with a diaphragm pump and then fully evacuating the reactor to a minimum of 10^{-6} Pa with a turbo pump. While under vacuum, the sample is heated to 343.2 K for a minimum of 8 h with an external heating coil surrounding the container connected to a remote temperature controller. The system is purged with CO_2 that can flow into the vessel until the desired pressure is reached. After that, the valve is closed, the temperature is set, and the system is considered at equilibrium when no change in weight is observed. The best result achieved in this paper was 0.308 at 59.11 bar and 303.15 K [2].

References

(1) Li, X.; Hou, M.; Han, B.; Wang, X.; Zou, L. Solubility of CO2 in a Choline Chloride + Urea Eutectic Mixture. *J. Chem. Eng. Data* **2008**, *53*, 548–550.

(2) Leron, R. B.; Caparanga, A.; Li, M. H. Carbon Dioxide Solubility in a Deep Eutectic Solvent Based on Choline Chloride and Urea at T = 303.15-343.15K and Moderate Pressures. *J. Taiwan Inst. Chem. Eng.* **2013**, *44*, 879–885.

(3) Leron, R. B.; Li, M. H. Solubility of Carbon Dioxide in a Choline Chloride-Ethylene Glycol Based Deep Eutectic Solvent. *Thermochim. Acta* **2013**, *551*, 14–19.

(4) Leron, R. B.; Li, M. H. Solubility of Carbon Dioxide in a Eutectic Mixture of Choline Chloride and Glycerol at Moderate Pressures. *J. Chem. Thermodyn.* **2013**, *57*, 131–136.

(5) Ali, E.; Hadj-Kali, M. K.; Mulyono, S.; Alnashef, I.; Fakeeha, A.; Mjalli, F.; Hayyan, A. Solubility of CO2 in Deep Eutectic Solvents: Experiments and Modelling Using the Peng-Robinson Equation of State. *Chem. Eng. Res. Des.* **2014**, *92*, 1898–1906.

(6) Chen, Y.; Ai, N.; Li, G.; Shan, H.; Cui, Y.; Deng, D. Solubilities of Carbon Dioxide in Eutectic Mixtures of Choline Chloride and Dihydric Alcohols. *J. Chem. Eng. Data* **2014**, *59*, 1247–1253.

(7) Li, G.; Deng, D.; Chen, Y.; Shan, H.; Ai, N. Solubilities and Thermodynamic Properties of CO2 in Choline-Chloride Based Deep Eutectic Solvents. *J. Chem. Thermodyn.* **2014**, *75*, 58–62.

(8) Lu, M.; Han, G.; Jiang, Y.; Zhang, X.; Deng, D.; Ai, N. Solubilities of Carbon Dioxide in the Eutectic Mixture of Levulinic Acid (or Furfuryl Alcohol) and Choline Chloride. *J. Chem. Thermodyn.* **2015**, *88*, 72–77.

(9) Mirza, N. R.; Nicholas, N. J.; Wu, Y.; Mumford, K. A.; Kentish, S. E.; Stevens,

G. W. Experiments and Thermodynamic Modeling of the Solubility of Carbon Dioxide in Three Different Deep Eutectic Solvents (DESs). *J. Chem. Eng. Data* **2015**, *60*, 3246–3252.

(10) Ji, Y.; Hou, Y.; Ren, S.; Yao, C.; Wu, W. Phase Equilibria of High Pressure CO2 and Deep Eutectic Solvents Formed by Quaternary Ammonium Salts and Phenol. *Fluid Phase Equilib.* **2016**, *429*, 14–20.

(11) Deng, D.; Jiang, Y.; Liu, X.; Zhang, Z.; Ai, N. Investigation of Solubilities of Carbon Dioxide in Five Levulinic Acid-Based Deep Eutectic Solvents and Their Thermodynamic Properties. *J. Chem. Thermodyn.* **2016**, *103*, 212–217.

(12) Liu, X.; Gao, B.; Jiang, Y.; Ai, N.; Deng, D. Solubilities and Thermodynamic Properties of Carbon Dioxide in Guaiacol-Based Deep Eutectic Solvents. *J. Chem. Eng. Data* **2017**, *62*, 1448–1455.

(13) Haider, M. B.; Jha, D.; Marriyappan Sivagnanam, B.; Kumar, R. Thermodynamic and Kinetic Studies of CO2 Capture by Glycol and Amine-Based Deep Eutectic Solvents. *J. Chem. Eng. Data* **2018**, *63*, 2671–2680.

(14) Wang, J.; Cheng, H.; Song, Z.; Chen, L.; Deng, L.; Qi, Z. Carbon Dioxide Solubility in Phosphonium-Based Deep Eutectic Solvents: An Experimental and Molecular Dynamics Study. *Ind. Eng. Chem. Res.* **2019**, *58*, 17514–17523.

(15) Sarmad, S.; Nikjoo, D.; Mikkola, J. P. Amine Functionalized Deep Eutectic Solvent for CO2 Capture: Measurements and Modeling. *J. Mol. Liq.* **2020**, *309*, 1–11.

(16) Liu, F.; Chen, W.; Mi, J.; Zhang, J. Y.; Kan, X.; Zhong, F. Y.; Huang, K.; Zheng, A. M.; Jiang, L. Thermodynamic and Molecular Insights into the Absorption of H2S, CO2 , and CH4 in Choline Chloride plus Urea Mixtures. *AIChE J.* **2019**, *65*, 1–10.

(17) Ghaedi, H.; Ayoub, M.; Sufian, S.; Shariff, A. M.; Hailegiorgis, S. M.; Khan, S. N. CO2 Capture with the Help of Phosphonium-Based Deep Eutectic Solvents. *J. Mol.*

Liq. **2017**, *243*, 564–571.

(18) Li, X.; Liu, X.; Deng, D. Solubilities and Thermodynamic Properties of CO2 in Four Azole-Based Deep Eutectic Solvents. *J. Chem. Eng. Data* **2018**, *63*, 2091–2096.

(19) Rabhi, F.; Mutelet, F.; Sifaoui, H. Solubility of Carbon Dioxide in Carboxylic Acid-Based Deep Eutectic Solvents. *J. Chem. Eng. Data* **2021**, *66*, 702–711.

(20) Zubeir, L. F.; Van Osch, D. J. G. P.; Rocha, M. A. A.; Banat, F.; Kroon, M. C. Carbon Dioxide Solubilities in Decanoic Acid-Based Hydrophobic Deep Eutectic Solvents. *J. Chem. Eng. Data* **2018**, *63*, 913–919.

(21) Gu, Y.; Hou, Y.; Ren, S.; Sun, Y.; Wu, W. Hydrophobic Functional Deep Eutectic Solvents Used for Efficient and Reversible Capture of CO2. *ACS Omega* **2020**, *5*, 6809–6816.

(22) Ren, H.; Lian, S.; Wang, X.; Zhang, Y.; Duan, E. Exploiting the Hydrophilic Role of Natural Deep Eutectic Solvents for Greening CO2 Capture. *J. Clean. Prod.* **2018**, *193*, 802–810.

(23) Haider, M. B.; Jha, D.; Kumar, R.; Sivagnanam, M. Ternary Hydrophobic Deep Eutectic Solvents for Carbon Dioxide Absorption. *Int. J. Greenh. Gas Control* **2020**, *92*, 1–11.

(24) Zhang, K.; Hou, Y.; Wang, Y.; Wang, K.; Ren, S.; Wu, W. Efficient and Reversible Absorption of CO2 by Functional Deep Eutectic Solvents. *Energy and Fuels* **2018**, *32*, 7727–7733.

(25) Altamash, T.; Amhamed, A. I.; Aparicio, S.; Atilhan, M. Combined Experimental and Theoretical Study on High Pressure Methane Solubility in Natural Deep Eutectic Solvents. *Ind. Eng. Chem. Res.* **2019**, *58*, 8097–8111.

(26) Cui, G.; Liu, J.; Lyu, S.; Wang, H.; Li, Z.; Wang, J. Efficient and Reversible SO2 Absorption by Environmentally Friendly Task-Specific Deep Eutectic Solvents of

PPZBr + Gly. *ACS Sustain. Chem. Eng.* **2019**, *7*, 14236–14246.

(27) Deng, D.; Han, G.; Jiang, Y. Investigation of a Deep Eutectic Solvent Formed by Levulinic Acid with Quaternary Ammonium Salt as an Efficient SO 2 Absorbent. *New J. Chem.* **2015**, *39*, 8158–8164.

(28) Sun, S.; Niu, Y.; Xu, Q.; Sun, Z.; Wei, X. Efficient SO2 Absorptions by Four Kinds of Deep Eutectic Solvents Based on Choline Chloride. *Ind. Eng. Chem. Res.* **2015**, *54*, 8019–8024.

(29) Yang, D.; Hou, M.; Ning, H.; Zhang, J.; Ma, J.; Yang, G.; Han, B. Efficient SO2 Absorption by Renewable Choline Chloride–Glycerol Deep Eutectic Solvents. *Green Chem.* **2013**, *15*, 2261–2265.

(30) Liu, X.; Gao, B.; Deng, D. SO2 Absorption/Desorption Performance of Renewable Phenol-Based Deep Eutectic Solvents. *Sep. Sci. Technol.* **2018**, *53*, 2150–2158.

(31) Deng, D.; Liu, X.; Gao, B. Physicochemical Properties and Investigation of Azole-Based Deep Eutectic Solvents as Efficient and Reversible SO2 Absorbents. *Ind. Eng. Chem. Res.* **2017**, *56*, 13850–13856.

(32) Yang, X.; Zhang, Y.; Liu, F.; Chen, P.; Zhao, T.; Wu, Y. Deep Eutectic Solvents Consisting of EmimCl and Amides: Highly Efficient SO2 Absorption and Conversion. *Sep. Purif. Technol.* **2020**, *250*, 1–8.

(33) Hou, S.; Zhang, C.; Jiang, B.; Zhang, H.; Zhang, L.; Yang, N.; Zhang, N.; Xiao, X.; Tantai, X. Investigation of Highly Efficient and Reversible Absorption of SO2 Using Ternary Functional Deep Eutectic Solvents. *ACS Sustain. Chem. Eng.* **2020**, *8*, 16241–16251.

(34) Wu, X.; Guan, R.; Zheng, W. T.; Huang, K. New Deep Eutectic Solvents Formed by 1-Ethyl-3-Methylimidazolium Chloride and Dicyandiamide: Physiochemical

Properties and SO2 Absorption Performance. *J. Taiwan Inst. Chem. Eng.* **2021**, *119*, 45–51.

(35) Deng, D.; Zhang, C.; Deng, X.; Gong, L. Efficient Absorption of Low Partial Pressure SO2 by 1-Ethyl-3-Methylimidazolium Chloride plus N-Formylmorpholine Deep Eutectic Solvents. *Energy and Fuels* **2020**, *34*, 665–671.

(36) Zhang, J.; Yu, L.; Gong, R.; Li, M.; Ren, H.; Duan, E. Role of Hydrophilic Ammonium-Based Deep Eutectic Solvents in SO2 Absorption. *Energy and Fuels* **2020**, *34*, 47–81.

(37) Zhang, Z.; Wu, W.; Liu, Z.; Han, B.; Gao, H.; Jiang, T. A Study of Tri-Phasic Behavior of Ionic Liquid-Methanol-CO2 Systems at Elevated Pressures. *Phys. Chem. Chem. Phys.* **2004**, *6*, 2352–2357.

(38) Wang, G.; Hou, W.; Xiao, F.; Geng, J.; Wu, Y.; Zhang, Z. Low-Viscosity Triethylbutylammonium Acetate as a Task-Specific Ionic Liquid for Reversible CO2 Absorption. *J. Chem. Eng. Data* **2011**, *56*, 1125–1133. https://doi.org/10.1021/je101014q.

(39) Soriano, A. N.; Doma, B. T.; Li, M. H. Solubility of Carbon Dioxide in 1-Ethyl-3-Methylimidazolium Tetrafluoroborate. *J. Chem. Eng. Data* **2008**, *53*, 2550–2555.

(40) Alioui, O.; Benguerba, Y.; Alnashef, I. M. Investigation of the CO2-Solubility in Deep Eutectic Solvents Using COSMO-RS and Molecular Dynamics Methods. *J. Mol. Liq.* **2020**, *307*, 1–9.

(41) Haghbakhsh, R.; Raeissi, S. Modeling the Phase Behavior of Carbon Dioxide Solubility in Deep Eutectic Solvents with the Cubic Plus Association Equation of State. *J. Chem. Eng. Data* **2018**, *63*, 897–906.

(42) Haider, M. B.; Jha, D.; Marriyappan Sivagnanam, B.; Kumar, R. Modelling and Simulation of CO2 Removal from Shale Gas Using Deep Eutectic Solvents. *J. Environ.*

Chem. Eng. **2019**, *7*, 1–9.

(43) Zubeir, L. F.; Held, C.; Sadowski, G.; Kroon, M. C. PC-SAFT Modeling of CO2 Solubilities in Deep Eutectic Solvents. *J. Phys. Chem. B* **2016**, *120*, 2300–2310.

(44) Dietz, C. H. J. T.; van Osch, D. J. G. P.; Kroon, M. C.; Sadowski, G.; van Sint Annaland, M.; Gallucci, F.; Zubeir, L. F.; Held, C. PC-SAFT Modeling of CO2 Solubilities in Hydrophobic Deep Eutectic Solvents. *Fluid Phase Equilib.* **2017**, *448*, 94–98.

(45) Kamgar, A.; Mohsenpour, S.; Esmaeilzadeh, F. Solubility Prediction of CO2, CH4, H2, CO and N2 in Choline Chloride/Urea as a Eutectic Solvent Using NRTL and COSMO-RS Models. *J. Mol. Liq.* **2017**, *247*, 70–74.

(46) Haider, M. B.; Kumar, R. Solubility of CO2 and CH4 in Sterically Hindered Amine-Based Deep Eutectic Solvents. *Sep. Purif. Technol.* **2020**, *248*, 1 –10.

CAPÍTULO 3

MATERIAIS E MÉTODOS

1. Materiais

O gás avaliado foi o dióxido de carbono (CO_2). Os reagentes utilizados para sintetizar os ESs foram: Cloreto de colina (ChCl), glicerol, etilenoglicol, 1,3 propanodiol, ácido glicólico, ácido lático e ácido malônico conforme apresentados na Tabela 1. Todos os reagentes utilizados foram de grau analítico.

Tabela 1. Pureza e fonte dos compostos utilizados nesse trabalho

Nome químico	Número CAS	Pureza	Fonte
Dióxido de carbono	124-38-9	99,8%	White Martins
Cloreto de colina	67-48-1	≥ 98,5%	Sigma Aldrich
Etilenoglicol	107-21-1	99,5%	Merck
Glicerol	56-81-5	99%	Anidrol
1,3 propanodiol	504-63-2	≥ 98%	Sigma Aldrich
Ácido glicólico	79-14-1	99,7%	Acros
Ácido lático	50-21-5	99,5%	Sigma Aldrich
Ácido malônico	141-82-2	99%	Sigma Aldrich

Fonte: Autoria própria

2. Metodologia experimental

2.1. Preparação dos ESs

Foram produzidos seis ESs utilizando o cloreto de colina (ChCl) como HBA, e diferentes moléculas como HBD em diferentes frações molares, de acordo com a Tabela 2. Devido à definição de DESs apresentada, optou-se por chamar todas as misturas desse trabalho de ESs, uma vez que se trabalhou com diversas frações molares que nem sempre correspondem à do eutético profundo.

Os ESs foram produzidos utilizando a metodologia de aquecimento brando combinado com agitação proposta por Abbott et al. (2003). Inicialmente, os reagentes foram secos em estufa a vácuo por pelo menos 72 horas a 353,15 K, a fim de reduzir ao máximo o teor de água presente nos mesmos. Em seguida, foram pesadas quantidades previamente conhecidas de cada componente, conforme a fração molar, para uma massa total de 100 g, em um Erlenmeyer de 250 ml que foi colocado em um banho de glicerina com agitação recíproca a 333,15 K por 120 min, ou até a formação de um líquido límpido e homogêneo. Os ESs formados foram então transferidos para

frascos âmbar e armazenados à temperatura ambiente em um dessecador para que absorvessem o mínimo de água possível.

Tabela 2. Composição dos ESs que foram estudados no projeto

HBA (1)	HBD (2)	Fração molar (x_1)	Abreviação	Referência
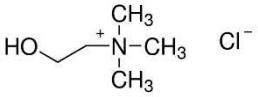 Cloreto de colina	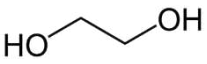 Etilenoglicol	0,30; 0,33; 0,40; 0,45	ChCl:ETGLY	(SILVA et al., 2020)
	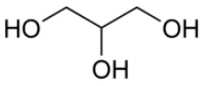 Glicerol	0,45; 0,50; 0,55	ChCl:GLY	(SILVA et al., 2020)
	 1,3 propanodiol	0,33; 0,40; 0,45	ChCl:1,3PROP	(SILVA et al., 2020)
	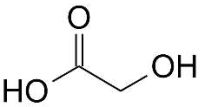 Ácido glicólico	0,15; 0,40	ChCl:AC GLY	(CRESPO et al., 2018)
	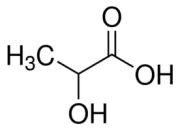 Ácido lático	0,50; 0,55	ChCl:AC LAT	(CRESPO et al., 2018)
	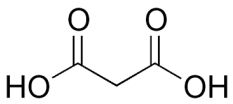 Ácido malônico	0,30; 0,35; 0,55	ChCl:AC MAL	(CRESPO et al., 2018)

Fonte: Autoria própria

2.2. Determinação do equilíbrio de fases a altas pressões

Nesse trabalho foi utilizado o método estático sintético para a obtenção de dados experimentais de equilíbrio de fases a altas pressões. A técnica já é consolidada consiste em introduzir em uma célula de equilíbrio quantidades precisas da substância pura para que se possa conhecer a composição global da mistura. Em seguida, ajustam-se as condições de temperatura e pressão para que uma solução homogênea seja formada, e então, encontra-se a pressão ou temperatura na qual ocorre a transição de fases (LANZA, 2004; NDIAYE, 2004; DALMOLIN, 2013).

A Figura 1 apresenta um diagrama esquemático do aparato experimental utilizado. Esse aparato é formado por um reservatório de solvente na forma de um cilindro de gás, que também pode desempenhar o papel de fluido de pressurização (1), uma bomba do tipo seringa de alta pressão (ISCO, modelo 260L, Lincoln, USA) (2), utilizada por permitir facilmente o controle da pressão e quantificação de volume de solvente deslocado. A temperatura do fluido na bomba é controlada através de um banho termostático (TECNA, modelo TE-184) (3). O aparato ainda conta com um transdutor absoluto de pressão para monitoramento (4), uma célula de equilíbrio de volume variável (5), que é um cilindro de aço inoxidável 316L com capacidade máxima de 2,7 x 10^{-5} m^3 (diâmetro interno de 17,2 mm e comprimento de 146,5 mm) considerando a presença do pistão móvel, e com conexões remontadas a cada experimento.

Figura 1. Diagrama esquemático do aparato experimental de equilíbrio de fases a altas pressões

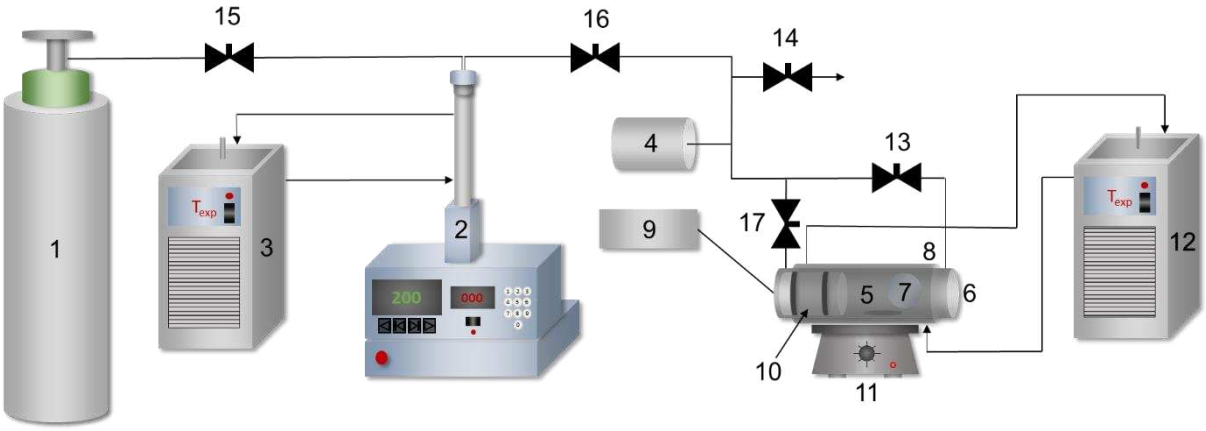

Fonte: Autoria própria

Na conexão frontal da célula há uma janela de safira (6) para que a transição de fases seja visualmente observada, e na lateral, há outra janela de safira, menor (7), para a entrada de luz. Para a fixação das janelas são utilizados dois anéis de vedação (Figura 2), que podem ser feitos de borracha, teflon ou cobre. É recomendado para temperaturas próximas a ambiente ou menores a utilização dos anéis de vedação de borracha e/ou teflon. Já para temperaturas mais elevadas (acima de 343,15 K), é recomendado o uso dos anéis de cobre, pois os de teflon podem deformar e causar vazamento no sistema e/ou trincas nas janelas de safira, o que compromete a operação do equipamento (LANZA, 2004). Dessa maneira, nesse trabalho foram utilizados os anéis de cobre e teflon por serem mais resistentes nas condições em que o trabalho foi desenvolvido.

Figura 2. Anéis de vedação. (A) anel de cobre; (B) anel de teflon; (C) posicionamento das janelas de safira na célula de equilíbrio

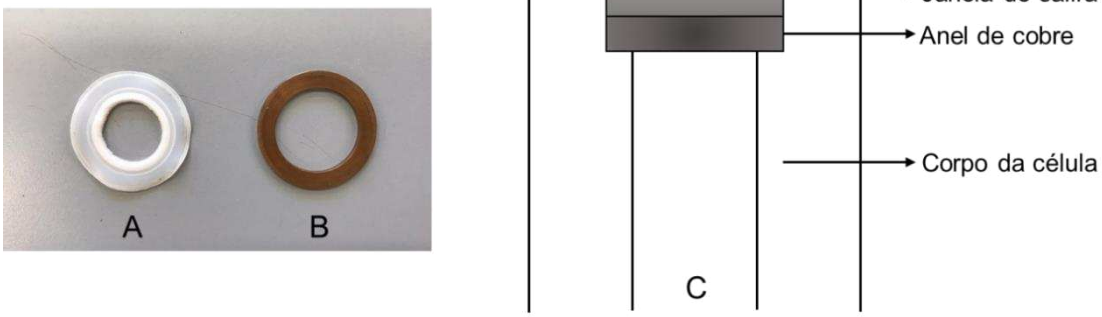

Fonte: Autoria própria

Na Figura 1 está ilustrada também a parte frontal da célula que ainda conta com conexões desmontáveis para a alimentação dos componentes da mistura e inserção de um indicador de temperatura tipo PT-100 (8 e 9) para controle da temperatura de operação. O controle de pressão dentro da célula é feito através de um pistão móvel (10), de aço inoxidável 316L, que possui 17 mm de diâmetro interno, 28 mm de comprimento e dois anéis de Buna- N90 *O-rings* localizados em suas extremidades, como exibido na Figura 3(B). Os anéis permitem que o pistão deslize pelo interior da célula e garantem a vedação entre o fundo, que contém o fluido que será usado para pressurizar o sistema, e a frente da célula que contém a mistura a ser estudada.

Entretanto, a montagem do pistão é uma etapa crítica, pois os anéis de vedação devem estar igualmente dispostos, ou seja, ambos devem ser colocados no pistão e aparafusados com a mesma intensidade. Caso os anéis que são ajustados através de parafusos estejam muito comprimidos, o pistão não deslocará dentro da célula em baixas pressões e, em altas pressões, poderá deslocar-se brutalmente devido ao rompimento do anel, o que por sua vez causará a passagem da substância de estudo, o ES, para o fundo da célula. Se os anéis estiverem pouco comprimidos também ocorrerá a passagem dos fluidos e consequente mistura entre os componentes da parte frontal da célula com o fluido de pressurização.

Figura 3. Pistão móvel. (A) pistão desmontado, visão de cada componente; (B) pistão montado, posição horizontal

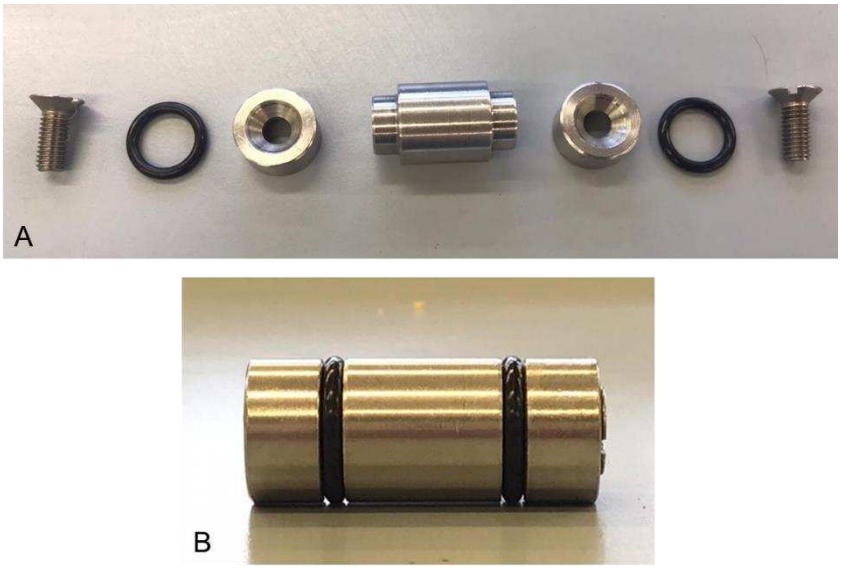

Fonte: Autoria própria

Depois de montado, o pistão é colocado dentro da célula pela parte de trás da mesma, que é fechada em seguida. Pela parte da frente é colocada uma barra magnética recoberta com teflon e que tem por função homogeneizar o sistema através do uso de uma placa de agitação (11) colocada logo abaixo da célula. Por último, é feita a conexão frontal com a janela de safira para visualização, ou seja, a célula é completamente fechada e vedada.

No diagrama da Figura 1 há também o sistema de resfriamento da célula de equilíbrio que está envolta por uma camisa metálica. Nesse sistema de resfriamento, mantido por um banho termostático (12), etilenoglicol é recirculado, na temperatura desejada, mantendo a temperatura do sistema constante.

O sistema possui ainda válvulas agulha, que são usadas para a alimentação do fluido de pressurização do sistema (13), para descarga e alívio do sistema (14), garantindo a segurança durante a operação; válvulas esfera para interromper o fluxo na linha de gás (15 e 16) e uma válvula de uma via (*check-valve*) (17), que garante que pressões elevadas não retornem o gás para o cilindro.

2.2.1. Determinação do equilíbrio de fases dos ESs puros a altas pressões

A determinação do equilíbrio de fases dos ESs puros pode ser realizada como uma operação isobárica. Na qual, uma quantidade conhecida de ES a uma determinada fração molar é inserida na célula, a fim de completar um volume de

aproximadamente 10 mL, com o auxílio de uma seringa na conexão frontal, devido à alta viscosidade do composto que não pode ser inserido através das conexões desmontáveis. Em seguida, a pressão no fundo da célula, que inicialmente está a 5,5 MPa, pressão de vapor do CO_2, aproximadamente, é reduzida e mantida em 2 MPa, por questões de segurança, uma vez que o ES está a temperatura e pressão ambiente. A fim de eliminar o ar atmosférico dentro da célula, a conexão do termopar é parcialmente fechada, e a de fundo é aberta. A pressão é então pré-fixada através da inserção de gás, o fluido de pressurização, pela bomba seringa na parte de trás do pistão, ou seja, aumenta-se a pressão do sistema. Estabilizada a pressão, a temperatura é reduzida vagarosamente, até que a transição de fases sólido-líquido seja observada, ou seja, uma temperatura de transição é determinada a uma dada pressão. Esse procedimento é feito em triplicata. Nesse trabalhou avaliou-se as transições a 6, 10, 14, 20 e 25 MPa.

As transições observadas acontecem conforme apresentado nas Figura 4 e 5, na qual cada etapa representa a vista da janela de safira frontal da célula, no sentido da diminuição da temperatura no sistema isobárico.

Figura 4. Visualização das transições de fases sólido-líquido a altas pressões, isobaricamente através do método estático sintético

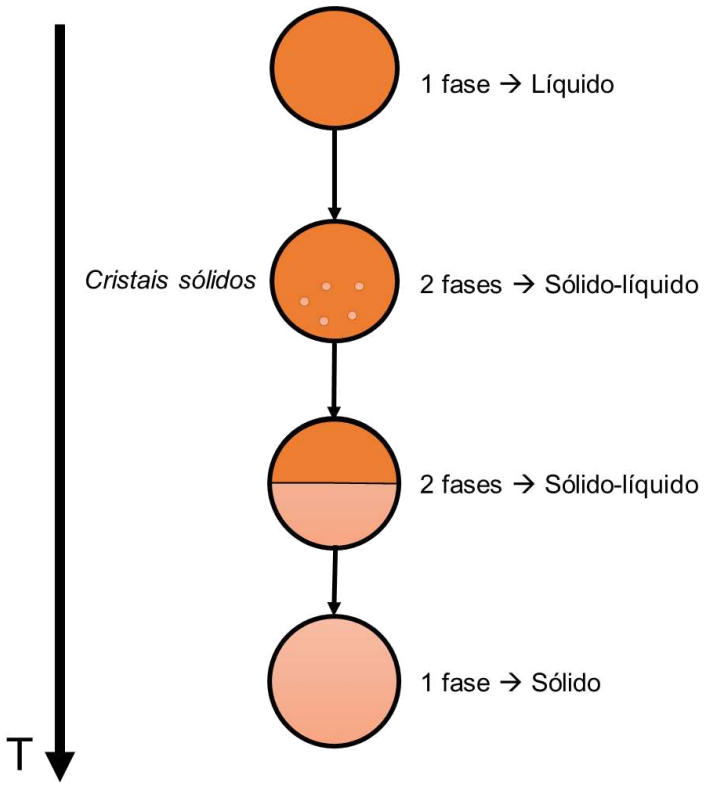

Fonte: Autoria própria

Figura 5. Vista da janela frontal da célula de pressão a 9 MPa: (A) ChCl:ETGLY líquido na temperatura de 30 °C; (B) transição sólido-líquido na temperatura de 26,9 °C; (C) ChCl:ETGLY completamente sólido na temperatura 26,5 °C.

Fonte: Autoria própria

2.2.2. Determinação do equilíbrio de fases ESs e CO_2

Para a determinação do equilíbrio de fases entre os ESs e o CO_2 - solubilidade, o experimento foi realizado isotermicamente e com o auxílio de duas bombas seringa. A primeira bomba continha o CO_2, que foi inserido juntamente com o ES na parte frontal da célula, e a segunda bomba foi preenchida com etanol para alimentar o fundo da célula. A utilização de duas bombas se fez necessária, pois algumas transições foram encontradas em pressões baixas, menores que a pressão de vapor do CO_2, o que aumentaria muito o esforço da bomba, fato que não acontece com o etanol, que é líquido. Para esses experimentos, escolheu-se a composição eutética de cada ES para ser estudada.

Inicialmente, escolhe-se as composições de ES e CO_2 desejadas e uma quantidade conhecida do componente menos volátil, o ES, é colocado na célula com o auxílio de uma seringa na conexão frontal. Para confirmar a ausência de ar atmosférico dentro da célula deve ser feita uma troca de atmosfera pela rápida passagem de pequena quantidade do solvente CO_2. A pressão na bomba contendo CO_2 é então fixada em 10 MPa e a temperatura em 278,15 K, e somente quando se atinge essas condições o volume de CO_2 necessário para se obter a composição global pré-estabelecida é lentamente adicionado à célula. O volume de solvente é calculado com base na diferença do volume interno da bomba, a densidade, nas condições desejadas, é obtida através do método de Hankinson-Brobst-Thomson (HBT) e através dessas informações a massa de solvente é computada (THOMSON; BROBST; HANKINSON, 1982).

O sistema é então submetido a temperatura desejada, e a pressão da célula é aumentada após a estabilização da temperatura, pela injeção de etanol na parte de trás do pistão, auxiliada pela bomba seringa, até que se observe uma única fase líquida. A mistura é então homogeneizada por cerca de 4 horas através de agitação contínua. A seguir, a pressão é vagarosamente reduzida (0,3 a 0,5 MPa/min), isotermicamente, até que se observe a transição de fases, ou seja, uma pressão de transição é determinada em uma dada temperatura. Esse procedimento é feito em triplicata para cada temperatura e composição global.

As transições observadas acontecem conforme apresentado na Figura 6, em que cada etapa representa a vista da janela de safira localizada na frente da célula, com a diminuição da pressão mantendo-se o sistema isotérmico. As transições apresentadas na Figura 6, não necessariamente foram observadas em um único experimento, a figura representa possíveis transições que podem ser observadas.

Figura 6. Visualização das transições de fases líquido-vapor a altas pressões, isotermicamente através do método estático sintético

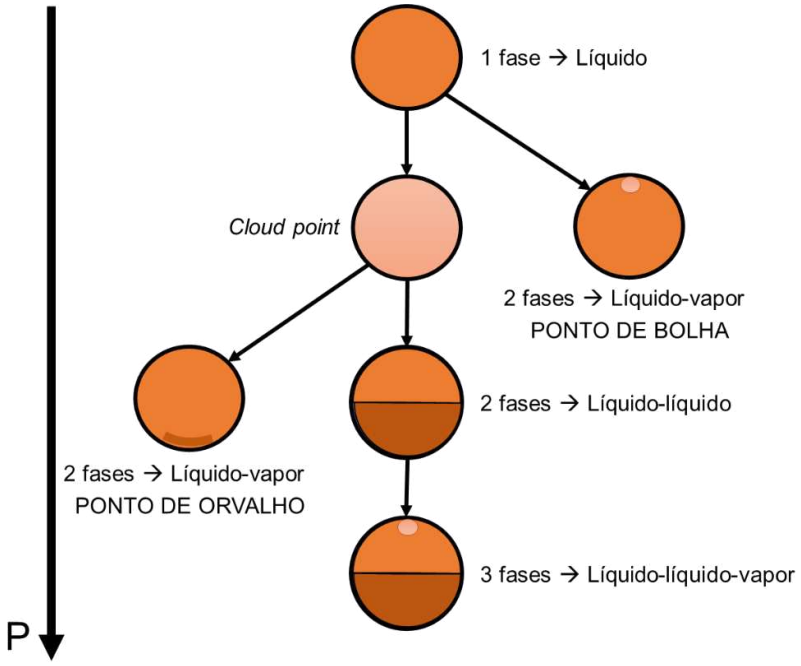

Fonte: Autoria própria

Na Figura 7 é apresentada uma foto da vista frontal da unidade experimental de equilíbrio de fases a altas pressões, com destaque para o cilindro de CO_2 (A), a bomba do tipo seringa (B), a célula de equilíbrio (C), a válvula esfera para interromper o fluxo na linha que o solvente percorre (D) e a válvula de alívio/segurança (E).

Figura 7. Vista frontal da unidade experimental de equilíbrio de fases a altas pressões

Fonte: Autoria própria

Os sistemas que foram determinadas as solubilidades estão dispostos na Tabela 3 com a faixa de temperatura de interesse.

Tabela 3. Sistemas e composições de CO_2 que foram estudados nesse trabalho

Soluto (1)	Solvente (2)	x_{CO2}	Temperatura (K)
ChCl:ETGLY	CO_2	0,01; 0,05; 0,10; 0,20	298,15 K – 333,15K
ChCl:GLY	CO_2	0,01; 0,05; 0,10; 0,15	298,15 K – 333,15K
ChCl:1,3PROP	CO_2	0,01; 0,05; 0,10; 0,15	298,15 K – 333,15K
ChCl:AC GLY	CO_2	0,01; 0,05; 0,15; 0,07	298,15 K – 333,15K
ChCl:AC LAT	CO_2	0,01; 0,05; 0,10; 0,20	298,15 K – 333,15K
ChCl:AC MAL	CO_2	0,01; 0,05; 0,07; 0,10	298,15 K – 333,15K

2.3. Densidade dos ESs a altas pressões

As densidades dos ESs foram medidas nas temperaturas 293,15 K, 298,15 K, 313,15 K, 333,15 e 353,15 K e na faixa de pressão 1 – 50 MPa usando um DMA-HPM, juntamente com a unidade amPDS 5, um densímetro de alta pressão da Anton Paar, Áustria. O equipamento realiza medidas de densidade de gases e líquidos sob condições de temperatura (T) e pressão (P) variando de 263,15 K a 473,15 K e 0 a 140 MPa. A célula de medição foi termostatizada através da circulação de um fluido termorregulador, com uma estabilidade de temperatura de ±0,01 K, por meio da circulação de um banho termostático (Julabo MC). Verificou-se que a incerteza padrão sobre a temperatura era de 0,1 K. A pressão foi medida através de um transdutor de

pressão piezoresistivo de silicone (Kulite HEM 375) com uma precisão superior a 0,2%. O transdutor foi fixado diretamente na linha de aço inoxidável ¼", para reduzir o volume morto e colocado entre a célula de medição DMA-HPM e um pistão móvel.

O densímetro foi calibrado com água deionizada e nitrogênio, em uma ampla faixa de temperatura e pressão, indo de 293,15 a 363,15 K e 10 a 600 bar, respectivamente. O modo utilizado e sugerido pelo fabricante foi o *Wide Range*, o qual aplica uma equação polinomial (Equação 1) para correlacionar o período de oscilação registrado pelo osciloscópio interno com a densidade do fluido analisado.

$$\rho = AA + AB.\partial t + AC.\partial d + AD.\partial t^2 + AE.\partial d^2 + (AF + AG.\partial t + AH.\partial d + AI.\partial t^2 + AJ.\partial d^2).\partial p^2 + AK.\partial p^4 \quad (1)$$

Em que ρ é a densidade do fluido, ∂t é a temperatura, ∂d é a pressão, ∂p é o período de oscilação e AA à AK são os coeficientes polinomiais de ajuste.

3. Descrição dos modelos

3.1. Modelagem termodinâmica utilizando o software Multiflash

O Multiflash é um software da empresa KBC, que permite modelar e resolver o comportamento de fase de misturas complexas e substâncias puras. O Multiflash pode modelar quaisquer fases, incluindo hidratos, ceras, asfaltenos e incrustações de haletos. Ele apresenta um banco de dados com mais de 300 componentes puros, acesso ao banco de dados do *Design Institute for Physical Properties* (DIPPR) com mais de 2.200 compostos e a possibilidade de incluir componentes com base em dados suplementares. Os modelos disponíveis no Multiflash incluem diversas equações de estados para representar óleo, condensados, gás natural, CO_2, água, vapor, glicóis, refrigerantes, polímeros e outros produtos químicos.

O Multiflash disponibiliza algumas ferramentas que possibilitam a interface com outros aplicativos, facilitando o compartilhamento de dados e informações. Neste trabalho foi utilizado o suplemento do Microsoft Excel. Por meio dessa configuração, foi possível obter o *script* de cada simulação realizada e transferir para o Microsoft Excel, onde também foram realizados os estudos e análises.

O *script* pode ser entendido como uma "identidade", a qual contém todas as informações necessárias de cada simulação, como por exemplo: a composição do fluido, propriedades críticas e termofísicas, parâmetros do modelo termodinâmico

utilizado e os valores do parâmetro de interação binária (k_{ij}). Assim, para cada simulação realizada, foi selecionado um *script* e este compartilhado com o Microsoft Excel.

Nesse trabalho, o Multiflash foi utilizado para modelar a solubilidade de CO_2 em treze DESs em uma ampla faixa de temperatura (303,15 a 343,15 K) e pressão (0,06 a 12 MPa), utilizando as equações de estado Peng-Robinson 78 e *Cubic Plus Association* (CPA), conforme apresentado no Capítulo 4: "*Carbon Dioxide Solubility in Deep Eutectic Solvents: Modelling using Cubic Plus Association and Peng-Robinson Equations of State*". Por meio do *script*, foi possível calcular as curvas solubilidade para as equações de estado CPA e PR78. Além disso, o software foi utilizado para modelar, usando a CPA, os dados experimentais de densidade em altas pressões de seis DESs, conforme apresentado no Capítulo 6: *"Characterization by SLE phase diagrams and density of Eutectic Solvents based on ChCl, alcohols and acids at high pressures".*

3.1.1. Equação de estado Peng-Robinson

A solubilidade do CO_2 nos ESs foi modelada utilizando a equação de Peng-Robinson (PENG; ROBINSON, 1976; MIRZA et al., 2015), definida da seguinte forma:

$$P = \frac{RT}{V_m - b} - \frac{a(T)}{V_m(V_m + b) + b(V_m - b)} \tag{1}$$

Em que, V_m é o volume molar, T é a temperatura, P é a pressão, e R é a constante universal dos gases. O parâmetro de energia física a e o parâmetro de co-volume b são funções das propriedades críticas – temperatura (T_c) e pressão (P_c) - e são calculados para cada componente de acordo com as Equações 2 e 3, respectivamente:

$$a_i = 0.45724 \frac{RT_{c_i}^2}{P_{c_i}} \left[1 + m_i \left(1 - \sqrt{\frac{T}{T_{c_i}}} \right) \right]^2 \tag{2}$$

$$b_i = 0.0778 \frac{RT_{c_i}}{P_{c_i}} \tag{3}$$

Com,

$$m_i = 0.37464 + 1.54226\omega_i - 0.26992\omega_i^2 \tag{4}$$

Se $\omega_i < 0{,}49$. A equação de Peng-Robinson (PENG; ROBINSON, 1978) foi modificada para considerar moléculas cujo $\omega_i > 0{,}49$, de acordo com a expressão:

$$m_i = 0.37964 + 1.4850\omega_i - 0.16442\omega_i^2 + 0.01667\omega_i^3 \quad (5)$$

Nesse trabalho, foi considerada a equação de Peng-Robinson 78, uma vez que os ESs apresentam normalmente fatores acêntricos superiores a 0,49.

As forças predominantes entre as moléculas de diferentes componentes, que formam a mistura, foram descritas considerando as regras de mistura. Assim, os parâmetros a_i e b_i da mistura são determinados utilizando as regras de mistura de um único fluido:

$$a = \sum_{i=1}^{N_c}\sum_{j=1}^{N_c} x_i x_j \left(1 - k_{ij}\right)\sqrt{a_i a_j} \quad (6)$$

E

$$b = \sum_{i=1}^{N_c} x_i b_i \quad (7)$$

Em que, x_i é a fração molar do componente, k_{ij} é o parâmetro de interação binária ajustado com base nos dados experimentais de equilíbrio vapor-líquido (VLE) entre o CO_2 e o ES, dado por:

$$A = \frac{aP}{R^2T^2} \quad (8)$$

$$B = \frac{bP}{RT} \quad (9)$$

Uma vez determinados estes parâmetros, o fator de compressibilidade (Z) pode ser obtido usando a seguinte equação que é a equação Peng-Robinson cúbica em Z:

$$Z^3 - (1 - B)Z^2 + (A - 2B - 3B^2)Z - (AB - B^2 - B^3) = 0 \quad (10)$$

O coeficiente de fugacidade do componente i pode ser calculado por:

$$\phi_i = \exp\left[(Z-1)\frac{b_i}{B} - \ln(Z-B) - \frac{A}{2\sqrt{2}B} \times \left(\frac{2\sum_j y_i a_{ij}}{A} - \frac{b_i}{B}\right)\ln\left(\frac{Z + \left(1+\sqrt{2}\right)B}{Z + \left(1+\sqrt{2}\right)B}\right)\right] \quad (11)$$

As fugacidades individuais foram determinadas com base nos coeficientes de fugacidade e na abordagem $\phi - \phi$, em que as fases líquidas e vapor foram consideradas iguais.

$$f_i^L = f_i^V \tag{12}$$

Com,

$$f_i^V = y_i \phi_i^V P \tag{13}$$

$$f_i^L = x_i \phi_i^L P \tag{14}$$

Foi utilizado um método iterativo para resolver a Equação 12, que deve satisfazer simultaneamente duas restrições:

$$\sum_i x_i = 1 \tag{15}$$

$$\sum_i y_i = 1 \tag{16}$$

3.1.2. Equação Cubic Plus Association (CPA)

A equação CPA é composta pela clássica equação de Soave-Redlich-Kwong (SRK) e a associação com a termodinâmica estatística. A pressão é fornecida pela Equação 17 (KONTOGEORGIS et al., 1996, 1999):

$$P = \frac{RT}{V_m - b} - \frac{\mathrm{a}(T)}{V_m(V_m + b)} - \frac{1}{2}\frac{RT}{V_m}\left(1 + \rho\frac{\partial \ln g}{\partial \rho}\right)\sum_i x_i \sum_{A_i}\left(1 - X_{A_i}\right) \tag{17}$$

Em que, x_i é a fração molar do componente i e ρ é a densidade molar ($\rho = 1/V_m$). O parâmetro de energia física ($\mathrm{a}(T)$) é calculado utilizando a Equação 18:

$$\mathrm{a}(T) = \mathrm{a}_0\left(1 + c_1\left(1 - \sqrt{T_r}\right)\right)^2 \tag{18}$$

Com $T_r = \frac{T}{T_c}$, em que T_c é a temperatura crítica.

X_{A_i} representa a fração molar dos sítios A na molécula i que não foram ligados a outros sítios ativos, fornecida pela seguinte Equação:

$$X_{Ai} = \frac{1}{1 + \rho \sum_j x_j \sum_{B_j} X_{Bj} \Delta^{A_i B_j}} \tag{19}$$

Em que, $\Delta^{A_iB_j}$ é a força de associação dada pela Equação 20, que descreve os laços de associação entre duas moléculas diferentes com dois sítios ativos.

$$\Delta^{A_iB_j} = g(V_m)^{ref}\left[\exp\left(\frac{\varepsilon^{A_iB_j}}{RT}\right) - 1\right] b_{ij}\beta^{A_iB_j} \tag{20}$$

Na Equação 20, $\varepsilon^{A_iB_j}$ é a energia da associação, $\beta^{A_iB_j}$ é o volume de associação, e $g(V_m)^{ref}$ é a função de distribuição radial do fluido de referência (esferas rígidas) - definidas por Elliot; Suresh; Donohue, (1990) como:

$$g(V_m) = \frac{1}{1 - 1.9\eta} \tag{21}$$

Com,

$$\eta = \frac{1}{4} b\rho \tag{22}$$

$$b_{ij} = \frac{b_i + b_j}{2} \tag{23}$$

Portanto, são necessários cinco parâmetros para descrever um componente puro usando a CPA: a_0, b e c_1 na parte física, $\varepsilon^{A_iB_j}$ e $\beta^{A_iB_j}$ na parte da associação. O termo de co-volume b está presente em ambas as partes da equação. Esses parâmetros são otimizados por meio do ajuste de dados de pressão de vapor e/ou densidade líquida dentro de uma faixa de temperaturas desejadas. Para compostos não auto-associantes, os parâmetros otimizados são apenas os da equação SRK.

Para ampliar a CPA a misturas, são utilizadas regras de mistura convencionais no termo físico para a energia e o co-volume b. Para o parâmetro de energia $a_{ij}(T)$, é utilizada a seguinte regra de média geométrica:

$$\mathrm{a}(T) = \sum_i \sum_j x_i x_j \mathrm{a}_{ij}(T) \tag{24}$$

Com

$$\mathrm{a}_{ij}(T) = \sqrt{\mathrm{a}_i(T)\mathrm{a}_j(T)}\left(1 - k_{ij}\right) \tag{25}$$

Enquanto o co-volume b da mistura é dado por:

$$b = \sum_i x_i b_i \tag{26}$$

Se a mistura for formada por compostos não-associativos, o parâmetro de interação binária k_{ij} é o único parâmetro ajustável.

Embora o termo de associação não exija regras de mistura, as misturas que apresentam moléculas de associação cruzada requerem regras de combinação dos parâmetros de energia e volume de associação para calcular o valor da força de associação. As regras adequadas para a CPA foram a combinação das regras CR-1 e a de Elliott (VOUTSAS; YAKOUMIS; TASSIOS, 1999).

$$\varepsilon^{A_iB_j} = \varepsilon^{A_iB_i} + \varepsilon^{A_jB_j} \tag{27}$$

$$\beta^{A_iB_j} = \sqrt{\beta^{A_iB_i}\beta^{A_jB_j}} \tag{28}$$

$$\Delta^{A_iB_j} = \sqrt{\Delta^{A_iB_i}\Delta^{A_jB_j}} \tag{29}$$

Misturas em que apenas um composto tem ligações associativas, enquanto o outro permanece inerte são comuns, implicando apenas na ocorrência de ligações associativas. Folas et al., (2006) chamam tal processo de "solvatação", que descreve a indução da ligação de hidrogênio entre compostos de associação polar e compostos inertes da mistura. Estes casos consideram uma ligação de associação entre compostos polares e inertes, exigindo a otimização do parâmetro de volume ($\beta^{A_iB_j}$) a partir dos dados experimentais. O parâmetro de energia ($\varepsilon^{A_iB_j}$) é calculado utilizando a regra de combinação CR-1 modificada (FOLAS et al., 2006).

$$\varepsilon^{A_iB_j} = \frac{\varepsilon_{associating}}{2} \tag{30}$$

3.1.3. Determinação das propriedades necessárias dos ESs

Como os solventes eutéticos não estão presentes na base de dados do *software* Multiflash, é indispensável a sua inclusão por meio dos dados necessários. Para cada modelo termodinâmico utilizado, o Multiflash exige uma certa quantidade de dados do componente puro. Para a equação Peng-Robinson 78 são exigidas as propriedades críticas (pressão, temperatura e fator acêntrico), a massa molar do componente, a capacidade calorífica a pressão constante (Cp) do gás perfeito (caso não haja dados, pode ser considerada zero). Para a equação CPA são exigidas todas as propriedades descritas acima além da pressão de vapor (desconsiderada para os ESs), a densidade do líquido saturado e os parâmetros físicos e de associação ($a_0, b, c_1, \varepsilon, \beta$).

3.1.3.1. Correlação da densidade do líquido saturado

Para a determinação da correlação da densidade do líquido saturado (mol/m³) foi necessário inicialmente dados de densidade dos ESs a pressão atmosférica e em diversas temperaturas. Em seguida, de acordo com as opções oferecidas pelo Multiflash, escolhe-se uma correlação para que seja determinada a densidade calculada. Para este trabalho, escolheu-se a equação 100 da DIPPR:

$$\rho = a_1 + a_2 T + a_3 T^2 + a_4 T^3 + a_5 T^4 \tag{31}$$

Então, não se considerando os coeficientes a_4 e a_5, chutou-se valores para os demais coeficientes para o cálculo das densidades, os desvios absolutos médios (do inglês, *average absolute deviations*, %AARD) foram calculados (Equação 32), e através do suplemento Solver do Microsoft Excel, a média dos %AARDs foram minimizados utilizando a função objetivo indicada pela Equação 33 para encontrar os valores corretos dos parâmetros.

$$\%AARD(\rho) = \frac{|\rho^{exp} - \rho^{calc}|}{\rho^{exp}} \times 100 \tag{32}$$

$$OF = \min \left| \sum_{i=1}^{N_p} \left(\frac{\rho_i^{exp} - \rho_i^{calc}}{\rho_i^{exp}} \right) \right| \tag{33}$$

Em que, ρ_i^{cal} é a densidade calculada; ρ_i^{exp} é a densidade experimental e N_p é a quantidade de dados experimentais.

3.1.3.2. Cálculo das propriedades críticas dos ESs

Independentemente da EoS utilizada, a modelagem termodinâmica requer as propriedades críticas dos ESs - que não são facilmente encontradas na literatura. As propriedades críticas dos ESs foram calculadas utilizando o método modificado de Lydersen-Joback-Reid proposto por Valderrama e Rojas, (2009) (JOBACK E REID, 1987; LYDERSEN, 1955), e diferentes razões molares de HBA e HBD utilizando a regra de mistura Lee-Kesler (LYDERSEN, 1955). A pressão crítica e o volume foram calculados utilizando o método de Lydersen, enquanto a temperatura normal de ebulição e as temperaturas críticas foram calculadas utilizando o método Joback-Reid.

O método Joback de contribuição de grupo foi escolhido porque calcula propriedades críticas sem quaisquer dados experimentais e mostra boa precisão para moléculas de massa molar elevada, tais como os ESs. Além disso, os ESs foram preparados usando sais com natureza iônica semelhante à dos líquidos iônicos - tal como determinado com sucesso pelo método modificado Lydersen-Joback-Reid (SHAHBAZ et al., 2011; HAGHBAKHSH; RAEISSI, 2017; HAIDER et al., 2018).

O ponto de ebulição normal (T_b), a temperatura crítica (T_c), a pressão crítica (P_c) e o volume crítico (V_c) foram calculados para cada HBA e HBD como se segue:

$$T_b = 198.2 + \sum n\Delta T_{bM} \tag{34}$$

$$T_c = \frac{T_b}{[0.5703 + 1.0121 \sum n\Delta T_M - (\sum n\Delta T_M)^2]} \tag{35}$$

$$P_c = \frac{M}{(0.2573 + \sum n\Delta P_M)^2} \tag{36}$$

$$V_c = 6.75 + \sum n\Delta V_M \tag{37}$$

Em que, ΔT_{bM}, ΔT_M, ΔP_M e ΔV_M são constantes do método modificado Lydersen-Joback-Reid, M é a massa molecular (g.mol^{-1}), e n é o número de cada grupo de contribuição.

O fator acêntrico de cada HBA e HBD foi calculado de acordo com a equação proposta por Valderrama e Robles, (2007).

$$\omega = \frac{(T_b - 43)(T_c - 43)}{(T_c - T_b)(0.7T_c - 43)} \log\left(\frac{P_c}{P_b}\right) - \frac{(T_c - 43)}{(T_c - T_b)} \log\left(\frac{P_c}{P_b}\right) + \log\left(\frac{P_c}{P_b}\right) - 1 \tag{38}$$

Em que T_c é a temperatura crítica, P_c é a pressão crítica, T_b é a temperatura de ebulição normal e P_b é a pressão de ebulição normal (0,101325 MPa).

As propriedades críticas dos ESs foram calculadas pelas regras de mistura de Lee-Kesler, como se segue:

$$T_{cm} = \frac{1}{V_{cm}^{\frac{1}{4}}} \sum_i \sum_j y_i y_j V_{cm}^{\frac{1}{4}} T_{cij} \tag{39}$$

$$V_{cm} = \sum_i \sum_j y_i y_j V_{cij} \tag{40}$$

$$\omega_m = \sum_i y_i \omega_i \tag{41}$$

$$T_{cij} = \left(T_{ci} T_{cj}\right)^{\frac{1}{2}} k'_{ij} \tag{42}$$

$$V_{cij} = \frac{1}{8}\left(V_{ci}^{\frac{1}{3}} + V_{cj}^{\frac{1}{3}}\right)^3 \tag{43}$$

$$P_{cm} = 0.2905 - 0.085\omega_m \frac{RT_{cm}}{V_{cm}} \tag{44}$$

Em que, m está relacionado com a mistura e i e j com os componentes puros, y é a fração molar de cada componente, e k'_{ij} são os parâmetros binários. Devido à falta de dados experimentais, k'_{ij} foi considerado como 1.

3.1.3.3. Predição dos parâmetros da CPA para os ESs

Como mencionado no Tópico 3.1.2, são necessários cinco parâmetros para descrever os componentes puros: três parâmetros físicos (a_0, b, c_1), o volume ($\beta^{A_i B_j}$) e a energia ($\varepsilon^{A_i B_j}$). No entanto, estes parâmetros para os ESs não são facilmente encontrados na literatura.

Sendo assim, os parâmetros dos componentes puros foram determinados ajustando os seus dados à densidade líquida e à pressão de vapor numa faixa de temperaturas entre 293,15 e 343,15 K. Como a pressão de vapor dos ESs é insignificante, apenas os dados de densidade líquida foram considerados para otimizar os parâmetros da CPA. Embora vários estudos tenham determinado a solubilidade do CO_2 nos ESs, existem poucos dados na literatura que apresentam a densidade dos ESs numa grande faixa de temperatura, o que limita a determinação dos parâmetros da CPA que são necessários. Assim, os critérios de seleção dos ESs utilizados neste trabalho foram: existir tanto dados de densidade dos ESs como dados de solubilidade de CO_2 nos ESs.

Inicialmente, foram calculadas as densidades utilizando o *script* do Multiflash para a CPA que continha apenas as propriedades críticas e os parâmetros calculados para a densidade do líquido saturado, chutando assim valores para os cinco parâmetros da equação. Em seguida, os valores de %AARD entre os dados calculados e experimentais foram obtidos de acordo com a Equação 45.

$$AARD\% = \frac{1}{N_p}\sum_{i}^{N_p}\left|\frac{\rho_i^{cal} - \rho_i^{exp}}{\rho_i^{exp}}\right| \times 100 \quad (45)$$

Após o cálculo das densidades líquidas usando a programação do Multiflash, a soma dentro dos parênteses da Equação 45 foi minimizada usando uma função objetivo no Solver do Microsoft Excel (Equação 46), variando os parâmetros de modo a encontrá-los e consequentemente o valor da densidade líquida calculada.

$$OF = \min\left[\sum_{i=1}^{N_p}\left(\frac{\rho_i^{cal} - \rho_i^{exp}}{\rho_i^{exp}}\right)\right] \quad (46)$$

Os ESs foram modelados utilizando duas estratégias: (i) como componente pseudo-puro e (ii) como componente individual. Efetivamente utilizado na literatura (DIETZ et al., 2017; HAGHBAKHSH; RAEISSI, 2017; HAGHBAKHSH et al., 2021; RABHI; MUTELET; SIFAOUI, 2021) a abordagem pseudo-pura considera os ESs como um componente pseudo-puro com massa molar média calculada pela razão molar de HBA e HBD. Para garantir que a auto-associação de HBA e HBD formaria uma ligação de hidrogênio, foram atribuídos dois sítios de associação 2B para os ESs. A segunda estratégia consistiu em ajustar a densidade líquida de cada componente do ES (HBA e HBD), considerando tanto a auto-associação como a associação cruzada entre os HBAs e HBDs. Embora considerado como um componente inerte na maioria dos estudos, os esquemas de associação 2B e 4C foram também considerados para o CO_2 (TSIVINTZELIS et al., 2011; HAGHBAKHSH; RAEISSI, 2017). Como os estudos que abordam a solubilidade de CO_2 nos ESs são ainda incipientes na literatura, este estudo avança o conhecimento modelando a solubilidade de CO_2 nos ESs, considerando o CO_2 como inerte, com esquemas de associação 2B e 4C e também de solvatação.

A Figura 8 apresenta o fluxograma ilustrando o passo a passo do processo de cálculo dos AARDs% e da otimização dos parâmetros da CPA.

Figura 8. Fluxograma do processo de obtenção dos parâmetros da CPA para os ESs

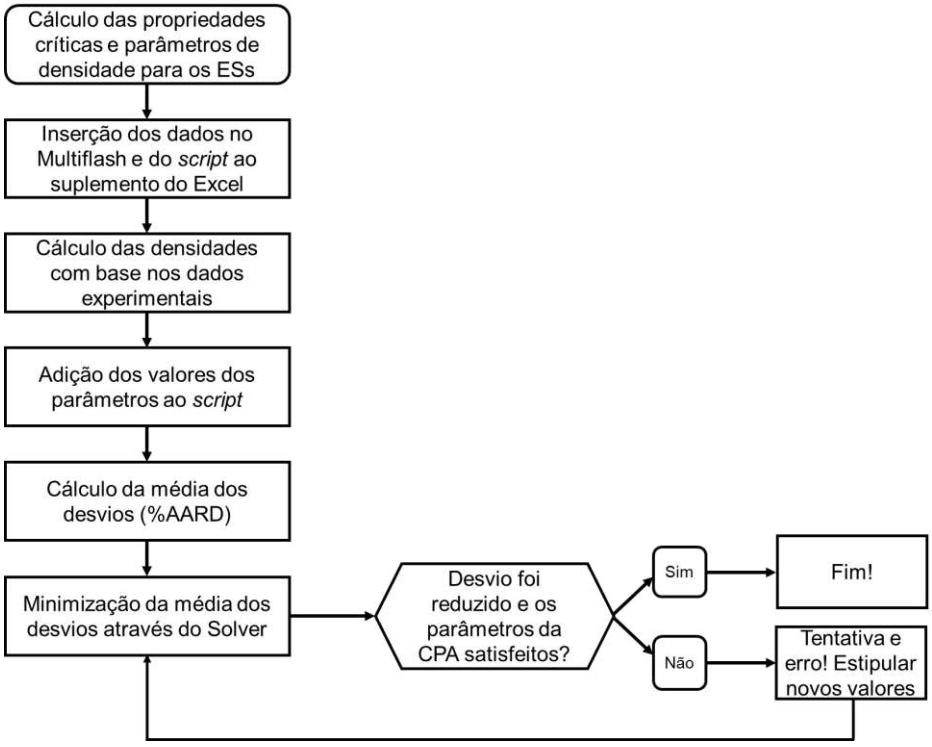

Fonte: Autoria própria

3.1.4. Modelagem da solubilidade do CO_2 nos ESs através das equações Peng-Robinson 78 e CPA

Para a modelagem da solubilidade do CO_2 nos ESs usando ambas as equações de estado foram utilizadas a mesma abordagem. Entretanto, enquanto a equação de Peng-Robinson 78 dispensa os dados experimentais de densidade e/ou pressão de vapor dos pseudo-componentes ESs, exigindo apenas as suas propriedades críticas, a equação CPA exige esses dados além dos seus 5 parâmetros anteriormente citados.

Os dados experimentais foram modelados considerando duas hipóteses para o parâmetro de interação binária (k_{ij}), nomeadamente: (i) $k_{ij} = 0$ e (ii) considerando uma tendência linear de k_{ij} com a temperatura (Equação 47), caso em que o parâmetro foi ajustado aos dados calculados de solubilidade, com os valores dos coeficientes (a_0 e a_1).

$$k_{ij} = a_0 + a_1 T \tag{47}$$

k_{ij} é o parâmetro de interação binária, a_0 e a_1 são as constantes e T é a temperatura em Kelvin.

Sendo assim, utilizando os dados experimentais de solubilidade, temperatura e pressão, determinou-se os valores de pressão calculados através do *script* do Multiflash, adotando valores para os parâmetros a_0 e a_1. Em seguida, calculou-se o %AARD de acordo com a Equação 48, e por fim utilizou-se uma função objetivo (Equação 49) para minimizar os desvios, encontrando assim os valores para o k_{ij} dependente da temperatura.

$$AARD\% = \frac{1}{N_p}\sum_{i}^{N_p}\left|\frac{P_i^{exp} - P_i^{calc}}{P_i^{exp}}\right| \times 100 \tag{48}$$

$$OF = \min\left[\sum_{i=1}^{N_p}\left(\frac{P_i^{exp} - P_i^{calc}}{P_i^{exp}}\right)\right] \tag{49}$$

Em que N_pé o número de dados experimentais, P_i^{exp}é a pressão experimental, e P_i^{calc} é a pressão calculada pelo Multiflash.

Essa metodologia foi utilizada tanto para o ES como um pseudo-componente quanto para o ES como um componente individual. A única diferença é que para o pseudo-componente tem-se um único k_{ij} e para o componente individual, o sistema é considerado um ternário, e, portanto, possui três k_{ij} (k_{12} , k_{13}, k_{23}).

A Figura 9 apresenta o fluxograma ilustrando o passo a passo do processo de cálculo dos AARDs% e da otimização dos valores de k_{ij}.

Figura 9. Fluxograma do processo de obtenção dos valores de k_{ij} para os sistemas CO_2+ESs

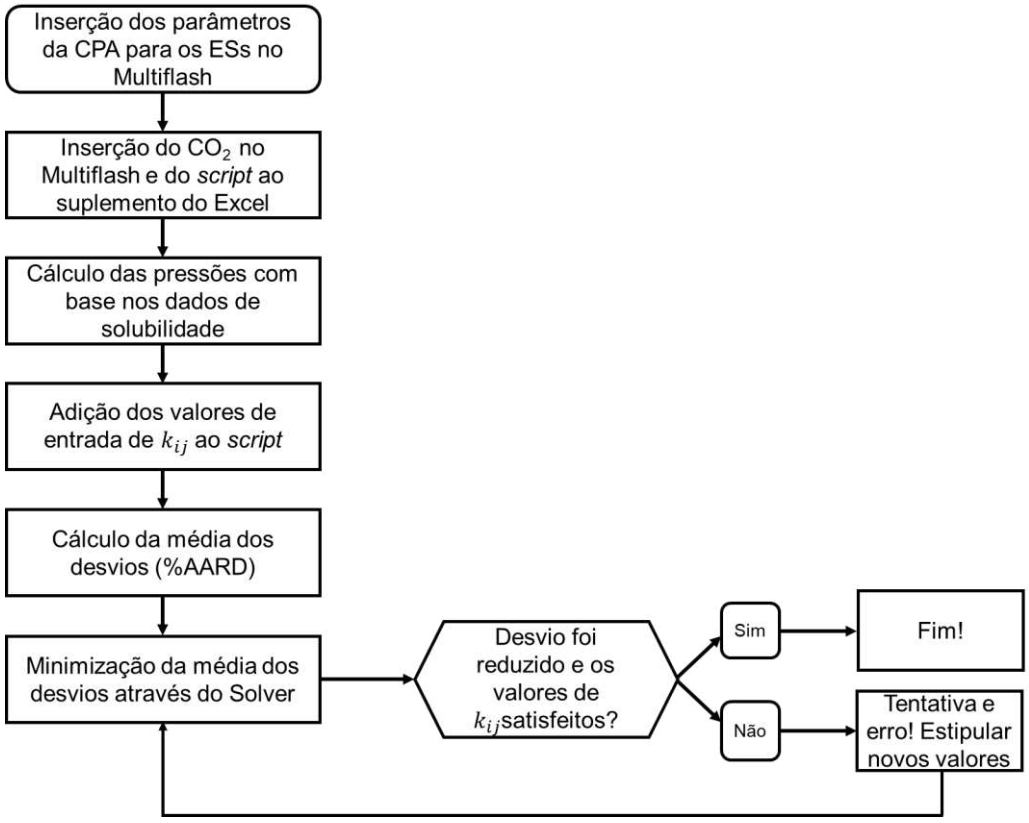

Fonte: Autoria própria

3.2. Modelagem termodinâmica utilizando o COSMO-RS

O COSMO-RS (do inglês, *Conductor-like Screening Model for Realistic Solvents*) é um software que calcula as propriedades termodinâmicas de fluidos e soluções com base em dados mecânicos quânticos. As propriedades do COSMO-RS têm poder de previsão fora do conjunto de parametrização, em oposição aos modelos empíricos. Ele prediz instantaneamente propriedades termodinâmicas, como solubilidade, coeficientes de partição e de atividade, pressão de vapor, diagramas de equilíbrio líquido-vapor de misturas binárias e ternárias (ELV/ELL), energias de excesso, azeótropos, entre outros.

Ele é um modelo termodinâmico preditivo que combina o modelo de solvatação dielétrica contínua conhecido como COSMO e a termodinâmica estatística (KLAMT, 1995). Neste sentido, o COSMO-RS utiliza a interação entre uma cavidade contendo uma molécula e um meio dielétrico, gerado através de cálculos baseados na Teoria Funcional da Densidade Química Quântica (DFT), como um estado de referência a partir do qual as energias de interação entre as moléculas podem ser inferidas (KLAMT, 2005). Através da termodinâmica estatística, a definição de um conjunto de

pequenos segmentos de superfície de diferentes moléculas interagindo entre si, juntamente com o estabelecimento de uma função de partição, a partir da qual a energia de Gibbs do sistema pode ser derivada, permite o cálculo das propriedades da solução a partir do COSMO-RS (KLAMT, 2005).

De fato, o contato entre as moléculas no estado de referência do COSMO provoca o aparecimento de energias de interação, que contribuem para a energia global de Gibbs. A partir da energia de Gibbs, é possível derivar potenciais químicos, permitindo assim ao COSMO-RS calcular os equilíbrios termodinâmicos. O modelo, em essência, depende apenas da geometria da molécula e da densidade da carga de polarização para determinar as condições de equilíbrio dos sistemas multicomponentes, o que constitui uma vantagem notável sobre as abordagens empíricas ou semiempíricas. Para calcular a solubilidade dos gases, o modelo aplica um procedimento interativo, em que para cada componente j, a sua fração molar (x_j) é variada até a sua pressão parcial (p_j) seja igual a um valor de porosidade parcial de referência (imputado ao COSMO-RS). Cada pressão parcial do componente é descrita pela Equação 50 (COSMOTHERM, 2021a).

$$p_j = p_j^0 x_j \gamma_j \qquad (50)$$

Em que, p_j^0 e γ_j são a pressão de vapor e o coeficiente de atividade do componente j, respectivamente.

O presente trabalho, visou avaliar o potencial do COSMO-RS para representar dados de solubilidade de CO_2, CH_4 e H_2S em 17 ESs baseados em ChCl encontrados na literatura, a 313,15 K, e na faixa de pressão entre 1 e 125 bar, conforme apresentado no Capítulo 5: *"Prediction of greenhouse gas solubility in Eutectic Solvents using COSMO-RS".* Além disso, foi investigado o efeito de três razões molares diferentes do ES composto por ChCl e ureia na solubilidade do CO_2, CH_4 e H_2S.

Para isso, o software COSMOtherm (versão 21.0) (COSMOTHERM, 2021b) com o nível de parametrização BP_TZVPD_FINE_21.ctd foi aplicado para estimar os dados de solubilidade dos gases do efeito de estufa nos solventes eutéticos. Todos os arquivos *.cosmo* necessários para os gases e alguns precursores dos ESs (fenol, etilenoglicol e glicerol) foram recuperados da base de dados COSMOtherm TZVPD-FINE. Para o ChCl e todos os HBDs em falta na base de dados, os ficheiros de entrada foram obtidos com o software COSMOconfX 2021 acoplado ao pacote TmoleX

(versão 4.5) utilizando o modelo BP-TZVPD-FINE-COSMO+GAS_18 (STEFFEN et al., 2010). O ChCl foi tratado seguindo a abordagem da mistura eletroneutra (DIEDENHOFEN; KLAMT, 2010), e os dados de solubilidade previstos foram corrigidos para os dados de solubilidade à escala laboratorial (COSMOTHERM, 2021a). Detalhes adicionais para o procedimento de cálculo da solubilidade de gás com o COSMOtherm estão disponíveis no manual de referência do *software* (COSMOTHERM, 2021a). Além disso, todos os conformadores de cada molécula foram considerados nas simulações.

Referências bibliográficas

ABBOTT, A. P. et al. Novel solvent properties of choline chloride / urea mixtures. **The Royal Society of Chemistry**, v. 1, p. 70–71, 2003.

COSMOTHERM, B. **Reference manual**. [s.l: s.n.].

COSMOTHERM, B. **Release 2021**. [s.l: s.n.]. Disponível em: <http://www.3ds.com>.

CRESPO, E. A. et al. The Role of Polyfunctionality in the Formation of [Ch]Cl-Carboxylic Acid-Based Deep Eutectic Solvents. **Industrial and Engineering Chemistry Research**, v. 57, n. 32, p. 11195–11209, 2018.

DALMOLIN, I. A. L. **Uso de sementes de uva, um resíduo da agroindústria vinícula, empregando tecnologias supercríticas**. 2013. Universidade Estadual de Campinas, 2013.

DIEDENHOFEN, M.; KLAMT, A. COSMO-RS as a tool for property prediction of IL mixtures—A review. **Fluid Phase Equilibria**, v. 294, n. 1–2, p. 31–38, jul. 2010. Disponível em: <https://linkinghub.elsevier.com/retrieve/pii/S0378381210000695>.

DIETZ, C. H. J. T. et al. PC-SAFT modeling of CO2 solubilities in hydrophobic deep eutectic solvents. **Fluid Phase Equilibria**, v. 448, p. 94–98, 2017. Disponível em: <http://dx.doi.org/10.1016/j.fluid.2017.03.028>.

ELLIOT, R. J.; SURESH, S. J.; DONOHUE, M. D. A Simple Equation of State for Nonspherical and Associating Molecules. **Industrial and Engineering Chemistry Research**, v. 29, p. 1476–1485, 1990.

FOLAS, G. K. et al. Application of the cubic-plus-association equation of state to mixtures with polar chemicals and high pressures. **Industrial and Engineering Chemistry Research**, v. 45, p. 1516–1526, 2006.

HAGHBAKHSH, R. et al. Experimental investigation of carbon dioxide solubility in the deep eutectic solvent (1 ChCl + 3 triethylene glycol) and modeling by the CPA EoS. **Journal of Molecular Liquids**, v. 330, p. 1–12, 2021. Disponível em: <https://doi.org/10.1016/j.molliq.2021.115647>.

HAGHBAKHSH, R.; RAEISSI, S. Modeling the Phase Behavior of Carbon Dioxide Solubility in Deep Eutectic Solvents with the Cubic Plus Association Equation of State. **Journal of Chemical and Engineering Data**, v. 63, p. 897–906, 2017.

HAIDER, M. B. et al. Thermodynamic and Kinetic Studies of CO2 Capture by Glycol and Amine-Based Deep Eutectic Solvents. **Journal of Chemical and Engineering Data**, v. 63, p. 2671–2680, 2018.

JOBACK, K. G.; REID, R. C. Estimation of Pure-Component Properties from Group-Contributions. **Chemical Engineering Communications**, v. 57, p. 233–243, 1987.

KLAMT, A. Conductor-like screening model for real solvents: A new approach to the quantitative calculation of solvation phenomena. **Journal of Physical Chemistry**, v. 99, n. 7, p. 2224–2235, 1995.

KLAMT, A. **COSMO-RS From Quantum Chemistry to Fluid Phase Thermodynamics and Drug Design**. 1st Editio ed. [s.l.] Elsevier Science, 2005.

KONTOGEORGIS, G. M. et al. An Equation of State for Associating Fluids. **Industrial and Engineering Chemistry Research**, v. 35, p. 4310–4318, 1996.

KONTOGEORGIS, G. M. et al. Multicomponent phase equilibrium calculations for water–methanol–alkane mixtures. **Fluid Phase Equilibria**, v. 158–160, p. 201–209, jun. 1999. Disponível em: <https://linkinghub.elsevier.com/retrieve/pii/S0378381299000606>.

LANZA, M. **Comportamento de Fases dos Óleos de Oliva, Soja e Mamona em n-Butano e Propano a Alta Pressão**. 2004. URI-Campus de Erechim, Erechim/RS, 2004.

LYDERSEN, A. L. **Estimation of critical properties of organic compounds by the method of group contibutions**. [s.l: s.n.].

MIRZA, N. R. et al. Experiments and Thermodynamic Modeling of the Solubility of Carbon Dioxide in Three Different Deep Eutectic Solvents (DESs). **Journal of Chemical and Engineering Data**, v. 60, p. 3246–3252, 2015.

NDIAYE, P. M. **Equilíbrio de Fases de Óleos Vegetais e de Biodiesel em CO2, Propano e n- Butano**. 2004. Universidade Federal do Rio de Janeiro, Escola de Química, Rio de Janeiro/RJ, 2004.

PENG, D. Y.; ROBINSON, D. B. A New Two-Constant Equation of State. **Industrial and Engineering Chemistry Fundamentals**, v. 15, p. 59–64, 1976.

PENG, D. Y.; ROBINSON, D. B. **The Characterization of the Heptanes and Heavier**

Fractions for the GPA Peng-Robinson Programs. [s.l.] Gas Processors Association, 1978.

RABHI, F.; MUTELET, F.; SIFAOUI, H. Solubility of Carbon Dioxide in Carboxylic Acid-Based Deep Eutectic Solvents. **Journal of Chemical and Engineering Data**, v. 66, p. 702–711, 2021.

SHAHBAZ, K. et al. Prediction of deep eutectic solvents densities at different temperatures. **Thermochimica Acta**, v. 515, n. 1–2, p. 67–72, 2011. Disponível em: <http://dx.doi.org/10.1016/j.tca.2010.12.022>.

SILVA, L. P. et al. Eutectic Mixtures Based on Polyalcohols as Sustainable Solvents: Screening and Characterization. **ACS Sustainable Chemistry & Engineering**, v. 8, n. 40, p. 15317–15326, 12 out. 2020. Disponível em: <https://pubs.acs.org/doi/10.1021/acssuschemeng.0c05518>.

STEFFEN, C. et al. TmoleX-A graphical user interface for TURBOMOLE. **Journal of Computational Chemistry**, v. 31, p. 2967–2970, 19 ago. 2010. Disponível em: <https://onlinelibrary.wiley.com/doi/10.1002/jcc.21576>.

THOMSON, G. H.; BROBST, K. R.; HANKINSON, R. W. An improved correlation for densities of compressed liquids and liquid mixtures. **AIChE Journal**, v. 28, n. 4, p. 671–676, 1982.

TSIVINTZELIS, I. et al. Modeling phase equilibria for acid gas mixtures using the CPA equation of state. Part II: Binary mixtures with CO2. **Fluid Phase Equilibria**, v. 306, p. 38–56, 2011. Disponível em: <http://dx.doi.org/10.1016/j.fluid.2011.02.006>.

VALDERRAMA, J. O.; ROBLES, P. A. Critical properties, normal boiling temperature, and acentric factor of another 200 ionic liquids. **Industrial and Engineering Chemistry Research**, v. 46, p. 1338–1344, 2007.

VALDERRAMA, J. O.; ROJAS, R. E. Critical properties of ionic liquids. Revisited. **Industrial and Engineering Chemistry Research**, v. 48, p. 6890–6900, 2009.

VOUTSAS, E. C.; YAKOUMIS, I. V.; TASSIOS, D. P. Prediction of phase equilibria in water/alcohol/alkane systems. **Fluid Phase Equilibria**, v. 158–160, p. 151–163, jun. 1999. Disponível em: <https://linkinghub.elsevier.com/retrieve/pii/S0378381299001314>.

CAPÍTULO 4

Carbon Dioxide Solubility in Deep Eutectic Solvents: Modelling using Cubic Plus Association and Peng-Robinson Equations of State

(Artigo publicado na *Process Safety and Environmental Protection*
DOI: 10.1016/j.psep.2022.04.075)

Fernanda Paludetto Pelaquim[a], Raphaela Gabrí Bitencourt[b], Antonio Marinho Barbosa Neto[c], Irede Angela Lucini Dalmolin[d], Mariana Conceição da Costa[a2*].

[a] School of Chemical Engineering, University of Campinas – UNICAMP, Avenida Albert Einstein 500, ZIP Code 13083-852, Campinas, SP, Brazil

[b] Goiano Federal Institute – IF Goiano, Estrada Sul Gôiana Highway, ZIP Code 75901970, Rio Verde, GO, Brazil

[c] ThermoPhase, Petroleum Engineering Department, State University of Santa Catarina – UDESC, Avenida Lourival Cesário Pereira, ZIP Code 88336-275, Balneário Camboriú, SC, Brazil

[d] Academic Department of Engineering, Universidade Tecnológica Federal do Paraná (UTFPR), Linha Santa Bárbara, ZIP Code 85601-970, Francisco Beltrão, PR, Brazil

2 * Corresponding author.

E-mail address: mcdcosta@unicamp.br (M.C. Costa)

phone number: +551935213962.

Abstract

Carbon Dioxide (CO_2) is the greenhouse gas that most contributes to global warming and climate change due to fossil fuels combustion, transportation, and other industrial process. Carbon capture, storage, and utilization (CCSU) is an effective method to reduce CO_2 emission. Chemical absorption is the most straightforward technology for post-combustion CO_2, and monoethanolamine (MEA) has been proved to be the most efficient chemical solvent. However, MEA is not environment friend, thus indicating the need for developing eco-friendly absorbers for CO_2 capture, such as Deep Eutectic Solvents (DESs). Despite recent experimental studies investigating CO_2 solubility in DESs, thermodynamic modelling is important to understand the system behavior. Thus, this study modelled CO_2 solubility in thirteen DESs found in a large range of temperature (from 303.15 to 343.15 K) and pressure range (from 0.06 to 12 MPa). Cubic-Plus Association (CPA) and Peng-Robinson equations of state were used to compare efficiency. The results indicate that fitting the binary interaction parameter (k_{ij}) promotes a better reproduction result than considering k_{ij} equals zero Despite all association schemes of CO_2 providing accurate results, the 4C association scheme (two electron acceptors and two electron donors) resulted in better equilibrium description. Both models describe experimental data very well, yet the individual component presents better results than pseudo-component approach, corroborating with DESs definition.

Keywords: Carbon Dioxide; Carbon capture, storage, and utilization; Deep Eutectic Solvents; Cubic-Plus Association; CO_2 solubility.

1. Introduction

The increase of CO_2 atmospheric levels is associated with human population growth and dependency on commercial energy. Most global CO_2 emissions come from the fossil fuels (Abdelkareem et al., 2018; Elsaid et al., 2020; Li et al., 2020). The imbalance in the CO_2 cycle caused by fossil fuels combustion for transportation, and other industrial processes increased pre-industrial atmospheric CO_2 levels from 280 ppm to around 411 ppm in 2020. Greenhouse gases (GHGs) emissions has increased the global temperature by 1 °C when compared with pre-industrial levels, showing its effects on sea levels, floods, droughts, and infectious diseases (Joshi et al., 2011).

In this context, the Paris Agreement aims to hold global average temperature increase, cutting CO_2 emissions by at least 40% by 2030 compared to 1990 (2030 climate & energy framework). For that, negative anthropogenic CO_2 emissions must be reduced by 45% until 2030 and reach zero emissions around 2050 (IPCC, 2018; Pachauri et al., 2014). In an attempt to reduce the negative effects of fossil fuels on the environment, a number of researches have investigated cost-effective renewable energy sources (Mohamed et al., 2017) and process with low or no environmental impacts (Rabaia et al., 2021).

Carbon capture, storage and utilization (CCSU) likewise comprises an effective method to reduce CO_2 emissions and it is a potentially scalable technology (Tapia et al., 2016; Zhang et al., 2020), which consists of separating and transporting CO_2 produced industrially to be stored in a safe place and converted into more valuable substances or products.

Nowadays, CCSU technologies can absorb around 85–95% of CO_2 produced by a power plant. CO_2 can be captured by three different methods; these are: (i) post-combustion, (ii) pre-combustion, and (iii) oxy-fuel combustion (Deng et al., 2015; Pires

et al., 2011; Sarmad et al., 2017; Schmelz et al., 2020; Tapia et al., 2016; Wilberforce et al., 2021). Post-combustion is the most used capture system due to its relative ease to retrofit and remove CO_2 from burning fossil fuel through physical or chemical absorption/adsorption mechanisms (Ben-Mansour et al., 2016; Chao et al., 2021).

Absorption is the most straightforward technology among post-combustion ones, which separate CO_2 from flue gas by using a regenerable liquid sorbent (Leung et al., 2014; Li et al., 2020). Monoethanolamine (MEA) is an affordable absorber with high reactivity and selectivity (Aaron and Tsouris, 2005), low cost, abundant solvent, uncomplicated retrofitting (Sultan et al., 2021), thus being considered the most effective chemical solvent to capture CO_2 by chemical absorption showing efficiency over 90% (Abdul Halim et al., 2015; Aroonwilas and Veawab, 2004). However, MEA may promote degradation, causing solvent loss, equipment corrosion, and volatile organic compounds (VOCs) emission. Moreover, amine emissions promote a series of implication to both the environment and human health (Akbari and Valeh-e-Sheyda, 2019; Leung et al., 2014; Rochelle, 2012). Thus, studies must develop eco-friendly and cost-effective absorbers for capturing CO_2 and replacing aqueous amine solutions, such as Deep Eutectic Solvents (DESs) (Ghaedi et al., 2020; Haider et al., 2020; Li et al., 2008; Rabhi et al., 2021; Sarmad et al., 2020; Zubeir et al., 2018).

DESs are a mixture composed of two or more pure compounds, including hydrogen-bond acceptors (HBAs) and hydrogen-bond donors (HBDs), whose eutectic point temperature is below that of an ideal liquid mixture (Martins et al., 2018). These low-cost solvents present good biodegradability and low toxicity, besides being easy to prepare and producing very little byproduct generation. Moreover, DESs also have high thermal and chemical stability, task-specificity, non-flammability, and negligible vapor pressures (Hansen et al., 2021; Krishnan et al., 2020; Song et al., 2020). HBA

and HBDs enable an immense number of combinations, so that DESs may be used in several different applications, such as gas capture and separation (Gu et al., 2020; Haghbakhsh et al., 2021; Haider and Kumar, 2020; Rabhi et al., 2021).

Over the years, several studies sought to determine experimentally the solubility of CO_2 in different DESs, considering distinct techniques, HBAs and HBDs, molar ratio, temperature and pressure range (Aboshatta and Magueijo, 2021; Ansarypur et al., 2022; Cichowska-Kopczyńska et al., 2021; Gu et al., 2020; Haghbakhsh et al., 2021; Haider et al., 2021; Liu et al., 2022; Pishro et al., 2021; Qin et al., 2021; Rabhi et al., 2021). However, thermodynamic modelling is crucial for providing a better understanding about the system behavior. According to a review conducted by Pelaquim et al., (2021), articles containing experimental and modeling data are a minor parcel of the literature, accounting for 23% of the published papers.

Some studies have addressed the thermodynamic modelling of CO_2 solubility in DESs, most of which used Perturbed Chain-Statistical Associating Fluid Theory (PC-SAFT) (Dietz et al., 2017; Rabhi et al., 2021; Zubeir et al., 2016) or Peng-Robinson equations of state (Ali et al., 2014; Haider et al., 2019, 2018; Haider and Kumar, 2020; Mirza et al., 2015). Haider and Kumar, (2020) determined CO_2 solubility in amine-based DESs using Non-Random Two liquids (NRTL) model and Peng-Robinson equation of state to predict experimental data. The results indicate a better fit for NRTL than Peng-Robinson. However, studies modelling experimental data of systems formed by DESs are still scarce in the literature, so that model results cannot be used to predict CO_2 solubility in any type of DESs.

To expand the thermodynamic modelling of CO_2 solubility in DESs and provide a better understanding on CO_2 and DES behavior in the mutual solubility, it could also consider the Cubic-Plus Association equation of state (CPA EoS). Based on the

combination of: the classic Soave–Redlich–Kwong (SRK) EoS with the association term from statistical thermodynamics, which considers the presence of compounds capable of hydrogen bonding (Kontogeorgis et al., 1996), this equation describe the complex equilibria behavior of mixtures formed by hydrocarbons, polar and associating compounds (Kontogeorgis and Folas, 2009). Only two studies in the literature - both from Haghbakhsh et al., (2021) and Haghbakhsh and Raeissi, (2017) - model CO_2 solubility in DES using CPA EoS and showing good results when compared to experimental data.

In this study, it was used the CPA and Peng-Robinson 78 EoS to describe the behavior of 13 binary mixtures found in literature (from Deng et al., (2016); Ji et al., (2016); Leron et al., (2013); Leron and Li, (2013b, 2013a); Li et al., (2014) and Wang et al., (2019)) formed by DES and CO_2 in a large temperature (303.15–343.15 K) and pressure range (0.06–12 MPa), using the pseudo-component and individual component approaches. Experimental data was not accompanied by modeling results on the original paper. This work used Multiflash software from KBC that has a comprehensive PVT (pressure, volume, temperature) and physical properties package that quickly and reliably allows the complete modeling of the phase behavior of complex mixtures and pure substances through equations of state. Thus, the needed parameters were adjusted from experimental data to both models (CPA and Peng-Robinson 78).

2. Model Description

2.1. Peng-Robinson Equation of State

CO_2 solubility in DESs was modelled using the Peng-Robinson EoS (Mirza et al., 2015; Peng and Robinson, 1976), defined as follows:

$$P = \frac{RT}{V_m - b} - \frac{a(T)}{V_m(V_m + b) + b(V_m - b)} \quad (1)$$

where V_m is the molar volume, T is the temperature, P is the pressure, and R is the universal gas constant. The physical energy parameter a and co-volume parameter b are functions of the critical properties - temperature (T_c) and pressure (P_c). More details of Peng-Robinson EoS are presented in the Supporting Information.

The component i fugacity coefficient can be calculated by:

$$\phi_i = \exp\left[(Z-1)\frac{b_i}{B} - \ln(Z-B) - \frac{A}{2\sqrt{2}B} \times \left(\frac{2\sum_j y_i a_{ij}}{A} - \frac{b_i}{B}\right) \ln\left(\frac{Z + \left(1+\sqrt{2}\right)B}{Z + \left(1+\sqrt{2}\right)B}\right)\right] \quad (2)$$

Individual fugacities were determined based on fugacities coefficients and $\phi - \phi$ approach, whereby liquid and vapor phases were considered as equal.

$$f_i^L = f_i^V \quad (3)$$

with,

$$f_i^V = y_i \phi_i^V P \quad (4)$$

$$f_i^L = x_i \phi_i^L P \quad (5)$$

An iterative method was used to solve Equation (3), which must simultaneously satisfy two constraints:

$$\sum_i x_i = 1 \tag{6}$$

$$\sum_i y_i = 1 \tag{7}$$

2.2. Cubic-Plus Association Equation of State

The CPA equation is composed by the classic SRK equation and the association from statistical thermodynamics. Pressure is provided by Equation (8) (Kontogeorgis et al., 1999, 1996):

$$P = \frac{RT}{V_m - b} - \frac{\mathrm{a}(T)}{V_m(V_m + b)} - \frac{1}{2}\frac{RT}{V_m}\left(1 + \rho\frac{\partial \ln g}{\partial \rho}\right)\sum_i x_i \sum_{A_i}\left(1 - X_{A_i}\right) \tag{8}$$

where x_i is the molar fraction of component i and ρ is the molar density ($\rho = 1/V_m$). All details of CPA EoS are presented in the Supporting Information.

2.2.1. CPA parameter estimation for DESs

As mentioned in the Supporting Information, five parameters are required to describe pure components: three physical parameters (a_0, b, c_1), the volume ($\beta^{A_iB_j}$) and energy ($\varepsilon^{A_iB_j}$). However, these parameters for DESs are often unavailable in the literature.

Pure-component parameters were determined by fitting their data to liquid density and vapor pressure in a 293.15 – 343.15 K temperature range, k_{ij} was fitted to VLE (DES + CO_2) in a given of pressure and temperature range. As the vapor pressure of DESs is insignificant, only liquid density data were considered to optimize their CPA parameters. Although several studies have determined the solubility of CO_2 in DESs, there are a few in literature that present the density of DESs in a range of

temperature, which limit the determination of the CPA parameters that are needed. Thus, the criteria for selecting the DESs used in this work were: to have both data of DESs density and data of CO_2 solubility in DESs

DESs were modelled using two strategies: (i) the pseudo-pure component and (ii) the individual component. Effectively used in the literature (Dietz et al., 2017; Haghbakhsh et al., 2021; Haghbakhsh and Raeissi, 2017; Rabhi et al., 2021), the pseudo-pure approach considers DESs as a pseudo-pure component with average molar mass calculated by the molar ratio of HBA and HBD. To guarantee that the HBA and HBD self-association would form a hydrogen bond, two association sites of 2B scheme were assigned for DESs. The second strategy consists of fitting the liquid density of each DES component (HBA and HBD), except glycerol and ethylene glycol, considering both the self - and cross-association between HBA and HBD. Although deemed as an inert component in most studies, the 2B or 4C association schemes were also considered for CO_2 (Haghbakhsh and Raeissi, 2017; Tsivintzelis et al., 2011). As studies addressing CO_2 solubility in DESs are still incipient in the literature, this study advances knowledge by modelling CO_2 solubility in DESs considering this element as inert, with 2B and 4C association schemes and solvation too.

2.3. DESs' critical properties

Regardless of the EoS used, thermodynamic modelling requires DESs critical properties — which are not easily found in the literature. Critical properties of ionic liquids were calculated using the modified Lydersen−Joback−Reid method proposed by Valderrama and Rojas, (2009) (Joback and Reid, 1987; Lydersen, 1955;), and different molar ratios of HBA and HBD using the Lee-Kesler mixing rule (Lydersen, 1955). Critical pressure and volume were calculated using the Lydersen

method, while normal boiling and critical temperatures were calculated using the Joback–Reid method.

The Joback group-contribution method was choose because it calculates critical properties without any experimental data and shows good accuracy for high-mass molecules such as DESs. Moreover, DESs were prepared using salts with similar ionic nature to ionic liquids — as successfully determined by the modified Lydersen−Joback−Reid method (Haghbakhsh and Raeissi, 2017; Haider et al., 2018; Shahbaz et al., 2011). All calculation report is detailed in Supporting Information.

3. Results and Discussion

Table 1 presents a comparison between the most used models to predict the CO_2 solubility in DESs, including CPA EoS. The information of Table 1 is regarding the application of each model and its ability to predict the density of DESs and the CO_2 solubility in DESs. It is possible to observe that all models are capable of predict the CO_2 solubility. Thus, the models can be used in a very pragmatic approach to screen DESs for prediction of CO_2 solubilities in them, saving time compared to experimental methods, for example. In this work, CPA EoS was used in order to increase knowledge about its prediction, since only two studies used this model.

Table 5. Comparison between NRTL, Peng-Robinson (PR), PC-SAFT and CPA models concerning their ability to predict the density of DESs and the CO_2 solubility in DESs.

Model	Application	Ability to predict density of DESs	Ability to predict CO_2 solubility in DESs
NRTL	Based on the local composition concept, NRTL is useful to partially miscible systems, to describe LLE data (Maximo et al., 2019; Renon and Prausnitz, 1968)	NOT APPLICABLE [a]	Kamgar et al.,(2017) and Haider and Kumar, (2020) indicated that NRTL model can predicts the CO_2 solubility in DESs at all ranges of temperature and pressure, better than COSMO-RS and PR, with %AARD no longer than 4.20
Peng-Robinson	PR is suitable to predict the density of systems containing hydrocarbons, water, air, and combustion gases, and to estimate the VLE data (Ali et al., 2014; Peng and Robinson, 1976)	NOT APPLICABLE [a]	Ali et al., (2014); Haider et al., (2020, 2018) and Haider and Kumar, (2020) showed that there is a good agreement between experimental and calculated results using PR.
PC-SAFT	PC-SAFT has been used for systems containing polar, nonpolar and associating compounds (Gross and Sadowski, 2001; Zubeir et al., 2016)	The comparison between the density of DESs calculated using PC-SAFT and the experimental data showed %AARDs no longer than 0.06 from Zubeir et al., (2016); 0.15 for Dietz et al., (2017); and 0.01 for Rabhi et al., (2021)	Dietz et al., (2017); Rabhi et al., (2021) and Zubeir et al., (2016) used PC-SAFT and proved that the model can represent CO_2 solubility in DESs with good accuracy.
CPA	CPA can be used to calculate the phase equilibria of binary and multicomponent systems containing different inert and/or associating compounds, in a broad range of thermodynamic conditions (Kontogeorgis et al., 1996; Oliveira et al., 2011)	The comparison between the density of DESs calculate by CPA and the experimental data result in a %AARD is no longer than 0.35 according to Haghbakhsh and Raeissi, (2017)	According to Haghbakhsh and Raeissi, (2017), CPA is a suitable model to predict the density of mixtures involving CO_2 and DESs, with %AARD no longer than 19.30

a Peng Robinson and NRTL models does not require density data to describe CO_2 solubility.

Table 2 presents CO_2 solubilities in DESs within a wide temperature (303.15–343.15 K) and pressure range (0.063–11.820 MPa) used in this work, considering 353 experimental data found in the literature.

Table 6. CO_2 solubilities, temperature, and pressure ranges of the studied DESs.

DES (2B)	Temperature range (K)	Pressure range (MPa)	CO_2 solubility range (x_1)	N_p	Ref.
ChCl:Ethylene glycol 1:2	303.15 – 343.15	0.236 – 6.323	0.006 – 0.275	40	(Leron and Li, 2013a)
ChCl:Urea 1:2	303.15 – 343.15	0.299 – 5.911	0.017 – 0.384	34	(Leron et al., 2013)
ChCl:Phenol 1:3	293.15 – 333.15	0.104 – 11.820	0.003 – 0.274	27	(Ji et al., 2016; Li et al., 2014)
ChCl:Glycerol 1:2	303.15 – 343.15	0.187 – 6.347	0.006 – 0.398	40	(Leron and Li, 2013b)
TBPB:Phenol 1:4	313.15 – 333.15	0.164 – 1.578	0.018 – 0.205	18	(Wang et al., 2019)
TBPB:Diethylene glycol 1:4	313.15 – 333.15	0.094 – 1.398	0.013 – 0.212	18	(Wang et al., 2019)
ATPPB:Phenol 1:4	313.15 – 333.15	0.183 – 1.345	0.020 – 0.213	18	(Wang et al., 2019)
ATPPB:Phenol 1:6	313.15 – 333.15	0.160 – 1.387	0.021 – 0.195	18	(Wang et al., 2019)
ACC:Levulinic acid 1:3	303.15 – 333.15	0.066 – 0.576	0.003 – 0.038	28	(Deng et al., 2016)
TEAC:Levulinic acid 1:3	303.15 – 333.15	0.066 – 0.585	0.003 – 0.034	28	(Deng et al., 2016)
TEAB:Levulinic acid 1:3	303.15 – 333.15	0.069 – 0.588	0.003 – 0.032	28	(Deng et al., 2016)
TBAC:Levulinic acid 1:3	303.15 – 333.15	0.063 – 0.592	0.004 – 0.045	28	(Deng et al., 2016)
TBAB:Levulinic acid 1:3	303.15 – 333.15	0.070 – 0.586	0.004 – 0.043	28	(Deng et al., 2016)
TOTAL				353	

a Choline Chloride; b tetrabutylphosphonium bromide; c allyltriphenylphosphonium bromide; d Acetylcholine chloride; e Tetraethylammonium chloride; f Tetraethylammonium bromide; g Tetrabutylammonium chloride; h Tetrabutylammonium bromide

3.1. Peng-Robinson 78 modelling for pseudo-component approach

The use of Peng-Robinson 78 EoS (PR78) to model CO_2 solubility in DESs dispenses with experimental data on density and/or vapor pressure of DESs pseudo-component, requiring only its critical properties.

This study compared the results of CO_2 solubility in thirteen DESs obtained by PR78 EoS using the mixing rules proposed by van der Waals and Twu (Twu, 1986) — based on a correlation of the nomograph for kinematic viscosity of the American Petroleum Institute (API) and a mixing rule for blending oils, as shown in Table S3. Average Absolute Relative Deviation (AARD%) calculated by Equation (9) shows that both mixing rules works equally for these systems, showing differences of 0.10% for ChCl (choline chloride):Glycerol system in 1:2 molar ratio. The mixing rules presented low deviations (up to 11.46% using van der Waals and 11.49% using Twu), which indicates that PR78 is able to properly predict CO_2 solubility in all DESs studied. As a consequence, all subsequently data were modeled considering van der Waals mixing rule.

$$AARD\% = \frac{1}{N_p}\sum_{i}^{N_p}\left|\frac{x_i^{cal} - x_i^{exp}}{x_i^{exp}}\right| \times 100 \quad (9)$$

where N_p is the number of experimental data, x^{exp} is the experimental solubility, and x^{cal} is the Peng-Robinson 78-calculated solubility.

Experimental data was modeled by PR78 EoS considering two assumptions for the binary interaction parameter (k_{ij}), namely: (i) $k_{ij} = 0$ and (ii) considering a linear trend of k_{ij} with temperature (Equation (10)), in which case the parameter was fitted to experimental data on solubility, with the coefficients values ($a_0\ and\ a_1$) presented in Table S3.

$$k_{ij} = a_0 + a_1 T \quad (10)$$

k_{ij} is the binary interaction parameter, a_0 and a_1 are the constants and T is the temperature in Kelvin.

Figure 1 shows the evolution of k_{ij} as a function of temperature of some DESs considered in this study. In all cases, except for those DES formed with phenol and the DES formed by TBPB:Diethylene Glycol 1:4 molar ratio, k_{ij} values increase linearly with the temperature increase. On the contrary, DES formed with phenol and TBPB:Diethylene Glycol 1:4 molar ratio exhibit a reduction of k_{ij} values with the temperature increase as Rabhi et al., (2021) observed in their work in which the CO_2 solubility in DESs was modelled by PC-SAFT. The k_{ij} behavior as a function of temperature is presented in Figure S1 of Supporting Information for the other DESs studied.

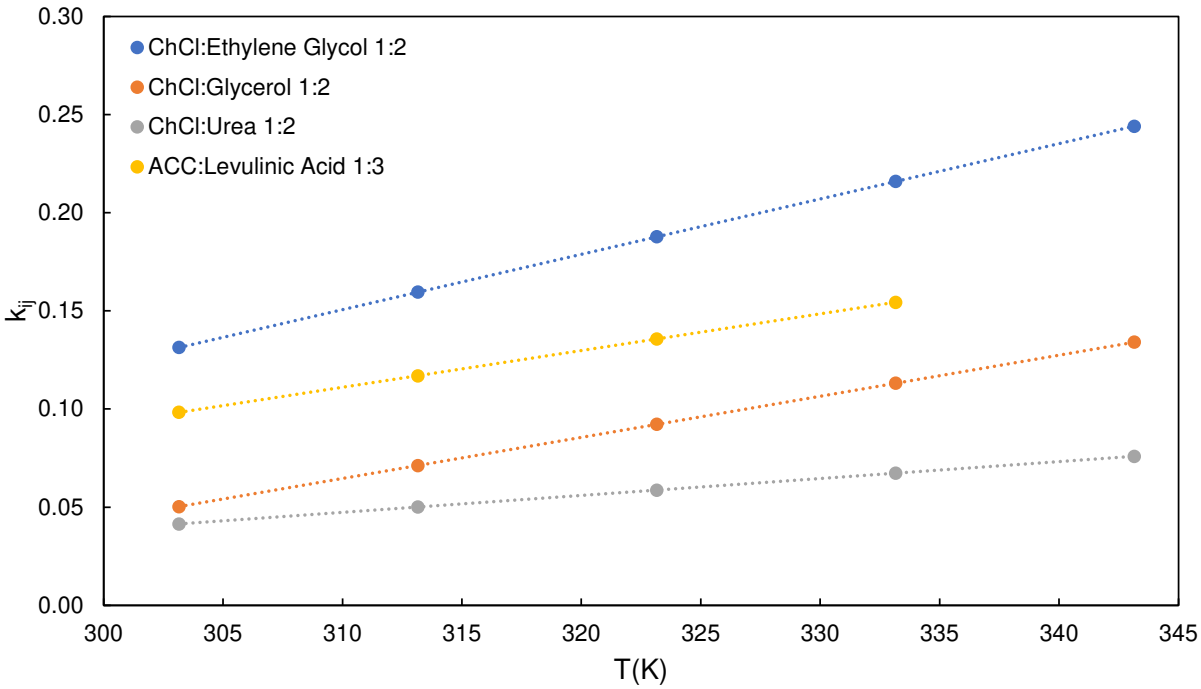

Figure 9. PR78 interaction parameter $\boldsymbol{k_{ij}}$ as a function of temperature.

The influence of the binary interaction parameter (k_{ij}) on the results considering $k_{ij} = 0$ and fitting k_{ij} values to experimental data were evaluated. Table 3 present the comparison of the AARD% of CO_2 solubility in DESs with or without k_{ij} and Figure 2 shows this comparison of ChCl:Ethylene Glycol 1:2 molar ratio. For TBPB (tetrabutylphosphonium bromide):Phenol 1:4 molar ratio and TBPB:Diethylene glycol

1:4 molar ratio, k_{ij} had smaller influence on AARD%. When considering the other systems, $k_{ij} = 0$ led to non-acceptable AARD% values, despite showing good results to fitted k_{ij}. As shown in Figure 2 PR78 describes very well the CO_2 solubility in all DESs with fitted k_{ij} values. ChCl:Ethylene Glycol 1:2 molar ratio, for example, shows a 10.46 deviation at 333.15 K when considering the k_{ij}, increasing to 78.62 without such variable. Deviations using PR78 increase with pressure increase because the equation accuracy is affected by the b/V_c magnitude, in which V_c is the predicted critical volume (Peng and Robinson, 1976).

Table 7. Comparison of the AARD% of CO_2 solubility in DESs with or without $\boldsymbol{k_{ij}}$ for PR78 EoS and the solvation for CPA EoS.

DES	%AARD PR78 (van der Waals)		%AARD PR78 (Twu)		%AARD CPA
	$\boldsymbol{k_{ij} = 0}$	$\boldsymbol{k_{ij} \neq 0}$	$\boldsymbol{k_{ij} = 0}$	$\boldsymbol{k_{ij} \neq 0}$	**Solvation**
ChCl[a]:Ethylene glycol 1:2	72.70	11.46	72.88	11.49	15.05
ChCl:Urea 1:2	33.40	6.76	33.62	6.77	8.14
ChCl:Phenol 1:3	74.71	4.12	74.49	4.10	11.56
ChCl:Glycerol 1:2	49.13	8.57	49.75	8.67	11.59
TBPB[b]:Phenol 1:4	8.15	7.10	7.99	7.10	11.48
TBPB:Diethylene glycol 1:4	9.53	8.13	9.46	8.13	20.79
ATPPB[c]:Phenol 1:4	33.62	7.65	34.67	7.68	7.68
ATPPB:Phenol 1:6	28.86	4.78	27.75	4.82	8.32
ACC[d] Levulinic acid 1:3	56.00	3.27	55.99	3.28	3.11
TEAC[e]:Levulinic acid 1:3	63.23	2.67	63.27	2.68	2.71
TEAB[f]:Levulinic acid 1:3	64.06	2.01	64.09	2.01	2.04
TBAC[g]:Levulinic acid 1:3	52.64	3.12	52.75	3.14	3.53
TBAB[h]:Levulinic acid 1:3	54.71	1.76	54.80	1.76	1.89
Average of deviation	43.99	5.49	46.27	5.51	7.02

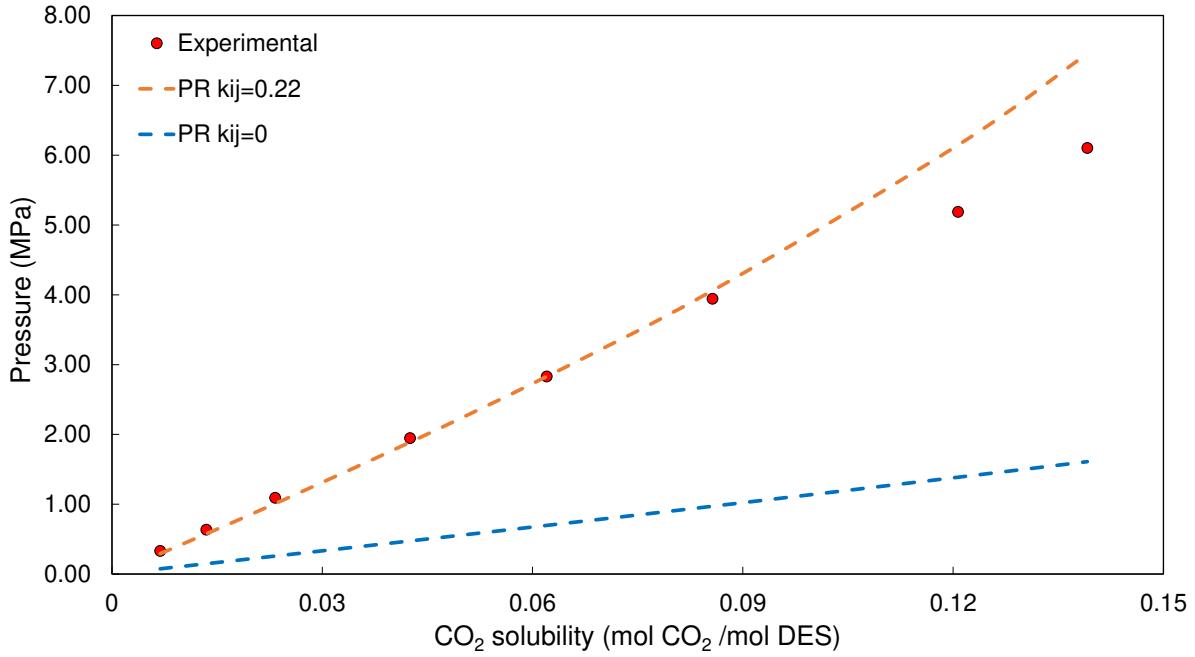

Figure 10. Comparison of modelling results of CO_2 solubility in ChCl:Ethylene Glycol 1:2 molar ratio at 333.15 K using PR78 considering $\boldsymbol{k_{ij} = 0}$ and $\boldsymbol{k_{ij} \neq 0}$.

3.2. Cubic Plus Association modeling for pseudo-component approach

The same systems were modelled using CPA EoS according to the temperature and density range presented in Table 4. CPA parameters are derived from experimental data on density of pure DESs. Although rather scarce in the literature, 105 experimental data were found on density, which were used to calculate CPA parameters and a CPA-calculated density. AARD% values between the calculated and experimental data were obtained according to Equation (11) and presented in Table 4.

$$AARD\% = \frac{1}{N_p}\sum_{i}^{N_p}\left|\frac{\rho_i^{cal} - \rho_i^{exp}}{\rho_i^{exp}}\right| \times 100 \qquad (11)$$

where N_p is the number of experimental data, ρ^{exp} is the experimental density, and ρ^{cal} is the CPA-calculated density.

Table 8. Temperature and density ranges at 0.10 MPa for each DESs studied.

DES (2B)	Molecular weight ($g.mol^{-1}$)	Temperature range (K)	Density range (mol/m^3)	N_p	Density AARD%	Ref.
ChCl:Ethylene glycol 1:2	89.919	298.15 – 333.15	12473.7 – 12703.9	8	0.05	(Leron et al., 2012)
ChCl:Urea 1:2	91.883	293.15 – 363.15	13288.6 – 13872.8	8	0.19	(Yadav and Pandey, 2014)
ChCl:Phenol 1:3	105.489	293.15 – 318.15	10234.2 – 10380.1	6	0.01	(Guo et al., 2013)
ChCl:Glycerol 1:2	107.900	298.15 – 333.15	10848.3 – 11040.1	8	0.04	(Leron et al., 2012)
TBPB:Phenol 1:4	143.156	293.15 – 333.15	7300.7 – 7496.0	5	0.03	(Wang et al., 2019)
TBPB:Diethylene glycol 1:4	152.763	293.15 – 333.15	6934.8 – 7130.3	5	0.09	(Wang et al., 2019)
ATPPB:Phenol 1:4	151.941	293.15 – 333.15	7529.7 – 7718.8	5	0.01	(Wang et al., 2019)
ATPPB:Phenol 1:6	135.418	293.15 – 333.15	8336.0 – 8569.5	5	0.16	(Wang et al., 2019)
ACC:Levulinic acid 1:3	132.501	293.15 – 343.15	8346.9 – 8635.0	11	0.01	(Deng et al., 2016)
TEAC:Levulinic acid 1:3	128.512	293.15 – 343.15	8254.4 – 8537.4	11	0.04	(Deng et al., 2016)
TEAB:Levulinic acid 1:3	139.625	293.15 – 343.15	8154.9 – 8430.7	11	0.03	(Deng et al., 2016)
TBAC:Levulinic acid 1:3	156.566	293.15 – 343.15	6377.1 – 6606.9	11	0.01	(Deng et al., 2016)
TBAB:Levulinic acid 1:3	167.678	293.15 – 343.15	6347.0 – 6563.3	11	0.02	(Deng et al., 2016)
TOTAL		293.15 – 343.15	6347.0 – 13872.8	105	0.05	

AARD% values presented in Table 4 (0.05 % on average) ratify the good fitting of experimental data by CPA EoS. To understand each DESs density behavior, Figure 3 present the plot of density versus temperature.

Figure 3 shows that density decreases with increases in temperature due to thermal expansion for all cases. This occurs because heating a substance promotes the acceleration and spreading of molecules, which start to occupy a larger volume and consequently reduces density (Leron and Li, 2012).

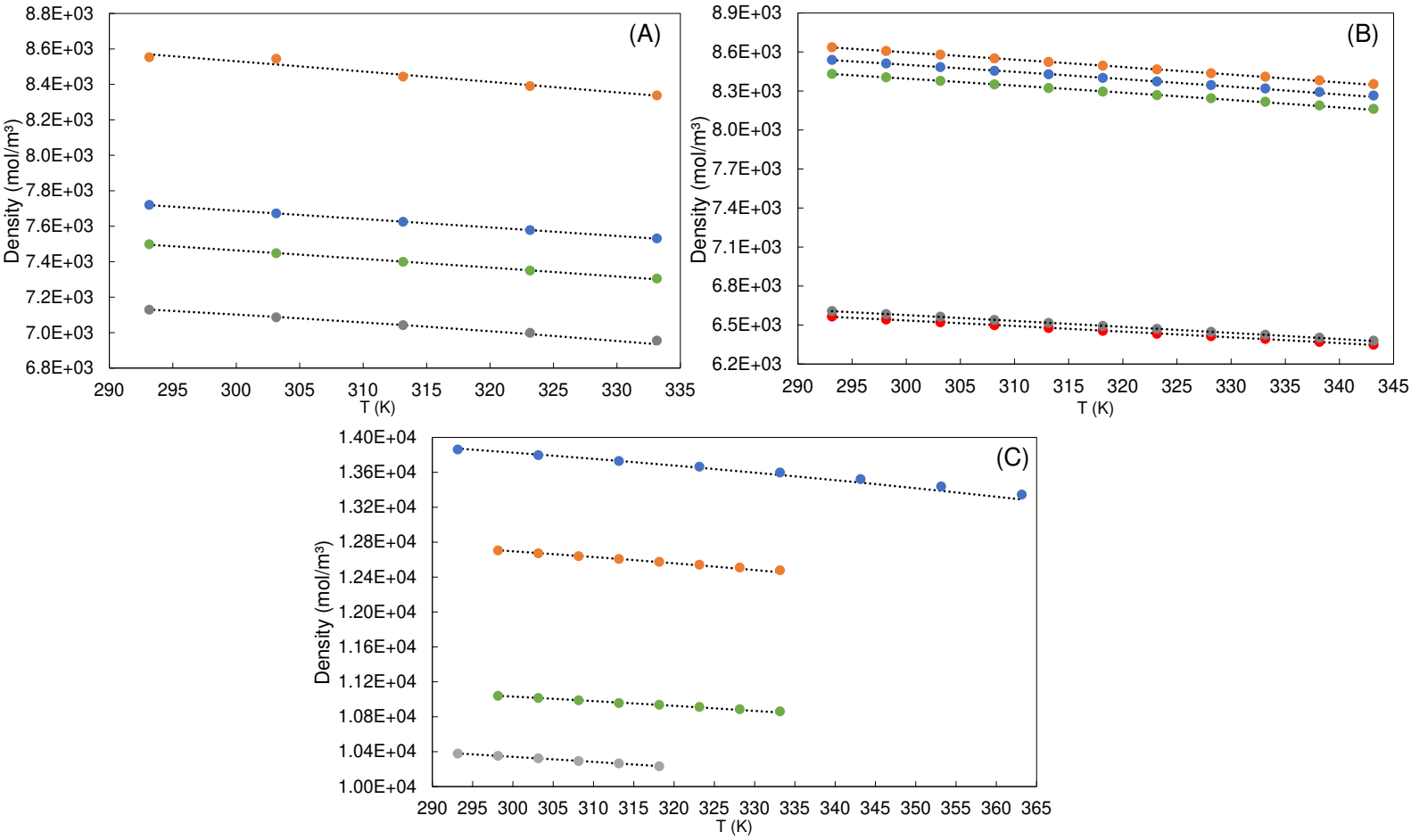

Figure 11. Comparison between densities calculated by the CPA EoS (dotted lines) and experimental data for (A) • ATPPB:phenol (1:6) • ATPPB:phenol (1:4) • TPPB:phenol (1:4) • TPPB: Diethylene glycol (1:4) (Wang et al., 2019); (B) • ACC:Levulinic acid (1:3) • TEAC:Levulinic acid (1:3) • TEAB:Levulinic acid (1:3) • TBAC:Levulinic acid (1:3) • TBAB:Levulinic acid (1:3) (Deng et al., 2016); (C) • ChCl:Urea (1:2) (Francisco et al., 2013) • ChCl:Ethylene Glycol (1:2) (Yadav and Pandey, 2014) • ChCl:glycerol (1:2) (Leron et al., 2012) • ChCl:phenol (1:3) (Leron et al., 2012).

As shown in Figure 3(A), the increase in ATPPB:phenol DES molar ratio from 1:4 to 1:6 leads to an increase in DES density, which may be explained by the highest dispersive forces of phenol, leading to a higher material packing (Zubeir et al., 2016) and conferring to greater density to this molecule when compared with ATPPB. The change in the HBA from ATPPB to TBPB with phenol at 1:4 molar ratio promotes a

reduction in density, possibly due to the smaller density of TBPB compared to ATPPB. HBA interactions occur between Br^- and hydrogen atoms in the -C-C=C group in $ATPP^+$, which is attributable to the strong steric hindrance of benzene rings in the $ATPP^+$ cation, promoting a high density (Wang et al., 2019). HBD change from phenol to diethylene glycol with TBPB at 1:4 molar ratio leads to a decrease in density. Although phenol and diethylene glycol present similar densities (respectively, 1.07 g/cm³ (Cole, 1960) and 1.12 g/cm³ (Awwad et al., 2002)), phenol presents an aromatic ring which could increase its density when mixed with TBPB.

Figure 3(B) shows that the ACC:levulinic acid DES presents the highest density at 1:3 molar ratio due to its chain length and ester functional group, allowing intermolecular forces to act more strongly. When comparing the TEAC:levulinic acid, TEAB:levulinic acid, TBAC:levulinic acid and TBAB:Levulinic acid DESs as to chain length, it was verified that chain decrease led to an increase in density due to TEAB and TEAC smaller ramification and higher density. Changing TBAC or TEAC chloride to TBAB or TEAB bromide promotes a decrease in density due to the difference between the two halogens, whereby bromide electronegativity is lower than that of chloride (Deng et al., 2016).

Figure 3(C) shows that ChCl:urea DES presents the highest density among the DESs, followed by ChCl:ethylene glycol, ChCl:glycerol and ChCl:phenol. This is due to the fact that urea has two amine groups and a carbonyl that bonds most powerfully to ChCl, glycerol has a largest alkyl chain and three hydroxyl groups, and ethylene glycol has two hydroxyl groups. In a study conducted by Crespo et al., (2019), the authors showed that DESs density increase with increased excess molar volume, thus indicating that CPA EoS provides a good fitting to experimental data on density and suggesting that pure-components parameters will likewise fit well.

Table 5 presents the critical properties of the studied DESs. As previously stated, these properties are required to adjust the CPA parameters of the pseudo-component DESs calculated according the modified Lydersen−Joback−Reid method. Table 6 shows the optimized CPA parameters of DESs used to calculate liquid density, and AARD%. The CPA parameters of pure DESs were optimized using Equation (12). After the calculation of the liquid densities using a Multiflash programing and CPA estimated parameters, the sum inside the square brackets of Equation (12) was minimized using Solver from Microsoft Excel varying the parameters in order to found them and consequently the liquid density value.

$$OF = \min\left[\sum_{i=1}^{N_p}\left(\frac{\rho_i^{cal} - \rho_i^{exp}}{\rho_i^{exp}}\right)\right] \quad (12)$$

where N_p is the number of data points, ρ_i^{cal} is the liquid densities calculated using CPA and ρ_i^{exp} is the experimental liquid densities.

Table 9. Calculated critical properties and acentric factor of the studied DESs.

HBA	HBD	Molar ratio	Molecular weight (g.mol^{-1})	T_c (K)	ω	P_c (MPa)
ChCl	Ethylene glycol	1:2	89.919	602.000	0.915	4.099
ChCl	Urea	1:2	91.883	644.444	0.651	4.954
ChCl	Phenol	1:3	105.489	655.663	0.512	4.789
ChCl	Glycerol	1:2	107.900	680.672	1.225	3.346
TBPB	Phenol	1:4	143.156	694.584	0.511	3.827
TBPB	Diethylene glycol	1:4	152.763	500.926	0.997	3.347
ATPPB	Phenol	1:4	151.941	751.768	0.484	4.273
ATPPB	Phenol	1:6	135.418	727.637	0.469	4.657
ACC	Levulinic acid	1:3	132.501	744.573	0.772	3.429
TEAC	Levulinic acid	1:3	128.512	716.343	0.757	3.266

TEAB	Levulinic acid	1:3	139.625	728.300	0.760	3.291
TBAC	Levulinic acid	1:3	156.566	759.050	0.839	2.725
TBAB	Levulinic acid	1:3	167.678	769.287	0.842	2.743

Table 10. Optimized CPA parameters of pseudo-component DESs and deviation from experimental data.

DES	a_0 (J m³/mol²)	b (m³/mol)	C_1	ε (J/mol)	β	AARD% in ρ (this study)	AARD% in ρ (Haghbakhsh and Raeissi, 2017)
ChCl:Ethylene glycol 1:2	$1.0 \cdot 10^{-5}$	$4.306\ 10^{-5}$	0.835	0.538	986.694	0.05	0.35
ChCl:Urea 1:2	$1.0 \cdot 10^{-5}$	$3.894\ 10^{-5}$	0.835	0.520	969.816	0.19	0.17
ChCl:Phenol 1:3	$2.0 \cdot 10^{-5}$	$3.903\ 10^{-5}$	0.110	0.474	978.208	0.01	0.07
ChCl:Glycerol 1:2	$3.0 \cdot 10^{-5}$	$8.133\ 10^{-5}$	0.810	0.816	973.658	0.04	0.15
TBPB :Phenol 1:4	$3.0 \cdot 10^{-5}$	$5.480\ 10^{-5}$	0.830	0.790	938.770	0.03	-
TBPB:Diethylene glycol 1:4	$5.0 \cdot 10^{-5}$	$3.783\ 10^{-5}$	0.830	0.777	922.699	0.09	-
ATPPB:Phenol 1:4	$9.0 \cdot 10^{-5}$	$5.805\ 10^{-5}$	0.900	0.795	893.233	0.01	-
ATPPB:Phenol 1:6	$5.0 \cdot 10^{-5}$	$4.877\ 10^{-5}$	0.500	0.800	892.302	0.16	-
ACC:Levulinic acid 1:3	$2.0 \cdot 10^{-5}$	$9.848\ 10^{-5}$	0.500	0.779	828.070	0.01	-
TEAC:Levulinic acid 1:3	$4.0 \cdot 10^{-5}$	$7.169\ 10^{-5}$	0.100	1.898	903.766	0.04	0.10
TEAB:Levulinic acid 1:3	$4.0 \cdot 10^{-5}$	$7.998\ 10^{-5}$	0.100	1.199	899.862	0.03	0.11
TBAC:Levulinic acid 1:3	$1.7\ 10^{-4} \cdot$	$1.358\ 10^{-4}$	0.110	0.524	962.611	0.01	0.20
TBAB:Levulinic acid 1:3	$1.7 \cdot 10^{-4}$	$1.207\ 10^{-4}$	0.110	0.641	948.009	0.02	0.21
Average of deviation						0.05	0.17

As shown in Table 6, a_0 and b parameters present no significant changes among the DESs — except for TBAC:Levulinic acid 1:3 and TBAB:levulinic acid 1:3, which present values 10 times higher than those fitted for other DESs. The deviations of CPA parameters did not exceed 0.19%, thus that CPA EoS is able to predict these solvents liquid density. In our study, the average AARD was equal to 0.05% – more three times lower than that found by Haghbakhsh and Raeissi, (2017), which was equal

to 0.17%. Such a difference may be different fitting methods used and/or by the software used for modeling.

CO_2 solubility curves in DESs were modelled considering no association scheme for CO_2 (inert), CO_2 solvation — in which the β_{ij} parameter must be fitted — 2B (with one electron acceptor and one electron donor) and 4C association schemes (with two electron acceptor and two electron donor). Table 7 presents the CPA parameters of CO_2 in each association scheme. These parameters were used to model experimental data on CO_2 solubility at different temperatures and pressures, as shown in Table 2. To compare each analyzed case, AARD% pressure was calculated according to Equation (13).

Table 11. CPA parameters of CO_2 in different association schemes (Oliveira et al., 2011).

Association Schemes	a_0 (J.m³/mol²)	b (m³/mol)	C_1	ε (J/mol)	β	AARD% in ρ	AARD% in P
CO_2 (inert)	0.35	2.72 10^{-5}	0.76			0.22	0.83
CO_2 (2B)	0.34	2.73 10^{-5}	0.77	1237.14	0.1202	0.15	1.23
CO_2 (4C)	0.34	2.76 10^{-5}	0.77	731.77	0.0642	0.15	0.31

$$AARD\% = \frac{1}{N_p}\sum_{i}^{N_p}\left|\frac{P_i^{cal} - P_i^{exp}}{P_i^{exp}}\right| \times 100 \qquad (13)$$

where N_p is the number of experimental data, P^{exp} is the experimental pressure, and P^{cal} is the CPA-calculated pressure.

Experimental data was modeled by CPA EoS also considering $k_{ij} = 0$ and k_{ij} have a linear trend with temperature in which case the parameter was fitted to experimental data on solubility, with the coefficients values $(a_0 \; and \; a_1)$ presented in Table S2.

Figure 4 presents experimental data and CPA modelling results of CO_2 solubility in ChCl:Urea 1:2 and TBAB:Levulinic acid 1:3 molar ratios at different temperatures considering CO_2 as inert. The results indicate that temperature increase promotes a decrease in CO_2 solubility. Figure 4(B) also shows that deviation decreases with increased temperature, going from 13.66% at 303.15 K to 2.88% at 343.15 K. Such finding indicates that CPA modelling is enhanced at higher temperatures. The average AARD% for ChCl:Urea 1:2 molar ratio is 8.14% (Table 3) and for TBAB:Levulinic acid 1:3 molar ratio is 1.89% (Table 3), showing that CPA is able to describe experimental data.

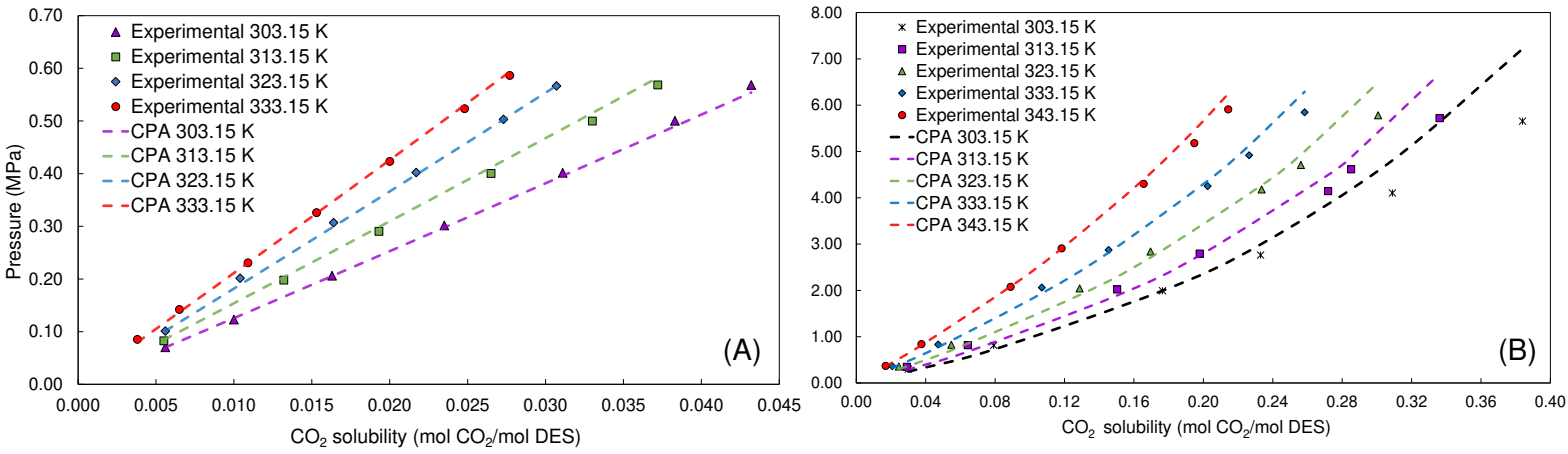

Figure 12. Experimental and CPA modelling of CO_2 solubility at 303.15 K, 313.15 K, 323.15 K, 333.15 K and 343.15 K in (A) TBAB:Levulinic acid 1:3; (B) ChCl:Urea 1:2 considering CO_2 as inert and fitted $\boldsymbol{k_{ij}}$

Table 8 and Figure 5 show AARD% considering $k_{ij} = 0$ or fitted k_{ij}. In ACC:Levulinic acid 1:3 molar ratio at 333.15 K, for example, deviation was 217.36%. Once assumed $k_{ij} = 0$, and thus excluded any strong molecular interactions other than the hydrogen bonds of the association term, this result was expected. For inert CO_2, no interactions were considered (Tsivintzelis et al., 2011). Thus, AARD% is enhanced for all DESs in all association schemes when fitted k_{ij} is taken into account.

Table 12. Comparison between AARD% of CO_2 solubility in some DESs with or without k_{ij} in different CO_2 association schemes for CPA EoS

DES	%AARD CPA CO_2 Solvation	%AARD CPA CO_2 Inert		%AARD CPA CO_2 2B		%AARD CPA CO_2 4C	
	$k_{ij} \neq 0$	$k_{ij} = 0$	$k_{ij} \neq 0$	$k_{ij} = 0$	$k_{ij} \neq 0$	$k_{ij} = 0$	$k_{ij} \neq 0$
ChCl:Ethylene glycol 1:2	15.05	676.68	14.05	163.08	11.33	187.71	7.20
ChCl:Urea 1:2	8.14	192.97	8.75	667.50	30.75	604.71	22.99
ChCl:Phenol 1:3	11.56	100.00	11.54	100.00	9.29	139.38	6.86
ChCl:Glycerol 1:2	11.59	734.57	11.40	56.61	11.74	58.47	8.86
TBPB:Diethylene glycol 1:4	20.52	100.00	19.45	629.90	6.78	174.97	6.51
ACC:Levulinic acid 1:3	3.11	404.68	2.83	83.28	3.77	92.74	3.21
TBAC:Levulinic acid 1:3	3.53	92.52	3.12	90.76	3.87	98.21	4.12
TBAB:Levulinic acid 1:3	1.89	371.08	1.54	92.12	2.01	98.42	2.24
Average of deviation	9.42	334.06	9.08	235.41	9.94	181.83	7.75

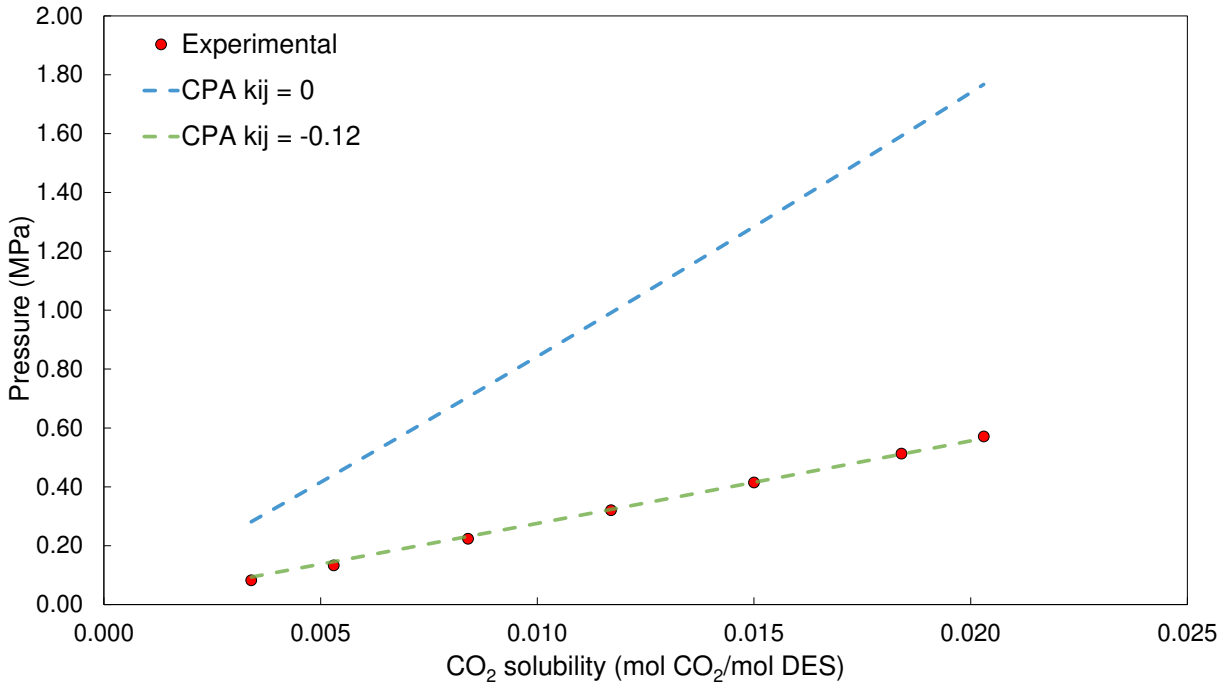

Figure 13. Comparison between CPA modelling of CO_2 solubility in ACC:Levulinic acid 1:3 molar ratio at 333.15 K with and without the $k_{ij} = 0$, considering CO_2 as inert.

Rabhi et al., (2021) also evaluated CO_2 solubility in different DESs (tetrabutylammonium bromide (TBABr):octanoic acid 1:2, TBABr:decanoic acid 1:2 and DL-menthol:dodecanoic acid 2:1 in a 293.15–393.15 K temperature range and a pressure up to 122.9 bar, correlating these data using PC-SAFT. They considered DESs as a pseudo-pure component, in which the deviations seem to rise with the temperature increase, what is a quite different behavior in comparison to this study results, but both with the same data trend. It was also analyzed the k_{ij} behavior considering it temperature-dependent and independent. The results show the linearly decrease of k_{ij}values with the temperature increase, on the contrary of this study. In addition, large deviations from experimental data were observed when k_{ij} was considered independent, as observed in this study. Consequently, both models (PC-SAFT and CPA) proved to present good agreement with the experimental data.

Table 8 allow to compare AARD% between experimental data and CPA EoS using different CO_2 association schemes. Figure 6 shows the results for three DESs that solubilize CO_2 under high (1–9 MPa) (Figure 6(A)), moderate (0.20–1.60 MPa) (Figure 6(B)) and low pressures (010 – 0.70 MPa) (Figure 6(C)). Figure 6 indicates that deviation will be smaller as smaller the pressure range regardless of the association schemes, thus approaching model results from experimental data. Figure 6(A) evinces that, for the highest-pressure range, deviation is higher when CO_2 is considered inert (14.05%) than for the 2B (11.33%) and 4C association schemes (7.20%). As shown in Table 8, this behavior is also observed for ChCl:Ethylene glycol 1:2, ChCl:Urea 1:2, ChCl:Phenol 1:3, and ChCl:Glycerol 1:2 DESs, where errors are smaller for the 4C association scheme than for 2B and inert. Different from inert CO_2, which requires high values of binary interaction parameters, the 4C association scheme demonstrates the enhancement

in consider explicitly the specific polar interactions between CO_2 molecules in the model (Oliveira et al., 2011). Despite that, all association schemes have acceptable errors. These results differ from those obtained by Haghbakhsh and Raeissi, (2017), who indicate no improvement errors between 2B, 3B, 4C association schemes and inert and solvation. This difference may be related to the method used to data modelling.

Moreover, slightly better results were obtained when CO_2 was considered as inert, in which case only the binary interaction parameter was adjusted, than for solvation, in which both binary interaction and cross-volume association were adjusted. This extra adjustable parameter adds more complexity to the modelling approach (Tsivintzelis et al., 2011).

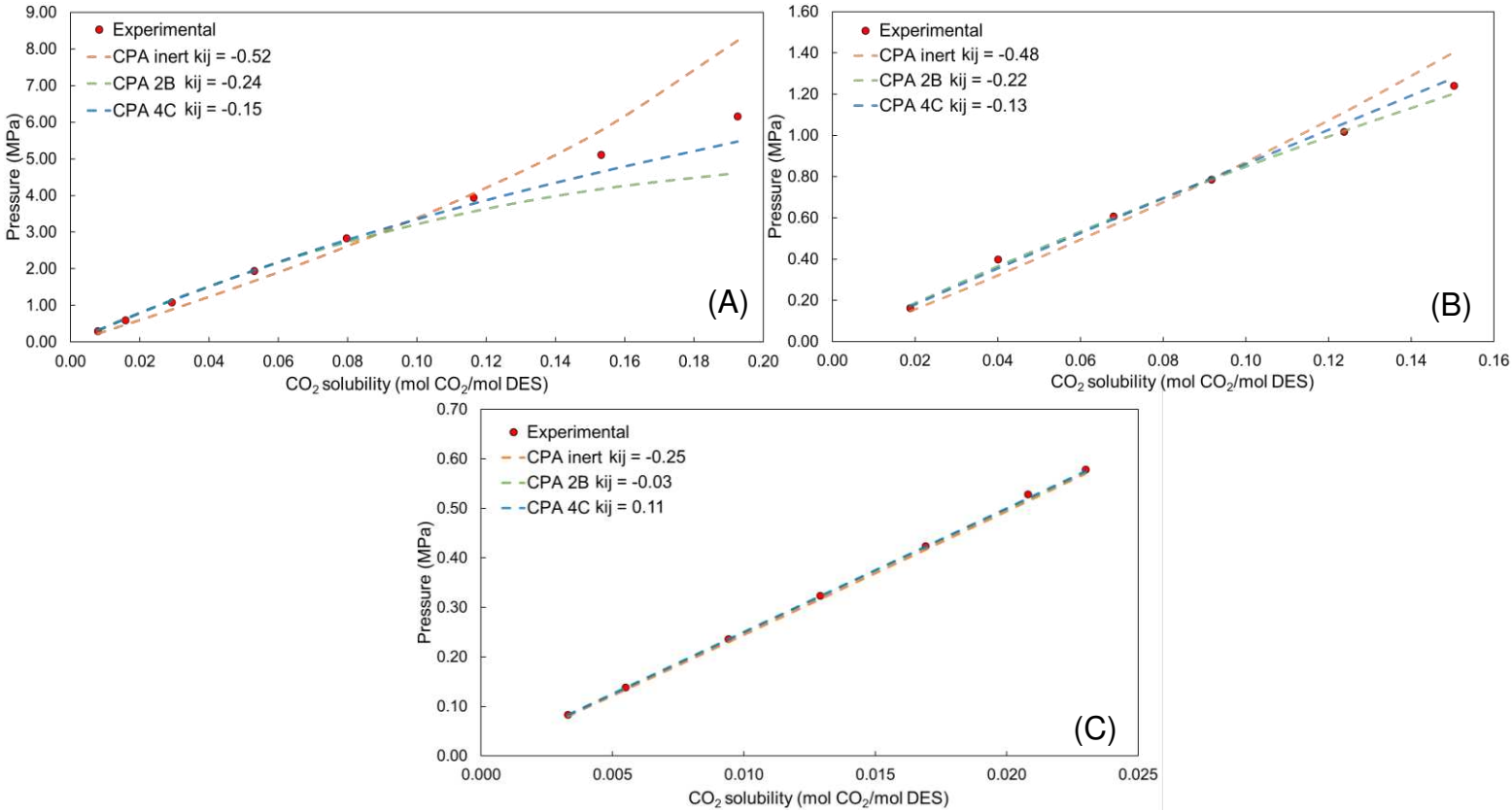

Figure 14. Comparison between CPA modelling of CO_2 solubility in different association schemes at 323.15 K in (A) ChCl:Ethylene Glycol 1:2; (B) TBPB:Phenol

1:3;
(C) TEAB:Levulinic acid 1:3 considering the fitted k_{ij}.

PR78 and CPA were also compared in their best configuration, i.e., with fitted binary interaction parameter, as shown in Figure 7 and Table 3. For all systems analyzed considering CO_2 as inert, PR78 showed better results than CPA due to its smaller deviation — an expected outcome, given than CPA is far more complex than PR78 EoS, thus making it a good fit for modelling CO_2 solubility in DESs. This may be verified through CO_2 solubility in TBPB:Diethylene Glycol 1:4 molar ratio at 313.15 K (9.53% for PR and 20.52% for CPA), as shown in Figure 7. Considering ACC:Levulinic acid 1:3, TEAC:Levulinic acid 1:3, TEAB:Levulinic acid 1:3, TBAC:Levulinic acid 1:3, and TBAB:Levulinic acid 1:3 DESs, this difference was very low due to the small pressure range (0.065 – 0.60 MPa).

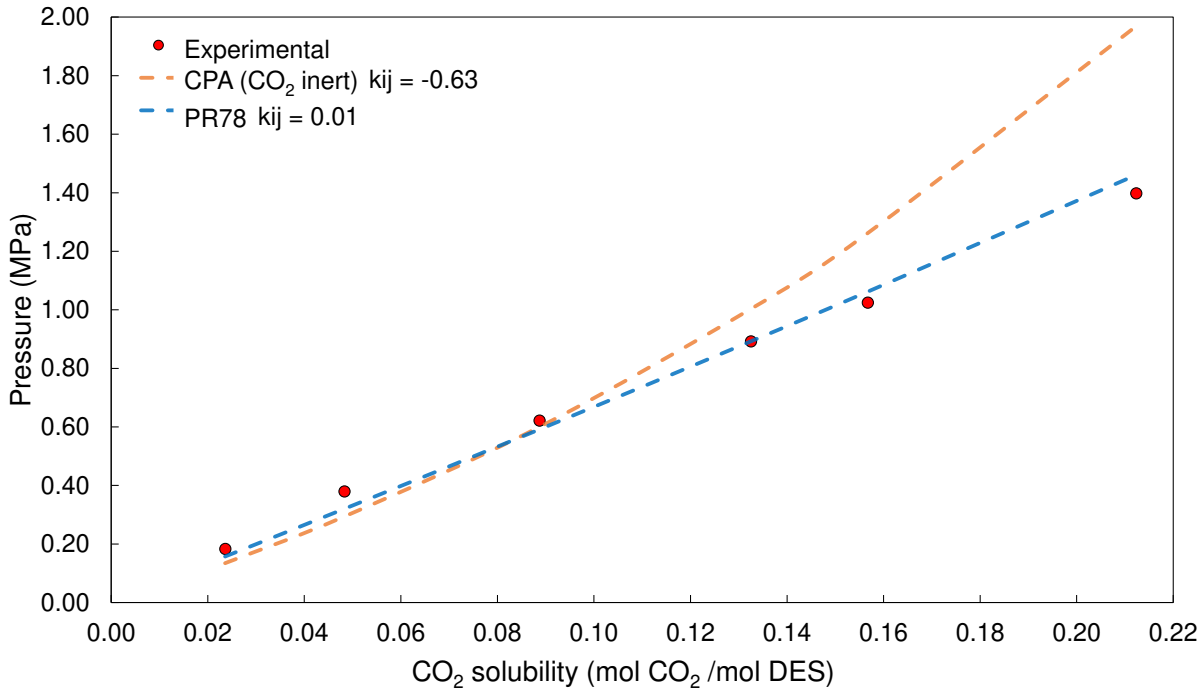

Figure 15. Comparison between CPA and Peng-Robinson 78 EoS modelling for CO_2 solubility in TBPB:Diethylene Glycol 1:4 at 313.15 K.

When considering k_{ij} as equal to zero, both CPA and PR78 EoSs presented unacceptable deviations. The deviations of PR78 were smaller than those of CPA,

probably because the Peng-Robinson 78 presents a single term that makes the equation mathematically simpler, which contributes for the better adjustment of k_{ij}. CPA EoS is more complex due to its association term, thus hampering the adjustment of k_{ij}. Furthermore, the pure-DESs parameters were adjusted for CPA EoS which might have influenced the uncertainties.

3.3. Peng-Robinson 78 and CPA modelling for individual approach

The individual component approach consists of fitting the density of each DES individual component aqueous solutions while considering components self-association and the interaction between each component and CO_2 as inert. This study was conducted by modelling ChCl:Ethylene glycol 1:2, ChCl:Urea 1:2, ChCl:Phenol 1:3, and ChCl:Glycerol 1:2 DESs.

Firstly, CPA parameters were optimized for ChCl, phenol and urea that are mixed to form the DESs using experimental data on density in a given temperature range. Table S4 shows the temperature (293.15–353.15 K) and density (6,960.1–16,623.1 mol.m^{-3}) ranges used as reference. The CPA parameters were not adjusted for those HBD for which the Multiflash software had such parameters in its own database (ethylene glycol and glycerol). Table 9 presents the CPA parameters and the deviations for choline chloride, urea and phenol, calculated using experimental data, and glycerol and ethylene glycol collected from the Multiflash database. The results confirm that CPA is able to predict density with deviations no greater than 0.05% for ChCl, phenol and urea. For ethylene glycol and glycerol this information can not be drawn because Multiflash does not provide the deviations.

Table 13. Optimized CPA parameters for each DES component.

Components	a_0 (J m³/mol²)	b (m³/mol)	C_1	ε (J/mol)	β	AARD% in ρ
Choline Chloride	0.020	$3.872\ 10^{-4}$	0.835	0.769	960.868	0.05
Phenol	0.002	$2.378\ 10^{-5}$	0.110	0.465	837.618	0.003
Urea	0.001	$9.490\ 10^{-5}$	0.800	0.497	993.735	0.02
Ethylene Glycol	1.082	$3.154\ 10^{-5}$	0.674	17932	0.051	NA[a]
Glycerol				21352.2	0.054	NA[a]

a Not applicable. The CPA parameters of both components come from Multiflash database and no AARD% were given.

Table 10 shows the AARD% results for both PR78 and CPA considering CO_2 as inert for the four systems studied. As setting k_{ij} values to zero led to non-equitable results, it was found optimal linear dependent-temperature binary interaction parameters, as in the pseudo-component approach, by fitting to the experimental data (Tables S5 and S6).

Table 10 and Figure 8 show that individual component is better than the pseudo-component approach for all studied systems for both CPA and PR78, as the deviation is smallest. As DESs are not a pseudo-component, but rather a mixture of two or more components (Martins et al., 2018), the individual component approach is expected to predict experimental data better than the pseudo-component one. When comparing both models, ChCl:Ethylene glycol 1:2 DES was the only one to present a better result in CPA than in PR78. For the others DESs, both models reached similar results and showed good agreement with experimental data. When considering CPA individual component approach, it was found temperature increase to affect predictions — thus corroborating the results reported by Zubeir et al., (2016) study. This may be due to the fact that components parameters were only fitted at 298.15K. In contrast, temperature increase provided best predictions in both the individual and pseudo-component approached for PR78.

Table 14. AARD% comparisons using pseudo-component and individual approaches for CPA with CO_2 inert and Peng-Robinson 78

DES	T (K)	$\overline{P_{exp}}$ (MPa)[a]	AARD% CPA (CO_2 Inert)			AARD% Peng-Robinson 78		
			Pseudo	Individual	$\overline{P_{cal}}$ (MPa)[b]	Pseudo	Individual	$\overline{P_{cal}}$ (MPa)
ChCl:Ethylene glycol 1:2	303.15	2.64	19.26	1.77	3.06	13.47	14.47	2.79
	313.15	2.68	20.33	2.79	3.01	13.14	17.23	3.17
	323.15	2.75	16.92	2.26	2.99	14.19	17.26	3.33
	333.15	2.76	10.67	2.40	2.94	9.40	11.45	3.00
	343.15	2.82	8.07	6.32	3.17	7.48	10.74	2.76
ChCl:Urea 1:2	303.15	3.60	13.67	4.59	2.41	9.73	7.86	2.34
	313.15	2.92	10.57	2.45	2.93	7.87	5.94	2.78
	323.15	2.96	8.74	1.20	2.98	6.36	4.36	2.98
	333.15	3.02	5.64	1.08	3.03	5.40	3.97	3.05
	343.15	3.08	2.88	4.05	2.95	4.72	3.49	2.93
ChCl:Phenol 1:3	293.15	0.31	1.84	6.62	0.32	2.12	1.95	0.31
	303.15	0.32	20.60	6.74	0.30	7.31	7.22	0.30
	313.15	0.31	16.91	6.00	0.30	4.18	4.16	0.31
	323.15	0.32	6.72	9.72	0.33	2.87	3.23	0.32
ChCl:Glycerol 1:2	303.15	2.72	9.79	2.52	2.70	1.59	1.47	2.67
	313.15	2.76	8.76	5.92	3.01	5.64	5.15	2.97
	323.15	2.75	25.20	23.84	2.32	23.18	23.28	2.31
	333.15	2.87	8.75	9.03	3.28	8.09	7.52	3.23
	343.15	2.92	5.49	5.93	3.07	4.93	4.84	3.01

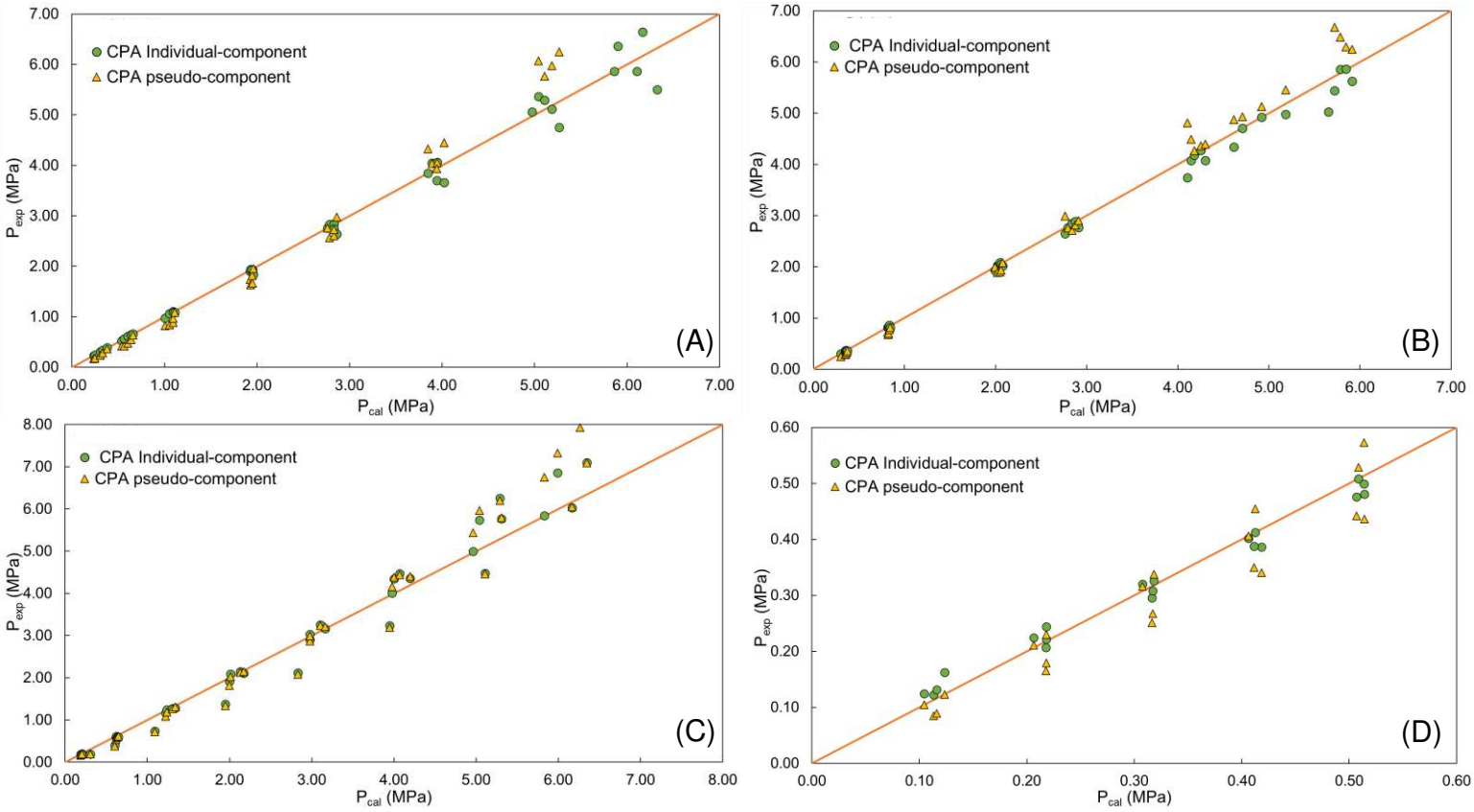

Figure 16. Comparison between pseudo-component and individual approach using CPA with CO_2 as inert for (A) ChCl:Ethylene Glycol 1:2, (B) ChCl:Urea 1:2, (C) ChCl:Glycerol1:2 and (D) ChCl:Phenol 1:3.

4. Conclusions

The phase behavior of CO_2 in 13 DESs were modelled using CPA and PR78 equations of state, adding over 300 experimental data. Using the pseudo-component and individual component approaches, both density and CO_2 solubility in DESs were modelled in a wide temperature and pressure range. This study also investigated the binary interaction parameter (k_{ij}) as equal or not to zero for both models. To understand the behavior of CO_2 in DES with different association schemes, it was considered DESs as a component with two association sites (2B) and CO_2 as inert with two or four association sites (2B and 4C, respectively) when using CPA EoS, as well as the case of solvation.

The results show that CPA adequately predicts these solvents liquid density, proving that the Cubic-Plus Association technique can be used to optimize parameters of pseudo- and individual components. Both equations managed to predict the experimental data, however the deviation was smaller in PR78 – for most DESs – than in CPA. The binary interaction parameter was considered equal to zero or fitted using CO_2 solubility in DES experimental data, showing that only fitted k_{ij} can reproduce experimental results with good accuracy. All CO_2 association schemes presented good accuracy, especially 4C, which showed smaller deviation – for most DESs – when compared with the other schemes.

The results also indicate that the individual component approach presents better results for both CPA considering CO_2 as inert and PR78 EoS — for DES are considered a mixture of components rather than a pseudo-component. Thus, both equations of state are suitable for modelling CO_2 solubility in DESs.

Acknowledgement:

The authors would like to thank the São Paulo Research Foundation (FAPESP – 2018/19198-9 and 2014/21252-0), Coordination for the Improvement of Higher Education Personnel - Brasil (CAPES) – Finance Code 001, the National Council for Scientific and Technological Development (CNPq – 306666/2020-0), and the Fund for the Support of Education, Research and Extension (FAEPEX/UNICAMP) for the financial support. The authors also thank the Human Resources Program of the National Agency of Petroleum, Natural Gas and Biofuels (PRH-ANP); to KBC for the authorized use of Multiflash software; and the Espaço da Escrita – Pró-Reitoria de Pesquisa - UNICAMP – for the language services provided.

References

2030 climate & energy framework [WWW Document], n.d. URL https://ec.europa.eu/clima/policies/strategies/2030_en (accessed 5.19.21).

Aaron, D., Tsouris, C., 2005. Separation of CO2 from flue gas: A review. Sep. Sci. Technol. 40, 321–348. https://doi.org/10.1081/SS-200042244

Abdelkareem, M.A., El Haj Assad, M., Sayed, E.T., Soudan, B., 2018. Recent progress in the use of renewable energy sources to power water desalination plants. Desalination 435, 97–113. https://doi.org/10.1016/j.desal.2017.11.018

Abdul Halim, H.N., Shariff, A.M., Tan, L.S., Bustam, M.A., 2015. Mass transfer performance of CO2 absorption from natural gas using monoethanolamine (MEA) in high pressure operations. Ind. Eng. Chem. Res. 54, 1675–1680. https://doi.org/10.1021/ie504024m

Aboshatta, M., Magueijo, V., 2021. A comprehensive study of co2 absorption and desorption by choline-chloride/levulinic-acid-based deep eutectic solvents. Molecules 26. https://doi.org/10.3390/molecules26185595

Akbari, M., Valeh-e-Sheyda, P., 2019. CO2 equilibrium solubility in and physical properties for monoethanolamine glycinate at low pressures. Process Saf. Environ. Prot. 132, 116–125. https://doi.org/10.1016/j.psep.2019.10.003

Ali, E., Hadj-Kali, M.K., Mulyono, S., Alnashef, I., Fakeeha, A., Mjalli, F., Hayyan, A., 2014. Solubility of CO2 in deep eutectic solvents: Experiments and modelling using the Peng-Robinson equation of state. Chem. Eng. Res. Des. 92, 1898–1906. https://doi.org/10.1016/j.cherd.2014.02.004

Ansarypur, G., Bayareh, M., Jahangiri, A., 2022. Experimental investigation and thermodynamic modeling of CO2 absorption by a chemical solution. J. Therm. Anal. Calorim. 147, 1689–1697. https://doi.org/10.1007/s10973-021-10554-3

Aroonwilas, A., Veawab, A., 2004. Characterization and Comparison of the CO 2 Absorption Performance into Single and Blended Alkanolamines in a Packed Column. Ind. Eng. Chem. Res. 43, 2228–2237. https://doi.org/10.1021/ie0306067

Awwad, A.M., Al-Dujaili, A.H., Salman, H.E., 2002. Relative permittivities, densities, and refractive indices of the binary mixtures of sulfolane with ethylene glycol, diethylene glycol, and poly(ethylene glycol) at 303.15 K. J. Chem. Eng. Data 47, 421–424. https://doi.org/10.1021/je010259c

Ben-Mansour, R., Habib, M.A., Bamidele, O.E., Basha, M., Qasem, N.A.A., Peedikakkal, A., Laoui, T., Ali, M., 2016. Carbon capture by physical adsorption: Materials, experimental investigations and numerical modeling and simulations - A review. Appl. Energy 161, 225–255. https://doi.org/10.1016/j.apenergy.2015.10.011

Chao, C., Deng, Y., Dewil, R., Baeyens, J., Fan, X., 2021. Post-combustion carbon capture. Renew. Sustain. Energy Rev. 138, 110490. https://doi.org/10.1016/j.rser.2020.110490

Cichowska-Kopczyńska, I., Warmińska, D., Nowosielski, B., 2021. Solubility of carbon dioxide in deep eutectic solvents based on 3-amino-1-propanol and tetraalkylammonium salts at low pressure. Materials (Basel). 14, 1–14. https://doi.org/10.3390/ma14030594

Cole, P.J., 1960. The Density of Solid Phenol. J. Chem. Eng. Data 5, 367. https://doi.org/10.1021/je60007a036

Crespo, E.A., Costa, J.M.L., Palma, A.M., Soares, B., Martín, M.C., Segovia, J.J., Carvalho, P.J., Coutinho, J.A.P., 2019. Thermodynamic characterization of deep eutectic solvents at high pressures. Fluid Phase Equilib. 500, 1–13. https://doi.org/10.1016/j.fluid.2019.112249

Deng, D., Han, G., Jiang, Y., 2015. Investigation of a deep eutectic solvent formed by levulinic acid with quaternary ammonium salt as an efficient SO 2 absorbent. New J. Chem. 39, 8158–8164. https://doi.org/10.1039/C5NJ01629K

Deng, D., Jiang, Y., Liu, X., Zhang, Z., Ai, N., 2016. Investigation of solubilities of carbon dioxide in five levulinic acid-based deep eutectic solvents and their thermodynamic properties. J. Chem. Thermodyn. 103, 212–217. https://doi.org/10.1016/j.jct.2016.08.015

Dietz, C.H.J.T., van Osch, D.J.G.P., Kroon, M.C., Sadowski, G., van Sint Annaland,

M., Gallucci, F., Zubeir, L.F., Held, C., 2017. PC-SAFT modeling of CO2 solubilities in hydrophobic deep eutectic solvents. Fluid Phase Equilib. 448, 94–98. https://doi.org/10.1016/j.fluid.2017.03.028

Elsaid, K., Kamil, M., Sayed, E.T., Abdelkareem, M.A., Wilberforce, T., Olabi, A., 2020. Environmental impact of desalination technologies: A review. Sci. Total Environ. 748, 1–19. https://doi.org/10.1016/j.scitotenv.2020.141528

Francisco, M., González, A.S.B., García De Dios, S.L., Weggemans, W., Kroon, M.C., 2013. Comparison of a low transition temperature mixture (LTTM) formed by lactic acid and choline chloride with choline lactate ionic liquid and the choline chloride salt: Physical properties and vapour-liquid equilibria of mixtures containing water and ethanol. RSC Adv. 3, 23553–23561. https://doi.org/10.1039/c3ra40303c

Ghaedi, H., Zhao, M., Clough, P.T., Anthony, E.J., Fennell, P.S., 2020. High CO2 absorption in new amine based-transition-temperature mixtures (deep eutectic analogues) and reporting thermal stability, viscosity and surface tension: Response surface methodology (RSM). J. Mol. Liq. 316, 1–11. https://doi.org/10.1016/j.molliq.2020.113863

Gross, J., Sadowski, G., 2001. Perturbed-chain SAFT: An equation of state based on a perturbation theory for chain molecules. Ind. Eng. Chem. Res. 40, 1244–1260. https://doi.org/10.1021/ie0003887

Gu, Y., Hou, Y., Ren, S., Sun, Y., Wu, W., 2020. Hydrophobic Functional Deep Eutectic Solvents Used for Efficient and Reversible Capture of CO2. ACS Omega 5, 6809–6816. https://doi.org/10.1021/acsomega.0c00150

Guo, W., Hou, Y., Ren, S., Tian, S., Wu, W., 2013. Formation of deep eutectic solvents by phenols and choline chloride and their physical properties. J. Chem. Eng. Data 58, 866–872. https://doi.org/10.1021/je300997v

Haghbakhsh, R., Keshtkar, M., Shariati, A., Raeissi, S., 2021. Experimental investigation of carbon dioxide solubility in the deep eutectic solvent (1 ChCl + 3 triethylene glycol) and modeling by the CPA EoS. J. Mol. Liq. 330, 1–12. https://doi.org/10.1016/j.molliq.2021.115647

Haghbakhsh, R., Raeissi, S., 2017. Modeling the Phase Behavior of Carbon Dioxide Solubility in Deep Eutectic Solvents with the Cubic Plus Association Equation of State. J. Chem. Eng. Data 63, 897–906. https://doi.org/10.1021/acs.jced.7b00472

Haider, M.B., Jha, D., Kumar, R., Sivagnanam, M., 2020. Ternary hydrophobic deep eutectic solvents for carbon dioxide absorption. Int. J. Greenh. Gas Control 92, 1–11. https://doi.org/10.1016/j.ijggc.2019.102839

Haider, M.B., Jha, D., Marriyappan Sivagnanam, B., Kumar, R., 2019. Modelling and simulation of CO2 removal from shale gas using deep eutectic solvents. J. Environ. Chem. Eng. 7, 1–9. https://doi.org/10.1016/j.jece.2018.10.061

Haider, M.B., Jha, D., Marriyappan Sivagnanam, B., Kumar, R., 2018. Thermodynamic and Kinetic Studies of CO2 Capture by Glycol and Amine-Based Deep Eutectic Solvents. J. Chem. Eng. Data 63, 2671–2680. https://doi.org/10.1021/acs.jced.8b00015

Haider, M.B., Kumar, R., 2020. Solubility of CO2 and CH4 in sterically hindered amine-based deep eutectic solvents. Sep. Purif. Technol. 248, 117055. https://doi.org/10.1016/j.seppur.2020.117055

Haider, M.B., Maheshwari, P., Kumar, R., 2021. CO2 capture from flue gas using phosphonium based deep eutectic solvents: Modeling and simulation approach. J. Environ. Chem. Eng. 9, 106727. https://doi.org/10.1016/j.jece.2021.106727

Hansen, B.B., Spittle, S., Chen, B., Poe, D., Zhang, Y., Klein, J.M., Horton, A., Adhikari, L., Zelovich, T., Doherty, B.W., Gurkan, B., Maginn, E.J., Ragauskas, A., Dadmun, M., Zawodzinski, T.A., Baker, G.A., Tuckerman, M.E., Savinell, R.F., Sangoro, J.R., 2021. Deep Eutectic Solvents: A Review of Fundamentals and Applications. Chem. Rev. 121, 1232–1285. https://doi.org/10.1021/acs.chemrev.0c00385

Hester, R.E., Harrison, R.M., 2010. Carbon Capture: Sequestration and Storage. The Royal Society of Chemistry, Cambridge.

IPCC, 2018. Global warming of 1,5 °C an IPCC Special Report on the Impacts of Global Warming of 1.5 °C above Pre-industrial Levels and Related Global Greenhouse Gas Emission Pathways, in the Context of Strengthening the Global Response to the

Threat of Climate Change.

IPCC, 2005. IPCC special report on carbon dioxide capture and storage. Prepared by working group III of the Intergovernmental Panel on Climate Change.

Ji, Y., Hou, Y., Ren, S., Yao, C., Wu, W., 2016. Phase equilibria of high pressure CO2 and deep eutectic solvents formed by quaternary ammonium salts and phenol. Fluid Phase Equilib. 429, 14–20. https://doi.org/10.1016/j.fluid.2016.08.020

Joback, K.G., Reid, R.C., 1987. Estimation of Pure-Component Properties from Group-Contributions. Chem. Eng. Commun. 57, 233–243. https://doi.org/10.1080/00986448708960487

Joshi, M., Hawkins, E., Sutton, R., Lowe, J., Frame, D., 2011. Projections of when temperature change will exceed 2°C above pre-industrial levels. Nat. Clim. Chang. 1, 407–412. https://doi.org/10.1038/nclimate1261

Kamgar, A., Mohsenpour, S., Esmaeilzadeh, F., 2017. Solubility prediction of CO2, CH4, H2, CO and N2 in Choline Chloride/Urea as a eutectic solvent using NRTL and COSMO-RS models. J. Mol. Liq. 247, 70–74. https://doi.org/10.1016/j.molliq.2017.09.101

Kontogeorgis, G.M., Folas, G.K., 2009. Thermodynamic Models for Industrial Applications: From Classical and Advanced Mixing Rules to Association Theories, Thermodynamic Models for Industrial Applications: From Classical and Advanced Mixing Rules to Association Theories. https://doi.org/10.1002/9780470747537

Kontogeorgis, G.M., V. Yakoumis, I., Meijer, H., Hendriks, E., Moorwood, T., 1999. Multicomponent phase equilibrium calculations for water–methanol–alkane mixtures. Fluid Phase Equilib. 158–160, 201–209. https://doi.org/10.1016/S0378-3812(99)00060-6

Kontogeorgis, G.M., Voutsas, Epaminondas, C., Yakoumis, Iakovos, V., Tassios, Dimitrios, P., 1996. An Equation of State for Associating Fluids. Ind. Eng. Chem. Res. 35, 4310–4318. https://doi.org/10.1021/ie071397j

Krishnan, A., Gopinath, K.P., Vo, D.V.N., Malolan, R., Nagarajan, V.M., Arun, J., 2020. Ionic liquids, deep eutectic solvents and liquid polymers as green solvents in carbon

capture technologies: a review. Environ. Chem. Lett. 18, 2031–2054. https://doi.org/10.1007/s10311-020-01057-y

Leron, R.B., Caparanga, A., Li, M.H., 2013. Carbon dioxide solubility in a deep eutectic solvent based on choline chloride and urea at T = 303.15-343.15K and moderate pressures. J. Taiwan Inst. Chem. Eng. 44, 879–885. https://doi.org/10.1016/j.jtice.2013.02.005

Leron, R.B., Li, M.H., 2013a. Solubility of carbon dioxide in a choline chloride-ethylene glycol based deep eutectic solvent. Thermochim. Acta 551, 14–19. https://doi.org/10.1016/j.tca.2012.09.041

Leron, R.B., Li, M.H., 2013b. Solubility of carbon dioxide in a eutectic mixture of choline chloride and glycerol at moderate pressures. J. Chem. Thermodyn. 57, 131–136. https://doi.org/10.1016/j.jct.2012.08.025

Leron, R.B., Li, M.H., 2012. High-pressure volumetric properties of choline chloride-ethylene glycol based deep eutectic solvent and its mixtures with water. Thermochim. Acta 546, 54–60. https://doi.org/10.1016/j.tca.2012.07.024

Leron, R.B., Soriano, A.N., Li, M.H., 2012. Densities and refractive indices of the deep eutectic solvents (choline chloride+ethylene glycol or glycerol) and their aqueous mixtures at the temperature ranging from 298.15 to 333.15K. J. Taiwan Inst. Chem. Eng. 43, 551–557. https://doi.org/10.1016/j.jtice.2012.01.007

Leung, D.Y.C., Caramanna, G., Maroto-Valer, M.M., 2014. An overview of current status of carbon dioxide capture and storage technologies. Renew. Sustain. Energy Rev. 39, 426–443. https://doi.org/10.1016/j.rser.2014.07.093

Li, F., Hemmati, A., Rashidi, H., 2020. Industrial CO2 absorption into methyldiethanolamine/piperazine in place of monoethanolamine in the absorption column. Process Saf. Environ. Prot. 142, 83–91. https://doi.org/10.1016/j.psep.2020.06.006

Li, G., Deng, D., Chen, Y., Shan, H., Ai, N., 2014. Solubilities and thermodynamic properties of CO2 in choline-chloride based deep eutectic solvents. J. Chem. Thermodyn. 75, 58–62. https://doi.org/10.1016/j.jct.2014.04.012

Li, X., Hou, M., Han, B., Wang, X., Zou, L., 2008. Solubility of CO2 in a choline chloride + urea eutectic mixture. J. Chem. Eng. Data 53, 548–550. https://doi.org/10.1021/je700638u

Liu, X., Ao, Q., Shi, S., Li, S., 2022. CO2capture by alcohol ammonia based deep eutectic solvents with different water content. Mater. Res. Express 9. https://doi.org/10.1088/2053-1591/ac47c6

Lydersen, A.L., 1955. Estimation of critical properties of organic compounds by the method of group contibutions. Madison.

Martins, M.A.R., Pinho, S.P., Coutinho, J.A.P., 2018. Insights into the Nature of Eutectic and Deep Eutectic Mixtures. J. Solution Chem. 1–3. https://doi.org/10.1007/s10953-018-0793-1

Maximo, G.J., Carareto, N.D.D., Costa, M.C., 2019. Thermodynamics of Phase Equilibria in Food Engineering, 1st ed, Thermodynamics of Phase Equilibria in Food Enhineering. Elsevier. https://doi.org/10.1016/C2016-0-01686-8

Mirza, N.R., Nicholas, N.J., Wu, Y., Mumford, K.A., Kentish, S.E., Stevens, G.W., 2015. Experiments and Thermodynamic Modeling of the Solubility of Carbon Dioxide in Three Different Deep Eutectic Solvents (DESs). J. Chem. Eng. Data 60, 3246–3252. https://doi.org/10.1021/acs.jced.5b00492

Mohamed, H.O., Obaid, M., Sayed, E.T., Abdelkareem, M.A., Park, M., Liu, Y., Kim, H.Y., Barakat, N.A.M., 2017. Graphite Sheets as High-Performance Low-Cost Anodes for Microbial Fuel Cells Using Real Food Wastewater. Chem. Eng. Technol. 40, 2243–2250. https://doi.org/10.1002/ceat.201700058

Oliveira, M.B., Queimada, A.J., Kontogeorgis, G.M., Coutinho, J.A.P., 2011. Evaluation of the CO2 behavior in binary mixtures with alkanes, alcohols, acids and esters using the Cubic-Plus-Association Equation of State. J. Supercrit. Fluids 55, 876–892. https://doi.org/10.1016/j.supflu.2010.09.036

Pachauri, R.K., Allen, M.R., Barros, V.R., Broome, J., Cramer, W., Christ, R., Church, J.A., Clarke, L., Dahe, Q., Dasgupta, P., Dubash, N.K., Edenhofer, O., Elgizouli, I., Field, C.B., Forster, P., Friedlingstein, P., Fuglestvedt, J, J.P., 2014. Climate Change

2014: Synthesis Report. Contribution of Working Groups I, II and III to the Fifth Assessment Report of the Intergovernmental Panel on Climate Change. Geneva, Switzerland.

Pelaquim, F.P., Barbosa Neto, A.M., Dalmolin, I.A.L., Costa, M.C. da, 2021. Gas Solubility Using Deep Eutectic Solvents: Review and Analysis. Ind. Eng. Chem. Res. acs.iecr.1c00947. https://doi.org/10.1021/acs.iecr.1c00947

Peng, D.Y., Robinson, D.B., 1976. A New Two-Constant Equation of State. Ind. Eng. Chem. Fundam. 15, 59–64. https://doi.org/10.1021/i160057a011

Pires, J.C.M., Martins, F.G., Alvim-Ferraz, M.C.M., Simões, M., 2011. Recent developments on carbon capture and storage: An overview. Chem. Eng. Res. Des. 89, 1446–1460. https://doi.org/10.1016/j.cherd.2011.01.028

Pishro, K.A., Murshid, G., Mjalli, F.S., Naser, J., 2021. Carbon dioxide solubility in amine-based deep eutectic solvents: Experimental and theoretical investigation. J. Mol. Liq. 325, 115133. https://doi.org/10.1016/j.molliq.2020.115133

Qin, H., Song, Z., Cheng, H., Deng, L., Qi, Z., 2021. Physical absorption of carbon dioxide in imidazole-PTSA based deep eutectic solvents. J. Mol. Liq. 326, 1–7. https://doi.org/10.1016/j.molliq.2021.115292

Rabaia, M.K.H., Abdelkareem, M.A., Sayed, E.T., Elsaid, K., Chae, K.J., Wilberforce, T., Olabi, A.G., 2021. Environmental impacts of solar energy systems: A review. Sci. Total Environ. 754, 1–19. https://doi.org/10.1016/j.scitotenv.2020.141989

Rabhi, F., Mutelet, F., Sifaoui, H., 2021. Solubility of Carbon Dioxide in Carboxylic Acid-Based Deep Eutectic Solvents. J. Chem. Eng. Data 66, 702–711. https://doi.org/10.1021/acs.jced.0c00844

Renon, H., Prausnitz, J.M., 1968. Local compositions in thermodynamic excess functions for liquid mixtures. AIChE J. 14, 135–144. https://doi.org/10.1002/aic.690140124

Rochelle, G.T., 2012. Thermal degradation of amines for CO2 capture. Curr. Opin. Chem. Eng. 1, 183–190. https://doi.org/10.1016/j.coche.2012.02.004

Sarmad, S., Mikkola, J.P., Ji, X., 2017. Carbon Dioxide Capture with Ionic Liquids and

Deep Eutectic Solvents: A New Generation of Sorbents. ChemSusChem 10, 324–352. https://doi.org/10.1002/cssc.201600987

Sarmad, S., Nikjoo, D., Mikkola, J.P., 2020. Amine functionalized deep eutectic solvent for CO2 capture: Measurements and modeling. J. Mol. Liq. 309, 1–11. https://doi.org/10.1016/j.molliq.2020.113159

Schmelz, W.J., Hochman, G., Miller, K.G., 2020. Total cost of carbon capture and storage implemented at a regional scale: northeastern and midwestern United States. Interface Focus 10, 1–15. https://doi.org/10.1098/rsfs.2019.0065

Shahbaz, K., Mjalli, F.S., Hashim, M.A., Alnashef, I.M., 2011. Prediction of deep eutectic solvents densities at different temperatures. Thermochim. Acta 515, 67–72. https://doi.org/10.1016/j.tca.2010.12.022

Song, Z., Song, Z., Hu, X., Wu, H., Mei, M., Linke, S., Zhou, T., Zhou, T., Qi, Z., Sundmacher, K., Sundmacher, K., 2020. Systematic Screening of Deep Eutectic Solvents as Sustainable Separation Media Exemplified by the CO2 Capture Process. ACS Sustain. Chem. Eng. 8, 8741–8751. https://doi.org/10.1021/acssuschemeng.0c02490

Sultan, T., Zabiri, H., Shahbaz, M., Maulud, A.S., 2021. Performance Evaluation of the Fast Model Predictive Control Scheme on a CO2 Capture Plant through Absorption/Stripping System. Process Saf. Environ. Prot. 157, 218–236. https://doi.org/10.1016/j.psep.2021.11.018

Tapia, J.F.D., Lee, J.Y., Ooi, R.E.H., Foo, D.C.Y., Tan, R.R., 2016. Planning and scheduling of CO2 capture, utilization and storage (CCUS) operations as a strip packing problem. Process Saf. Environ. Prot. 104, 358–372. https://doi.org/10.1016/j.psep.2016.09.013

Tsivintzelis, I., Kontogeorgis, G.M., Michelsen, M.L., Stenby, E.H., 2011. Modeling phase equilibria for acid gas mixtures using the CPA equation of state. Part II: Binary mixtures with CO2. Fluid Phase Equilib. 306, 38–56. https://doi.org/10.1016/j.fluid.2011.02.006

Twu, C.H., 1986. Generalized method for predicting viscosities of petroleum fractions.

AIChE J. 32, 2091–2094. https://doi.org/10.1002/aic.690321221

Valderrama, J.O., Rojas, R.E., 2009. Critical properties of ionic liquids. Revisited. Ind. Eng. Chem. Res. 48, 6890–6900. https://doi.org/10.1021/ie900250g

Wang, J., Cheng, H., Song, Z., Chen, L., Deng, L., Qi, Z., 2019. Carbon Dioxide Solubility in Phosphonium-Based Deep Eutectic Solvents: An Experimental and Molecular Dynamics Study. Ind. Eng. Chem. Res. 58, 17514–17523. https://doi.org/10.1021/acs.iecr.9b03740

Wilberforce, T., Olabi, A.G., Sayed, E.T., Elsaid, K., Abdelkareem, M.A., 2021. Progress in carbon capture technologies. Sci. Total Environ. 761, 1–11. https://doi.org/10.1016/j.scitotenv.2020.143203

Yadav, A., Pandey, S., 2014. Densities and viscosities of (choline chloride + urea) deep eutectic solvent and its aqueous mixtures in the temperature range 293.15 K to 363.15 K. J. Chem. Eng. Data 59, 2221–2229. https://doi.org/10.1021/je5001796

Zhang, Z., Pan, S., Li, H., Cai, J., Ghani, A., John, E., Manovic, V., 2020. Recent advances in carbon dioxide utilization. Renew. Sustain. Energy Rev. 125, 1–17. https://doi.org/10.1016/j.rser.2020.109799

Zubeir, L.F., Held, C., Sadowski, G., Kroon, M.C., 2016. PC-SAFT Modeling of CO2 Solubilities in Deep Eutectic Solvents. J. Phys. Chem. B 120, 2300–2310. https://doi.org/10.1021/acs.jpcb.5b07888

Zubeir, L.F., Van Osch, D.J.G.P., Rocha, M.A.A., Banat, F., Kroon, M.C., 2018. Carbon Dioxide Solubilities in Decanoic Acid-Based Hydrophobic Deep Eutectic Solvents. J. Chem. Eng. Data 63, 913–919. https://doi.org/10.1021/acs.jced.7b00534

Supporting Information

1. Model Description

1.1. Peng-Robinson Equation of State

CO_2 solubility in DESs was modelled using the Peng-Robinson EoS (Mirza et al., 2015; Peng and Robinson, 1976), defined as follows:

$$P = \frac{RT}{V_m - b} - \frac{a(T)}{V_m(V_m + b) + b(V_m - b)} \quad (1)$$

where V_m is the molar volume, T is the temperature, P is the pressure, and R is the universal gas constant. The physical energy parameter a and co-volume parameter b are functions of the critical properties - temperature (T_c) and pressure (P_c) - and are calculated for each component according to Equations (2) and (3), respectively:

$$a_i = 0.45724 \frac{RT_{c_i}^2}{P_{c_i}} \left[1 + m_i \left(1 - \sqrt{\frac{T}{T_{c_i}}}\right)\right]^2 \quad (2)$$

$$b_i = 0.0778 \frac{RT_{c_i}}{P_{c_i}} \quad (3)$$

with,

$$m_i = 0.37464 + 1.54226\omega_i - 0.26992\omega_i^2 \quad (4)$$

for $\omega_i < 0.49$. Peng-Robinson EoS (Peng and Robinson, 1978) was modified to consider molecules whose $\omega_i \geq 0.49$, according to the expression:

$$m_i = 0.37964 + 1.4850\omega_i - 0.16442\omega_i^2 + 0.01667\omega_i^3 \quad (5)$$

Hence DESs usually present acentric factors greater than 0.49.

The prevailing forces between molecules of different components, which forms the mixture were described considering the mixing rules. Thus, the a_i and b_i parameters of the mixture are determined using the one-fluid type mixing rules:

$$a = \sum_{i=1}^{N_c}\sum_{j=1}^{N_c} x_i x_j \left(1 - k_{ij}\right)\sqrt{a_i a_j} \tag{6}$$

and,

$$b = \sum_{i=1}^{N_c} x_i b_i \tag{7}$$

where x_i is the molar fraction of the component i and k_{ij} is the binary interaction parameter fitted based on CO_2 experimental data — DES vapor-liquid equilibrium (VLE) — given by:

$$A = \frac{aP}{R^2T^2} \tag{8}$$

$$B = \frac{bP}{RT} \tag{9}$$

Once these parameters are determined, the compressibility factor (Z) can be obtained using the following equation — which is the Peng-Robinson EoS cubic in Z:

$$Z^3 - (1 - B)Z^2 + (A - 2B - 3B^2)Z - (AB - B^2 - B^3) = 0 \tag{10}$$

The fugacity coefficient of component i can be calculated by:

$$\phi_i = \exp\left[(Z-1)\frac{b_i}{B} - \ln(Z-B) - \frac{A}{2\sqrt{2}B} \times \left(\frac{2\sum_j y_i a_{ij}}{A} - \frac{b_i}{B}\right)\ln\left(\frac{Z + \left(1+\sqrt{2}\right)B}{Z + \left(1+\sqrt{2}\right)B}\right)\right] \tag{11}$$

Individual fugacities were determined based on fugacities coefficients and $\phi - \phi$ approach, whereby liquid and vapor phases were considered as equal.

$$f_i^L = f_i^V \tag{12}$$

with,

$$f_i^V = y_i \phi_i^V P \tag{13}$$

$$f_i^L = x_i \phi_i^L P \tag{14}$$

An iterative method was used to solve Equation (3), which must simultaneously satisfy two constraints:

$$\sum_i x_i = 1 \tag{15}$$

$$\sum_i y_i = 1 \tag{16}$$

1.2. Cubic-Plus Association Equation of State

The CPA equation is composed by the classic SRK equation and the association from statistical thermodynamics. Pressure is provided by Equation (8) (Kontogeorgis et al., 1999, 1996):

$$P = \frac{RT}{V_m - b} - \frac{\mathrm{a}(T)}{V_m(V_m + b)} - \frac{1}{2}\frac{RT}{V_m}\left(1 + \rho\frac{\partial \ln g}{\partial \rho}\right)\sum_i x_i \sum_{A_i}\left(1 - X_{A_i}\right) \tag{17}$$

where x_i is the molar fraction of component i and ρ is the molar density ($\rho = 1/V_m$). The physical energy parameter ($\mathrm{a}(T)$) is calculated using Equation (18):

$$\mathrm{a}(T) = \mathrm{a}_0 \left(1 + c_1\left(1 - \sqrt{T_r}\right)\right)^2 \quad (18)$$

with $T_r = \frac{T}{T_c}$, where T_c is the critical temperature.

X_{A_i} represents the mole fraction of sites A in molecule i that were not bonded to other active sites, provided by the following Equation:

$$X_{Ai} = \frac{1}{1 + \rho \sum_j x_j \sum_{B_j} X_{Bj} \Delta^{A_i B_j}} \quad (19)$$

where $\Delta^{A_i B_j}$ is the association strength given by Equation (20), which describes the association bonds between two different molecules with two active sites.

$$\Delta^{A_i B_j} = g(V_m)^{ref} \left[\exp\left(\frac{\varepsilon^{A_i B_j}}{RT}\right) - 1\right] b_{ij} \beta^{A_i B_j} \quad (20)$$

In Equation (20), $\varepsilon^{A_i B_j}$ is the association energy, $\beta^{A_i B_j}$ is the association volume, and $g(V_m)^{ref}$ is the radial distribution function for reference fluid (rigid spheres) — defined by Elliot et al., (1990) as:

$$g(V_m) = \frac{1}{1 - 1.9\eta} \quad (21)$$

with

$$\eta = \frac{1}{4} b\rho \quad (22)$$

and

$$b_{ij} = \frac{b_i + b_j}{2} \quad (23)$$

To specify the suitable association scheme, which is the way that CO_2 interacts with other molecules, is an important step. The X_{Ai} value for the association compounds depends on the number and type of pure compounds association sites. Huang and Radosz, (1990) proposed the association schemes.

Therefore, five parameters are necessary to describe a pure component using CPA EoS: a_0, b, and c_1 in the physical part, $\varepsilon^{A_iB_j}$ and $\beta^{A_iB_j}$ in the association part. The co-volume term b is present in both parts of the EoS. These parameters are optimized by fitting vapor pressure and/or liquid density data within a desired temperature range. For non-self-associating compounds, optimized parameters are only those of SRK.

To extend CPA EoS to mixtures, conventional mixing rules are employed in the physical term for energy and co-volume b. For the energy parameter $a_{ij}(T)$, the following geometric mean rule is used:

$$a(T) = \sum_i \sum_j x_i x_j a_{ij}(T) \tag{24}$$

with

$$a_{ij}(T) = \sqrt{a_i(T) a_j(T)}\left(1 - k_{ij}\right) \tag{25}$$

while the mixture co-volume b is given by:

$$b = \sum_i x_i b_i \tag{26}$$

If the mixture is composed by non-associating compounds, the binary interaction parameter k_{ij} is the only adjustable parameter.

Although the association term requires no mixing rules, mixtures presenting cross-association molecules require combining rules for the association energy and

volume parameters to calculate the association strength value. The suitable rules for CPA were CR-1 and Elliott's combining rules (Voutsas et al., 1999).

$$\varepsilon^{A_iB_j} = \frac{\varepsilon^{A_iB_i} + \varepsilon^{A_jB_j}}{2} \tag{27}$$

$$\beta^{A_iB_j} = \sqrt{\beta^{A_iB_i}\beta^{A_jB_j}} \tag{28}$$

$$\Delta^{A_iB_j} = \sqrt{\Delta^{A_iB_i}\Delta^{A_jB_j}} \tag{29}$$

Mixtures in which only one compound has association bonds while the other remains inert are common, implying only the occurrence of association bonds. Folas et al., (2006) call such a process "solvation," describing the induction of hydrogen-bond between polar associating and inert compounds upon mixing. These cases consider one association bond between polar and inert compounds, requiring the optimization of the volume parameter ($\beta^{A_iB_j}$) from experimental data. The energy parameter ($\varepsilon^{A_iB_j}$) is calculated using the modified CR-1 combining rule (Folas et al., 2006).

$$\varepsilon^{A_iB_j} = \frac{\varepsilon_{associating}}{2} \tag{30}$$

1.3. DESs' critical properties

Regardless of the EoS used, thermodynamic modelling requires DESs critical properties — which are not easily found in the literature. Critical properties of ionic liquids were calculated using the modified Lydersen−Joback−Reid method proposed by Valderrama and Rojas, (2009) (Joback and Reid, 1987; Lydersen, 1955;), and different molar ratios of HBA and HBD using the Lee-Kesler mixing rule (Lydersen, 1955). Critical pressure and volume were calculated using the Lydersen

method, while normal boiling and critical temperatures were calculated using the Joback–Reid method.

The Joback group-contribution method was choose because it calculates critical properties without any experimental data and shows good accuracy for high-mass molecules such as DESs. Moreover, DESs were prepared using salts with similar ionic nature to ionic liquids — as successfully determined by the modified Lydersen−Joback−Reid method (Haghbakhsh and Raeissi, 2017; Haider et al., 2018; Shahbaz et al., 2011).

Normal boiling point (T_b), critical temperature (T_c), critical pressure (P_c) and critical volume (V_c) were calculated for each HBA and HBD as follow:

$$T_b = 198.2 + \sum n\Delta T_{bM} \tag{31}$$

$$T_c = \frac{T_b}{[0.5703 + 1.0121 \sum n\Delta T_M - (\sum n\Delta T_M)^2]} \tag{32}$$

$$P_c = \frac{M}{(0.2573 + \sum n\Delta P_M)^2} \tag{33}$$

$$V_c = 6.75 + \sum n\Delta V_M \tag{34}$$

where ΔT_{bM}, ΔT_M, ΔP_M and ΔV_M are constants of the modified Lydersen–Joback–Reid method (presented in Table S1), M is the molecular mass (g.mol^{-1}), and n is the number of each contribution group.

Each HBA and HBD acentric factor was calculated according to the equation proposed by Valderrama and Robles (2007):(Valderrama and Robles, 2007)

$$\omega = \frac{(T_b - 43)(T_c - 43)}{(T_c - T_b)(0.7T_c - 43)} \log\left(\frac{P_c}{P_b}\right) - \frac{(T_c - 43)}{(T_c - T_b)} \log\left(\frac{P_c}{P_b}\right) + \log\left(\frac{P_c}{P_b}\right) - 1 \tag{35}$$

where T_c is the critical temperature and P_c critical pressure (calculated by Equation 32 and 33, respectively), T_b is the normal boiling temperature and P_b is the normal boiling pressure (0.101325 MPa).

DES critical properties were calculated by the Lee–Kesler mixing rules, as follows:

$$T_{cm} = \frac{1}{V_{cm}^{\frac{1}{4}}} \sum_i \sum_j y_i y_j V_{cm}^{\frac{1}{4}} T_{cij} \tag{36}$$

$$V_{cm} = \sum_i \sum_j y_i y_j V_{cij} \tag{37}$$

$$\omega_m = \sum_i y_i \omega_i \tag{38}$$

$$T_{cij} = \left(T_{ci} T_{cj}\right)^{\frac{1}{2}} k'_{ij} \tag{39}$$

$$V_{cij} = \frac{1}{8}\left(V_{ci}^{\frac{1}{3}} + V_{cj}^{\frac{1}{3}}\right)^3 \tag{40}$$

$$P_{cm} = 0.2905 - 0.085\omega_m \frac{RT_{cm}}{V_{cm}} \tag{41}$$

where m is related to the mixture and i and j to the pure components, y is the mole fraction of each component, and k'_{ij} is the binary parameters. Due to the lack of experimental data, k'_{ij} was considered as 1.

2. Complementary Results

Table S15. Groups considered for Modified Lydersen–Joback–Reid method.

Group	ΔT_{bM} (K)	ΔT_M (K)	ΔP_M (bar)	ΔV_M (cm³.mol⁻¹)
Without rings				
−CH3	23.58	0.0275	0.3031	66.81
−CH2−	22.88	0.0159	0.2165	57.11
>CH−	21.74	0.0002	0.114	45.7
>C<	18.18	-0.0206	0.0539	21.78
=CH2	24.96	0.017	0.2493	60.37
=CH-	18.25	0.0182	0.1866	49.92
ΞC<	24.14	-0.0003	0.0832	34.9
=C=	26.15	-0.0029	0.0934	33.85
ΞCH	0	0.0078	0.1429	43.97
ΞC−	0	0.0078	0.1429	43.97
−OH (alcohol)	92.88	0.0723	0.1343	30.4
−O−	22.42	0.0051	0.13	15.61
>C=O	94.97	0.0247	0.2341	69.76
−CHO	72.24	0.0294	0.3128	77.46
−COOH	169.06	0.0853	0.4537	88.6
−COO-	0	0.0377	0.4139	84.76
HCOO-	0	0.036	0.4752	97.77
=O (other)	-10.5	0.0273	0.2042	44.03
−NH2	73.23	0.0364	0.1692	49.1
>NH	50.17	0.0119	0.0322	78.96
>N−	11.74	-0.0028	0.0304	26.7
−N=	74.6	0.0172	0.1541	45.54
−CN	125.66	0.0506	0.3697	89.32
−NO2	152.54	0.0448	0.4529	123.62
−F	-0.03	0.0228	0.2912	31.47
−Cl	38.13	0.0188	0.3738	62.08
−Br	66.86	0.0124	0.5799	76.6
−I	93.84	0.0148	0.9174	100.79
With rings				
−CH2−	27.15	0.0116	0.1982	51.64
>CH−	21.78	0.0081	0.1773	30.56
=CH−	26.73	0.0114	0.1693	42.55
>C<	21.32	-0.018	0.0139	17.62
=C<	31.01	0.0051	0.0955	31.28
−O−	31.22	0.0138	0.1371	17.41
−OH (phenol)	76.34	0.0291	0.0493	-17.44
>C=O	94.97	0.0343	0.2751	59.32
>NH	52.82	0.0244	0.0724	27.61
>N−	0	0.0063	0.0538	25.17
−N=	57.55	-0.0011	0.0559	42.15
Other groups				
−B −	24.56	0.0352	0.0348	22.45
−P	34.86	-0.0084	0.1776	67.01
−SO2	147.24	-0.0563	-0.0606	112.19

Table S216. Constant values used to determine the binary interaction parameter using CPA EoS in each studied DES and association scheme for CO_2 and its respective AARD%.

DES	CO_2 solvation				CO_2 2B			CO_2 4C		
	a_0	a_1	β_{ij}	AARD%	a_0	a_1	AARD %	a_0	a_1	AARD %
ChCl + EtGLY[a] 1:2	-2.833	0.007	0	15.05	-3.125	0.009	11.33	-3.230	0.009	7.20
ChCl + Urea 1:2	-2.304	0.005	0.006	8.14	-2.584	0.007	30.75	-2.580	0.007	22.99
ChCl + PH[b] 1:3	-2.397	0.006	-0.015	11.56	-2.657	0.007	9.29	-3.338	0.010	6.87
ChCl + GLY[c] 1:2	-1.258	0.003	0.006	11.59	-1.363	0.004	11.74	-1.505	0.005	8.86
TBPB + PH 1:4	-1.159	0.002	0.006	11.48	-1.309	0.003	6.27	-1.564	0.004	4.88
TBPB + DEG[d] 1:4	-3.347	0.009	0.006	20.52	-4.221	0.012	6.78	-4.393	0.013	6.51
ATPPB + PH 1:4	0.169	-0.001	0.006	7.68	-1.120	0.003	4.36	-1.078	0.003	6.55
ATPPB + PH 1:6	-1.421	0.003	0.006	8.32	-1.392	0.003	8.27	-1.487	0.004	5.38
ACC + LA[e] 1:3	-0.669	0.002	0.007	3.11	-0.806	0.003	3.77	-0.824	0.003	3.21
TEAC + LA 1:3	-1.169	0.003	0.009	2.71	-1.217	0.004	2.93	-1.273	0.005	2.72
TEAB + LA 1:3	-0.920	0.002	0.007	2.04	-1.119	0.004	2.35	-1.156	0.004	2.10
TBAC+ LA 1:3	-0.316	0.0008	0.007	3.53	-0.747	0.003	3.87	-0.760	0.004	4.12
TBAB + LA 1:3	-0.443	0.0009	0.007	1.89	-0.674	0.003	2.01	-0.669	0.003	2.24

a Ethylene Glycol, b Phenol, c Glycerol, d Diethylene Glycol, e Levulinic acid

Table S3. Constant values used to determine the binary interaction parameter using Peng-Robinson 78 and Peng-Robinson with Twu Model in each studied DES and its respective AARD%.

DES	PR78			PR78 (TWU)		
	a_0	a_1	AARD %	a_0	a_1	AARD %
ChCl + Ethylene glycol 1:2	-0.724	0.00281	11.46	-0.723	0.00282	11.49
ChCl + Urea 1:2	-0.220	0.00086	6.76	-0.233	0.00090	6.77
ChCl + Phenol 1:3	0.026	0.00054	4.12	0.005	0.00061	4.10
ChCl + Glycerol 1:2	-0.584	0.00209	8.57	-0.583	0.00209	8.67
TBPB + Phenol 1:4	0.153	-0.00047	7.10	0.126	-0.00038	7.10
TBPB + Diethylene glycol 1:4	0.488	-0.00152	8.13	0.467	-0.00146	8.13
ATPPB + Phenol 1:4	0.167	-0.00067	7.65	0.167	-0.00067	7.68
ATPPB + Phenol 1:6	0.013	-0.00016	4.78	0.013	-0.00016	4.82
ACC + Levulinic acid 1:3	-0.468	0.00187	3.27	-0.471	0.00188	3.28
TEAC + Levulinic acid 1:3	-0.204	0.00113	2.67	-0.215	0.00117	2.68
TEAB + Levulinic acid 1:3	-0.188	0.00109	2.01	-0.208	0.00116	2.01
TBAC+ Levulinic acid 1:3	-0.219	0.00108	3.12	-0.237	0.00114	3.14
TBAB + Levulinic acid 1:3	-0.172	0.00094	1.76	-0.191	0.00100	1.76

Table S4. Temperature and density ranges at 1 bar for each HBA and HBD investigated to use the individual approach.

DES (2B)	Temperature range (K)	Density range (mol/m³)	N_p	AARD% in ρ	Ref.
Choline Chloride	293.15 – 353.15	6960.1 – 7149.2	13	0.05	(Francisco et al., 2013)
Phenol	318.15 – 343.15	10970.5 – 11200.0	6	0.003	(Cunha et al., 2013)
Urea	293.15 – 313.15	16523.2 – 16623.1	3	0.02	(Sadeghi et al., 2012)
TOTAL			22	0.024	

Table S5. Constant values used to determine the binary interaction parameter in the individual approach, modelling with CPA and CO_2 inert.

Components	CPA (CO_2 Inert)					
	k_{12}		k_{13}		k_{23}	
	a_0	a_1	a_0	a_1	a_0	a_1
CO_2 (1) + ChCl (2) + EtGLY (3)	-2.942	0.012	-0.017	-5.50E-04	-1.989	0.004
CO_2 (1) + ChCl (2) + Urea (3)	-5.703	6.80E-04	2.913	-0.007	-12.456	-0.004
CO_2 (1) + ChCl (2) + Phenol (3)	-0.215	0.002	-2.417	0.005	-2.403	0.006
CO_2 (1) + ChCl (2) + Glycerol (3)	-1.291	0.005	-1.870	0.005	-1.599	0.001

Table S6. Constant values used to determine the binary interaction parameter in the individual approach, modelling with Peng-Robinson 78.

Components	Peng-Robinson 78					
	k_{12}		k_{13}		k_{23}	
	a_0	a_1	a_0	a_1	a_0	a_1
CO_2 (1) + ChCl (2) + EtGLY (3)	-0.723	0.003	-0.724	0.003	-0.724	0.003
CO_2 (1) + ChCl (2) + Urea (3)	-0.304	0.001	-0.022	8.62E-04	-0.022	8.62E-04
CO_2 (1) + ChCl (2) + Phenol (3)	-0.029	0.009	0.409	-7.80E-04	0.409	-7.80E-04
CO_2 (1) + ChCl (2) + Glycerol (3)	-0.700	0.003	-0.584	0.002	-0.584	0.002

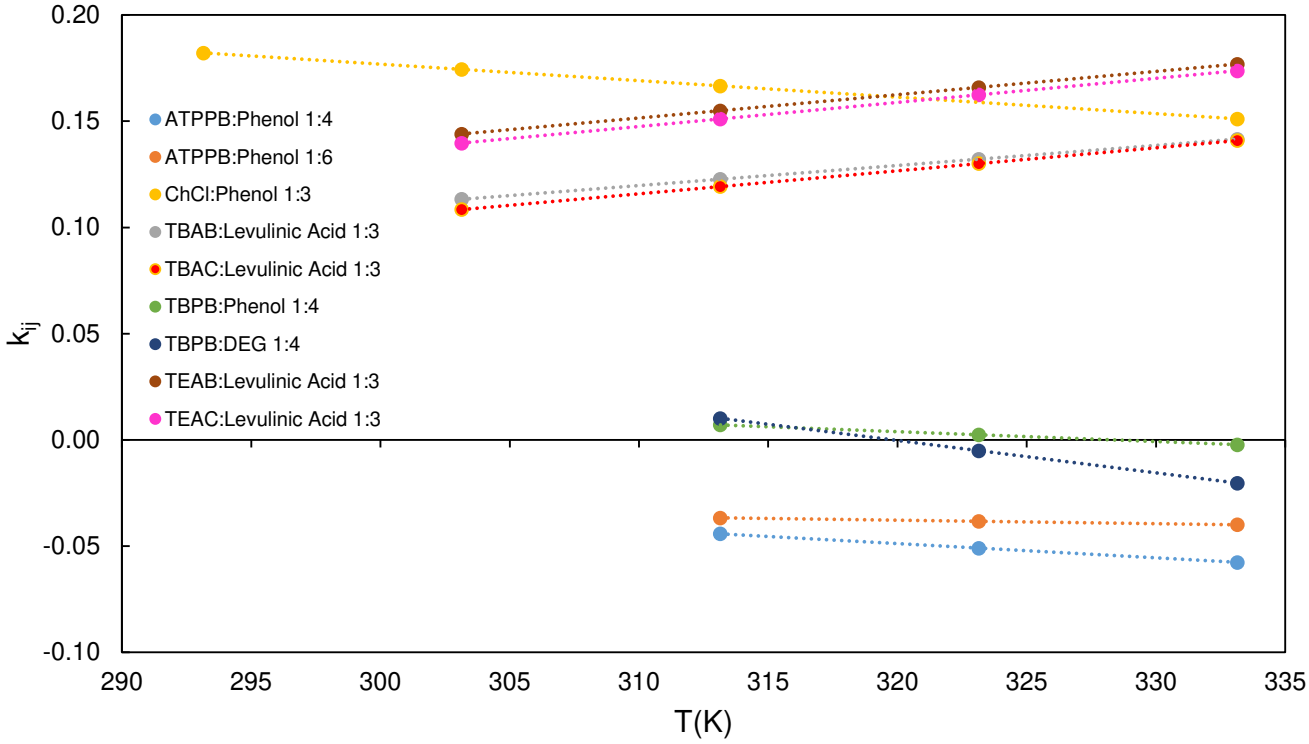

Figure S17. PR78 interaction parameter k_{ij} as a function of temperature.

3. Reference

Cunha, D.L., Coutinho, J.A.P., Daridon, J.L., Reis, R.A., Paredes, M.L.L., 2013. Experimental densities and speeds of sound of substituted phenols and their modeling with the prigogine-flory-patterson model. J. Chem. Eng. Data 58, 2925–2931. https://doi.org/10.1021/je4003256

Elliot, R.J., Suresh, S.J., Donohue, M.D., 1990. A Simple Equation of State for Nonspherical and Associating Molecules. Ind. Eng. Chem. Res. 29, 1476–1485. https://doi.org/10.1021/ie00107a014

Folas, G.K., Kontogeorgis, G.M., Michelsen, M.L., Stenby, E.H., 2006. Application of the cubic-plus-association equation of state to mixtures with polar chemicals and high pressures. Ind. Eng. Chem. Res. 45, 1516–1526. https://doi.org/10.1021/ie0509241

Francisco, M., González, A.S.B., García De Dios, S.L., Weggemans, W., Kroon, M.C., 2013. Comparison of a low transition temperature mixture (LTTM) formed by lactic acid and choline chloride with choline lactate ionic liquid and the choline chloride salt: Physical properties and vapour-liquid equilibria of mixtures containing water and ethanol. RSC Adv. 3, 23553–23561. https://doi.org/10.1039/c3ra40303c

Haghbakhsh, R., Raeissi, S., 2017. Modeling the Phase Behavior of Carbon Dioxide Solubility in Deep Eutectic Solvents with the Cubic Plus Association Equation of State. J. Chem. Eng. Data 63, 897–906. https://doi.org/10.1021/acs.jced.7b00472

Haider, M.B., Jha, D., Marriyappan Sivagnanam, B., Kumar, R., 2018. Thermodynamic and Kinetic Studies of CO2 Capture by Glycol and Amine-Based Deep Eutectic Solvents. J. Chem. Eng. Data 63, 2671–2680. https://doi.org/10.1021/acs.jced.8b00015

Huang, S.H., Radosz, M., 1990. Equation of State for Small, Large, Polydisperse, and Associating Molecules. Ind. Eng. Chem. Res. 29, 2284–2294. https://doi.org/10.1021/ie00107a014

Joback, K.G., Reid, R.C., 1987. Estimation of Pure-Component Properties from Group-Contributions. Chem. Eng. Commun. 57, 233–243. https://doi.org/10.1080/00986448708960487

Kontogeorgis, G.M., V. Yakoumis, I., Meijer, H., Hendriks, E., Moorwood, T., 1999. Multicomponent phase equilibrium calculations for water–methanol–alkane mixtures. Fluid Phase Equilib. 158–160, 201–209. https://doi.org/10.1016/S0378-3812(99)00060-6

Kontogeorgis, G.M., Voutsas, Epaminondas, C., Yakoumis, Iakovos, V., Tassios,

Dimitrios, P., 1996. An Equation of State for Associating Fluids. Ind. Eng. Chem. Res. 35, 4310–4318. https://doi.org/10.1021/ie071397j

Lydersen, A.L., 1955. Estimation of critical properties of organic compounds by the method of group contibutions. Madison.

Mirza, N.R., Nicholas, N.J., Wu, Y., Mumford, K.A., Kentish, S.E., Stevens, G.W., 2015. Experiments and Thermodynamic Modeling of the Solubility of Carbon Dioxide in Three Different Deep Eutectic Solvents (DESs). J. Chem. Eng. Data 60, 3246–3252. https://doi.org/10.1021/acs.jced.5b00492

Peng, D.Y., Robinson, D.B., 1978. The Characterization of the Heptanes and Heavier Fractions for the GPA Peng-Robinson Programs. Gas Processors Association.

Peng, D.Y., Robinson, D.B., 1976. A New Two-Constant Equation of State. Ind. Eng. Chem. Fundam. 15, 59–64. https://doi.org/10.1021/i160057a011

Sadeghi, M., Held, C., Samieenasab, A., Ghotbi, C., Abdekhodaie, M.J., Taghikhani, V., Sadowski, G., 2012. Thermodynamic properties of aqueous salt containing urea solutions. Fluid Phase Equilib. 325, 71–79. https://doi.org/10.1016/j.fluid.2012.04.003

Shahbaz, K., Mjalli, F.S., Hashim, M.A., Alnashef, I.M., 2011. Prediction of deep eutectic solvents densities at different temperatures. Thermochim. Acta 515, 67–72. https://doi.org/10.1016/j.tca.2010.12.022

Valderrama, J.O., Robles, P.A., 2007. Critical properties, normal boiling temperature, and acentric factor of another 200 ionic liquids. Ind. Eng. Chem. Res. 46, 1338–1344. https://doi.org/10.1021/ie071055d

Valderrama, J.O., Rojas, R.E., 2009. Critical properties of ionic liquids. Revisited. Ind.

Eng. Chem. Res. 48, 6890–6900. https://doi.org/10.1021/ie900250g

Voutsas, E.C., Yakoumis, I. V., Tassios, D.P., 1999. Prediction of phase equilibria in water/alcohol/alkane systems. Fluid Phase Equilib. 158–160, 151–163. https://doi.org/10.1016/S0378-3812(99)00131-4

CAPÍTULO 5

Prediction of Greenhouse Gases Solubility in Eutectic Solvents using COSMO-RS

(Artigo submetido na edição especial da Science and Technology for Energy Transition)

Fernanda Paludetto Pelaquim[a], Sérgio M. Vilas-Boas[a,b,c], Débora Costa do Nascimento[a], Pedro Carvalho[c], Antonio Marinho Barbosa Neto[d], Mariana Conceição da Costa[a3*].

a School of Chemical Engineering, University of Campinas – UNICAMP, Avenida Albert Einstein 500, ZIP Code 13083-852, Campinas, SP, Brazil

b Centro de Investigação de Montanha (CIMO), Instituto Politécnico de Bragança, Campus de Santa Apolónia, ZIP Code 5300-253, Bragança, Portugal

c CICECO − Aveiro Institute of Materials, Department of Chemistry, University of Aveiro, ZIP Code 3810-193, Aveiro, Portugal

dThermoPhase, Petroleum Engineering Department, State University of Santa Catarina – UDESC, Avenida Lourival Cesário Pereira, ZIP Code 88336-275, Balneário Camboriú, SC, Brazil

3 * Corresponding author.

E-mail address: mcdcosta@unicamp.br (M.C. Costa)

phone number: +551935213962.

Abstract

Over the past few years, eutectic solvents (ESs) have been drawing the scientific community's attention because they are usually more environmentally friendly than traditional organic solvents. One of the applications of ESs is in the gas capture field, where they are considered promising absorbers to replace amine- (MEA, DEA, or MDEA processes), methanol- (Retinol process), dimethyl ethers of polyethylene glycol- (Selexol process), N-methyl-2-pyrrolidone- (Purisol process), propylene carbonate- (Fluor solvent process), or morpholine-based (Morphysorb process) solvents on CO_2 capture of atmosphere. Although several studies have reported experimental gas solubility data in ESs, especially for CO_2, only a small number of the existing options are covered. In fact, resorting to experimental methods to obtain the solubility data seems unfeasible considering the vast number of possible eutectic mixtures. Therewith, theoretical predictions of gas solubility in ESs are valuable for the fast pre-screening of prospective solvents. In this work, the ability of the COSMO-RS thermodynamic model to represent solubility data of CO_2, CH_4, and H_2S in 17 Choline Chloride-based (ChCl) ESs was evaluated. The experimental data were collected from the literature at different molar ratios, at 298.15 K or 313.15 K, and in the pressure range from 1 to 125 bar. COSMO-RS offers a qualitative description of these gases' solubility, which was expected due to the model's fully predictive character.

Keywords: carbon dioxide, methane, COSMO-RS, solubility, high pressure, eutectic solvents.

1. Introduction

The increasing evidence of an imminent global and systemic environmental crisis has led the scientific community to develop more sustainable products and processes [1]. In this context, green chemistry has emerged as one of the main topics in chemistry, aiming to create products and processes to reduce or eliminate the use and generation of hazardous substances [2]. One of the major green chemistry issues is replacing traditional organic solvents, usually volatile and toxic, for more sustainable options, the so-called alternative solvents [3], such as eutectic solvents (ESs).

A eutectic mixture is often defined as a mixture of components that, at fixed proportions, have a melting temperature lower than the melting points of pure compounds [4]. The term DES is often attributed to eutectic mixtures formed by at least two components, a hydrogen bond donor (HBD) and a hydrogen bond acceptor (HBA), with a eutectic point temperature (and a solid-liquid phase behavior) below that of an ideal liquid mixture, as reported by Martins et al., (2018) [5]. Otherwise, the mixture can be called simply a eutectic solvent (ESs), which is observed for most systems reported in the literature.

The ESs reported in the literature have attracted considerable interest from environmental, economic, and technological viewpoints [6], due to their low prices, low vapor pressure, nonflammability, biocompatibility, biodegradability, and easy preparation processes [7–9]. Consequently, both DESs and ESs have received great attention in recent decades due to their potential to replace organic solvents in various applications, such as media for extracting and purifying biocompounds [10], hydrate inhibitors [11,12], metal processing and metal decomposition agents [13–15], two-phase aqueous system forming agents [16,17], and gas capture media [18,19].

Regarding gas capture, the continuous increase in fossil fuel usage for

transportation and electricity, along with land misuse and other human activities, have led to excessive greenhouse gas (GHGs) emissions, especially carbon dioxide (CO_2) [20,21]. According to the International Energy Agency (IEA) global energy review on CO_2 emission in 2021 [22], global energy-related CO_2 emissions rose by 6%, corresponding to 36.3 billion tons of CO_2 released to the atmosphere, the largest registered level in history in absolute terms. Nonetheless, mitigating GHGs emissions is mandatory because of their negative effects on climate change [23]. The most effective action toward reducing CO_2 emissions would involve replacing fossil fuels with renewable energy sources [24]. However, fossil-fuel-based power plants continue to be the most viable process for electricity and power generation due to their lower price [25,26]. For this reason, technologies to capture flue gases seek to provide a more realistic approach to reducing emissions in the next few years [27].

Developing strategies such as CO_2 capture, utilization, and storage (CCUS) technology could greatly contribute to reducing CO_2 emissions. These technologies can be divided into precombustion, oxyfuel combustion, and post-combustion capture [20,28]. The latter is a suitable alternative to reduce CO_2 emissions in coal-fired power plants [20]. In post-combustion technology, CO_2 is separated from the flue gases through absorption, membrane separation, adsorption, or a combination of these technologies [29,30]. Alternatively, amine-based (like, MEA, DEA, or MDEA) aqueous solutions have traditionally been used as chemical solvents to capture CO_2 due to their excellent absorption capacity, high reactivity, high selectivity, and low price. However, amine-based processes may undergo solvent loss or degradation, equipment corrosion, and emission of volatile organic compounds (VOCs). Regarding physical absorption, which is the case of most ESs, Selexol is a commercial process that uses dimethyl ether of polyethylene glycol (DEPG) as a solvent, and it is applied for the

selective removal of hydrogen and CO_2. This solvent presents low vapor pressure, chemical and thermal stability, and non-corrosive and non-toxic nature; however, the high solubility of DEPG, increases the pumping cost. These drawbacks have propelled the development of new materials for CO_2 capture, such as ESs [31–33].

The efficiency of different ESs in physically absorbing CO_2 has been mainly addressed over the years by evaluating experimental CO_2 solubility in the liquid phase [18,21,34–36]. Nevertheless, almost infinite possibilities of HBA and HBD combinations can result in ESs, and performing experimental solubility studies in all cases becomes unfeasible. Thus, theoretical predictions of CO_2 solubility in ESs are recommended for fast pre-screening prospective solvents [37,38]. In recent studies, classical thermodynamic models such as Non-random two-liquid model (NRTL) [19,39] or equations of state such as PC-SAFT, Cubic Plus Association (CPA), and Peng-Robinson [40–43], paired with the equilibrium isofugacity criteria, have been successfully used to describe gas solubility in organic solvents and ESs.

Although the models mentioned above often deliver good representations of the solubility data, they are semi-empirical approaches that require experimental thermophysical data, such as density, vapor pressure, and heat capacity, to fit the model's parameters. Unfortunately, these data are not easily found in the literature [38,42]. More predictive models, such as the Conductor-like Screening Model for Real Solvents (COSMO-RS) [44–46] arise as attractive tools to describe the phase behavior of systems lacking experimental thermophysical data[45–47]. COSMO-RS has shown to be useful for solvent screening purposes [47–49] due to its predictive character with a qualitative accuracy [21,44]. The model estimates the thermodynamic equilibria of fluids using a statistical thermodynamic approach combined with quantum chemical calculations.

Despite the topic's relevance, only a few studies aiming at modeling CO_2 solubility in ESs have been reported [40,45,51,52]. In this context, this work aims to evaluate the potentialities of COSMO-RS in describing the solubility of CO_2, CH_4, and H_2S in 17 ChCl-based ESs at 313.15 K and pressures ranging from 1 to 125 bar, and whose data is reported in the literature. The model's performance was compared with the results achieved with more empyrical thermodynamic approaches reported in previous studies, such as the PC-SAFT, CPA, and Peng-Robinson equations of state [42].

2. Materials and Methods

2.1. Eutectic Solvent database collection

Experimental gas solubility data in ESs were collected from the literature [31,53–61]. A database comprising the compounds' molecular structure and polarization charge density (cosmo file) was built, allowing us to infer the COSMO-RS predictive accuracy. In this study, 208 solubility data points of CO_2, CH_4, and H_2S in 17 different ESs, at 313.15 K and pressures varying from 1 to 125 bar, were gathered from the literature. All these data are compiled in Table 17.

Choline chloride was chosen as the common HBA, and 15 HBDs were selected, including ethylene glycol, glycerol, phenol, urea, 1,4 butanediol, 2,3 butanediol, 1,2 propanediol, diethylene glycol, triethylene glycol, levulinic acid, furfuryl alcohol, guaiacol, lactic acid, malonic acid, and phenylacetic acid. The HBA:HBD molar ratios of 1:2, 1:3, and 1:4 were considered for CO_2 solubility calculation, while the molar ratio of 1:1 was considered for CH_4 calculation due to the scarcity of experimental data. The only exception was for the ES composed of ChCl (HBA) and urea (HBD), where HBA:HBD molar ratios equal to 1:1.5, 1:2, and 1:2.5 were studied.

Table 17. ChCl-based ESs molar ratio, gas solubility range, and pressure range of the systems analyzed in this study.

Gas	HBD	Molar ratio (HBA:HBD)	Pressure range (bar)	Gas solubility (x_1)	Reference
CO_2	Ethylene Glycol	1:2	2.48 – 59.02	0.008 – 0.230	Leron and Li (2013)[50]
CO_2	Glycerol	1:2	1.91 – 59.91	0.019 – 0.331	Leron and Li (2013)[51]
CO_2	Phenol	1:2; 1:3; 1:4	1.16 – 127.40	0.003 – 0.275	Ji et al., (2016)[52], Li et al., (2014)[53]
CO_2	Urea	1:1.5; 1:2; 1:2.5	10.70 – 125.00	0.046 – 0.309	Li et al., (2008)[54], Liu et al., (2019)[55]
CO_2	1,4 butanediol	1:3; 1:4	1.12 – 5.07	0.003 – 0.012	Chen et al. (2014)[56]
CO_2	2,3 butanediol	1:3; 1:4	1.11 – 5.29	0.003 – 0.014	Chen et al. (2014)[56]
CO_2	1,2 propanediol	1:3; 1:4	1.21 – 5.25	0.002 – 0.012	Chen et al. (2014)[56]
CO_2	Diethylene Glycol	1:3; 1:4	1.16 – 5.18	0.003 – 0.015	Li et al., (2014)[53]
CO_2	Triethylene Glycol	1:3; 1:4	1.14 – 5.19	0.004 – 0.020	Li et al., (2014)[53]
CO_2	Levulinic acid	1:3; 1:4	0.60 – 5.80	0.003 – 0.027	Lu et al., (2015)[57]
CO_2	Furfuryl alcohol	1:3; 1:4	0.70 – 5.82	0.002 – 0.018	Lu et al., (2015)[57]
CO_2	Guaiacol	1:3; 1:4	0.53 – 5.43	0.001 – 0.016	Liu et al., (2017)
CH_4	Lactic acid	1:1	0.05 – 49.93	0.004 – 0.287	Altamash et al., (2019)[58]
CH_4	Malonic acid	1:1	0.05 – 49.93	0.004 – 0.281	Altamash et al., (2019)[58]
CH_4	Phenylacetic acid	1:1	0.05 – 49.92	0.005 – 0.0322	Altamash et al., (2019)[58]
CH_4	Urea	1:1.5; 1:2; 1:2.5	0.10 – 2.03	4E-05 – 0 001	Liu et al., (2019)[55]
H_2S	Urea	1:1.5; 1:2; 1:2.5	0.10 – 2.02	0.002 – 0.055	Liu et al., (2019)[55]

2.2. COSMO-RS

The COSMO-RS is a predictive activity coefficient model that combines the dielectric continuum solvation model, known as COSMO, and statistical thermodynamics [44]. Hereupon, COSMO-RS uses the interaction between a cavity containing a molecule and a dielectric media, generated through quantum chemistry Density Functional Theory (DFT) based calculations, as a reference state from which interaction energies between molecules can be inferred [46]. Through statistical thermodynamics, the definition of an ensemble of pairwise small surface segments of different molecules interacting with each other, along with the establishment of a partition function from which the Gibbs energy of the system can be derived, enables the calculation of solution properties from COSMO-RS [46].

In fact, the contact between molecules in the reference state of COSMO causes the appearance of interaction energies, which contribute to the overall Gibbs energy. From the Gibbs energy, it is possible to derive chemical potentials, thus allowing COSMO-RS to calculate thermodynamic equilibria. The model, in essence, depends only on the molecule's geometry and polarization charge density to determine equilibrium conditions for multicomponent systems, which is a notable advantage over empirical or semi-empirical approaches. To describe the vapor-liquid phase diagram at a fixed pressure (isobaric) or fixed temperature (isothermal), the activity coefficient model computes a list of concentrations that cover the whole range of mole fractions of the system and calculates the excess enthalpy and Gibbs-free energy, the species chemical potentials and activity coefficients, the total vapor pressure of the system and the concentrations of the species in the gas phase. The total pressure of the system is obtained using the modified Raoult's law:

$$p = \sum_i p_i^{\sigma} x_i \gamma_i \qquad (1)$$

COSMO-RS assumes ideal behavior in the gas phase, being the species vapor mole fractions obtained from the ratio of the total pressure and partial vapor pressures

$$p_j = p_j^{\sigma} x_j \gamma_j \tag{2}$$

$$y_i = \frac{p_i^{\sigma} x_i \gamma_i}{p} \tag{3}$$

where p_j^{σ} and γ_j are the vapor pressure and the activity coefficient of component *j*, respectively.

In the present work, the COSMOtherm software (version 21.0) [59] with the BP_TZVPD_FINE_21.ctd level of parametrization was used to estimate the solubility data of the greenhouse gases in the eutectic mixtures. All the required cosmo files for the gases and some ES precursors (phenol, ethylene glycol, and glycerol) were retrieved from the COSMOtherm TZVPD-FINE database. For ChCl and all the HBD missing in the database, the input files were obtained with the COSMOconfX 2021 software coupled to the TmoleX (version 4.5) package using the BP-TZVPD-FINE-COSMO+GAS_18 template [60]. ChCl was treated following the electroneutral mixture approach [61]. Additional details for the gas solubility calculation procedure with COSMOtherm are available in the software reference manual [62]. Moreover, all conformers of each molecule were considered in the simulations.

3. Results and Discussion

The solubilities predicted with COSMO-RS were compared against the experimental data presented in Table 17, which includes solubility of CO_2, CH_4, and H_2S in 17 different ES with various HBA:HBD molar ratios (1:1, 1:1.5,1:2, 1:2.5, 1:3 and 1:4and), at 313.15 K and pressure ranging from 1 to 125 bar. The Average Relative Deviation (ARD) for each *pTx* data set, according to Eq (4), was calculated to evaluate the COSMO-RS capability to describe the experimental data.

$$ARD = \frac{1}{N_p}\sum_{i=1}^{N_p}\frac{\left|x_i^{exp} - x_i^{cal}\right|}{x_i^{cal}} \quad (4)$$

where N_p is the number of experimental data, i is the analyzed gas (CO_2, CH_4, and H_2S), x_i^{exp} is the experimental gas solubility, and x_i^{cal} is the gas solubility calculated with COSMO-RS.

All the 208 experimental data points were plotted against the predicted results (further discussed in the next sections), and the corresponding ARDs are listed in Tables S1 – S33 of the Supporting Information (SI).

3.1. CO_2 solubility in ESs at 1:2 (ChCl:HBD) molar ratio

The experimental and predicted solubility data of CO_2 in ESs at 1:2 HBA:HBD molar ratio are depicted in **Erro! Fonte de referência não encontrada.**. For all of these ESs COSMO-RS could qualitatively describe the experimental data, presenting ARDs varying between 26% and 81%. Although COSMO-RS underestimated the solubilities of all ESs, except ChCl:Ethylene Glycol, the model provided similar curve trends as those reported in the literature [50].

The best results were obtained for the ESs containing diols as the HBD, the ChCl:Glycerol (ARD = 26%) and ChCl:Ethylene glycol (ARD = 34%), while higher deviations were observed for ChCl:Urea (58%) and ChCl:Phenol (ARD = 81%). For example, the experimental CO_2 solubility data, x_{CO2}, in ChCl:Glycerol was 0.31 at 313.15 K and 59.91 bar, and the COSMO-RS predicted value was 0.285, corresponding to an ARD of 14%. In contrast, the experimental CO_2 solubility in ChCl:Phenol at the same temperature and 64.5 bar was 0.186, about five times the value predicted with COSMO-RS (x_{CO2}^{cal} = 0.036). In general, for all the studied dataset, the COSMO-RS prediction is more qualitative, which means that it is able to single out the best solvents from the worst ones as shown in **Erro! Fonte de referência não encontrada.**(C).

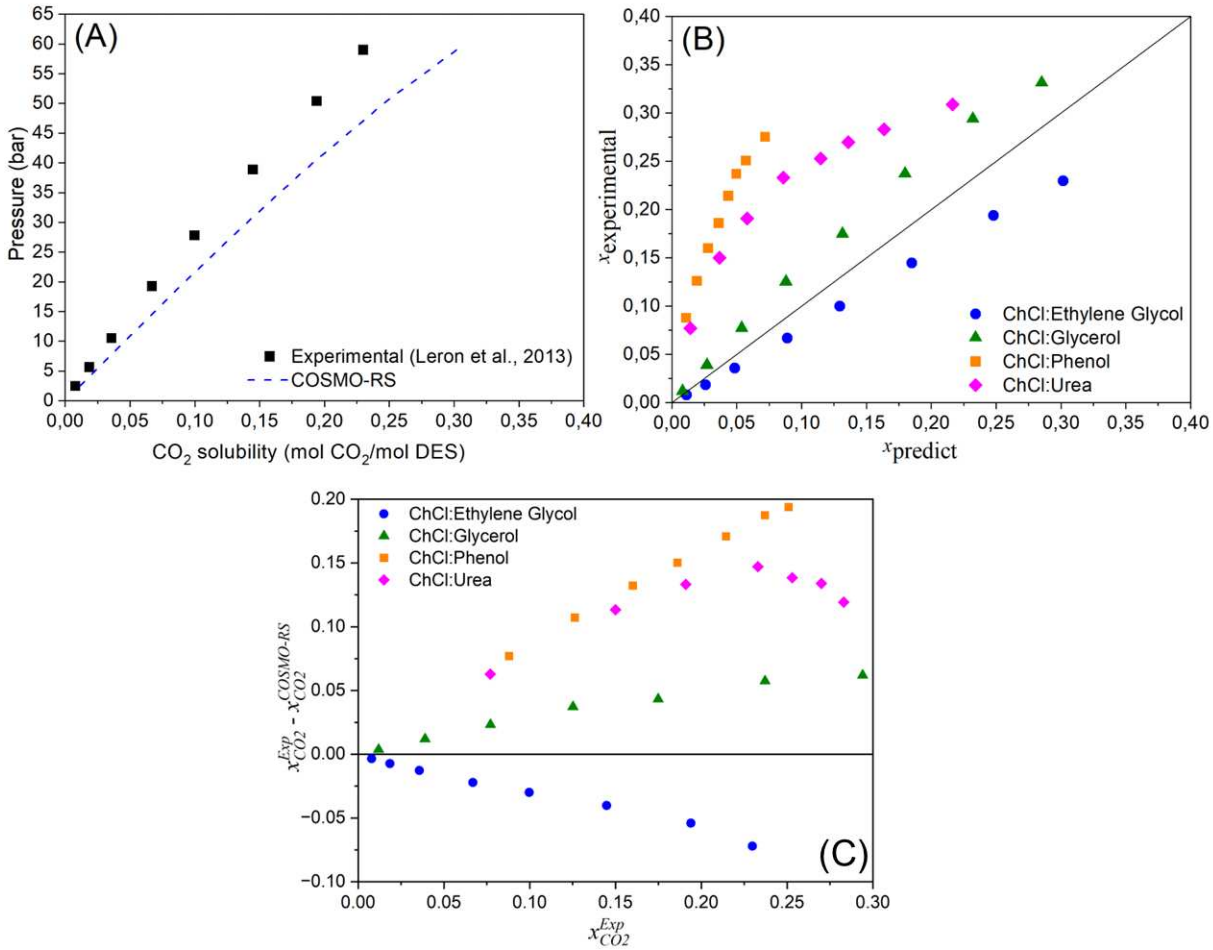

Figure 18. (A) Comparison of the experimental solubility of CO_2 in ChCl:Ethylene glycol (at 1:2 HBA:HBD molar ratio) with the COSMO-RS predictions; (B) Experimental x_{CO2} vs. x_{CO2} predicted with COSMO-RS; (C) solubility differences.

The experimental CO_2 solubility ranks as ChCl:Glycerol > ChCl:Ethyelene Glycol = ChCl:Urea > ChCl:Phenol. Since the HBA is the same for all ESs, the difference between the CO_2 solubility values is attributed to the HBDs. As glycerol has a longer chain length than ethylene glycol and urea, and more hydroxyl groups than the other HBDs, the free volume of this ES is higher [42]. Consequently, there is more free space for CO_2 hosting in glycerol-based ES than in the others. Although the solubility rank obtained with COSMO-RS is slightly different from the experimental trend (ChCl:Glycerol = ChCl:Ethyelene Glycol > ChCl:Urea > ChCl:Phenol), the model

identifies ChCl:Phenol as the ES with the least solubilization capacity, while confirms that the ESs containing the diols as HBD provide the highest solubility values.

Erro! Fonte de referência não encontrada.(A) compares the CO_2 solubility in ChCl:Ethylene glycol and the COSMO-RS predictions. As can be seen, an increase in the pressure leads to an increase in the experimental CO_2 solubility values; COSMO-RS also describes this behavior well. Similar trends were observed for the other studied ESs. This result is even more evident for ChCl:Urea and ChCl:Phenol, which exhibits experimental CO_2 solubility up to 130 bar. These large deviations seen in Figure 18 were an expected outcome as COSMO-RS assumes the incompressibility of the liquid state and the ideality of the gas phase, computing only pressure-independent activity coefficients, and not fugacity coefficients. To improve the prediction results for high-pressure systems, Moity et al., (2012) emphasize the necessity to combine COSMO-RS and an equation of state (EoS) [63].

Liu et al., (2020) [37] also predicted the CO_2 solubility in ChCl:Phenol at 313.15 K and at low pressures (between 1.22 and 5.03 bar) using COSMO-RS (with the BP_TZVP_C30_1401 level of parametrization). The authors obtained solubility predictions one order of magnitude higher than the experimental data, resulting in ARDs much higher than those obtained in this work. It is also possible to compare the results of this study with those of Pelaquim et al., (2022) [42] that used Cubic Plus Association (CPA) and Peng-Robinson equations of state (EoSs) to model the CO_2 solubility in ESs. The authors considered the ESs as individual components, as shown in Table 18, and adjusted the binary interaction parameters (k_{ij}). According to Table 18, it is possible to observe that EoSs (both CPA and Peng-Robinson) described the CO_2 solubility in the three ESs much better than COSMO-RS, as proved by the ARDs.

This was an expected outcome due to the fully predictive character of COSMO-RS, which does not require any experimental thermodynamic properties as an input.

Table 18. Comparison between the ARDs obtained in this study and those reported by Pelaquim et al., (2022) for the predicted CO_2 solubility in three ESs at 1:2 molar ratio and 313.15 K.

HBA	HBD	Pressure (bar)	%ARD in x for COSMO-RS[a]	%ARD in x for Peng-Robinson[42]	%ARD in x for CPA[42]
ChCl	Ethylene Glycol	26.80 – 27.80	33.81	17.23	2.79
ChCl	Glycerol	27.60 – 29.78	25.64	5.15	5.92
ChCl	Urea	28.50 – 29.20	58.31	5.94	2.45

3.2. CO_2 solubility in ESs at 1:3 and 1:4 molar ratios

Tables S8 – S25 of the Supporting Information and Figure 19Figure 20 present the experimental and COSMO-RS predicted CO_2 solubility in 9 ESs at 313.15 K, pressure range from 0.50 to 6.00 bar, 1:3 and 1:4 molar ratios as well as the ARDs. In all cases, COSMO-RS poorly predicted the experimental CO_2 solubilities, delivering higher values than those obtained experimentally. The obtained ARDs varied between 51% (ChCl:Levulinic acid, at 1:4) and 303% (ChCl:Guaiacol, at 1:3). It can be seen that the CO_2 solubility in these ESs is much lower compared to the solubility in the same ESs at the 1:2 molar ratio presented in Section 3.1, which is not fully captured by COSMO-RS, that often overestimates the solubility data in the ESs at 1:3 and 1:4 molar ratios. (Figure 19(B) and Figure 20(B)). This was an expected outcome since the data pressures found at 1:3 and 1:4 molar ratios are up to ten times lower than the pressures data at 1:2 molar ratio (Tables S3, S11, and S20 of Supporting Information for ChCl:Phenol). And as previously discussed, an increase in pressure leads to higher solubility. Despite the higher solubility value observed at 1:2 molar ratio, a relation was

not found concerning the HBA:HBD proportion since the available solubility data at 1:3 molar ratio were typically measured at lower pressure ranges than those reported for ESs at 1:2 proportion.

As in the previous section, the deviations between predicted values and the experimental data increase with pressure increase, as shown in Figure 19(A) and Figure 20(A). Three factors influence the deviation between experimental data and those predicted by COSMO-RS: pressure, temperature, and the molar ratio [64]. The pressure increase, as mentioned before, is responsible for the deviation enlargement. On the other hand, the molar ratio causes a reduction of the deviations in almost all mixtures, especially for ChCl:Levulinic Acid (from 111.32 to 51.04%).

Once again, it is possible to compare the predicted CO_2 solubility in ChCl:Phenol with COSMO-RS to the results obtained in our previous work [42] with CPA and Peng-Robinson EoSs, at 1:3 molar ratio, 313.15 K, and 3 bar [42]. At those conditions, the COSMO-RS model shows an ARD of 187%, whereas ARDs of 6% and 4% were obtained with CPA and Peng-Robinson EoS, respectively. Moreover, it is possible to compare this study's results with those of Liu et al. (2020) [37]. In this case, the solubility predictions obtained in this work are closer to the experimental values than those provided by Liu et al. (2020) [37] for all ESs and pressures at a 1:3 molar ratio (HBA:HBD).

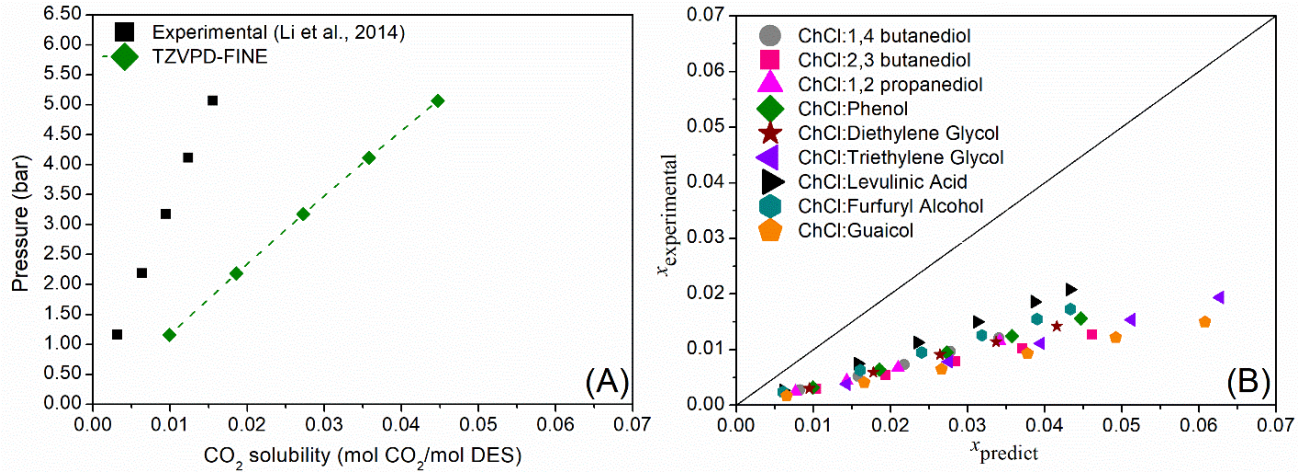

Figure 19. (A) Comparison of the experimental solubility of CO_2 in ChCl:Phenol at 1:3 molar ratio (HBA:HBD). with the COSMO-RS predictions; (B) Experimental x_{CO2} vs. predicted x_{CO2} with COSMO-RS.

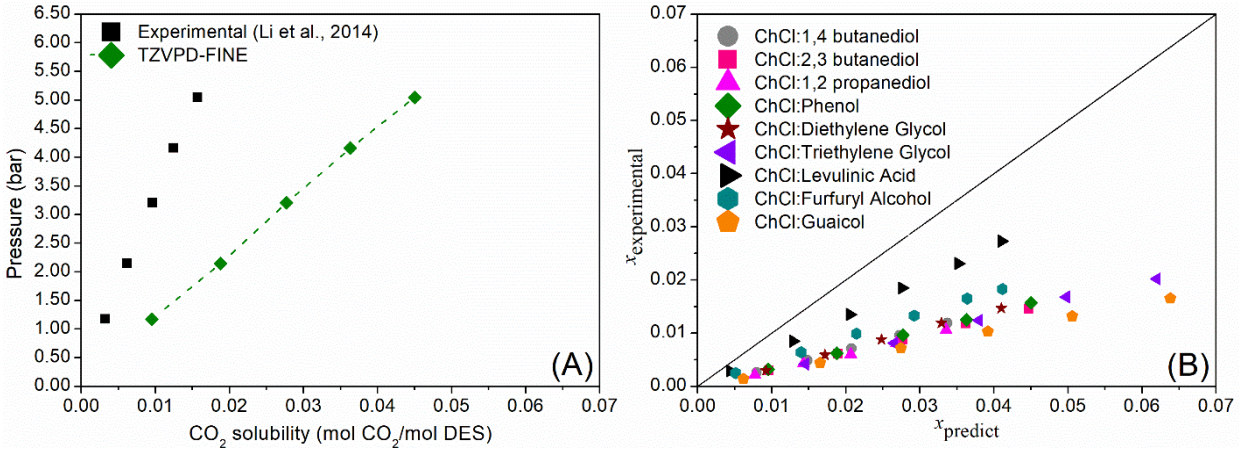

Figure 20. (A) Comparison of the experimental solubility of CO_2 in ChCl:Phenol at 1:4 molar ratio (HBA:HBD). with the COSMO-RS predictions; (B) Experimental x_{CO2} vs. predicted x_{CO2} with COSMO-RS.

3.3. CH_4 solubility in ESs at 1:1 molar ratio

Experimental and thermodynamic studies on CH_4 solubility in ESs are scarce in the literature [19,39,55,58,65,66]. Consequently, a few ESs have been studied for this application in a limited range of molar ratios. In this work, the solubilities of CH_4 in ESs composed of choline chloride as HBA, and lactic acid, malonic acid, or phenylacetic acid as HBD (at 1:1 molar ratio) were estimated, at 298.15 K, in the pressure range

(0.05–50) bar. The results are presented in Tables S26-S28 of the SI and compared to the experimental data reported by Altamash et al. (2019) [58] below.

In this scenario, COSMO-RS underestimates the solubility data by one or two orders of magnitude, generally resulting in ARDs larger than 80%. Despite the large deviations, the predicted curves suggest that the solubility increases as the pressure increases, which is confirmed by the experimental data. Regarding the CH_4 absorption performance, the experimental solubility data exhibit the following order: ChCl:Lactic acid > ChCl:Phenylacetic acid > ChCl:Malonic acid due to the C−OH···CH_4 or C=O···CH_4 interactions [19]. Although COSMO-RS confirms that the ES with malonic acid delivers the lowest solubility data, the model suggests that ChCl:Phenylacetic acid would present a higher CH_4 solubilization capacity than ChCl:Lactic acid in the studied conditions.

Although no thermodynamic modeling is available to describe the CH_4 solubility in the ESs analyzed by Altamash et al. (2019) [58], Haider and Kumar (2020) [19] modeled the CH_4 solubility in ESs composed of Tetrabutyl Ammonium Bromide (TBAB):2-Methylaminoethanol (MAE), Benzyltriethyl ammonium Chloride (BTEACl):MAE, TBAB:2-Ethylaminoethanol (EAE) and BTEACl:EAE using NRTL model and Peng-Robinson EoS. They observed that both models fit well with the experimental results; however, the NRTL model was slightly better than the Peng-Robinson EoS. Therefore, classical thermodynamic modeling again represented the experimental data better than COSMO-RS.

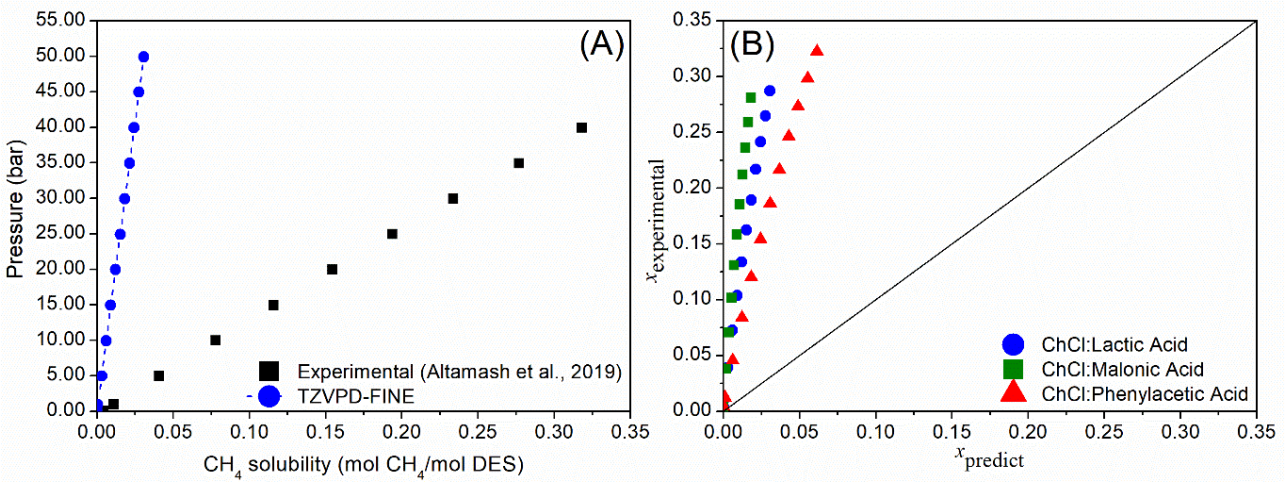

Figure 21. (A) Comparison of the experimental solubility of CO_2 in ChCl:Lactic Acid at 1:1 molar ratio (HBA:HBD) with the COSMO-RS predictions; (B) Experimental x_{CO2} vs. x_{CO2} predicted with COSMO-RS.

3.4. CO_2, CH_4, and H_2S solubilities in ChCl:Urea at different molar ratios

Experimental solubility data of other gases like H_2S, HCl, N_2, and SO_2 in ESs are scarce in the literature [19,58,67–71]. Nonetheless, studies addressing modeling, prediction, or molecular strategies to obtain such data are even rarer. Only one study used COSMO-RS to predict the CO_2, CH_4, and H_2S solubilities in ChCl:Urea at different temperatures than 313.15 K was found [39]. In the present study, COSMO-RS was applied to represent the solubility of H_2S, CO_2, and CH_4 in ChCl:Urea in three different molar ratios (1:1.5, 1:2, and 1:2.5), at 313.15 K, and in the pressure range varying between 0.1 and 2 bar. The results are compared with the experimental data measured by Liu et al. (2019) [55] in Figure 22 and Tables S5 – S7 and S29 – S34 of the SI.

In most cases, the model can predict the correct order of magnitude of the solubility data, presenting ARDs varying between 37% and 81%. The smallest deviations were found for the H_2S solubilities (37% < ARD < 72%), whereas ARDs superior to 71% were obtained for CO_2. In general, COSMO-RS underestimates the

solubility values of CO_2 and CH_4 (Figure 22), diverging from the data analyzed by Kamgar et al. (2017) [39]. In contrast, the opposite behavior was registered for H_2S.

Unlike the previous cases, COSMO-RS adequately estimates the correct experimental solubility order for the ChCl:Urea ES: H_2S > CO_2 > CH_4. This behavior was expected since H_2S forms stronger hydrogen bonds with ChCl:Urea than CO_2, while CH_4, a rigid and inert molecule, presents only weak van der Waals interactions. The strengths of site-to-site interaction for H_2S, which is much stronger than for CO_2 and CH_4, follow the sequence of Cl (ChCl)---H (H_2S) > O (Urea)---H (H_2S) > O (ChCl)---H (H_2S) > N (Urea)---H (H_2S) > H (ChCl)---S (H_2S)> H (urea)---S (H_2S)> N (ChCl)---H (H_2S) [55].

Regarding the absorption capacity at different molar ratios, for H_2S both COSMO-RS and experimental data followed the order 1:1.5 >1:2> 1:2.5. These results are not similar to those found in the literature [55], as generally increasing the HBD molar ratio leads to an increase in the gas solubility. On the other hand, CO_2 and CH_4 experimental solubility data follow the order 1:2 > 1:1.5 ≈ 1:2.5, slightly different from that predicted COSMO-RS (1:2 ≈ 1:1.5> 1:2.5). Different from the H_2S, where absorption is governed by weak site-to-site interactions, the solubilization of CO_2 and CH_4 in mixtures of ChCl:Urea are driven by the solvent-free volume and not by the [55,72]. Since ChCl:Urea at a 1:2 molar ratio forms a DES (i.e., its melting point is lower than those of 1:1.5 and 1:2.5 molar ratios), promoting a tight aggregation of the molecules, and the extra free volume favors the gas absorption [55,72].

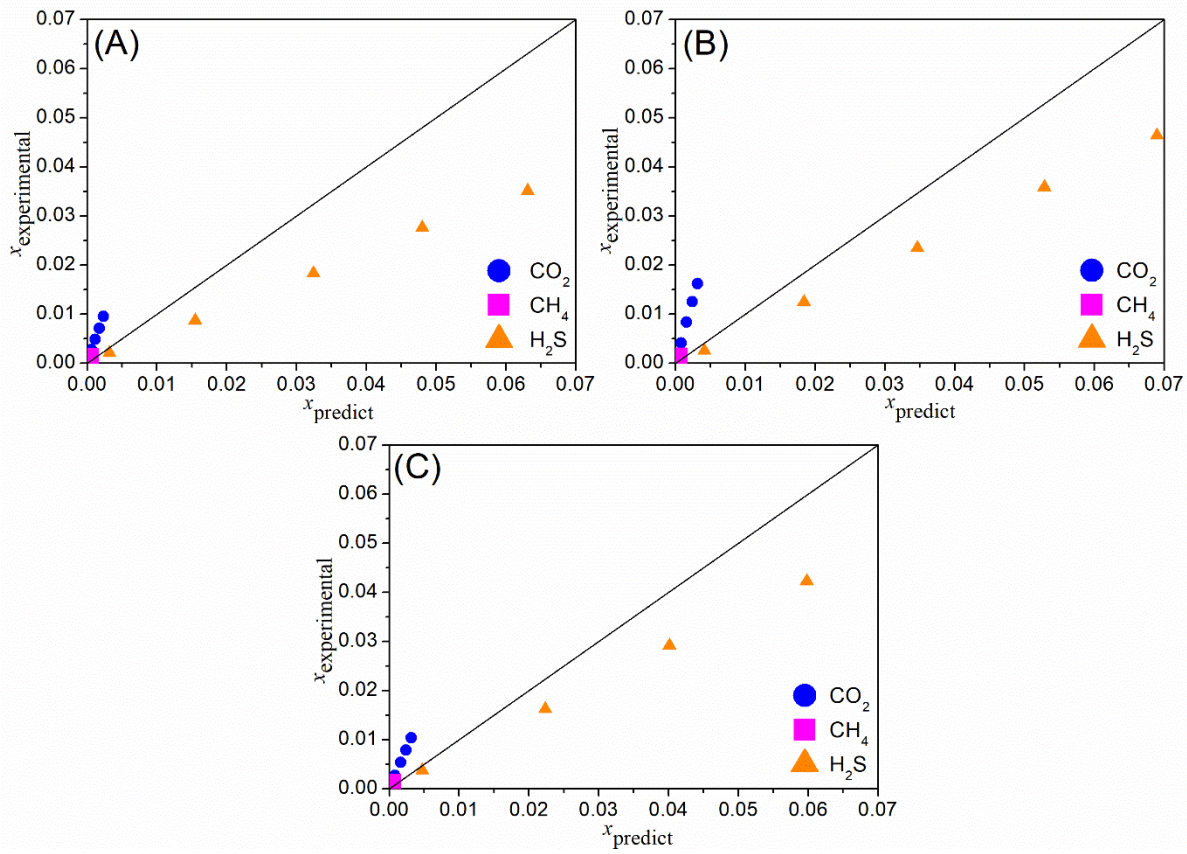

Figure 22. Comparison between the experimental solubility data with the predicted values with COSMO-RS of CO_2, CH_4, and H_2S in ChCl:Urea at (A) 1:2.5 molar ratio (HBA:HBD); (B) 1:1.5 molar ratio (HBA:HBD); and (C) 1:2 molar ratio (HBA:HBD).

4. Conclusion

In this study, the solubility of CO_2, CH_4, and H_2S in 17 ChCl-based ES retrieved from the literature, at 298.15 or 313.15 K and in the pressure range from 1 to 125 bar, were predicted using the COSMO-RS model. In addition, the effect of three different molar ratios of ChCl:urea on the solubility of CO_2, CH_4, and H_2S was investigated. Whenever possible, the results obtained in this study were compared with solubility values estimated with other thermodynamic models in previous works.

In general, the deviations obtained with COSMO-RS were larger than those achieved by CPA and Peng-Robinson EoSs, which was expected due to COSMO-RS's fully predictive nature. In most situations, the obtained ARDs were higher than 50%,

revealing that COSMO-RS provides only a qualitative picture of the investigated greenhouse gas solubility phenomenon. In a few cases for CO_2,(ChCl:Ethylene Glycol – 1:2, ChCl:Glycerol, ChCl:Levulinic acid – 1:4) and H_2S (ChCl:Urea – 1:1.5 and 1:2), the model offered a more quantitative description of the solubility data, achieving relative deviations inferior to 50%.

The experimental data reveal that an increase in pressure leads to an increase in solubility, which is also captured by the COMOS-RS predictions. The model underestimated the solubility data of CO_2 and CH_4 in ESs with molar ratios of 1:2 and 1:1, respectively. On the contrary, the CO_2 solubilities in 1:3 and 1:4 molar ratios ESs were overestimated by COSMO-RS. Regarding absorption capacity, COSMO-RS agreed with the experimental data or slightly missed the solubility order.

This study shows that COSMO-RS is a reliable tool for solvent screening purposes for light gases. Although the model is inadequate for quantitative purposes in many situations, it is suitable to identify solubility trends in eutectic mixtures, being capable of identifying promising ES to be further investigated as absorbers in the gas capture field.

Acknowledgment

The authors thank the São Paulo Research Foundation (FAPESP – 2018/19198-9 and 2014/21252-0), Coordination for the Improvement of Higher Education Personnel - Brasil (CAPES) – Finance Code 001, the National Council for Scientific and Technological Development (CNPq – 306666/2020-0), and the Fund for the Support of Education, Research and Extension (FAEPEX/ UNICAMP) for the financial support. The authors also thank the Human Resources Program of the National Agency of Petroleum, Natural Gas and Biofuels (PRH-ANP). This work was

developed within the scope of the project CICECO Aveiro Institute of Materials, UIDB/50011/2020, UIDP/50011/2020 & LA/P/0006/2020, financed by national funds through the FCT/MEC (PIDDAC).

References

[1] C.A. Marques, A.A.S.C. Machado, Environmental Sustainability: implications and limitations to Green Chemistry, Found Chem. 16 (2014) 125–147. https://doi.org/10.1007/s10698-013-9189-x.

[2] P. Anastas, N. Eghbali, Green Chemistry: Principles and Practice, Chem. Soc. Rev. 39 (2010) 301–312. https://doi.org/10.1039/B918763B.

[3] A. Paiva, R. Craveiro, I. Aroso, M. Martins, R.L. Reis, A.R.C. Duarte, Natural deep eutectic solvents - Solvents for the 21st century, ACS Sustain Chem Eng. 2 (2014) 1063–1071. https://doi.org/10.1021/sc500096j.

[4] S. Cherukuvada, A. Nangia, Eutectics as improved pharmaceutical materials: design, properties and characterization, Chem. Commun. 50 (2014) 906–923. https://doi.org/10.1039/C3CC47521B.

[5] M.A.R. Martins, S.P. Pinho, J.A.P. Coutinho, Insights into the Nature of Eutectic and Deep Eutectic Mixtures, J Solution Chem. (2018) 1–3. https://doi.org/10.1007/s10953-018-0793-1.

[6] B. Singh, H. Lobo, G. Shankarling, Selective N-Alkylation of Aromatic Primary Amines Catalyzed by Bio-catalyst or Deep Eutectic Solvent, Catal Letters. 141 (2011) 178–182. https://doi.org/10.1007/s10562-010-0479-9.

[7] Q. Zhang, K. De Oliveira Vigier, S. Royer, F. Jérôme, Deep eutectic solvents: Syntheses, properties and applications, Chem Soc Rev. 41 (2012) 7108–7146. https://doi.org/10.1039/c2cs35178a.

[8] B. Tang, K.H. Row, Recent developments in deep eutectic solvents in chemical sciences, Monatsh Chem. 144 (2013) 1427–1454. https://doi.org/10.1007/s00706-013-1050-3.

[9] D. Carriazo, M.C. Serrano, M.C. Gutiérrez, M.L. Ferrer, F. del Monte, Deep-eutectic solvents playing multiple roles in the synthesis of polymers and related materials, Chem Soc Rev. 41 (2012) 4996. https://doi.org/10.1039/c2cs15353j.

[10] H. Cheng, Z. Qi, Applications of deep eutectic solvents for hard-to-separate liquid systems, Sep Purif Technol. 274 (2021) 119027. https://doi.org/10.1016/j.seppur.2021.119027.

[11] V. Sivabalan, N. Hasnor, B. Lal, Z. Kassim, A.S. Maulud, Tetraethylammoniumacetate and tetraethylammonium bromide-based deep eutectic solvents as thermodynamic CO2 gas hydrate inhibitors, Applied Sciences (Switzerland). 10 (2020). https://doi.org/10.3390/app10196794.

[12] D. Lee, W. Go, J. Oh, J. Lee, I. Jo, K.S. Kim, Y. Seo, Thermodynamic inhibition effects of an ionic liquid (choline chloride), a naturally derived substance (urea), and their mixture (deep eutectic solvent) on CH4 hydrates, Chemical Engineering Journal. 399 (2020) 125830. https://doi.org/10.1016/j.cej.2020.125830.

[13] Y. Liao, S. Gong, G. Wang, T. Wu, X. Meng, Q. Huang, Y. Su, F. Wu, R.M. Kelly, A Novel Ternary Deep Eutectic Solvent for Efficient Recovery of Critical Metals from Spent Lithium-Ion Batteries Under Mild Conditions, SSRN Electronic Journal. (2022). https://doi.org/10.2139/ssrn.4124040.

[14] Z. Wang, M. Cheng, J. Bu, L. Cheng, J. Ru, Y. Hua, D. Wang, Understanding the electrochemical behavior of Sn(II) in choline chloride-ethylene glycol deep eutectic

solvent for tin powders preparation, Advanced Powder Technology. 33 (2022) 103670. https://doi.org/10.1016/j.apt.2022.103670.

[15] E.L. Smith, A.P. Abbott, K.S. Ryder, Deep Eutectic Solvents (DESs) and Their Applications, Chem Rev. 114 (2014) 11060–11082. https://doi.org/10.1021/cr300162p.

[16] R. Zhao, D. Pei, P. Yu, J. Wei, N. Wang, D. Di, Y. Liu, Aqueous two-phase systems based on deep eutectic solvents and their application in green separation processes, J Sep Sci. 43 (2020) 348–359. https://doi.org/10.1002/jssc.201900991.

[17] F.O. Farias, F.H.B. Sosa, L. Igarashi-Mafra, J.A.P. Coutinho, M.R. Mafra, Study of the pseudo-ternary aqueous two-phase systems of deep eutectic solvent (choline chloride:sugars) + K2HPO4 + water, Fluid Phase Equilib. 448 (2017) 143–151. https://doi.org/10.1016/j.fluid.2017.05.018.

[18] G. Ansarypur, M. Bayareh, A. Jahangiri, Experimental investigation and thermodynamic modeling of CO2 absorption by a chemical solution, J Therm Anal Calorim. 147 (2022) 1689–1697. https://doi.org/10.1007/s10973-021-10554-3.

[19] M.B. Haider, R. Kumar, Solubility of CO2 and CH4 in sterically hindered amine-based deep eutectic solvents, Sep Purif Technol. 248 (2020) 117055. https://doi.org/10.1016/j.seppur.2020.117055.

[20] F. Luo, X. Liu, S. Chen, Y. Song, X. Yi, C. Xue, L. Sun, J. Li, Comprehensive Evaluation of a Deep Eutectic Solvent Based CO2Capture Process through Experiment and Simulation, ACS Sustain Chem Eng. 9 (2021) 10250–10265. https://doi.org/10.1021/acssuschemeng.1c02722.

[21] O. Alioui, Y. Benguerba, I.M. Alnashef, Investigation of the CO2-solubility in deep eutectic solvents using COSMO-RS and molecular dynamics methods, J Mol Liq. 307 (2020) 113005. https://doi.org/10.1016/j.molliq.2020.113005.

[22] International Energy Agency, Global Energy Review: CO2 Emissions in 2021 Global emissions rebound sharply to highest ever level, 2022.

[23] D.A. Lashof, D.R. Ahuja, Relative contributions of greenhouse gas emissions to global warming, Nature. 344 (1990) 529–531. https://doi.org/10.1038/344529a0.

[24] No Title, (n.d.). https://doi.org/https://doi.org/10.1016/j.rser.2012.10.020.

[25] M. Höök, X. Tang, Depletion of fossil fuels and anthropogenic climate change—A review, Energy Policy. 52 (2013) 797–809. https://doi.org/10.1016/j.enpol.2012.10.046.

[26] G. García, S. Aparicio, R. Ullah, M. Atilhan, Deep Eutectic Solvents: Physicochemical Properties and Gas Separation Applications, Energy & Fuels. 29 (2015) 2616–2644. https://doi.org/10.1021/ef5028873.

[27] G. Luderer, V. Bosetti, M. Jakob, M. Leimbach, J.C. Steckel, H. Waisman, O. Edenhofer, The economics of decarbonizing the energy system—results and insights from the RECIPE model intercomparison, Clim Change. 114 (2012) 9–37. https://doi.org/10.1007/s10584-011-0105-x.

[28] F. Petrakopoulou, G. Tsatsaronis, Can Carbon Dioxide Capture and Storage from Power Plants Reduce the Environmental Impact of Electricity Generation?, Energy & Fuels. 28 (2014) 5327–5338. https://doi.org/10.1021/ef500925h.

[29] Y. Wang, L. Zhao, A. Otto, M. Robinius, D. Stolten, A Review of Post-combustion CO2 Capture Technologies from Coal-fired Power Plants, Energy Procedia. 114 (2017) 650–665. https://doi.org/10.1016/j.egypro.2017.03.1209.

[30] F.P. Pelaquim, A.M. Barbosa Neto, I.A.L. Dalmolin, M.C. da Costa, Gas Solubility Using Deep Eutectic Solvents: Review and Analysis, Ind Eng Chem Res. (2021) acs.iecr.1c00947. https://doi.org/10.1021/acs.iecr.1c00947.

[31] X. Liu, B. Gao, Y. Jiang, N. Ai, D. Deng, Solubilities and Thermodynamic Properties of Carbon Dioxide in Guaiacol-Based Deep Eutectic Solvents, J Chem Eng Data. 62 (2017) 1448–1455. https://doi.org/10.1021/acs.jced.6b01013.

[32] H. Ghaedi, M. Ayoub, S. Sufian, A.M. Shariff, S.M. Hailegiorgis, S.N. Khan, CO2 capture with the help of Phosphonium-based deep eutectic solvents, J Mol Liq. 243 (2017) 564–571. https://doi.org/10.1016/j.molliq.2017.08.046.

[33] N. Ramzan, M. Rizwan, M. Zaman, M. Adnan, A. Ullah, A. Gungor, U. Shakeel, A. ul Haq, Pre-combustion carbon dioxide capture: A thermo-economic comparison for dual-stage Selexol process and combined Sulfinol-Selexol process, Int J Energy Res. (2022). https://doi.org/10.1002/er.8674.

[34] G. Siani, M. Tiecco, P. Di Profio, S. Guernelli, A. Fontana, M. Ciulla, V. Canale, Physical absorption of CO2 in betaine/carboxylic acid-based Natural Deep Eutectic Solvents, J Mol Liq. 315 (2020) 1–7. https://doi.org/10.1016/j.molliq.2020.113708.

[35] H. Qin, Z. Song, H. Cheng, L. Deng, Z. Qi, Physical absorption of carbon dioxide in imidazole-PTSA based deep eutectic solvents, J Mol Liq. 326 (2021) 1–7. https://doi.org/10.1016/j.molliq.2021.115292.

[36] X. Liu, Q. Ao, S. Shi, S. Li, CO2capture by alcohol ammonia based deep eutectic solvents with different water content, Mater Res Express. 9 (2022). https://doi.org/10.1088/2053-1591/ac47c6.

[37] Y. Liu, H. Yu, Y. Sun, S. Zeng, X. Zhang, Y. Nie, S. Zhang, X. Ji, Screening Deep Eutectic Solvents for CO2 Capture With COSMO-RS, Front Chem. 8 (2020) 1–11. https://doi.org/10.3389/fchem.2020.00082.

[38] J. Wang, Z. Song, L. Chen, T. Xu, L. Deng, Z. Qi, Prediction of CO2 solubility in deep eutectic solvents using random forest model based on COSMO-RS-derived descriptors, Green Chemical Engineering. 2 (2021) 431–440. https://doi.org/10.1016/j.gce.2021.08.002.

[39] A. Kamgar, S. Mohsenpour, F. Esmaeilzadeh, Solubility prediction of CO2, CH4, H2, CO and N2 in Choline Chloride/Urea as a eutectic solvent using NRTL and COSMO-RS models, J Mol Liq. 247 (2017) 70–74. https://doi.org/10.1016/j.molliq.2017.09.101.

[40] R. Haghbakhsh, S. Raeissi, Modeling the Phase Behavior of Carbon Dioxide Solubility in Deep Eutectic Solvents with the Cubic Plus Association Equation of State, J Chem Eng Data. 63 (2017) 897–906. https://doi.org/10.1021/acs.jced.7b00472.

[41] R. Haghbakhsh, M. Keshtkar, A. Shariati, S. Raeissi, Experimental investigation of carbon dioxide solubility in the deep eutectic solvent (1 ChCl + 3 triethylene glycol) and modeling by the CPA EoS, J Mol Liq. 330 (2021) 1–12. https://doi.org/10.1016/j.molliq.2021.115647.

[42] F.P. Pelaquim, R.G. Bitencourt, A.M.B. Neto, I.A.L. Dalmolin, M.C. da Costa, Carbon dioxide solubility in Deep Eutectic Solvents: Modelling using Cubic Plus Association and Peng-Robinson equations of state, Process Safety and Environmental Protection. 163 (2022) 14–26. https://doi.org/10.1016/j.psep.2022.04.075.

[43] F. Rabhi, F. Mutelet, H. Sifaoui, Solubility of Carbon Dioxide in Carboxylic Acid-Based Deep Eutectic Solvents, J Chem Eng Data. 66 (2021) 702–711. https://doi.org/10.1021/acs.jced.0c00844.

[44] A. Klamt, Conductor-like screening model for real solvents: A new approach to the quantitative calculation of solvation phenomena, Journal of Physical Chemistry. 99 (1995) 2224–2235. https://doi.org/10.1021/j100007a062.

[45] A. Klamt, V. Jonas, T. Bürger, J.C.W. Lohrenz, Refinement and Parametrization of COSMO-RS, J Phys Chem A. 102 (1998) 5074–5085. https://doi.org/10.1021/jp980017s.

[46] F. Eckert, A. Klamt, Fast solvent screening via quantum chemistry: COSMO-RS approach, AIChE Journal. 48 (2002) 369–385. https://doi.org/10.1002/aic.690480220.

[47] H. Cheng, C. Liu, J. Zhang, L. Chen, B. Zhang, Z. Qi, Screening deep eutectic solvents for extractive desulfurization of fuel based on COSMO-RS model, Chemical Engineering and Processing - Process Intensification. 125 (2018) 246–252. https://doi.org/10.1016/j.cep.2018.02.006.

[48] K.A. Kurnia, S.P. Pinho, J.A.P. Coutinho, Evaluation of the Conductor-like Screening Model for Real Solvents for the Prediction of the Water Activity Coefficient at Infinite Dilution in Ionic Liquids, Ind Eng Chem Res. 53 (2014) 12466–12475. https://doi.org/10.1021/ie5021415.

[49] K. Paduszyński, An overview of the performance of the COSMO-RS approach in predicting the activity coefficients of molecular solutes in ionic liquids and derived properties at infinite dilution, Physical Chemistry Chemical Physics. 19 (2017) 11835–11850. https://doi.org/10.1039/C7CP00226B.

[50] R.B. Leron, M.H. Li, Solubility of carbon dioxide in a choline chloride-ethylene glycol based deep eutectic solvent, Thermochim Acta. 551 (2013) 14–19. https://doi.org/10.1016/j.tca.2012.09.041.

[51] R.B. Leron, M.H. Li, Solubility of carbon dioxide in a eutectic mixture of choline chloride and glycerol at moderate pressures, Journal of Chemical Thermodynamics. 57 (2013) 131–136. https://doi.org/10.1016/j.jct.2012.08.025.

[52] Y. Ji, Y. Hou, S. Ren, C. Yao, W. Wu, Phase equilibria of high pressure CO2 and deep eutectic solvents formed by quaternary ammonium salts and phenol, Fluid Phase Equilib. 429 (2016) 14–20. https://doi.org/10.1016/j.fluid.2016.08.020.

[53] G. Li, D. Deng, Y. Chen, H. Shan, N. Ai, Solubilities and thermodynamic properties of CO2 in choline-chloride based deep eutectic solvents, J Chem Thermodyn. 75 (2014) 58–62. https://doi.org/10.1016/j.jct.2014.04.012.

[54] X. Li, M. Hou, B. Han, X. Wang, L. Zou, Solubility of CO2 in a choline chloride + urea eutectic mixture, J Chem Eng Data. 53 (2008) 548–550. https://doi.org/10.1021/je700638u.

[55] F. Liu, W. Chen, J. Mi, J.Y. Zhang, X. Kan, F.Y. Zhong, K. Huang, A.M. Zheng, L. Jiang, Thermodynamic and molecular insights into the absorption of H2S, CO2 , and CH4 in choline chloride plus urea mixtures, AIChE Journal. 65 (2019) 1–10. https://doi.org/10.1002/aic.16574.

[56] Y. Chen, N. Ai, G. Li, H. Shan, Y. Cui, D. Deng, Solubilities of Carbon Dioxide in Eutectic Mixtures of Choline Chloride and Dihydric Alcohols, J Chem Eng Data. 59 (2014) 1247–1253. https://doi.org/10.1021/je400884v.

[57] M. Lu, G. Han, Y. Jiang, X. Zhang, D. Deng, N. Ai, Solubilities of carbon dioxide in the eutectic mixture of levulinic acid (or furfuryl alcohol) and choline chloride, J Chem Thermodyn. 88 (2015) 72–77. https://doi.org/10.1016/j.jct.2015.04.021.

[58] T. Altamash, A.I. Amhamed, S. Aparicio, M. Atilhan, Combined Experimental and Theoretical Study on High Pressure Methane Solubility in Natural Deep Eutectic Solvents, Ind Eng Chem Res. 58 (2019) 8097–8111. https://doi.org/10.1021/acs.iecr.9b00702.

[59] B. COSMOtherm, Release 2021, 2021.

[60] C. Steffen, K. Thomas, U. Huniar, A. Hellweg, O. Rubner, A. Schroer, TmoleX-A graphical user interface for TURBOMOLE, J Comput Chem. 31 (2010) 2967–2970. https://doi.org/10.1002/jcc.21576.

[61] M. Diedenhofen, A. Klamt, COSMO-RS as a tool for property prediction of IL mixtures—A review, Fluid Phase Equilib. 294 (2010) 31–38. https://doi.org/10.1016/j.fluid.2010.02.002.

[62] B. COSMOtherm, Reference manual, 2021.

[63] L. Moity, M. Durand, A. Benazzouz, C. Pierlot, V. Molinier, J.M. Aubry, Panorama of sustainable solvents using the COSMO-RS approach, Green Chemistry. 14 (2012) 1132–1145. https://doi.org/10.1039/c2gc16515e.

[64] Y. Liu, Z. Dai, Z. Zhang, S. Zeng, F. Li, X. Zhang, Y. Nie, L. Zhang, S. Zhang, X. Ji, Ionic liquids/deep eutectic solvents for CO2 capture: Reviewing and evaluating, Green Energy and Environment. 6 (2021) 314–328. https://doi.org/10.1016/j.gee.2020.11.024.

[65] H.S. Salehi, R. Hens, O.A. Moultos, T.J.H. Vlugt, Computation of gas solubilities in choline chloride urea and choline chloride ethylene glycol deep eutectic solvents

using Monte Carlo simulations, J Mol Liq. 316 (2020) 1–10. https://doi.org/10.1016/j.molliq.2020.113729.

[66] K. Kumar, S. Keshri, A. Bharti, S. Kumar, S. Mogurampelly, Solubility of Gases in Choline Chloride-Based Deep Eutectic Solvents from Molecular Dynamics Simulation, Ind Eng Chem Res. 61 (2022) 4659–4671. https://doi.org/10.1021/acs.iecr.1c04923.

[67] M. Ramdin, S.P. Balaji, J.M. Vicent-Luna, J.J. Gutiérrez-Sevillano, S. Calero, T.W. De Loos, T.J.H. Vlugt, Solubility of the precombustion gases CO2, CH4, CO, H2, N2, and H2S in the ionic liquid [bmim][Tf2N] from Monte Carlo simulations, Journal of Physical Chemistry C. 118 (2014) 23599–23604. https://doi.org/10.1021/jp5080434.

[68] J. Zhu, H. Shao, L. Feng, Y. Lu, H. Meng, C. Li, Absorptive separation of HCl gas by choline chloride-based deep eutectic solvents, J Mol Liq. 341 (2021) 116928. https://doi.org/10.1016/j.molliq.2021.116928.

[69] G. Cui, J. Liu, S. Lyu, H. Wang, Z. Li, J. Wang, Efficient and reversible SO2 Absorption by environmentally friendly task-specific deep eutectic solvents of PPZBr + Gly, ACS Sustain Chem Eng. 7 (2019) 14236–14246. https://doi.org/10.1021/acssuschemeng.9b03245.

[70] D. Yang, M. Hou, H. Ning, J. Zhang, J. Ma, G. Yang, B. Han, Efficient SO2 absorption by renewable choline chloride–glycerol deep eutectic solvents, Green Chemistry. 15 (2013) 2261–2265. https://doi.org/10.1039/c3gc40815a.

[71] S. Sun, Y. Niu, Q. Xu, Z. Sun, X. Wei, Efficient SO2 absorptions by four kinds of deep eutectic solvents based on choline chloride, Ind Eng Chem Res. 54 (2015) 8019–8024. https://doi.org/10.1021/acs.iecr.5b01789.

[72] A.P. Abbott, G. Capper, D.L. Davies, R.K. Rasheed, V. Tambyrajah, Novel solvent properties of choline chloride / urea mixtures, The Royal Society of Chemistry. (2003) 70–71. https://doi.org/10.1039/B210714G.

Supporting Information

1. CO_2 solubility in ESs

Table S19. Experimental data of CO_2 solubility in ChCl:Ethylene Glycol and COSMO-RS predictions at 1:2 molar ratio.

Gas	HBA(1)	HBD(2)	x_1	x_2	T (K)	P (bar)	Experimental Solubility	Predicted Solubility	RD	Ref.
CO_2	ChCl	Ethylene Glycol	0.333	0.667	313.500	2.480	7.85E-03	1.14E-02	44.72%	Leron et al., (2013)
						5.650	1.85E-02	2.59E-02	39.74%	
						10.550	3.56E-02	4.84E-02	35.89%	
						19.280	6.69E-02	8.90E-02	33.07%	
						27.820	9.97E-02	1.30E-01	30.09%	
						38.890	1.45E-01	1.85E-01	27.75%	
						50.400	1.94E-01	2.48E-01	27.87%	
						59.020	2.30E-01	3.02E-01	31.37%	
								ARD	33.81%	

Table S20. Experimental data of CO_2 solubility in ChCl:Glycerol and COSMO-RS predictions at 1:2 molar ratio.

Gas	HBA(1)	HBD(2)	x_1	x_2	T (K)	P (bar)	Experimental Solubility	Predicted Solubility	RD	Ref.
CO_2	ChCl	Glycerol	0.333	0.667	313.500	1.910	1.19E-02	8.28E-03	30.40%	Leron et al., (2013)
						6.220	3.90E-02	2.70E-02	30.77%	
						12.390	7.71E-02	5.39E-02	30.12%	
						20.120	1.25E-01	8.80E-02	29.74%	
						29.780	1.75E-01	1.32E-01	24.78%	
						40.020	2.37E-01	1.80E-01	24.22%	
						50.400	2.94E-01	2.32E-01	21.08%	
						59.910	3.31E-01	2.85E-01	13.96%	
								ARD	25.64%	

Table S21. Experimental data of CO_2 solubility in ChCl:Phenol and COSMO-RS predictions at 1:2 molar ratio.

Gas	HBA(1)	HBD(2)	x_1	x_2	T (K)	P (bar)	Experimental Solubility	Predicted Solubility	RD	Ref.
CO_2	ChCl	Phenol	0.333	0.667	313.150	19.900	8.80E-02	1.10E-02	87.49%	Leron et al., (2013)
						34.600	1.26E-01	1.92E-02	84.81%	
						50.100	1.60E-01	2.79E-02	82.60%	
						64.500	1.86E-01	3.59E-02	80.69%	
						78.000	2.14E-01	4.36E-02	79.68%	
						88.700	2.37E-01	4.96E-02	79.07%	
						101.700	2.51E-01	5.70E-02	77.27%	
						127.400	2.75E-01	7.18E-02	73.93%	
								ARD	80.69%	

Table S22. Experimental data of CO_2 solubility in ChCl:Urea and COSMO-RS predictions at 1:2 molar ratio and high pressures.

Gas	HBA(1)	HBD(2)	x_1	x_2	T (K)	P (bar)	Experimental Solubility	Predicted Solubility	RD	Ref.
CO_2	ChCl	Urea	0.333	0.667	313.500	125.000	3.09E-01	2.16E-01	30.00%	Li et al., (2008)
						104.600	2.83E-01	1.64E-01	42.14%	
						91.200	2.70E-01	1.36E-01	49.62%	
						79.600	2.53E-01	1.15E-01	54.70%	
						62.300	2.33E-01	8.58E-02	63.17%	
						43.700	1.91E-01	5.79E-02	69.71%	
						28.500	1.50E-01	3.67E-02	75.54%	
						11.300	7.70E-02	1.42E-02	81.61%	
								ARD	58.31%	

Table 23. Experimental data of CO_2 solubility in ChCl:Urea and COSMO-RS predictions at 1:2 molar ratio and low pressures.

Gas	HBA(1)	HBD(2)	x_1	x_2	T (K)	P (bar)	Experimental Solubility	Predicted Solubility	RD	Ref.
CO_2	ChCl	Urea	0.333	0.667	313.500	0.103	1.00E-03	1.79E-04	82.10%	Liu et al., (2019)
						0.508	4.17E-03	8.24E-04	80.23%	
						1.058	8.43E-03	1.55E-03	81.63%	
						1.539	1.26E-02	2.39E-03	80.97%	
						2.023	1.62E-02	3.13E-03	80.75%	
								ARD	81.14%	

Table S24. Experimental data of CO_2 solubility in ChCl:Urea and COSMO-RS predictions at 1:1.5 molar ratio.

Gas	HBA(1)	HBD(2)	x_1	x_2	T (K)	P (bar)	Experimental Solubility	Predicted Solubility	RD	Ref.
CO_2	ChCl	Urea	0.40	0.60	313.500	0.103	5.50E-04	1.59E-04	71.10%	Liu et al., (2019)
						0.508	2.69E-03	7.84E-04	70.85%	
						1.058	5.36E-03	1.63E-03	69.52%	
						1.539	7.89E-03	2.38E-03	69.86%	
						2.023	1.04E-02	3.13E-03	69.93%	
								ARD	70.25%	

Table S25. Experimental data of CO_2 solubility in ChCl:Urea and COSMO-RS predictions at 1:2.5 molar ratio.

Gas	HBA(1)	HBD(2)	x_1	x_2	T (K)	P (bar)	Experimental Solubility	Predicted Solubility	RD	Ref.
CO_2	ChCl	Urea	0.286	0.714	313.500	0.116	5.60E-04	1.19E-04	78.78%	Liu et al., (2019))
						0.534	2.79E-03	6.57E-04	76.46%	
						1.003	4.89E-03	1.17E-03	76.05%	
						1.548	7.18E-03	1.76E-03	75.54%	
						2.022	9.59E-03	2.35E-03	75.55%	
								ARD	76.48%	

Table S26. Experimental data of CO_2 solubility in ChCl:1,4 butanediol and COSMO-RS predictions at 1:3 molar ratio.

Gas	HBA(1)	HBD(2)	x_1	x_2	T (K)	P (bar)	Experimental Solubility	Predicted Solubility	RD	Ref.
CO_2	ChCl	1,4-butanediol	0.250	0.750	313.150	1.214	2.80E-03	8.23E-03	193.96%	Chen et al., (2014)
						2.331	5.20E-03	1.58E-02	203.81%	
						3.216	7.30E-03	2.18E-02	198.50%	
						4.102	9.70E-03	2.78E-02	186.47%	
						5.028	1.21E-02	3.41E-02	181.45%	
								ARD	192.84%	

Table S27. Experimental data of CO_2 solubility in ChCl:2,3 butanediol and COSMO-RS predictions at 1:3 molar ratio.

Gas	HBA(1)	HBD(2)	x_1	x_2	T (K)	P (bar)	Experimental Solubility	Predicted Solubility	RD	Ref.
CO_2	ChCl	2,3-butanediol	0.250	0.750	313.150	1.193	2.90E-03	1.04E-02	258.54%	Chen et al., (2014)
						2.224	5.40E-03	1.94E-02	259.09%	
						3.255	7.90E-03	2.84E-02	259.41%	
						4.249	1.02E-02	3.71E-02	263.57%	
						5.288	1.27E-02	4.62E-02	263.66%	
								ARD	260.85%	

Table S28. Experimental data of CO_2 solubility in ChCl:1,2 propanediol and COSMO-RS predictions at 1:3 molar ratio.

Gas	HBA(1)	HBD(2)	x_1	x_2	T (K)	P (bar)	Experimental Solubility	Predicted Solubility	RD	Ref.
CO_2	ChCl	1,2-propanediol	0.250	0.750	313.150	1.254	2.40E-03	7.68E-03	219.81%	Chen et al., (2014)
						2.178	4.40E-03	1.43E-02	225.44%	
						3.176	6.70E-03	2.10E-02	213.05%	
						4.205	9.30E-03	2.74E-02	194.66%	
						5.154	1.15E-02	3.41E-02	196.86%	
								ARD	209.96%	

Table S29. Experimental data of CO_2 solubility in ChCl:Phenol and COSMO-RS predictions at 1:3 molar ratio.

Gas	HBA(1)	HBD(2)	x_1	x_2	T (K)	P (bar)	Experimental Solubility	Predicted Solubility	RD	Ref.
CO_2	ChCl	Phenol	0.250	0.750	313.150	1.169	3.00E-03	9.47E-03	209.84%	Li et al., (2014)
						2.196	5.90E-03	1.78E-02	189.98%	
						3.270	9.10E-03	2.64E-02	187.12%	
						4.177	1.14E-02	3.37E-02	188.35%	
						5.157	1.42E-02	4.16E-02	186.54%	
								ARD	192.37%	

Table S30. Experimental data of CO_2 solubility in ChCl:Diethylene Glycol and COSMO-RS prediction at 1:3 molar ratio.

Gas	HBA(1)	HBD(2)	x_1	x_2	T (K)	P (bar)	Experimental Solubility	Predicted Solubility	RD	Ref.
CO_2	ChCl	Diethylene Glycoll	0.250	0.750	313.150	1.140	3.80E-03	1.43E-02	215.59%	Li et al., (2014)
						2.208	7.80E-03	2.76E-02	201.05%	
						3.182	1.11E-02	3.95E-02	190.28%	
						4.149	1.54E-02	5.12E-02	195.69%	
						5.106	1.94E-02	6.28E-02	192.79%	
								ARD	199.08%	

Table S31. Experimental data of CO_2 solubility in ChCl:Triethylene Glycol and COSMO-RS prediction at 1:3 molar ratio.

Gas	HBA(1)	HBD(2)	x_1	x_2	T (K)	P (bar)	Experimental Solubility	Predicted Solubility	RD	Ref.
CO_2	ChCl	Triethylene Glycoll	0.250	0.750	313.150	1.140	3.80E-03	1.43E-02	276.82%	Li et al., (2014)
						2.208	7.80E-03	2.76E-02	253.39%	
						3.182	1.11E-02	3.95E-02	255.94%	
						4.149	1.54E-02	5.12E-02	232.78%	
						5.106	1.94E-02	6.28E-02	223.47%	
								ARD	248.48%	

Table S32. Experimental data of CO_2 solubility in ChCl:Levulinic acid and COSMO-RS prediction at 1:3 molar ratio.

Gas	HBA(1)	HBD(2)	x_1	x_2	T (K)	P (bar)	Experimental Solubility	Predicted Solubility	RD	Ref.
CO_2	ChCl	Levulinic Acid	0.250	0.750	313.150	0.808	2.70E-03	6.08E-03	125.23%	Lu et al., (2015)
						2.100	7.50E-03	1.58E-02	110.23%	
						3.140	1.13E-02	2.35E-02	108.26%	
						4.176	1.50E-02	3.12E-02	108.29%	
						5.178	1.86E-02	3.87E-02	107.94%	
								ARD	111.32%	

Table S33. Experimental data of CO_2 solubility in ChCl:Furfuryl Alcohol and COSMO-RS prediction at 1:3 molar ratio.

Gas	HBA(1)	HBD(2)	x_1	x_2	T (K)	P (bar)	Experimental Solubility	Predicted Solubility	RD	Ref.
CO_2	ChCl	Furfuryl Alcohol	0.250	0.750	313.150	0.808	2.40E-03	6.07E-03	153.03%	Lu et al., (2015)
						2.146	6.30E-03	1.61E-02	155.38%	
						3.214	9.50E-03	2.41E-02	153.17%	
						4.267	1.26E-02	3.19E-02	152.97%	
						5.232	1.55E-02	3.90E-02	151.75%	
								ARD	152.31%	

Table S34. Experimental data of CO_2 solubility in ChCl:Guaiacol and COSMO-RS prediction at 1:3 molar ratio.

Gas	HBA(1)	HBD(2)	x_1	x_2	T (K)	P (bar)	Experimental Solubility	Predicted Solubility	RD	Ref.
CO_2	ChCl	Guaiacol	0.250	0.750	313.150	0.575	1.70E-03	6.54E-03	284.94%	Liu et al., (2017)
						1.457	4.10E-03	1.66E-02	305.00%	
						2.332	6.50E-03	2.66E-02	309.48%	
						3.303	9.30E-03	3.78E-02	306.09%	
						4.296	1.22E-02	4.92E-02	303.41%	
								ARD	302.35%	

Table S35. Experimental data of CO_2 solubility in ChCl:1,4 butanediol and COSMO-RS prediction at 1:4 molar ratio.

Gas	HBA(1)	HBD(2)	x_1	x_2	T (K)	P (bar)	Experimental Solubility	Predicted Solubility	RD	Ref.
CO_2	ChCl	1,4-butanediol	0.20	0.80	313.150	1.195	2.60E-03	7.93E-03	205.16%	Chen et al., (2014)
						2.232	4.90E-03	1.48E-02	202.54%	
						3.125	7.10E-03	2.08E-02	192.43%	
						4.100	9.60E-03	2.73E-02	183.88%	
						5.072	1.19E-02	3.37E-02	183.44%	
								ARD	193.49%	

Table S36. Experimental data of CO_2 solubility in ChCl:2,3 butanediol and COSMO-RS prediction at 1:4 molar ratio.

Gas	HBA(1)	HBD(2)	x_1	x_2	T (K)	P (bar)	Experimental Solubility	Predicted Solubility	RD	Ref.
CO_2	ChCl	2,3-butanediol	0.20	0.80	313.150	1.109	3.00E-03	9.64E-03	221.40%	Chen et al., (2014)
						2.172	6.10E-03	1.89E-02	210.02%	
						3.180	8.70E-03	2.77E-02	218.72%	
						4.149	1.18E-02	3.62E-02	207.06%	
						5.110	1.45E-02	4.47E-02	208.26%	
								ARD	213.09%	

Table S37. Experimental data of CO_2 solubility in ChCl:1,2 propanediol and COSMO-RS prediction at 1:4 molar ratio.

Gas	HBA(1)	HBD(2)	x_1	x_2	T (K)	P (bar)	Experimental Solubility	Predicted Solubility	RD	Ref.
CO_2	ChCl	1,2-propanediol	0.20	0.80	313.150	1.216	2.10E-03	7.71E-03	267.00%	Chen et al., (2014)
						2.252	4.30E-03	1.43E-02	232.49%	
						3.251	6.00E-03	2.07E-02	244.56%	
						4.214	8.10E-03	2.68E-02	231.40%	
						5.256	1.06E-02	3.35E-02	216.46%	
								ARD	238.38%	

Table S38. Experimental data of CO_2 solubility in ChCl:Phenol and COSMO-RS prediction at 1:4 molar ratio.

Gas	HBA(1)	HBD(2)	x_1	x_2	T (K)	P (bar)	Experimental Solubility	Predicted Solubility	RD	Ref.
CO_2	ChCl	Phenol	0.20	0.80	313.150	1.171	3.20E-03	9.53E-03	197.96%	Li et al., (2014)
						2.142	6.20E-03	1.88E-02	202.99%	
						3.204	9.60E-03	2.77E-02	188.18%	
						4.158	1.25E-02	3.63E-02	190.45%	
						5.045	1.57E-02	4.50E-02	186.52%	
								ARD	193.22%	

Table S39. Experimental data of CO_2 solubility in ChCl:Diethylene Glycol and COSMO-RS prediction at 1:4 molar ratio.

Gas	HBA(1)	HBD(2)	x_1	x_2	T (K)	P (bar)	Experimental Solubility	Predicted Solubility	RD	Ref.
CO_2	ChCl	Diethylene Glycoll	0.20	0.80	313.150	1.165	3.00E-03	9.22E-03	207.35%	Li et al., (2014)
						2.171	5.90E-03	1.72E-02	191.13%	
						3.135	8.80E-03	2.48E-02	181.80%	
						4.160	1.19E-02	3.29E-02	176.48%	
						5.182	1.47E-02	4.10E-02	178.80%	
								ARD	187.11%	

Table S40. Experimental data of CO_2 solubility in ChCl:Triethylene Glycol and COSMO-RS prediction at 1:4 molar ratio.

Gas	HBA(1)	HBD(2)	x_1	x_2	T (K)	P (bar)	Experimental Solubility	Predicted Solubility	RD	Ref.
CO_2	ChCl	Triethylene Glycoll	0.20	0.80	313.150	1.196	4.20E-03	1.45E-02	246.38%	Li et al., (2014)
						2.193	8.10E-03	2.65E-02	227.77%	
						3.152	1.24E-02	3.80E-02	206.39%	
						4.150	1.68E-02	4.98E-02	196.43%	
						5.190	2.02E-02	6.20E-02	206.95%	
								ARD	216.78%	

Table S41. Experimental data of CO_2 solubility in ChCl:Levulinic acid and COSMO-RS prediction at 1:4 molar ratio.

Gas	HBA(1)	HBD(2)	x_1	x_2	T (K)	P (bar)	Experimental Solubility	Predicted Solubility	RD	Ref.
CO_2	ChCl	Levulinic Acid	0.20	0.80	313.150	0.600	2.90E-03	4.37E-03	50.85%	Lu et al., (2015)
						1.769	8.50E-03	1.29E-02	51.51%	
						2.824	1.35E-02	2.05E-02	52.09%	
						3.801	1.85E-02	2.76E-02	49.22%	
						4.851	2.31E-02	3.52E-02	52.34%	
						5.659	2.73E-02	4.10E-02	50.25%	
								ARD	51.04%	

Table S42. Experimental data of CO_2 solubility in ChCl:Furfuryl Alcohol and COSMO-RS prediction at 1:3 molar ratio.

Gas	HBA(1)	HBD(2)	x_1	x_2	T (K)	P (bar)	Experimental Solubility	Predicted Solubility	RD	Ref.
CO_2	ChCl	Furfuryl Alcohol	0.20	0.80	313.150	0.703	2.50E-03	5.12E-03	104.68%	Lu et al., (2015)
						1.922	6.40E-03	1.40E-02	118.24%	
						2.954	9.90E-03	2.14E-02	116.56%	
						4.035	1.33E-02	2.92E-02	119.91%	
						5.028	1.65E-02	3.64E-02	120.64%	
						5.688	1.83E-02	4.12E-02	124.90%	
								ARD	117.49%	

Table 43. Experimental data of CO_2 solubility in ChCl:Guaiacol and COSMO-RS prediction at 1:4 molar ratio.

Gas	HBA(1)	HBD(2)	x_1	x_2	T (K)	P (bar)	Experimental Solubility	Predicted Solubility	RD	Ref.
CO_2	ChCl	Guaiacol	0.20	0.80	313.150	0.534	1.40E-03	6.18E-03	341.63%	Liu et al., (2017)
						1.425	4.40E-03	1.65E-02	275.92%	
						2.359	7.20E-03	2.75E-02	281.34%	
						3.355	1.03E-02	3.92E-02	280.28%	
						4.318	1.32E-02	5.06E-02	283.08%	
						5.429	1.65E-02	6.38E-02	286.76%	
								ARD	291.50%	

2. CH_4 solubility in ESs

Table S44. Experimental data of CH_4 solubility in ChCl:Lactic acid and COSMO-RS prediction at 1:1 molar ratio.

Gas	HBA(1)	HBD(2)	x_1	x_2	T (K)	P (bar)	Experimental Solubility	Predicted Solubility	RD	Ref.
CH_4	ChCl	Lactic Acid	0.50	0.50	298.15	0.051	4.25E-03	3.08E-05	99.27%	Altamash et al., (2019)
						0.929	1.09E-02	5.62E-04	94.85%	
						4.944	4.08E-02	2.99E-03	92.66%	
						9.946	7.81E-02	6.03E-03	92.28%	
						14.930	1.16E-01	9.06E-03	92.19%	
						19.928	1.55E-01	1.21E-02	92.17%	
						24.922	1.94E-01	1.52E-02	92.17%	
						29.910	2.34E-01	1.82E-02	92.19%	
						34.929	2.77E-01	2.13E-02	92.30%	
						39.922	3.18E-01	2.44E-02	92.32%	
						44.933	3.60E-01	2.75E-02	92.35%	
						49.933	4.03E-01	3.07E-02	92.39%	
								ARD	93.10%	

Table S45. Experimental data of CH_4 solubility in ChCl:Malonic acid and COSMO-RS prediction at 1:1 molar ratio.

Gas	HBA(1)	HBD(2)	x_1	x_2	T (K)	P (bar)	Experimental Solubility	Predicted Solubility	RD	Ref.
CH_4	ChCl	Malonic Acid	0.50	0.50	298.15	0.050	3.79E-03	1.80E-05	99.53%	Altamash et al., (2019)
						0.918	9.88E-03	3.30E-04	96.66%	
						4.940	3.73E-02	1.78E-03	95.24%	
						9.942	7.17E-02	3.59E-03	95.00%	
						14.938	1.06E-01	5.40E-03	94.93%	
						19.929	1.42E-01	7.22E-03	94.90%	
						24.924	1.77E-01	9.05E-03	94.90%	
						29.921	2.14E-01	1.09E-02	94.91%	
						34.914	2.54E-01	1.27E-02	94.98%	
						39.937	2.91E-01	1.46E-02	94.99%	
						44.928	3.30E-01	1.64E-02	95.01%	
						49.933	3.68E-01	1.83E-02	95.03%	
								ARD	95.51%	

Table S46. Experimental data of CH4 solubility in ChCl:Phenylacetic acid and COSMO-RS prediction at 1:1 molar ratio.

Gas	HBA(1)	HBD(2)	x_1	x_2	T (K)	P (bar)	Experimental Solubility	Predicted Solubility	RD	Ref.
CH_4	ChCl	Phenylacetic Acid	0.50	0.50	298.15	0.050	4.02E-03	6.13E-05	98.47%	Altamash et al., (2019)
						0.916	1.05E-02	1.12E-03	89.25%	
						4.946	3.96E-02	6.07E-03	84.69%	
						9.943	7.64E-02	1.22E-02	84.03%	
						14.938	1.14E-01	1.83E-02	83.88%	
						19.917	1.52E-01	2.44E-02	83.88%	
						24.923	1.90E-01	3.06E-02	83.94%	
						29.921	2.30E-01	3.67E-02	84.01%	
						34.936	2.72E-01	4.29E-02	84.24%	
						39.932	3.13E-01	4.91E-02	84.33%	
						44.935	3.54E-01	5.52E-02	84.40%	
						49.920	3.96E-01	6.14E-02	84.51%	
								ARD	85.80%	

Table S47. Experimental data of CH_4 solubility in ChCl:Urea and COSMO-RS prediction at 1:2 molar ratio.

Gas	HBA(1)	HBD(2)	x_1	x_2	T (K)	P (bar)	Experimental Solubility	Predicted Solubility	RD	Ref.
CH_4	ChCl	Urea	0.333	0.667	313.150	0.134	7.00E-05	1.75E-05	74.99%	Liu et al., (2019)
						0.527	2.80E-04	6.89E-05	75.41%	
						1.076	5.70E-04	1.41E-04	75.33%	
						1.536	8.10E-04	2.01E-04	75.22%	
						2.028	1.10E-03	2.65E-04	75.90%	
								ARD	75.37%	

Table S48. Experimental data of CH_4 solubility in ChCl:Urea and COSMO-RS prediction at 1:1.5 molar ratio.

Gas	HBA(1)	HBD(2)	x_1	x_2	T (K)	P (bar)	Experimental Solubility	Predicted Solubility	RD	Ref.
CH_4	ChCl	Urea	0.40	0.60	313.150	0.103	6.00E-05	1.56E-05	73.97%	Liu et al., (2019)
						0.509	2.50E-04	7.72E-05	69.12%	
						0.994	4.90E-04	1.51E-04	69.23%	
						1.505	6.90E-04	2.28E-04	66.91%	
						1.996	9.10E-04	3.03E-04	66.72%	
								ARD	69.19%	

Table S49. Experimental data of CH_4 solubility in ChCl:Urea and COSMO-RS prediction at 1:2.5 molar ratio.

Gas	HBA(1)	HBD(2)	x_1	x_2	T (K)	P (bar)	Experimental Solubility	Predicted Solubility	RD	Ref.
CH_4	ChCl	Urea	0.286	0.714	313.150	0.114	4.00E-05	1.37E-05	65.68%	Liu et al., (2019)
						0.503	2.60E-04	6.06E-05	76.70%	
						1.015	4.70E-04	1.22E-04	73.99%	
						1.520	7.20E-04	1.83E-04	74.57%	
						2.019	9.50E-04	2.43E-04	74.39%	
								ARD	73.07%	

3. H_2S solubility in ESs

Table S50. Experimental data of H_2S solubility in ChCl:Urea and COSMO-RS prediction at 1:2 molar ratio.

Gas	HBA(1)	HBD(2)	x_1	x_2	T (K)	P (bar)	Experimental Solubility	Predicted Solubility	RD	Ref.
H_2S	ChCl	Urea	0.333	0.667	313.150	0.117	2.58E-03	4.14E-03	60.40%	Liu et al., (2019)
						0.524	1.24E-02	1.84E-02	47.94%	
						0.994	2.35E-02	3.47E-02	47.36%	
						1.526	3.59E-02	5.28E-02	47.27%	
						2.004	4.64E-02	6.90E-02	48.68%	
								ARD	50.33%	

Table S51. Experimental data of H_2S solubility in ChCl:Urea and COSMO-RS prediction at 1:1.5 molar ratio.

Gas	HBA(1)	HBD(2)	x_1	x_2	T (K)	P (bar)	Experimental Solubility	Predicted Solubility	RD	Ref.
H_2S	ChCl	Urea	0.40	0.60	313.150	0.114	3.74E-03	4.72E-03	26.12%	Liu et al., (2019)
						0.547	1.62E-02	2.23E-02	37.61%	
						0.994	2.92E-02	4.01E-02	37.59%	
						1.500	4.23E-02	5.98E-02	41.39%	
						2.021	5.55E-02	7.96E-02	43.61%	
								ARD	37.27%	

Table S52. Experimental data of H_2S solubility $_{in}$ ChCl:Urea and COSMO-RS prediction at 1:2.5 molar ratio.

Gas	HBA(1)	HBD(2)	x_1	x_2	T (K)	P (bar)	Experimental Solubility	Predicted Solubility	RD	Ref.
H_2S	ChCl	Urea	0.286	0.714	313.150	0.099	2.11E-03	3.19E-03	51.22%	Liu et al., (2019)
						0.482	8.72E-03	1.55E-02	77.49%	
						1.014	1.84E-02	3.24E-02	76.67%	
						1.506	2.76E-02	4.80E-02	73.77%	
						1.985	3.51E-02	6.31E-02	79.66%	
								ARD	71.76%	

CAPÍTULO 6

Characterization by SLE phase diagrams and density of Eutectic Solvents based on ChCl, alcohols, and acids at high pressures

(Artigo em fase de correção e submissão)

Fernanda Paludetto Pelaquim[a], Monique de Jesus Amaral [b,c], Irede Angela Lucini Dalmolin[d], Elton Franceschi [b,c], Gustavo Rodrigues Borges [b,c], Claudio Dariva [b,c], Mariana Conceição da Costa[a4*].

[a] School of Chemical Engineering, University of Campinas – UNICAMP, Avenida Albert Einstein 500, ZIP Code 13083-852, Campinas, SP, Brazil

b Center for Studies on Colloidal Systems (NUESC) – Institute of Technology and Research (ITP), Av. Murilo Dantas, 300, Aracaju, SE, ZIP Code 49032-490, Brazil

[c] Tiradentes University (UNIT), Postgraduate Programme in Process Engineering (PEP), Av. Murilo Dantas, 300, Aracaju, SE, ZIP Code 49032-490, Brazil

[c] Academic Department of Engineering, Universidade Tecnológica Federal do Paraná (UTFPR), Linha Santa Bárbara, ZIP Code 85601-970, Francisco Beltrão, PR, Brazil

4 [*] Corresponding author.

E-mail address: mcdcosta@unicamp.br (M.C. Costa)

phone number: +551935213962.

Abstract

Deep eutectic solvents (DESs) and eutectic solvents (ESs) have been used in many applications in the chemical, pharmaceutical, and material fields over the last decade. Their application is usually at a fixed stoichiometric molar ratio that is not always optimized since the knowledge of thermophysical properties is required. However, the thermodynamic characterization of these solvents is often scarce in the literature, which makes it difficult to understand the mechanisms underlying DESs interactions and formation. Therefore, this work aims to determine the solid-liquid phase diagrams of six binary mixtures composed of choline chloride (ChCl) as hydrogen bond acceptor (HBA) and ethylene glycol, glycerol, 1,3 propanediol, malonic acid, glycolic acid, and lactic acid as hydrogen bond donors (HBD) under high pressure and to compare this data with those found in the literature at atmospheric pressure. Moreover, it is also an objective of this study to determine the density of the ChCl:ethylene glycol, ChCl:glycerol, ChCl:1,3 propanediol, and ChCl:glycolic acid mixtures in its eutectic composition under high pressures (1 – 50 MPa) and larger temperature ranges (293.15 – 353.15 K). These experimental data were then correlated using the modified Tait–Tammann equation, and the Cubic Plus Association (CPA) equation of state model considering the solvents as an individual components. The experimental results indicate a eutectic behavior for all ESs and a shift of the melting temperature with pressure increase. Regarding densities under high pressure, the ESs presented the expected behavior, i.e., the density decreases with the temperature rise, and increases with the pressure rise. CPA and the modified Tait–Tammann allowed accurate modeling of the density experimental data, with deviations no higher than 0.45%.

1. Introduction

The application of conventional organic solvents has grown over the years because most industrial processes such as synthesis, extraction, and separation depend on their use [1]. Large amounts of these solvents are used, reaching approximately 20,000,000 tons every year [2]. They are mostly comprised of alcohols and low molecular weight petrochemical derivatives. However, their excessive consumption causes problems in human health, process safety risks, eco-toxicity, and waste management concerns since their recycling in many chemical processes are difficult [2,3].

Therefore, in 2015, the United Nations delineated a new sustainability-centered plan entitled ‘‘Transforming Our World: The 2030 Agenda for Sustainable Development” to remove the organic solvents and chemical waste pollution from the environment [4]. Accordingly, it is crucial to reduce the consumption of toxic organic solvents and replace them with safer solvents.

Green chemistry is responsible to reduce the use and production of these harmful substances, searching for renewable sources. In addition, introduces sustainable concepts to develop greener and more sustainable routes, processes, and products such as the Deep Eutectic Solvents (DESs) and the Eutectic Solvents (ESs) [3]. DESs and ESs have emerged because they usually present thermal stability, high solvation ability, and low volatility. Besides, they are liquid at room temperature, non-combustible, inexpensive, easy to prepare, and usually show good biodegradability, biocompatibility, and sustainability [5,6].

DESs are a mixture composed of two or more pure compounds, including hydrogen-bond acceptors (HBAs) and hydrogen-bond donors (HBDs), whose eutectic

point temperature is below that of an ideal liquid mixture. If the mixture presented a eutectic point temperature that does not follow the statement above, thus it is called only Eutectic Solvent [7]. It is important to mention that a wide range of possible HBAs and HBDs can be found in the literature forming either DESs or ESs. However, which defines the green characteristic of any eutectic mixtures is the use of more eco-friendly components such as amines [8], sugars [9,10], alcohol and polyalcohol compounds [11,12], and organic acids [13–15] as HBD [16,17]. These compounds are preferred due to their chemical diversity, biodegradability, and sustainability. Also the use of nontoxic quaternary ammonium salts as HBA, especially choline chloride (ChCl), because of its biocompatibility and low price [1].

These sustainable solvents have been used in many applications in the chemical, pharmaceutical, and material fields. They can be used as a replacement for inorganic acids for hydrometallurgy [18–20], as a doping agent, and chiral source [21,22], as a versatile ramie fiber degumming [23–25], as CO2 capture [26,27], in membrane separation applications [28–30], as a candidate for lignocellulose dissolution and pretreatment [31,32], as an effective extractor [33–37], among others.

Although DESs and ESs are being applied in several fields, the authors usually select only a fixed stoichiometric molar ratio at the point where the mixtures are visually liquid at room temperature and report it as optimized, which is not always true. The decision of the suitable molar ratio of the DES/ES components and operating temperature must be based on the knowledge of their thermophysical properties (as density and viscosity) and the solid-liquid equilibria (SLE) phase diagrams which enhance the design, simulation, and optimization of industrial processes [1,7]. Nevertheless, these essential properties are scarce in the literature on atmospheric

pressure as well as on high pressures, in a limited temperature range, which makes difficult the knowledge of the mechanisms underlying DESs/ESs interactions and formation, consequently, the development of reliable thermodynamic models for simulation processes is compromised due to the lack of experimental data [17]. Crespo et al. (2018) [38] also showed that most ESs reported as DESs do not present large deviations from the ideal-mixture behavior and the eutectic composition relies on the used precursors.

Regarding the SLE phase diagrams, a research group has determined several phase diagrams of eutectic mixtures using especially ChCl, quaternary ammonium chlorides and betaine as HBAs, and polyalcohol, sugars, carboxylic acids, fatty acids and alcohols, organic chloride-based salt and terpenes as HBDs [14,17,38–43]. Despite of built a large database, the ESs were determined only at atmospheric pressure and their behavior under high pressures is unknown.

The density of ESs at atmospheric pressure has been determined by several authors, using a wide range of HBAs and HBDs [13,44–64]. However, the density of ESs at higher pressures was determined only by a few authors. Leron et al. (2012, 2012(1), (2012(2)) [65–67] reported some density values at pressures up to 50 MPa, but only at the temperature range (298.15 – 323.15 K) for ESs composed of ChCl as HBA, ethylene glycol, glycerol and urea as HBDs. Crespo et al. (2019) [1] measured the densities of the same ESs, however in larger temperature (283.15 – 363.15 K) and pressure (0.1 – 95 MPa) ranges. Sas et al. (2021) [68] were the last authors to report the density of the following ESs: menthol:octanoic acid, menthol:decanoic acid, menthol:dodecanoic acid and dodecanoic acid:octanoic acid at high pressures (0.1 – 60 MPa) and larger temperature range (293.15 – 413.15 K).

Unfortunately, the determination of these properties and their thermodynamic modeling is still poorly studied in the literature due to the complex hydrogen bonding interactions of ESs and the lack of trustworthy experimental data. Crespo et al. (2017, 2018, 2019) [38,39,69] and Pontes et al. (2017) [14] were the only ones to model the SLE phase diagrams of several ESs. The authors successfully modeled the SLE phase diagrams using the PC-SAFT equation of state (EoS). To our knowledge, only Crespo et al. (2019) [1] have modeled the density of ESs at higher pressures, using PC-SAFT, while Sas et al. (2021) [68] and Leron et al. (2012, 2012(1), 2012(2)) [66,67,70] used the modified Tait–Tammann equation, an empirical model, frequently used to correlate high-pressure density experimental data.

This research seeks to contribute to the knowledge of the physical properties of ESs. Therefore, the study was shared into two parts: Firstly, it was determined the solid-liquid phase diagrams of six binary mixtures composed of ChCl and different alcohol and acids, namely, ethylene glycol, glycerol, 1,3 propanediol, malonic acid, glycolic acid, and lactic acid using a high-pressure variable-volume view cell at high pressures (6, 10, 14, and 25 MPa). These results were compared with those presented in the literature and determined at atmospheric pressure. In the second part, it was determined the density of four mixtures formed by ChCl, three with alcohols compounds (ethylene glycol, glycerol, 1,3 propanediol) and one with an acid (glycolic acid) at the eutectic composition of such mixtures and under high pressures (1 – 50 MPa) and larger temperature ranges (293.15 – 353.15 K). Moreover, the density data were correlated using the modified Tait–Tammann equation and the CPA EoS employing Multiflash software. Furthermore, it was assumed an individual component approach to describe the density of experimental data.

2. Experimental Section

2.1. Materials

The materials employed to prepare the ESs used in this work along with their source, purity, melting properties, and chemical structure are detailed in Table 53**Erro! Fonte de referência não encontrada.**. All components were dried under vacuum, at room temperature and atmospheric pressure for 72 h, and then stored at room temperature in a desiccator.

Table 53. Source, purity, and melting properties of the components used in this work.

Component	CAS Number	Supplier	Mass purity (%)	T_m(K)	$\Delta_m H$ (kJ.mol^{-1})
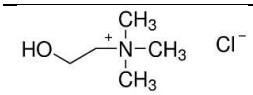 **Choline Chloride**	67-48-1	Sigma Aldrich	≥ 98,5%	597 [41]	4.30 [41]
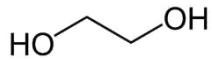 **Ethylene Glycol**	107-21-1	Merck	99,5%	256.60 [71]	9.50 [71]
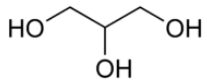 **Glycerol**	56-81-5	Anidrol	99%	293 [72]	18.28 [72]
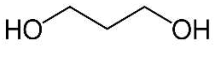 **1,3 propanediol**	504-63-2	Sigma Aldrich	≥ 98%	249 [72]	11.40 [72]
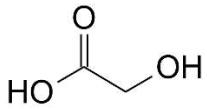 **Glycolic Acid**	79-14-1	Acros	99,7%	351.30 [73]	19.30 [73]
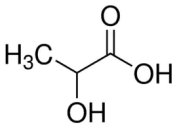 **Lactic Acid**	50-21-5	Sigma Aldrich	99,5%	289.90 [74]	11.34 [74]
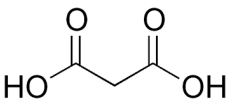 **Malonic Acid**	141-82-2	Sigma Aldrich	99%	407.50 [75]	23.10 [75]

2.2. Preparation of Eutectic Mixtures

Six ESs were prepared using choline chloride (ChCl) as a hydrogen bonding acceptor (HBA), and different hydrogen bonding donors (HBD) at different molar ratios, according to Table 54.

Table 54. Molar ratio (x_2) of the ChCl (1) based ESs.

Mixture components		Molar ratio (x_2)		Average of water content (%)
HBD (2)	System	SLE*	ρ*	
Ethylene Glycol (EG)	ChCl:EG	0.70; 0.67; 0.60; 0.55	0.67	0.75
Glycerol (GLY)	ChCl:GLY	0.55; 0.50; 0.45; 0.40	0.60	0.80
1,3 propanediol (PD)	ChCl:PD	0.67; 0.60;0.55	0.70	0.89
Glycolic Acid (GLY AC)	ChCl:GLY AC	0.60; 0.85	0.55	3.58
Lactic Acid (LAT AC)	ChCl:LAT AC	0.45; 0.50	0.50	1.09
Malonic Acid (MAL AC)	ChCl:MAL AC	0.70; 0.65; 0.45	0.50	1.23

*prepared for use in the measurements of solid-liquid phase diagrams (SLE) and density ($\boldsymbol{\rho}$) at high pressures.

The ESs were produced using the method of heating combined with stirring proposed by Abbott et al. (2003) [76]. Initially, previously known amounts of each component were weighed using an analytical balance with an accuracy of $\pm 2 \times 10^{-4} g$ (Shimadzu AUY220, Japan), according to the mole ratio, for a total mass of 100 g, into a 250 ml Erlenmeyer flask. The mixture was placed in a glycerin bath with reciprocal stirring at 333.15 K for 120 min, or until the formation of a clear and homogeneous liquid. Then, the water content of each molar ratio of the investigated ESs was measured using a Metrohm 831 Karl Fischer coulometer, with the Hydranal-Coulomat AG analyzer from Riedel-de Haën. The ESs formed were then transferred to amber flasks and stored at room temperature in a desiccator to avoid possible water absorption from the environment.

2.3. Phase equilibrium apparatus and procedure

In this work, the static synthetic method was used to obtain experimental data for phase equilibria at high pressures using a high-pressure variable-volume view cell. This apparatus (Figure 23) and experimental procedure have been employed in previous studies[77–80]. It is formed by a gas cylinder, which contains the pressurizing fluid (1), and a high-pressure syringe pump (ISCO 260L, Lincoln, USA) (2). The fluid temperature in the pump was controlled by a thermostatic bath (TECNA, model TE-184) (3). The system pressure was monitored by an absolute pressure transducer with a precision of ±0.03 MPa (Smar LD 301) (4). The high-pressure variable-volume view cell (5), with a maximum capacity of $2.7 \times 10^{-5}\ m^3$, presents two sapphire windows (6 and 7) for the visualization of the phase transitions, removable connections for feeding the mixture components, and the insertion of a PT-100 temperature indicator (8 and 9) to direct contact with the fluid inside the cell body. The pressure control was provided by a movable piston (10). The cell also is equipped with a jacket connected to a thermostatic bath (TECNA, model TE-184) (12) to control the temperature. The system was magnetically stirred (11) throughout the experimental procedure.

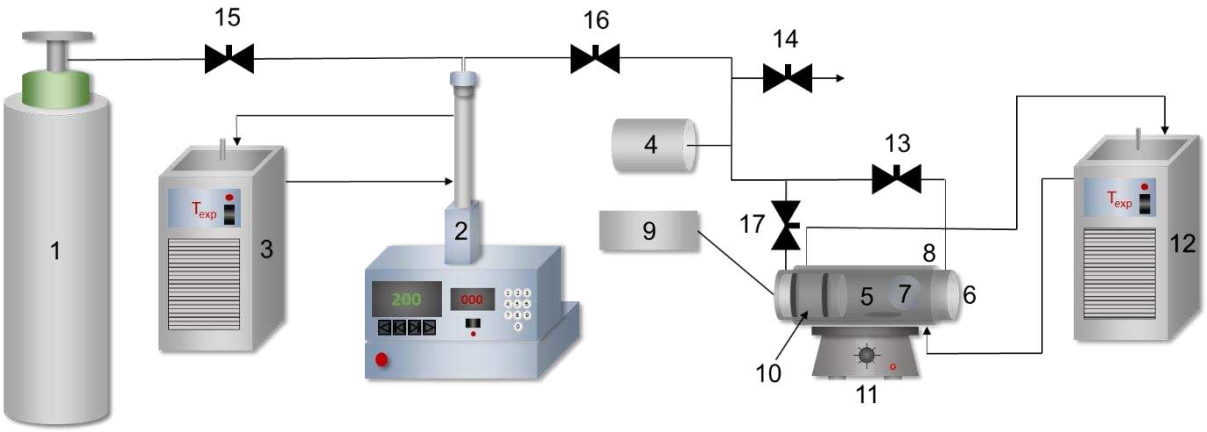

Figure 23. Schematic diagram of the experimental apparatus for phase equilibrium at high pressure. (1) gas cylinder; (2) syringe pump; (3 and 12) thermostatic baths; (4) absolute pressure transducer; (5) high-pressure variable-volume view cell; (6 and 7) sapphire windows; (8) removable connections; (9) PT-100 temperature indicator; (10) movable piston; (11) magnetic stirrer; (13 and 14) needle valves; (15 and 16) sphere valves; (17) micrometer valve.

Phase transitions were measured visually by manipulating the temperature using a thermostatic bath and a syringe pump with carbon dioxide as pressurizing fluid. The phase equilibrium determination of pure ESs was performed as an isobaric operation. Initially, a known amount of ES at a given molar ratio is inserted into the cell to complete a volume of approximately 10 mL at atmospheric pressure. Then, the cell was flushed with low-pressure gas to remove residual air. The pressure was pre-set by inserting the pressurization fluid through the syringe pump, increasing the pressure to the desired value for data acquisition. Once the required pressure is stabilized, the temperature is slowly reduced, until the solid-liquid phase transition is observed, i.e., a transition temperature is determined at a given pressure. This procedure occurs, on average, 12 hours to complete and was done in triplicate for each molar ratio. In this work, the phase transitions were evaluated at 6, 10, 14, 20, and 25 MPa.

2.4. Density of ESs at high pressures

The densities of ESs were measured at the temperatures 293.15 K, 298.15 K, 313.15 K, 333.15, and 353.15 K and pressure range 1 – 50 MPa using a density measuring module DMA HPM in combination with the evaluation unit mPDS 5, a high-pressure densimeter from Anton Paar, Austria. The measurement cell was thermostated by circulating a thermoregulatory fluid, with a temperature stability of ± 0.01 K through the circulation of a thermostatic bath (Julabo MC). The standard uncertainty on temperature was 0.1 K. Pressure was measured using a piezoresistive silicone pressure transducer (Kulite HEM 375) with an accuracy of better than 0.2%. The transducer was attached directly to a ¼" stainless steel line to reduce dead volume and placed between the DMA HPM measurement cell and a moving piston.

The densimeter was calibrated with deionized water and nitrogen over a wide temperature and pressure ranges from 293.15 to 363.15 K and 1 to 60 MPa, respectively. The mode used was the Wide Range, which applies a polynomial equation (Equation 1) to correlate the period of oscillation recorded by the internal oscilloscope with the density of the fluid analyzed.

$$\rho = AA + AB.\partial t + AC.\partial d + AD.\partial t^2 + AE.\partial d^2 + (AF + AG.\partial t + AH.\partial d + AI.\partial t^2 + AJ.\partial d^2).\partial p^2 + AK.\partial p^4 \quad (1)$$

3. Thermodynamic modeling

3.1. Modified Tait–Tammann Equation

The parameter of the modified Tait–Tammann equation were fitted to the liquid densities of ESs measured in this work according to Equation 2 [81].

$$\rho(T,p) = \frac{\rho^{ref}(T)}{1 - C.\ln\left(\frac{B(T)+p}{B(T)+p^{ref}}\right)} \quad (2)$$

Where ρ^{ref} is the density of the ES at a reference pressure (p^{ref}); $B(T)$ is a parameter that depends on temperature, and C is a temperature-independent parameter.

$$\rho^{ref}(T) = \sum_{i=0}^{2} a_i T^i \tag{3}$$

$$B(T) = \sum_{i=0}^{1} b_i T^i \tag{4}$$

The parameters of a_i from Equation 3 were optimized by fitting them to the experimental densities at reference pressure p^{ref} = 0.1 MPa. The coefficient C and the parameters of b_i were obtained by fitting the modified Tait–Tammann equation to the experimental data at high pressures.

3.2. Cubic Plus Association EoS

CPA EoS combines the classic Soave-Redlich-Kwong equation and the association term from statistical thermodynamics. Pressure is provided by Equation 5 [82,83]:

$$P = \frac{RT}{V_m - b} - \frac{\mathrm{a}(T)}{V_m(V_m + b)} - \frac{1}{2}\frac{RT}{V_m}\left(1 + \rho\frac{\partial \ln g}{\partial \rho}\right)\sum_i x_i \sum_{A_i}\left(1 - X_{A_i}\right) \tag{5}$$

where x_i is the molar fraction of component i; ρ is the molar density ($\rho = 1/V_m$); g is a simplified hard-sphere radial distribution function; and X_{A_i} represents the mole fraction of sites A in molecule i that were not bonded to other active sites. The equation can be also expressed in terms of compressibility factor (Z) as Equation 6.

$$Z = \frac{1}{1 - b\rho} - \frac{a\rho}{RT(1 + b\rho)} \tag{6}$$

Where a is the physical energy parameter calculated using Equation 7; and b is the co-volume parameter.

$$\mathrm{a}(T) = \mathrm{a}_0\left[1 + c_1\left(1 - \sqrt{T_r}\right)\right]^2 \quad (7)$$

with $T_r = \frac{T}{T_c}$, where T_c is the critical temperature. The critical properties of the studied HBA and HBDs were calculated by the modified Lydersen−Joback−Reid method (Table 55) [84,85], as explained in our last study [86].

To extend CPA EoS to mixtures, conventional van der Waals one-fluid mixing rules were employed in the physical term for energy and co-volume b. For the energy parameter $a_{ij}(T)$, the following geometric mean rule is used:

$$\mathrm{a}(T) = \sum_i \sum_j x_i x_j \mathrm{a}_{ij}(T) \quad (8)$$

with

$$\mathrm{a}_{ij}(T) = \sqrt{\mathrm{a}_i(T)\mathrm{a}_j(T)}\left(1 - k_{ij}\right) \quad (9)$$

And,

$$b = \sum_i x_i b_i \quad (10)$$

Table 55. Critical properties of the HBA and HBDs studied in this work.

Component	Molecular weight (g.mol^{-1})	T_c (K)	P_c (MPa)	ω
Choline chloride	139.62	622.97	3.05	0.76
Ethylene glycol	62.07	598.73	6.75	0.99
1,3 propanediol	76.09	621.75	5.51	1.00
Glycerol	92.04	715.99	6.32	1.46
Glycolic acid	76.05	674.80	6.75	0.97

3.3. CPA parameter estimation for ESs

Five parameters are needed to describe pure components: three physical parameters (a_0, b, c_1), the volume parameter ($\beta^{A_iB_j}$) and energy parameter ($\varepsilon^{A_iB_j}$). However, these parameters are not easily available in the literature for most precursors of ESs.

Two approaches can be assumed for modeling ESs, the pseudo-component, and the individual-component ones. Although the pseudo-component approach has been successfully used in the literature[87,88], in this study the individual component will be used because, in the last study of the research group, this approach was shown to be more appropriate for ESs as they are a mixture of HBAs and HBDs and not a new component as explained by Martins et al. (2018) [7].

The individual-component approach consists of treating each HBA and each HBD as a pure component. In such a case, the CPA parameters were obtained by fitting them to the liquid density of each HBA and HBD considering both the self and cross-association interactions. After parameters adjustment, they were used to calculate the density at high pressure by CPA EoS. The results from CPA were compared to experimental data determined in this work by average absolute relative deviation (AARD%) according to Equation 11. The AARD% minimization was done by the objective function of Equation 12 using Solver from Microsoft Excel to adjust the binary interaction parameters (k_{ij}).

$$AARD\% = \frac{1}{N_p}\sum_{i}^{N_p}\left|\frac{\rho_i^{cal} - \rho_i^{exp}}{\rho_i^{exp}}\right| \times 100 \qquad (11)$$

$$OF = \min\left[\sum_{i=1}^{N_p}\left(\frac{\rho_i^{cal} - \rho_i^{exp}}{\rho_i^{exp}}\right)\right] \quad (12)$$

where N_p is the number of experimental data, ρ^{exp} is the experimental density, and ρ^{cal} is the CPA-calculated density.

4. Results and Discussion

4.1. Solid-liquid equilibrium at high pressures

The temperature-composition (molar fraction of HBDs; x_2) diagrams are shown in Figure 24 - phase equilibrium experimental data at six pressures along with the phase equilibrium experimental data found in the literature at atmospheric pressure. All experimental data are detailed in Tables S1 – S6 of Supporting Information. Due to limitations of the high-pressure variable-volume view cell apparatus, it was not investigated all ESs molar ratios since the connections used in the unit support temperatures up to 343.15 K, and the thermostatic bath reaches temperatures up to 262.15 K. All the studied systems, such as depicted in Figure 24**Erro! Fonte de referência não encontrada.**, present a single eutectic point, which is expected for systems with immiscible components in the solid phase [17,89].

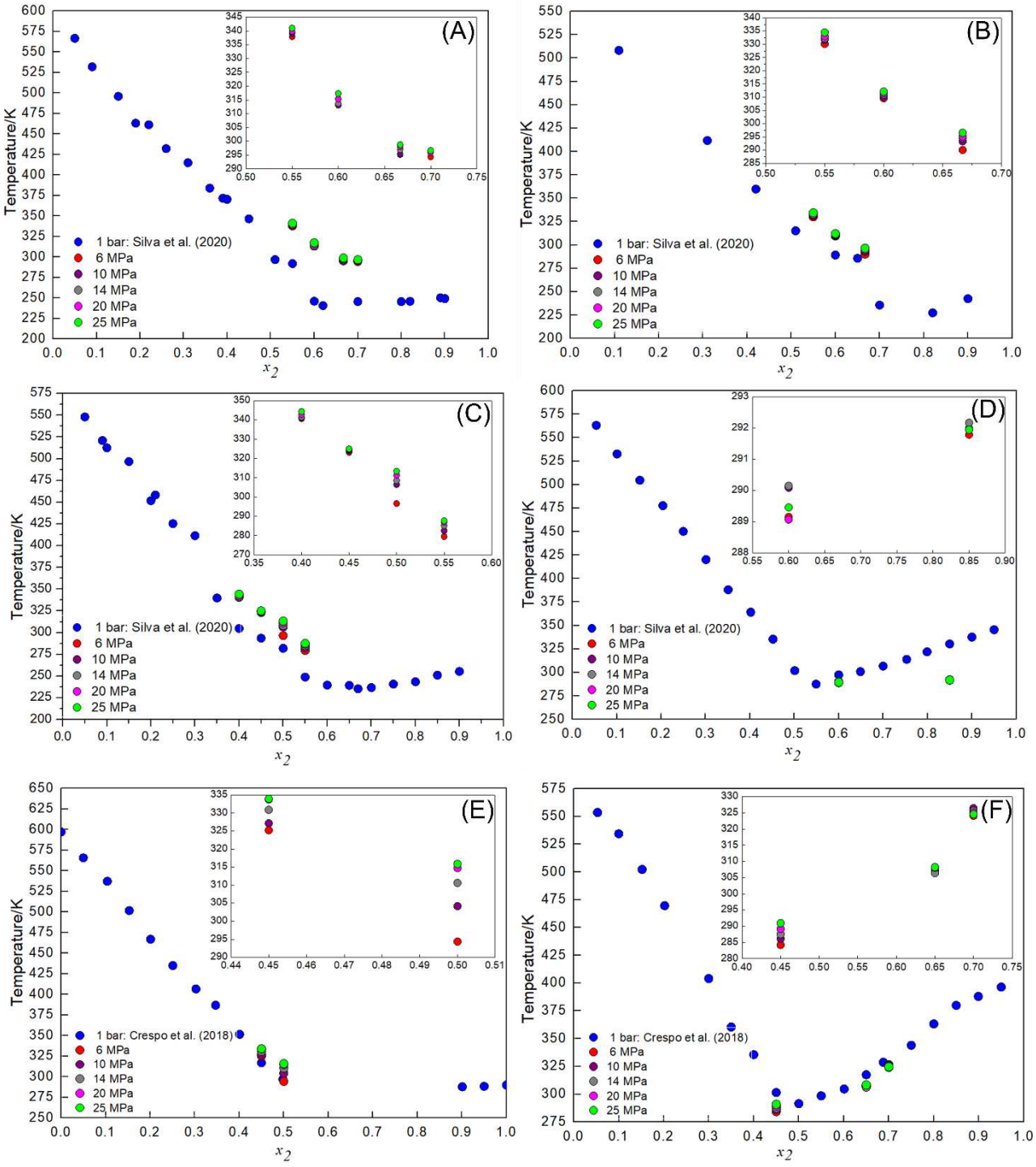

Figure 24. Solid-liquid phase diagrams at high pressures of binary mixtures composed of ChCl (1) and (A) ethylene glycol (2); (B) 1,3 propanediol (2); (C) glycerol (2); (D) glycolic acid (2); (E) lactic acid (2); (F) malonic acid (2).

Looking at Figure 24 one can notice that the eutectic temperature was found only for the ESs composed of ChCl:EG (Figure 24 (A)) at temperatures between 295

and 299 K and ChCl:MAL AC (Figure 24 (F)) at temperatures between 284 and 291 K. The eutectic temperature was not determined for the other systems due to apparatus limitations. However, the trend of the liquidus line of all systems remained the same as those at atmospheric pressure. In Figure 24 (A) it is possible to infer that the eutectic point is located between the mole ratios 0.67 and 0.70 of ethylene glycol, agreeing with the phase diagram found in the literature determined at atmospheric pressure [17]. And in **Erro! Fonte de referência não encontrada.** (F) the eutectic point occurs between 0.45 and 0.65 molar ratios of malonic acid, also agreeing with the literature on atmospheric pressure [89]. Therefore, the eutectic composition does not change with increasing pressure. This was also observed in SLE phase diagrams of fatty acids methyl and ethyl esters [90,91], fatty alcohols [92], and organic systems [93].

It can also be seen that the increase in melting temperature is relatively small between the pressures 6 – 25 MPa, but large between 0.1 – 6 MPa for all studied ESs (Table S1 – S6 of Supporting Information). For example, the increase in melting temperature of the ChCl:EG system (**Erro! Fonte de referência não encontrada. Erro! Fonte de referência não encontrada.**(A)) between 0.1 and 6 MPa ($\Delta T_{(6-0.1)MPa}$) was on average 54 K, whereas the temperature increases when pressure increases from 6 to 25 MPa ($\Delta T_{(25-6)MPa}$) is on average only 3.30 K. Tables S1 – S6 of Supporting information show that for both polyalcohol (ChCl:EG and ChCl:PD) and carboxylic acids-based ESs (ChCl:GLY AC and ChCl:LAT AC), the increase in HBD carbon chain length leads to a reduction of approximately 40 and 18 degrees in $\Delta T_{(6-0.1)MPa}$, for polyalcohol and carboxylic acids-based ESs respectively. In contrast to this behavior, an enlargement of approximately 1.2 and 15 degrees is observed in $\Delta T_{(25-6)MPa}$, for both families of ESs. To complement this observation, the existence of an

extra hydroxyl group for polyalcohol-based ESs, from ChCl:EG to ChCl:GLY, or an extra carboxylic group for carboxylic acids-based ESs, from ChCl: GLY AC to ChCl:MAL AC, shows the same influence on temperature. Unfortunately, more experimental data are required to deepen this discussion and to draw some conclusions about the topic.

These differences occur because pressure increases can lead the mixtures to states of smaller volume, i.e., more compact structures [94]. Therefore, the electrons tend to states of lower kinetic energy, and the pure component melting temperature subjected to high pressure will be higher than at atmospheric pressure [94]. In addition, at atmospheric pressure the molecules are not so tightly packed, so the energy required for a phase transition is lower, and consequently, the melting temperature will be lower. On the other hand, at higher pressures, the molecules are closer, and very tightly packed, requiring more energy for the phase transition, so the melting temperature will be higher as well [94]. Possibly, between 6 and 25 MPa, the molecules are as close as possible and the difference between the melting temperatures is smaller than at atmospheric pressure and 6 MPa.

Along with the previous explanation, it can be also justified by the water content of ESs. In this study the water content was no higher than 3.9%, however, in Silva et al. (2020) was no higher than 0.04% for polyalcohol ESs, and Crespo et al. (2018) was no higher than 1.3% for carboxylic acids ESs [17,89]. These differences may influence the results by slightly increasing the melting temperature of the system, but not changing the shape of the curve. When present in ESs, water is absorbed by the components forming strong interactions, and reducing the inter- and intramolecular interactions between HBA and HBD, which change their properties [95].

It is well known that an increase in water content reduces the viscosity and increases the conductivity, but only a few studies have evaluated the changes in melting temperature. Meng et al. (2016) showed that for the ES formed by ChCl and urea at a 1:2 molar ratio, the increase in the water content reduces the melting temperature from 298.15 K for the dry ES to approximately 276.15 K with a water addition of 10% [96], both system at atmospheric pressure (~0.1 MPa).

The ESs melting temperature seems to be influenced by the difference between the HBDs melting temperature and water melting temperature. For example, the urea melting temperature is approximately 406.15 K and water melts at 273.15 K, at atmospheric pressure (~0.1 MPa). In this case, the addition of water to urea-based ES causes a decrease in its melting temperature. Whereas, in this study, the melting temperature of ChCl:EG (**Erro! Fonte de referência não encontrada.** (A)) increases with water addition since the melting temperature of ethylene glycol is 260.61 K [97], 13 degrees lower than the water melting temperature at atmospheric pressure. Therefore, an ES formed by ethylene glycol will have its melting temperature increased, depending on the amount of ethylene glycol (molar ratio of HBA and HBD) and water. The same behavior was observed for ChCl:PD (**Erro! Fonte de referência não encontrada. Erro! Fonte de referência não encontrada.**(B)), ChCl:GLY (**Erro! Fonte de referência não encontrada.** (C)), and ChCl:LAT AC (**Erro! Fonte de referência não encontrada.** (E)). Whereas ChCl:GLY AC (**Erro! Fonte de referência não encontrada. Erro! Fonte de referência não encontrada.**(D)) and ChCl:MAL AC (**Erro! Fonte de referência não encontrada.** (F)) presented the opposite behavior since their melting temperature is much higher than the water at atmospheric pressure., 351.30 K [73], and 408.15 K [98] respectively.

Both low kinetic energy and high-water content influence SLE phase diagrams of ESs at high pressure. However, it is not already known the proportion in which each factor influences the liquidus line shift of the phase diagrams concerning the temperature axis. It is also important to mention that these data have never been reported in the literature to our knowledge, turning out to be relevant results even at larger water contents than the literature data at atmospheric pressure. Moreover, in industrial processes, ESs will hardly be used at low water contents because of the high solvent demand, and drying them is economically unfeasible.

Figure 25 shows PxT phase diagrams of ChCl:EG system at four molar ratios bringing another way to look at these discussions. One can notice that the pressure influences the melting temperature of the ESs in all molar ratios, since the increase in pressure causes an increase in the melting temperature, as previously explained. In Figure 25, the solid region is on the left side of the coexistence line and the liquid region, consequently, is on the right side. It may be noted that the coexistence line of solid and liquid phases moves toward the solid region as the amount of ethylene glycol rises in the mixture, gradually increasing the liquid phase region in the phase diagram. This behavior was observed in all polyalcohol-based and ChCl:LAT AC ESs studied and can be seen in Figures S1, S2, and S4 of Supporting Information. However, it is not observed for ChCl:MAL AC (Figure 26) and ChCl:GLY AC (Figure S3), the coexistence line moves in the direction of the liquid region as the quantity of malonic and glycolic acids increase in the mixture, gradually expanding the solid phase region of the phase diagram.

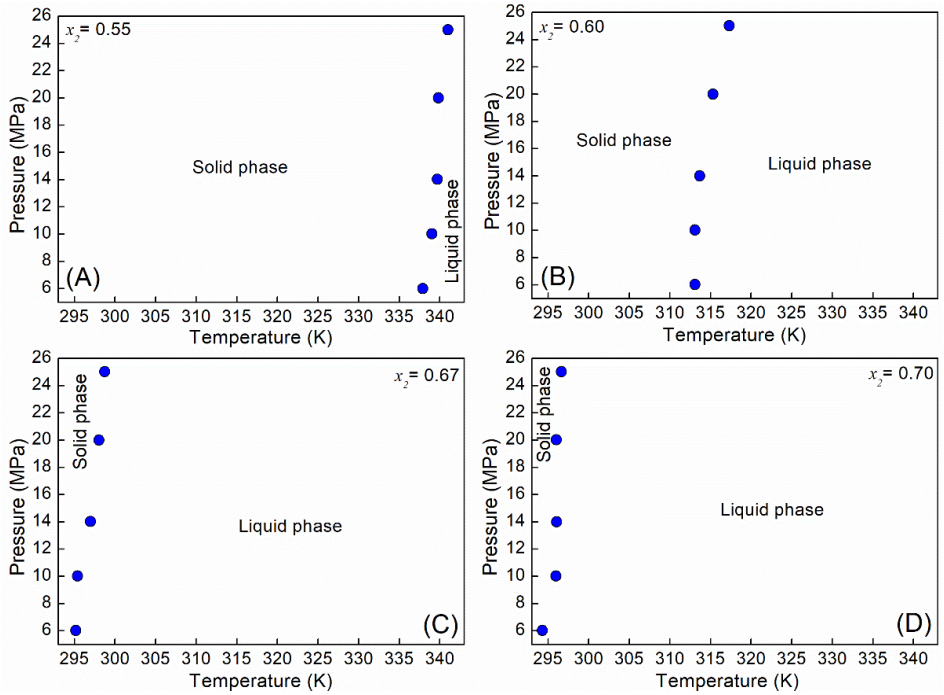

Figure 25. Phase diagrams P×T of the ES composed of ChCl (1) and ethylene glycol (2) at four molar ratios and five pressures.

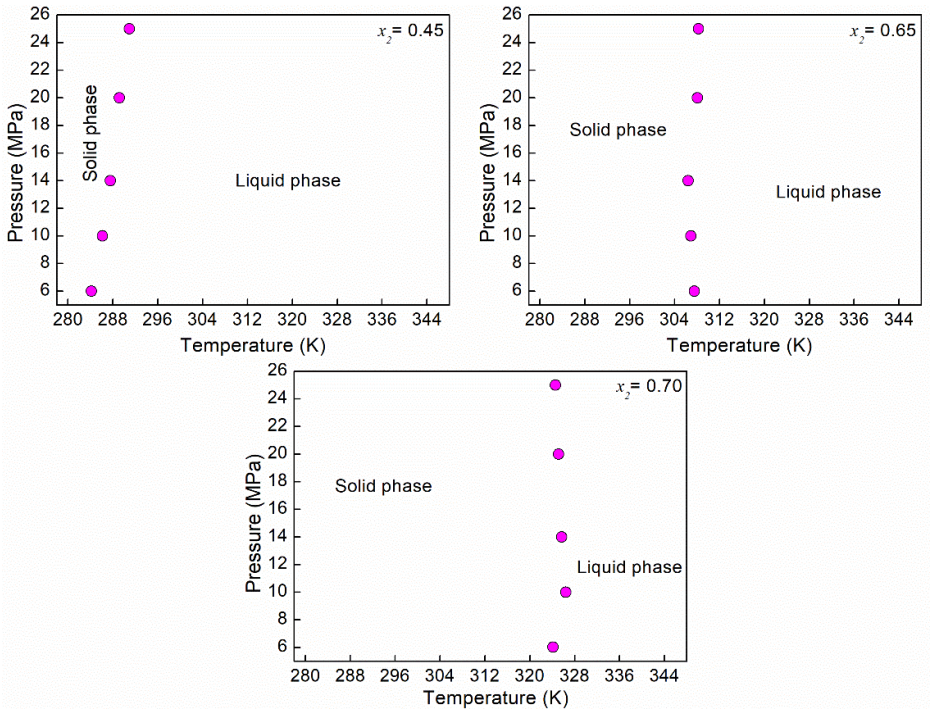

Figure 26. Phase diagrams P×T of the ES composed of ChCl (1) and malonic acid (2) at three molar ratios and five pressures.

4.2. Density of ESs at high pressure

The density of four ChCl-based ESs (ChCl combined with ethylene glycol, glycerol, 1,3 propanediol, and glycolic acid at 1:2, 1:1.5, 1:2.3 and 1:1.2 molar ratios, respectively) at a pressure ranging from 1 to 50 MPa and temperature ranging from 293.15 to 353.15 K were measured.

Figure 27 presents a comparison between the high-pressure data for ChCl:EG at pressures up to 50 MPa reported in this work with those reported by Crespo et al. (2019) [1] over a wide temperature and pressure range (283 – 363 K and 0.1 – 95 MPa). Another set of experimental data was reported by Leron et al. (2012) [70] at pressures up to 50 MPa but in a limited temperature range (298 – 323 K) hindering the comparison.

The comparison results show that the measured data in this study are in good agreement with those found in the literature as well as the percentage average deviations (calculated according to Equation 13) which are in the range of -0.3 to -0.6% (Figure 27(A)) and the density differences are no higher than -0.007 g.cm^{-3} (Figure 27 (B)).

$$\%ARD(\rho) = 100 \cdot \frac{\rho^{exp} - \rho^{lit}}{\rho^{exp}} \quad (13)$$

All data in this work present density values lower than those determined in the literature. These negative small differences can be associated with the higher water content of the ES in this study and minor discrepancies in the molar ratio of the mixtures. The deviations increase with the temperature increase in the order 293.15 < 313.15 < 333.15 < 353.15 K.

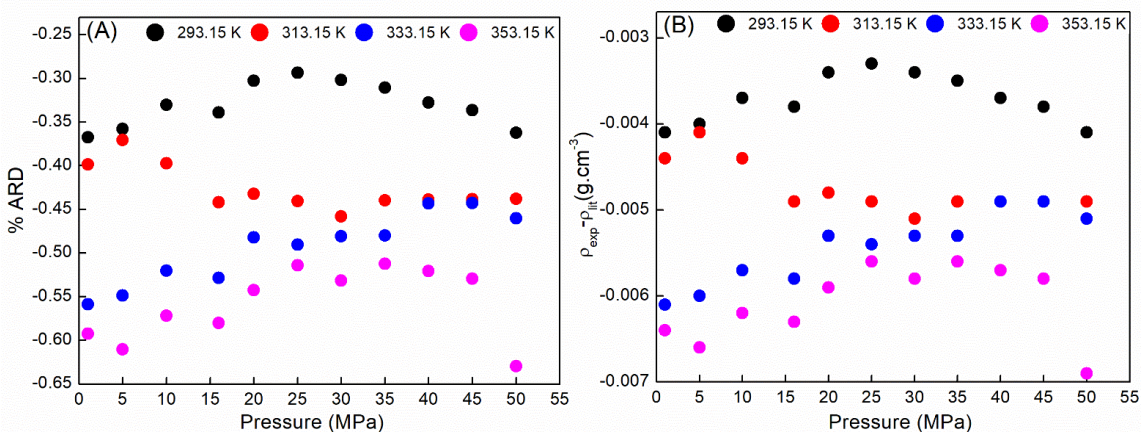

Figure 27. Comparison between density data for ChCl:EG at pressures up to 50 MPa measured in this work and those values reported in the literature [1] in four temperatures concerning (A) percentage average relative deviation (%ARD) and (B) density differences.

The densities measured in this work for ChCl-based ESs along with the CPA modeling and the modified Tammann-Tait fitting are sketched in Figure 28. All the density values are summarized in Tables S7 – S10 in Supporting Information.

According to Figure 28, density decreases with the temperature raise at a constant pressure, which is caused by the liquid thermal expansion [70]. Whereas, at a constant temperature, density tends to slightly increase with pressure raise due to compression [67]. The density almost did not change with pressure since ESs are considered practically incompressible liquids [67]. At the pressures (1 to 50 MPa) and temperature range (293.15 to 353.15 K) considered in this work, the temperature has a prominent impact on density than pressure, a behavior also found in the literature [1,66–68,70].

Concerning the HBDs influence on density values, it is observed an increase in ESs density in the following order: glycolic acid > glycerol > ethylene glycol > 1,3 propanediol. The explanation for this result can be related to the excess molar volume of the mixtures which is an additive property. The excess molar volume of binary

mixtures is known as a complex property due to its dependency on size, shape, chemical nature of the pure components, interactions between the solutes, and/or the solvents, and/or the solute-solvent, and structural effects [99].

As ChCl is the HBA for all ESs, the major influence on the excess molar volume is generated by the HBDs. ChCl presents a density of 1.1008 $g.cm^{-3}$ at 293.15 K and atmospheric pressure considering its densities of aqueous solutions measured by Francisco et al. (2013) [100]. At these conditions, the estimated excess molar volumes of the ESs are –4.03 $cm^3.mol^{-1}$ for ChCl:GLY AC, –1.70 $cm^3.mol^{-1}$ for ChCl:GLY, –0.96 $cm^3.mol^{-1}$ for ChCl:EG and –0.57 $cm^3.mol^{-1}$ for ChCl:PD. Therefore, the high negative excess molar volume values for ChCl:GLY AC indicate stronger and more favorable interactions than the other studied ESs, including ChCl:EG. Besides, the enthalpic effect in ChCl:GLY AC and ChCl:GLY agrees with the significative negative deviations from the ideal behavior observed by Crespo et al. (2018) [38] and Silva et al. (2020) [17] where the SLE phase diagrams were measured, since the interactions between HBA and HBD are stronger, decreasing the free volume, i.e., promoting an increase in density.

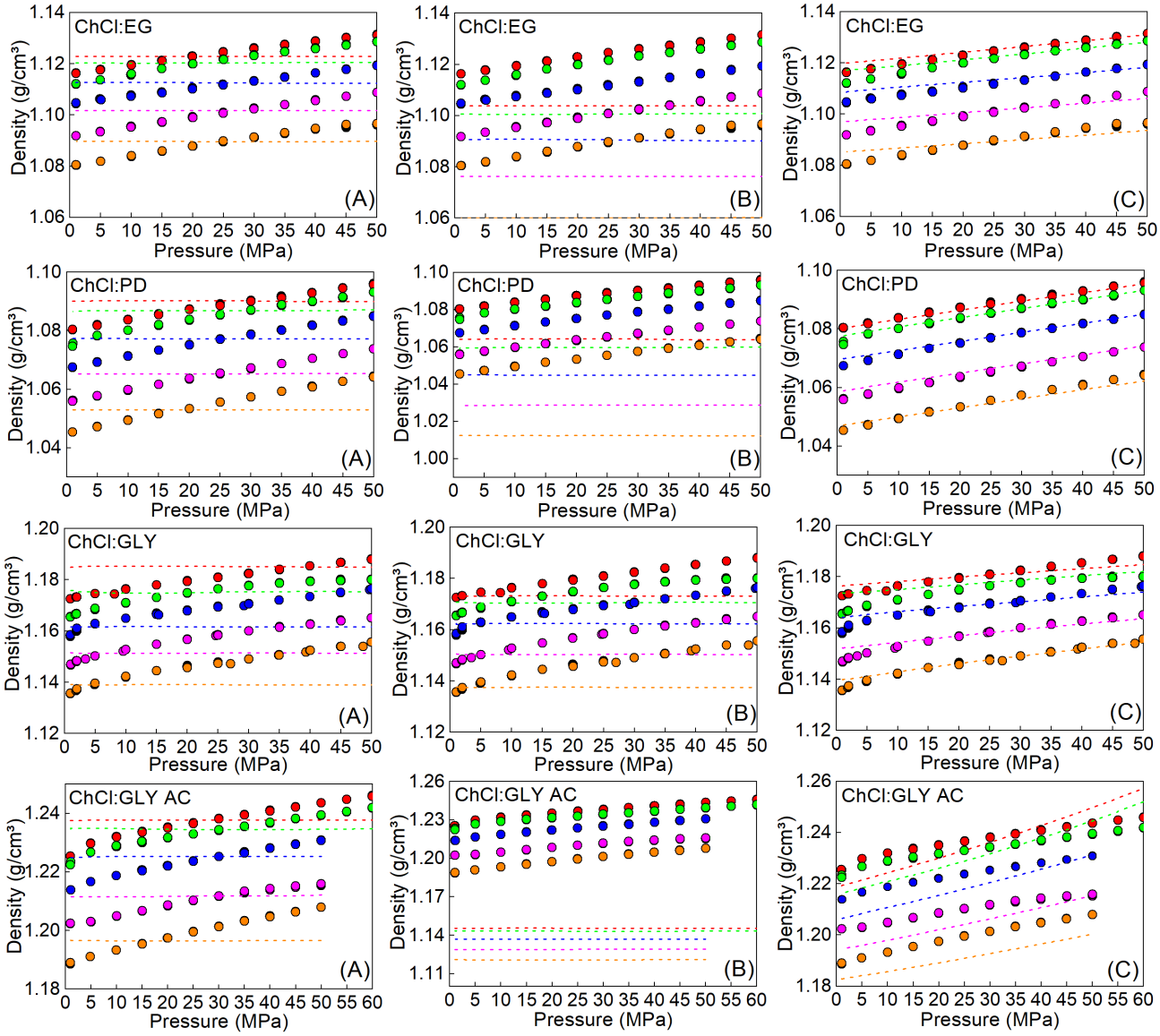

Figure 28. Densities measured at high pressures for ChCl-based ESs at (●) 293.15 K; (●) 298.15 K; (●) 313.15 K; (●) 333.15 K; (●) 353.15 K Symbols represent the experimental data and dashed lines represent (A) CPA correlation using a temperature-dependent binary interaction parameter; (B) CPA predictions using $k_{ij} = 0$; (C) modified Tammann-Tait fitting.

To correlate the experimental data was used the modified Tammann-Tait equation and the CPA EoS. The coefficients a_0, a_1, and a_2 of the Tammann-Tait equation (Equation 3) are shown in Table 56 and the coefficients b_0, b_1 and C of Equation 4 are shown in Table 57 with the respective average absolute deviation

(AAD%). It is possible to observe in Figure 29, that the values of the parameter B(T) decrease with temperature raise as reported for previous liquid systems [68,70,81,101]. In Figure 28 (C) and Table 57, it can be noted that the Tammann-Tait equation provided a good correlation with the densities as functions of temperature and pressure, with AADs% smaller than 0.45%. Despite the low AAD% values in this work, the literature has shown better correlations of the equation, with lower AAD%[66–68,70].

Table 56. Modified Tammann-Tait coefficients a_0, a_1, and a_2 of Equation 3.

ES	a_0 (kg.m^{-3})	a_1 (kg.m^{-3}K^{-1})	a_2 ($\times 10^4$ kg.m^{-3}K^{-2})
ChCl:EG	1253.035	-0.35494	-3.4083
ChCl:PD	1150.247	0.02403	-8.9701
ChCl:GLY	1338.205	-0.50538	-1.7771
ChCl:GLY AC	1438.761	-0.86898	4.0594

Table 57. Modified Tammann-Tait coefficients b_0, b_1, and C of Equation 4.

ES	b_0	b_1 (MPa)	C	AAD%[a]
ChCl:EG	399.98	-4.8243	-0.19623	0.159
ChCl:PD	741.34	-0.2104	0.20016	0.083
ChCl:GLY	750.15	-1.8100	0.03502	0.191
ChCl:AGLY AC	380.03	-2.0597	-0.08903	0.441

[a] $\text{AAD\%} = 100 \times \frac{1}{N_p} \sum_i^{N_p} \frac{|\rho_{i,exp} - \rho_{i,cal}|}{\rho_{i,exp}}$

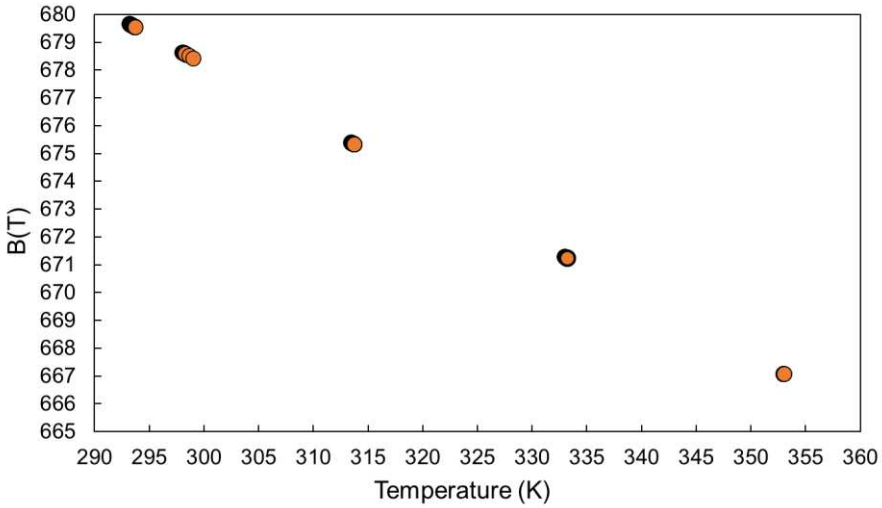

Figure 29. B(T) parameter behavior of Tammann-Tait equation with the temperature for ChCl (1):PD (2).

To describe the density experimental data by CPA EoS two steps are necessary. The first one consists of the optimization of the CPA parameters of each HBA and HBDs by density experimental data in a given temperature and density range (Table S11 of Supporting Information). The CPA parameters for some HBDs (ethylene glycol and glycerol) were not adjusted since Multiflash software already had such parameters in its database.

Table 58 shows the CPA-adjusted parameters and the deviations for ChCl, 1,3 propanediol, and glycolic acid calculated according to the Section 3.3 using density experimental data, and for ethylene glycol and glycerol obtained from the Multiflash database. One can see that CPA EoS predicts well the density of these components with deviations not higher than 0.03%. It is worth noting that ethylene glycol and glycerol do not present the deviations because Multiflash does not provide this information.

Table 58. Optimized CPA parameters for each ES component.

Component	a_0 (J.m³.mol^{-2})	b (m³.mol^{-1})	C_1	ε (J.mol^{-1})	β	AARD% in ρ
ChCl	4.252	1.564 E-04	1.576	5.267 E+04	5.903 E-05	0.005
EG				1.793 E+04	0.051	NA[a]
PD	2.074	8.131 E-05	1.876	3.255 E+04	2.87 E-03	0.010
GLY				2.135 E+04	0.054	NA[a]
GLY AC	1.995	7.206 E-05	1.844	5.525 E+04	4.139 E-05	0.031

[a] Not applicable. The CPA parameters of both components come from the Multiflash database and no AARD% were given.

The second step consists of ESs densities calculation at high pressures. As the density of the system components is one of the required properties of the model parametrization, it is supposed that the mixture density will be accurately described by the model with no binary interaction parameter (k_{ij}) [1].

Table **59** presents the density deviations for the studied ESs without any k_{ij}, and it is observed that CPA cannot describe densities at high pressure precisely, with deviations higher than 7% for ChCl:GLY AC. Figure 28 (B) shows more clearly the high deviations and demonstrates that the modified Tammann-Tait equation shows better results (Figure 28 (C)).

Due to the large deviation presented by CPA EoS without any k_{ij}, a linear trend of k_{ij} with the temperature (Equation 14) fitted to experimental data to enhance the CPA prediction and to take into account the temperature effect on experimental density.

Table **59** provides the constant values of Equation 14 and the deviations considering $k_{ij} \neq 0$, and Figure 28 (A) illustrates the results of the correlation. One can notice that the deviations are smaller, with values no greater than 0.50%, making the

CPA EoS a reasonable model to be used for density prediction at high pressures. Nevertheless, the experimental data slope and range differ from the ones provided by the CPA EoS since the analytic EoSs cannot describe the density temperature dependence. In comparison with the modified Tammann-Tait equation, even with $k_{ij} \neq 0$ adjustment, CPA presented higher deviations, an expected result due to the predictive nature of the modified Tammann-Tait equation and a smaller number of used parameters [101].

$$k_{ij} = a_0 + a_1 T \quad (14)$$

k_{ij} is the binary interaction parameter, a_0 and a_1 are the constants and T is the temperature in Kelvin.

Table 59. Constant values used to determine the binary interaction parameter ($\boldsymbol{k_{ij} \neq 0}$) and a comparison between AARD% in the ESs studied in this work with or without $\boldsymbol{k_{ij}}$.

Eutectic Solvent	$\boldsymbol{k_{ij} = a_0 + a_1 T(K)}$			$\boldsymbol{k_{ij} = 0}$
	$\boldsymbol{a_0}$	$\boldsymbol{a_1}$	**AARD%**	**AARD%**
ChCl:EG	-1.402	0.0014	0.365	2.132
ChCl:PD	0.262	-0.0017	0.450	2.937
ChCl:GLY	-5.073	0.0168	0.495	0.603
ChCl:GLY AC	-2.839	0.0060	0.385	7.134

5. Conclusions

In this work, the solid-liquid equilibrium phase diagrams of six ESs (ChCl:EG, ChCl:PD, ChCl:GLY, ChCl: GLY AC, ChCl: LAT AC, and ChCl:MAL AC) and the densities of four ESs at high pressures (ChCl:EG, ChCl:PD, ChCl:GLY and ChCl: GLY AC) were measured in a wide temperature and pressure ranges to enhance the

literature on the thermophysical properties of ESs. In particular, the solid-liquid equilibrium at high pressures was reported in this work for the first time.

All systems presented the same behavior of atmospheric pressure concerning the trend of the phase diagrams, i.e., a single eutectic point, with the eutectic composition not changing with pressure increase. The melting temperature increase is relatively small between the pressures 6 – 25 MPa but large between 0.1 – 6 MPa because the pressure raise led the mixtures to states of smaller volume, thus the energy for the phase transition is higher as well as the melting temperature. Besides, the water content of ESs studied in this work is higher than that at atmospheric pressure, which can influence the results by reducing the inter- and intramolecular interactions. Nevertheless, it cannot be measured the proportion in which each factor influences the liquidus line shift of the phase diagrams concerning the temperature axis.

Regarding densities at high pressure, it was possible to note that the data measured in this study agree with those from the literature for ChCl:EG. As expected, density decreases with temperature raise and increases with pressure raise. However, the influence of temperature on density is higher than pressure. The excess molar volume was measured for all ESs and shows that the high negative values for ChCl:GLY AC represents stronger and more favorable interactions.

Moreover, the modified Tammann-Tait equation and CPA EoS were used to correlate the experimental data. The first one provided a good correlation with density presenting AADs% smaller than 0.45%. CPA EoS was used considering the ESs as an individual component and showed deviations no higher than 0.50%. In comparison,

the modified Tammann-Tait presented better predictions, as expected, since the modified Tammann-Tait has a predictive nature and a smaller number of parameters.

Acknowledgments

The authors would like to thank the São Paulo Research Foundation (FAPESP – 2018/19198-9 and 2014/21252-0), Coordination for the Improvement of Higher Education Personnel - Brasil (CAPES) – Finance Code 001, the National Council for Scientific and Technological Development (CNPq – 306666/2020-0), and the Fund for the Support of Education, Research, and Extension (FAEPEX/ UNICAMP) for the financial support. The authors also thank the Human Resources Program of the National Agency of Petroleum, Natural Gas and Biofuels (PRH-ANP); KBC Process Technology Limited for the authorized use of Multiflash software; and the Espaço da Escrita – Pró-Reitoria de Pesquisa - UNICAMP – for the language services provided.

References

[1] E.A. Crespo, J.M.L. Costa, A.M. Palma, B. Soares, M.C. Martín, J.J. Segovia, P.J. Carvalho, J.A.P. Coutinho, Thermodynamic characterization of deep eutectic solvents at high pressures, Fluid Phase Equilib. 500 (2019) 1–13. https://doi.org/10.1016/j.fluid.2019.112249.

[2] J. Liu, X. Li, K. Ho Row, Development of deep eutectic solvents for sustainable chemistry, Journal of Molecular Liquids. 362 (2022) 119654. https://doi.org/10.1016/j.molliq.2022.119654.

[3] C.J. Clarke, W.C. Tu, O. Levers, A. Bröhl, J.P. Hallett, Green and Sustainable Solvents in Chemical Processes, Chemical Reviews. 118 (2018) 747–800. https://doi.org/10.1021/acs.chemrev.7b00571.

[4] The 2030 Agenda for sustainable development, 2016. https://doi.org/10.1201/b20466-7.

[5] B. Hashemi, F. Shiri, F. Svec, L. Nováková, Green solvents and approaches recently applied for extraction of natural bioactive compounds, Trends in Analytical Chemistry. 157 (2022) 1–10. https://doi.org/10.1016/j.trac.2022.116732.

[6] E.L. Smith, A.P. Abbott, K.S. Ryder, Deep Eutectic Solvents (DESs) and Their Applications, Chem Rev. 114 (2014) 11060–11082. https://doi.org/10.1021/cr300162p.

[7] M.A.R. Martins, S.P. Pinho, J.A.P. Coutinho, Insights into the Nature of Eutectic and Deep Eutectic Mixtures, J Solution Chem. (2018) 1–3. https://doi.org/10.1007/s10953-018-0793-1.

[8] H. Srinivasan, P.S. Dubey, V.K. Sharma, R. Biswas, S. Mitra, R. Mukhopadhyay, Molecular dynamics of acetamide based ionic deep eutectic solvents, in: AIP Conf. Proc. 1942, 2018: p. 110032. https://doi.org/10.1063/1.5029015.

[9] L.P. Silva, L. Fernandez, J.H.F. Conceição, M.A.R. Martins, A. Sosa, J. Ortega, S.P. Pinho, J.A.P. Coutinho, Design and Characterization of Sugar-Based Deep Eutectic Solvents Using Conductor-like Screening Model for Real Solvents, ACS Sustainable Chemistry & Engineering. 6 (2018) 10724–10734. https://doi.org/10.1021/acssuschemeng.8b02042.

[10] Z. Maugeri, P. Domínguez de María, Novel choline-chloride-based deep-eutectic-solvents with renewable hydrogen bond donors: levulinic acid and sugar-based polyols, RSC Adv. 2 (2012) 421–425. https://doi.org/10.1039/C1RA00630D.

[11] K. Shahbaz, F.S. Mjalli, M.A. Hashim, I.M. AlNashef, Prediction of deep eutectic solvents densities at different temperatures, Thermochimica Acta. 515 (2011) 67–72. https://doi.org/10.1016/j.tca.2010.12.022.

[12] K. Shahbaz, Farouq.S. Mjalli, M.A. Hashim, Inas.M. ALNashef, Using Deep Eutectic Solvents for the Removal of Glycerol from Palm Oil-Based Biodiesel, Journal of Applied Sciences. 10 (2010) 3349–3354. https://doi.org/10.3923/jas.2010.3349.3354.

[13] C. Florindo, F.S. Oliveira, L.P.N. Rebelo, A.M. Fernandes, I.M. Marrucho, Insights into the Synthesis and Properties of Deep Eutectic Solvents Based on Cholinium Chloride and Carboxylic Acids, ACS Sustainable Chemistry & Engineering. 2 (2014) 2416–2425. https://doi.org/10.1021/sc500439w.

[14] P.V.A. Pontes, E.A. Crespo, M.A.R. Martins, L.P. Silva, C.M.S.S. Neves, G.J. Maximo, M.D. Hubinger, E.A.C. Batista, S.P. Pinho, J.A.P. Coutinho, G. Sadowski, C. Held, Measurement and PC-SAFT modeling of solid-liquid equilibrium of deep eutectic solvents of quaternary ammonium chlorides and carboxylic acids, Fluid Phase Equilib. 448 (2017) 69–80. https://doi.org/10.1016/j.fluid.2017.04.007.

[15] A.P. Abbott, D. Boothby, G. Capper, D.L. Davies, R.K. Rasheed, Deep Eutectic Solvents formed between choline chloride and carboxylic acids: Versatile alternatives to ionic liquids, Journal of the American Chemical Society. 126 (2004) 9142–9147. https://doi.org/10.1021/ja048266j.

[16] M. Faggian, S. Sut, B. Perissutti, V. Baldan, I. Grabnar, S. Dall'Acqua, Natural Deep Eutectic Solvents (NADES) as a Tool for Bioavailability Improvement: Pharmacokinetics of Rutin Dissolved in Proline/Glycine after Oral Administration in Rats: Possible Application in Nutraceuticals, Molecules. 21 (2016) 1531. https://doi.org/10.3390/molecules21111531.

[17] L.P. Silva, M.A.R. Martins, J.H.F. Conceição, S.P. Pinho, J.A.P. Coutinho, Eutectic Mixtures Based on Polyalcohols as Sustainable Solvents: Screening and Characterization, ACS Sustain Chem Eng. 8 (2020) 15317–15326. https://doi.org/10.1021/acssuschemeng.0c05518.

[18] B. Li, Q. Li, Q. Wang, X. Yan, M. Shi, C. Wu, Deep eutectic solvent for spent lithium-ion battery recycling: comparison with inorganic acid leaching, Physical Chemistry Chemical Physics. 24 (2022) 19029–19051. https://doi.org/10.1039/D1CP05968H.

[19] B. Lu, R. Du, G. Wang, Y. Wang, S. Dong, D. Zhou, S. Wang, C. Li, High-efficiency leaching of valuable metals from waste Li-ion batteries using deep eutectic solvents, Environmental Research. 212 (2022) 113286. https://doi.org/10.1016/j.envres.2022.113286.

[20] L. V. Yelash, T. Kraska, Closed-Loops of liquid-liquid immiscibility in binary mixtures of equal sized molecules predicted with a simple theoretical equation of state, Berichte Der Bunsengesellschaft Für Physikalische Chemie. 102 (1998) 213–223. https://doi.org/10.1002/bbpc.19981020212.

[21] M. Wang, C. Li, M. Zhou, Z. Xia, Y. Huang, Natural deep eutectic solvent assisted synthesis and applications of chiral carbon dots, Green Chemistry. (2022). https://doi.org/10.1039/D2GC01949C.

[22] N. Xia, L. Xiong, S. Bi, F. Qian, P. Wang, Development of biocompatible DES/NADES as co-solvents for efficient biosynthesis of chiral alcohols, Bioprocess and Biosystems Engineering. 43 (2020) 1987–1997. https://doi.org/10.1007/s00449-020-02387-5.

[23] B. Ahmed, Q. Wu, J.G. et Al., Degumming of Hemp Fibers Using Combined Microwave Energy and Deep Eutectic Solvent Treatment, Research Square. (2022) 1–25. https://doi.org/https://doi.org/10.21203/rs.3.rs-1094469/v1.

[24] H. Huang, Q. Tang, G. Lin, Y. Liu, J. Yu, B. Ding, Z. Li, Anthraquinone-assisted deep eutectic solvent degumming of ramie fibers: Evaluation of fiber properties and degumming performance, Industrial Crops and Products. 185 (2022) 115115. https://doi.org/10.1016/j.indcrop.2022.115115.

[25] H. Huang, Q. Tang, G. Lin, C. Yu, H. Wang, Z. Li, High-efficiency and recyclable ramie cellulose fiber degumming enabled by deep eutectic solvent, Industrial Crops and Products. 171 (2021) 113879. https://doi.org/10.1016/j.indcrop.2021.113879.

[26] A. Al-Bodour, N. Alomari, A. Gutiérrez, S. Aparicio, M. Atilhan, High-pressure carbon dioxide solubility in terpene based deep eutectic solvents, Journal of Environmental Chemical Engineering. 10 (2022) 108237. https://doi.org/10.1016/j.jece.2022.108237.

[27] K. Kumar, S. Keshri, A. Bharti, S. Kumar, S. Mogurampelly, Solubility of Gases in Choline Chloride-Based Deep Eutectic Solvents from Molecular Dynamics Simulation, Ind Eng Chem Res. 61 (2022) 4659–4671. https://doi.org/10.1021/acs.iecr.1c04923.

[28] M. Xu, H. Dou, F. Peng, N. Yang, X. Xiao, X. Tantai, Y. Sun, B. Jiang, L. Zhang, Ultra-stable copper decorated deep eutectic solvent based supported liquid membranes for olefin/paraffin separation: In-depth study of carrier stability, Journal of Membrane Science. 659 (2022) 120775. https://doi.org/10.1016/j.memsci.2022.120775.

[29] G. Moradi, M. Rahimi, S. Zinadini, M. Shamsipur, N. Babajani, Natural deep eutectic solvent modified nanofiltration membranes with superior antifouling properties for pharmaceutical wastewater treatment, Chemical Engineering Journal. 448 (2022) 137704. https://doi.org/10.1016/j.cej.2022.137704.

[30] P. Zhang, W. Xiong, M. Shi, Z. Tu, X. Hu, X. Zhang, Y. Wu, Natural deep eutectic solvent-based gels with multi-site interaction mechanism for selective membrane separation of SO2 from N2 and CO2, Chemical Engineering Journal. 438 (2022) 135626. https://doi.org/10.1016/j.cej.2022.135626.

[31] H. Yu, Z. Xue, R. Shi, F. Zhou, T. Mu, Lignin dissolution and lignocellulose pretreatment by carboxylic acid based deep eutectic solvents, Industrial Crops and Products. 184 (2022) 115049. https://doi.org/10.1016/j.indcrop.2022.115049.

[32] F.H.B. Sosa, D.O. Abranches, A.M. da Costa Lopes, J.A.P. Coutinho, M.C. da Costa, Kraft Lignin Solubility and Its Chemical Modification in Deep Eutectic Solvents, ACS Sustainable Chemistry & Engineering. 8 (2020) 18577–18589. https://doi.org/10.1021/acssuschemeng.0c06655.

[33] S. Deniz, A.E. Ünlü, S. Takaç, Ultrasound-assisted natural deep eutectic solvent extraction of phenolic compounds from apple pomace, Separation Science and Technology. (2022) 1–12. https://doi.org/10.1080/01496395.2022.2112603.

[34] H. Suo, Z. Peng, Z. Guo, C. Wu, J. Liu, L. Wang, J. Xiao, X. Li, Deep eutectic solvent-based ultrasonic-assisted extraction of phenolic compounds from different

potato genotypes: Comparison of free and bound phenolic profiles and antioxidant activity, Food Chemistry. 388 (2022) 133058. https://doi.org/10.1016/j.foodchem.2022.133058.

[35] Q. Yu, F. Wang, Y. Jian, V.M. Chernyshev, Y. Zhang, Z. Wang, Z. Yuan, X. Chen, Extraction of flavonoids from Glycyrrhiza residues using deep eutectic solvents and its molecular mechanism, Journal of Molecular Liquids. 363 (2022) 119848. https://doi.org/10.1016/j.molliq.2022.119848.

[36] O. Zannou, H. Pashazadeh, C.M. Galanakis, A.S. Alamri, I. Koca, Carboxylic acid-based deep eutectic solvents combined with innovative extraction techniques for greener extraction of phenolic compounds from sumac (Rhus coriaria L.), Journal of Applied Research on Medicinal and Aromatic Plants. 30 (2022) 100380. https://doi.org/10.1016/j.jarmap.2022.100380.

[37] R.M. Dias, M.C. da Costa, Y.P. Jimenez, Perspectives of Using DES-Based Systems for Solid–Liquid and Liquid–Liquid Extraction of Metals from E-Waste, Minerals. 12 (2022) 1–20. https://doi.org/10.3390/min12060710.

[38] E.A. Crespo, L.P. Silva, M.A.R. Martins, M. Bülow, O. Ferreira, G. Sadowski, C. Held, S.P. Pinho, J.A.P. Coutinho, The Role of Polyfunctionality in the Formation of [Ch]Cl-Carboxylic Acid-Based Deep Eutectic Solvents, Ind Eng Chem Res. 57 (2018) 11195–11209. https://doi.org/10.1021/acs.iecr.8b01249.

[39] E.A. Crespo, L.P. Silva, M.A.R. Martins, L. Fernandez, J. Ortega, O. Ferreira, G. Sadowski, C. Held, S.P. Pinho, J.A.P. Coutinho, Characterization and Modeling of the Liquid Phase of Deep Eutectic Solvents Based on Fatty Acids/Alcohols and Choline Chloride, Ind Eng Chem Res. 56 (2017) 12192–12202. https://doi.org/10.1021/acs.iecr.7b02382.

[40] L.P. Silva, M.A.R. Martins, D.O. Abranches, S.P. Pinho, J.A.P. Coutinho, Solid-liquid phase behavior of eutectic solvents containing sugar alcohols, Journal of Molecular Liquids. 337 (2021) 116392. https://doi.org/10.1016/j.molliq.2021.116392.

[41] L. Fernandez, L.P. Silva, M.A.R. Martins, O. Ferreira, J. Ortega, S.P. Pinho, J.A.P. Coutinho, Indirect assessment of the fusion properties of choline chloride from solid-liquid equilibria data, Fluid Phase Equilibria. 448 (2017) 9–14. https://doi.org/10.1016/j.fluid.2017.03.015.

[42] D.O. Abranches, L.P. Silva, M.A.R. Martins, L. Fernandez, S.P. Pinho, J.A.P. Coutinho, Can cholinium chloride form eutectic solvents with organic chloride-based salts?, Fluid Phase Equilibria. 493 (2019) 120–126. https://doi.org/10.1016/j.fluid.2019.04.019.

[43] D.O. Abranches, L.P. Silva, M.A.R. Martins, S.P. Pinho, J.A.P. Coutinho, Understanding the Formation of Deep Eutectic Solvents: Betaine as a Universal Hydrogen Bond Acceptor, ChemSusChem. 13 (2020) 4916–4921. https://doi.org/10.1002/cssc.202001331.

[44] F.S. Mjalli, G. Murshid, S. Al-Zakwani, A. Hayyan, Monoethanolamine-based deep eutectic solvents, their synthesis and characterization, Fluid Phase Equilibria. 448 (2017) 30–40. https://doi.org/10.1016/j.fluid.2017.03.008.

[45] M. Hayyan, T. Aissaoui, M.A. Hashim, M.A. AlSaadi, A. Hayyan, Triethylene glycol based deep eutectic solvents and their physical properties, Journal of the Taiwan Institute of Chemical Engineers. 50 (2015) 24–30. https://doi.org/10.1016/j.jtice.2015.03.001.

[46] M.A. Sedghamiz, S. Raeissi, Physical properties of deep eutectic solvents formed by the sodium halide salts and ethylene glycol, and their mixtures with water,

Journal of Molecular Liquids. 269 (2018) 694–702. https://doi.org/10.1016/j.molliq.2018.08.045.

[47] R.K. Ibrahim, M. Hayyan, M.A. AlSaadi, S. Ibrahim, A. Hayyan, M.A. Hashim, Physical properties of ethylene glycol-based deep eutectic solvents, Journal of Molecular Liquids. 276 (2019) 794–800. https://doi.org/10.1016/j.molliq.2018.12.032.

[48] A. Yadav, S. Trivedi, R. Rai, S. Pandey, Densities and dynamic viscosities of (choline chloride+glycerol) deep eutectic solvent and its aqueous mixtures in the temperature range (283.15-363.15)K, Fluid Phase Equilibria. 367 (2014) 135–142. https://doi.org/10.1016/j.fluid.2014.01.028.

[49] A. Yadav, S. Pandey, Densities and viscosities of (choline chloride + urea) deep eutectic solvent and its aqueous mixtures in the temperature range 293.15 K to 363.15 K, Journal of Chemical and Engineering Data. 59 (2014) 2221–2229. https://doi.org/10.1021/je5001796.

[50] M.K. Alomar, M. Hayyan, M.A. Alsaadi, S. Akib, A. Hayyan, M.A. Hashim, Glycerol-based deep eutectic solvents: Physical properties, Journal of Molecular Liquids. 215 (2016) 98–103. https://doi.org/10.1016/j.molliq.2015.11.032.

[51] A. Hayyan, F.S. Mjalli, I.M. AlNashef, Y.M. Al-Wahaibi, T. Al-Wahaibi, M.A. Hashim, Glucose-based deep eutectic solvents: Physical properties, Journal of Molecular Liquids. 178 (2013) 137–141. https://doi.org/10.1016/j.molliq.2012.11.025.

[52] S. Benabid, Y. Benguerba, I.M. AlNashef, N. Haddaoui, Theoretical study of physicochemical properties of selected ammonium salt-based deep eutectic solvents, Journal of Molecular Liquids. 285 (2019) 38–46. https://doi.org/10.1016/j.molliq.2019.04.052.

[53] M.B. Taysun, E. Sert, F.S. Atalay, Physical properties of benzyl tri-methyl ammonium chloride based deep eutectic solvents and employment as catalyst, Journal

of Molecular Liquids. 223 (2016) 845–852. https://doi.org/10.1016/j.molliq.2016.07.148.

[54] K.R. Siongco, R.B. Leron, M.-H. Li, Densities, refractive indices, and viscosities of N,N-diethylethanol ammonium chloride–glycerol or –ethylene glycol deep eutectic solvents and their aqueous solutions, The Journal of Chemical Thermodynamics. 65 (2013) 65–72. https://doi.org/10.1016/j.jct.2013.05.041.

[55] S.P. Ijardar, Deep eutectic solvents composed of tetrabutylammonium bromide and PEG: Density, speed of sound and viscosity as a function of temperature, The Journal of Chemical Thermodynamics. 140 (2020) 105897. https://doi.org/10.1016/j.jct.2019.105897.

[56] N.F. Gajardo-Parra, M.J. Lubben, J.M. Winnert, Á. Leiva, J.F. Brennecke, R.I. Canales, Physicochemical properties of choline chloride-based deep eutectic solvents and excess properties of their pseudo-binary mixtures with 1-butanol, The Journal of Chemical Thermodynamics. 133 (2019) 272–284. https://doi.org/10.1016/j.jct.2019.02.010.

[57] R. Yusof, E. Abdulmalek, K. Sirat, M. Rahman, Tetrabutylammonium Bromide (TBABr)-Based Deep Eutectic Solvents (DESs) and Their Physical Properties, Molecules. 19 (2014) 8011–8026. https://doi.org/10.3390/molecules19068011.

[58] B. Nowosielski, M. Jamrógiewicz, J. Łuczak, M. Śmiechowski, D. Warmińska, Experimental and predicted physicochemical properties of monopropanolamine-based deep eutectic solvents, Journal of Molecular Liquids. 309 (2020) 113110. https://doi.org/10.1016/j.molliq.2020.113110.

[59] J.G. Lynam, N. Kumar, M.J. Wong, Deep eutectic solvents' ability to solubilize lignin, cellulose, and hemicellulose; thermal stability; and density, Bioresource Technology. 238 (2017) 684–689. https://doi.org/10.1016/j.biortech.2017.04.079.

[60] H.-Zhen. SU, J.-Mei. YIN, Q.-Shan. LIU, C.-Ping. LI, Properties of Four Deep Eutectic Solvents: Density, Electrical Conductivity, Dynamic Viscosity and Refractive Index, Acta Physico-Chimica Sinica. 31 (2015) 1468–1473. https://doi.org/10.3866/PKU.WHXB201506111.

[61] R.B. Leron, A.N. Soriano, M.H. Li, Densities and refractive indices of the deep eutectic solvents (choline chloride+ethylene glycol or glycerol) and their aqueous mixtures at the temperature ranging from 298.15 to 333.15K, Journal of the Taiwan Institute of Chemical Engineers. 43 (2012) 551–557. https://doi.org/10.1016/j.jtice.2012.01.007.

[62] W. Guo, Y. Hou, S. Ren, S. Tian, W. Wu, Formation of deep eutectic solvents by phenols and choline chloride and their physical properties, Journal of Chemical and Engineering Data. 58 (2013) 866–872. https://doi.org/10.1021/je300997v.

[63] J. Wang, H. Cheng, Z. Song, L. Chen, L. Deng, Z. Qi, Carbon Dioxide Solubility in Phosphonium-Based Deep Eutectic Solvents: An Experimental and Molecular Dynamics Study, Industrial and Engineering Chemistry Research. 58 (2019) 17514–17523. https://doi.org/10.1021/acs.iecr.9b03740.

[64] D. Deng, Y. Jiang, X. Liu, Z. Zhang, N. Ai, Investigation of solubilities of carbon dioxide in five levulinic acid-based deep eutectic solvents and their thermodynamic properties, Journal of Chemical Thermodynamics. 103 (2016) 212–217. https://doi.org/10.1016/j.jct.2016.08.015.

[65] R.B. Leron, M.H. Li, High-pressure volumetric properties of choline chloride-ethylene glycol based deep eutectic solvent and its mixtures with water, Thermochimica Acta. 546 (2012) 54–60. https://doi.org/10.1016/j.tca.2012.07.024.

[66] R.B. Leron, M.H. Li, High-pressure density measurements for choline chloride: Urea deep eutectic solvent and its aqueous mixtures at T = (298.15 to 323.15) K and

up to 50 MPa, Journal of Chemical Thermodynamics. 54 (2012) 293–301. https://doi.org/10.1016/j.jct.2012.05.008.

[67] R.B. Leron, D.S.H. Wong, M.-H. Li, Densities of a deep eutectic solvent based on choline chloride and glycerol and its aqueous mixtures at elevated pressures, Fluid Phase Equilib. 335 (2012) 32–38. https://doi.org/10.1016/j.fluid.2012.08.016.

[68] O.G. Sas, G.R. Ivaniš, M.L. Kijevčanin, B. González, A. Domínguez, I.R. Radović, High pressure densities and derived thermodynamic properties of deep eutectic solvents with menthol and saturated fatty acids, Journal of Chemical Thermodynamics. 162 (2021) 1–10. https://doi.org/10.1016/j.jct.2021.106578.

[69] E.A. Crespo, L.P. Silva, J.O. Lloret, P.J. Carvalho, L.F. Vega, F. Llovell, J.A.P. Coutinho, A methodology to parameterize SAFT-type equations of state for solid precursors of deep eutectic solvents: The example of cholinium chloride, Physical Chemistry Chemical Physics. 21 (2019) 15046–15061. https://doi.org/10.1039/c9cp02548k.

[70] R.B. Leron, M.H. Li, High-pressure volumetric properties of choline chloride-ethylene glycol based deep eutectic solvent and its mixtures with water, Thermochim Acta. 546 (2012) 54–60. https://doi.org/10.1016/j.tca.2012.07.024.

[71] T.E. Daubert, H.M. Sibul, C.C. Stebbins, R.P. Danner, R.L. Rowley, M.E. Adams, W. V Wilding, T.L. Marshall, Physical and Thermodynamic Properties of Pure Chemicals: DIPPR: Data Compilation: Core + Supplements 1−10, Taylor & Francis, 2000.

[72] S. Jabrane, J.M. Létoffé, P. Claudy, Study of the thermal behaviour of 1,3-propanediol and its aqueous solutions, Thermochimica Acta. 311 (1998) 121–127. https://doi.org/10.1016/S0040-6031(97)00416-4.

[73] V.N. Emel'yanenko, S.P. Verevkin, E.N. Stepurko, G.N. Roganov, M.K. Georgieva, Thermodynamic properties of glycolic acid and glycolide, Russian Journal of Physical Chemistry A. 84 (2010) 1301–1308. https://doi.org/10.1134/S0036024410080054.

[74] E.S. Domalski, E.D. Hearing, Heat Capacities and Entropies of Organic Compounds in the Condensed Phase. Volume III, Journal of Physical and Chemical Reference Data. 25 (1996) 1–525. https://doi.org/10.1063/1.555985.

[75] A.R. Hansen, K.D. Beyer, Experimentally Determined Thermochemical Properties of the Malonic Acid/Water System: Implications for Atmospheric Aerosols, The Journal of Physical Chemistry A. 108 (2004) 3457–3466. https://doi.org/10.1021/jp0376166.

[76] A.P. Abbott, G. Capper, D.L. Davies, R.K. Rasheed, V. Tambyrajah, Novel solvent properties of choline chloride / urea mixtures, The Royal Society of Chemistry. (2003) 70–71. https://doi.org/10.1039/B210714G.

[77] W.R. Giacomin Junior, C.A. Capeletto, F.A.P. Voll, M.L. Corazza, Phase Equilibrium Measurements and Thermodynamic Modeling of the Systems (CO 2 + Ethyl Levulinate) and (CO 2 + Levulinic Acid), Journal of Chemical & Engineering Data. 64 (2019) 2011–2017. https://doi.org/10.1021/acs.jced.8b01023.

[78] O.V. Junior, L. Ferreira-Pinto, V.F. Cabral, W.M. Giufrida, L. Cardozo-Filho, Experimental Measurements of the {CO 2 (1) + Acetone (2) + Ivermectin (3)} System at High Pressure, Journal of Chemical & Engineering Data. 64 (2019) 3786–3792. https://doi.org/10.1021/acs.jced.9b00072.

[79] N.G.O. Santos, E.A. Rebelatto, D.A. Mayer, M. Lanza, J. Vladimir Oliveira, High-pressure phase behavior of the quaternary system (carbon dioxide + dichloromethane

+ ε–caprolactone + poly(ε–caprolactone): Experimental data and PC-SAFT modeling, Fluid Phase Equilibria. 554 (2022) 113306. https://doi.org/10.1016/j.fluid.2021.113306.

[80] D. Borjan, D. Cör, M. Knez Marevci, I. Grčar, Ž. Knez, Phase Equilibrium Data of Tetrabutylurea, Tetramethylurea, and Tetramethylthiourea/Carbon Dioxide at Pressures up to 200 bar at 313.15 and 333.15 K, Journal of Chemical & Engineering Data. (2022). https://doi.org/10.1021/acs.jced.2c00079.

[81] J.H. Dymond, R. Malhotra, The Tait equation: 100 years on, Int J Thermophys. 9 (1988) 941–951. https://doi.org/10.1007/BF01133262.

[82] G.M. Kontogeorgis, C. Voutsas, Epaminondas, V. Yakoumis, Iakovos, P. Tassios, Dimitrios, An Equation of State for Associating Fluids, Industrial and Engineering Chemistry Research. 35 (1996) 4310–4318. https://doi.org/10.1021/ie071397j.

[83] G.M. Kontogeorgis, I. V. Yakoumis, H. Meijer, E. Hendriks, T. Moorwood, Multicomponent phase equilibrium calculations for water–methanol–alkane mixtures, Fluid Phase Equilibria. 158–160 (1999) 201–209. https://doi.org/10.1016/S0378-3812(99)00060-6.

[84] K.G. Joback, R.C. Reid, Estimation of Pure-Component Properties from Group-Contributions, Chemical Engineering Communications. 57 (1987) 233–243. https://doi.org/10.1080/00986448708960487.

[85] A.L. Lydersen, Estimation of critical properties of organic compounds by the method of group contibutions, Madison, 1955.

[86] F.P. Pelaquim, R.G. Bitencourt, A.M.B. Neto, I.A.L. Dalmolin, M.C. da Costa, Carbon dioxide solubility in Deep Eutectic Solvents: Modelling using Cubic Plus Association and Peng-Robinson equations of state, Process Safety and Environmental Protection. 163 (2022) 14–26. https://doi.org/10.1016/j.psep.2022.04.075.

[87] R. Haghbakhsh, M. Keshtkar, A. Shariati, S. Raeissi, Experimental investigation of carbon dioxide solubility in the deep eutectic solvent (1 ChCl + 3 triethylene glycol) and modeling by the CPA EoS, J Mol Liq. 330 (2021) 1–12. https://doi.org/10.1016/j.molliq.2021.115647.

[88] F. Rabhi, F. Mutelet, H. Sifaoui, Solubility of Carbon Dioxide in Carboxylic Acid-Based Deep Eutectic Solvents, J Chem Eng Data. 66 (2021) 702–711. https://doi.org/10.1021/acs.jced.0c00844.

[89] E.A. Crespo, L.P. Silva, M.A.R. Martins, M. Bülow, O. Ferreira, G. Sadowski, C. Held, S.P. Pinho, J.A.P. Coutinho, The Role of Polyfunctionality in the Formation of [Ch]Cl-Carboxylic Acid-Based Deep Eutectic Solvents, Industrial and Engineering Chemistry Research. 57 (2018) 11195–11209. https://doi.org/10.1021/acs.iecr.8b01249.

[90] A.C. Kouakou, K. Le Mapihan, J. Pauly, Solid–liquid equilibria under high pressure of pure fatty acid methyl esters, Fuel. 109 (2013) 297–302. https://doi.org/10.1016/j.fuel.2013.01.036.

[91] N.D.D. Carareto, M.C. Costa, A.J.A. Meirelles, J. Pauly, High pressure solid-liquid equilibrium of fatty acid ethyl esters binary systems, Fluid Phase Equilibria. 382 (2014) 158–163. https://doi.org/10.1016/j.fluid.2014.09.007.

[92] N.D. Dorighello Carareto, M.C. Costa, A.J.A. Meirelles, J. Pauly, High Pressure Solid-Liquid Equilibrium of Fatty Alcohols Binary Systems from 1-Dodecanol, 1-Tetradecanol, 1-Hexadecanol, and 1-Octadecanol, Journal of Chemical and Engineering Data. 60 (2015) 2966–2973. https://doi.org/10.1021/acs.jced.5b00330.

[93] M. Yang, T. Narita, Y. Tanaka, T. Sotani, S. Matsuo, Solid–liquid phase equilibria in binary (1-octanol + n-alkane) mixtures under high-pressure, Fluid Phase Equilibria. 204 (2003) 55–64. https://doi.org/10.1016/S0378-3812(02)00203-0.

[94] R.J. Hemley, Effects of High Pressure on Molecules, Annual Review of Physical Chemistry. 5 (2000) 763–800.

[95] F. Gabriele, M. Chiarini, R. Germani, M. Tiecco, N. Spreti, Effect of water addition on choline chloride/glycol deep eutectic solvents: Characterization of their structural and physicochemical properties, Journal of Molecular Liquids. 291 (2019) 111301. https://doi.org/10.1016/j.molliq.2019.111301.

[96] X. Meng, K. Ballerat-Busserolles, P. Husson, J.-M. Andanson, Impact of water on the melting temperature of urea + choline chloride deep eutectic solvent, New J. Chem. 40 (2016) 4492–4499. https://doi.org/10.1039/C5NJ02677F.

[97] J.B. Ott, J.R.E.X. Goates, J.D. Lamb, Solid-liquid phase equilibria in water-I-ethylene glycol, Journal of Chemical Thermodynamics. 4 (1972) 123–126.

[98] R.C. Wilhoit, Daniel. Shiao, Thermochemistry of Biologically Important Compounds. Heats of Combustion of Solid Organic Acids., Journal of Chemical & Engineering Data. 9 (1964) 595–599. https://doi.org/10.1021/je60023a038.

[99] I. Bahadur, T.M. Letcher, S. Singh, G.G. Redhi, P. Venkatesu, D. Ramjugernath, Excess molar volumes of binary mixtures (an ionic liquid+water): A review, J Chem Thermodyn. 82 (2015) 34–46. https://doi.org/10.1016/j.jct.2014.10.003.

[100] M. Francisco, A.S.B. González, S.L. García De Dios, W. Weggemans, M.C. Kroon, Comparison of a low transition temperature mixture (LTTM) formed by lactic acid and choline chloride with choline lactate ionic liquid and the choline chloride salt: Physical properties and vapour-liquid equilibria of mixtures containing water and ethanol, RSC Adv. 3 (2013) 23553–23561. https://doi.org/10.1039/c3ra40303c.

[101] M.J. Pratas, M.B. Oliveira, M.J. Pastoriza-Gallego, A.J. Queimada, M.M. Piñeiro, J.A.P. Coutinho, High-pressure biodiesel density: Experimental measurements, correlation, and cubic-plus-association equation of state (CPA EoS)

modeling, Energy and Fuels. 25 (2011) 3806–3814. https://doi.org/10.1021/ef200807m.

Supporting Information

1. Solid-liquid equilibrium at high pressure

Table S1. Experimental data (x_2, T) of the SLE system composed of choline chloride (1) and ethylene glycol (2) at high pressures[1].

Pressure (MPa)										$\Delta T_{(6-0.1)MPa}$	$\Delta T_{(25-6)MPa}$
6		10		14		20		25			
x_2	T (K)	x_2	T (K)	x_2	T (K)	x_2	T (K)	x_2	T (K)		
0.668	295.18	0.668	295.40	0.668	296.97	0.668	298.04	0.668	298.74	*	3.56
0.601	313.10	0.601	313.08	0.601	313.68	0.601	315.31	0.601	317.32	67.10	4.22
0.550	337.91	0.550	339.02	0.550	339.69	0.550	339.84	0.550	341.02	46.01	3.10
0.700	294.30	0.700	295.98	0.700	296.06	0.700	296.02	0.700	296.64	48.80	2.34
									Average	53.97	3.30

[1] Standard uncertainties (u) are: $u(T)$= 0.32 K, $u_r(p)$= 0.08, $u_r(x)$= 0.0003
* No data were found

Table S2. Experimental data (x_2, T) of the SLE system composed of choline chloride (1) and glycerol (2) at high pressures[1].

Pressure (MPa)										$\Delta T_{(6-0.1)MPa}$	$\Delta T_{(25-6)MPa}$
6		10		14		20		25			
x_2	T (K)	x_2	T (K)	x_2	T (K)	x_2	T (K)	x_2	T (K)		
0.401	340.65	0.401	341.01	0.401	341.47	0.401	342.71	0.401	344.35	33.05	3.70
0.450	323.15	0.450	323.91	0.450	324.53	0.450	324.82	0.450	324.98	29.55	1.83
0.500	296.60	0.500	306.38	0.500	308.49	0.500	311.20	0.500	313.40	5.70	16.80
0.549	279.50	0.549	282.50	0.549	285.16	0.549	286.90	0.549	287.67	29.60	8.17
									Average	24.48	7.62

[1] Standard uncertainties (u) are: $u(T)$= 0.56 K, $u_r(p)$= 0.02, $u_r(x)$= 0.0001

Table S3. Experimental data (x_2, T) of the SLE system composed of choline chloride (1) and 1,3 propanediol (2) at high pressures[1].

Pressure (MPa)										$\Delta T_{(6-0.1)MPa}$	$\Delta T_{(25-6)MPa}$
6		10		14		20		25			
x_2	T (K)	x_2	T (K)	x_2	T (K)	x_2	T (K)	x_2	T (K)		
0.667	290.04	0.667	293.24	0.667	294.58	0.667	295.07	0.667	296.54	7.04	6.49
0.601	309.60	0.601	310.22	0.601	311.05	0.601	311.56	0.601	312.12	20.40	2.52
0.550	330.07	0.550	331.72	0.550	332.28	0.550	332.96	0.550	334.47	*	4.40
									Average	13.72	4.47

[1] Standard uncertainties (u) are: $u(T)$= 0.32 K, $u_r(p)$= 0.08, $u_r(x)$= 0.0003
* No data were found

Table S4. Experimental data (x_2, T) of the SLE system composed of choline chloride (1) and glycolic acid (2) at high pressures[1].

Pressure (MPa)										$\Delta T_{(6-0.1)MPa}$	$\Delta T_{(25-6)MPa}$
6		10		14		20		25			
x_2	T (K)	x_2	T (K)	x_2	T (K)	x_2	T (K)	x_2	T (K)		
0.600	289.15	0.600	290.09	0.600	290.15	0.600	289.07	0.600	289.46	8.23	0.31
0.850	291.79	0.850	291.99	0.850	292.17	0.850	291.95	0.850	291.95	38.49	0.16
								Average		23.36	0.24

[1] Standard uncertainties (u) are: $u(T)$= 0.42 K, $u_r(p)$= 0.07, $u_r(x)$= 0.0001

Table S5. Experimental data (x_2, T) of the SLE system composed of choline chloride (1) and lactic acid (2) at high pressures[1].

Pressure (MPa)										$\Delta T_{(6-0.1)MPa}$	$\Delta T_{(25-6)MPa}$
6		10		14		20		25			
x_2	T (K)	x_2	T (K)	x_2	T (K)	x_2	T (K)	x_2	T (K)		
0.449	325.20	0.449	327.13	0.449	330.85	0.449	333.75	0.449	333.95	8.32	8.75
0.500	294.33	0.500	304.15	0.500	310.60	0.500	314.72	0.500	315.89	2.62	21.56
								Average		5.47	15.16

[1] Standard uncertainties (u) are: $u(T)$= 0.82 K, $u_r(p)$= 0.04, $u_r(x)$= 0.0002

Table S6. Experimental data (x_2, T) of the SLE system composed of choline chloride (1) and malonic acid (2) at high pressures[1].

Pressure (MPa)										$\Delta T_{(6-0.1)MPa}$	$\Delta T_{(25-6)MPa}$
6		10		14		20		25			
x_2	T (K)	x_2	T (K)	x_2	T (K)	x_2	T (K)	x_2	T (K)		
0.450	284.20	0.450	286.15	0.450	287.57	0.450	289.19	0.450	290.98	17.28	6.78
0.650	307.51	0.650	306.92	0.650	306.40	0.650	308.08	0.650	308.26	10.01	0.75
0.700	324.15	0.700	326.44	0.700	325.70	0.700	325.15	0.700	324.58	4.53	0.43
								Average		10.61	4.65

[1] Standard uncertainties (u) are: $u(T)$= 0.97 K, $u_r(p)$= 0.03, $u_r(x)$= 0.0001

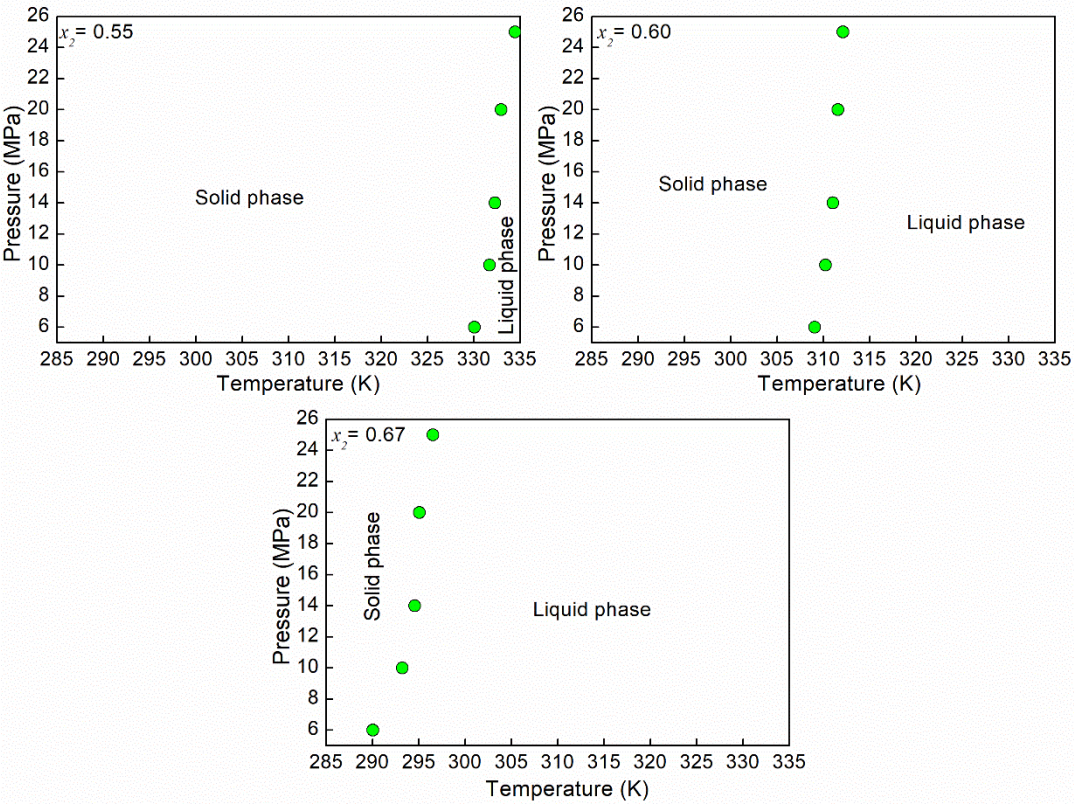

Figure S1. Phase diagrams P×T of the ES composed of ChCl (1) and 1,3 propanediol (2) at *three* molar ratios and five pressures.

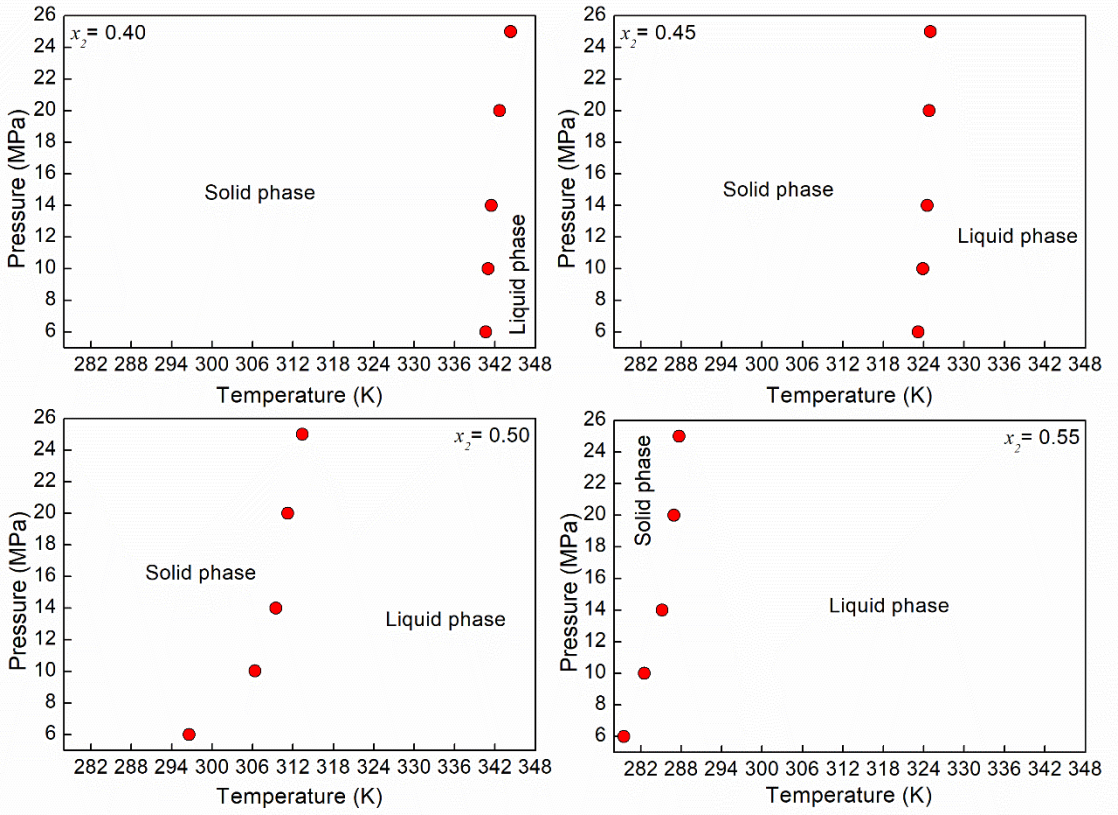

Figure S2. Phase diagrams P×T of the ES composed of ChCl (1) and glycerol (2) at four molar ratios and five pressures.

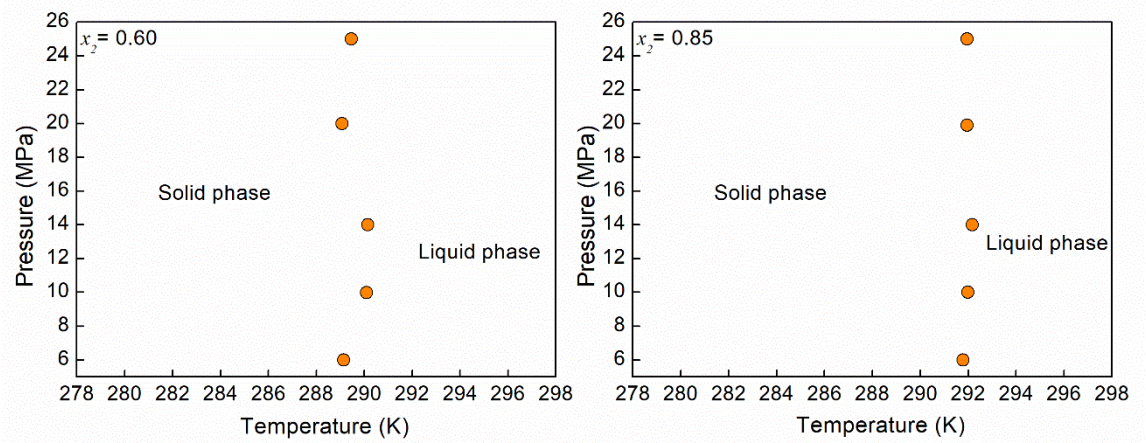

Figure S3. Phase diagrams P×T of the ES composed of ChCl (1) and glycolic acid (2) at *two* molar ratios and five pressures.

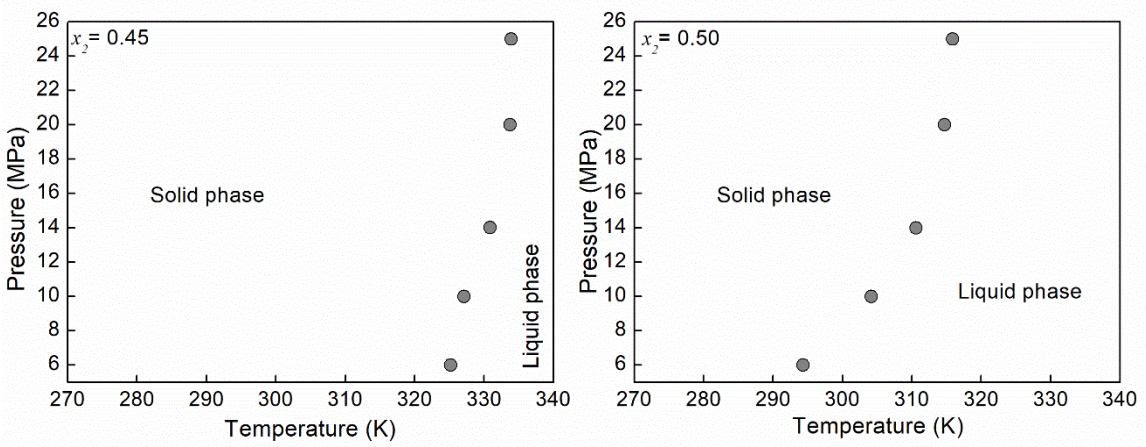

Figure S4. Phase diagrams P×T of the ES composed of ChCl (1) and lactic acid (2) at *two* molar ratios and five pressures.

2. Density at high pressure

Table S7. Experimental data of density as a function of pressure and temperature for the system composed of ChCl and ethylene glycol (1:2)[1].

	ρ (g.cm^{-3})				
Pressure (MPa)	**T (K)**				
	293.15	**298.15**	**313.15**	**333.15**	**353.15**
1.0	1.1162	1.1120	1.1046	1.0918	1.0804
5.0	1.1177	1.1137	1.1062	1.0934	1.0818
10.0	1.1195	1.1158	1.1075	1.0954	1.0839
15.0	1.1212	1.1181	1.1088	1.0972	1.0859
20.0	1.1229	1.1202	1.1103	1.0990	1.0877
25.0	1.1245	1.1216	1.1118	1.1007	1.0897
30.0	1.1260	1.1233	1.1132	1.1024	1.0912
35.0	1.1273	1.1247	1.1148	1.1040	1.0929
40.0	1.1287	1.1260	1.1163	1.1056	1.0945
45.0	1.1301	1.1273	1.1178	1.1072	1.0958
50.0	1.1313	1.1286	1.1193	1.1086	1.0963

[1] Standard uncertainties (u) are: $u(T)$= 0.007 K, $u_r(p)$= 0.01, $u_r(\rho)$= 7·10^{-4} g.cm^{-3}

Table S8. Experimental data of density as a function of pressure and temperature for the system composed of ChCl and glycerol (1:1.5)[1].

	ρ (g.cm^{-3})				
Pressure (MPa)	**T (K)**				
	293.15	**298.15**	**313.15**	**333.15**	**353.15**
1.0	1.1725	1.1656	1.1581	1.1469	1.1356
5.0	1.1746	1.1686	1.1629	1.1503	1.1393
10.0	1.1763	1.1710	1.1650	1.1524	1.1421
15.0	1.1779	1.1730	1.1666	1.1548	1.1445
20.0	1.1795	1.1748	1.1680	1.1568	1.1461
25.0	1.1809	1.1764	1.1693	1.1584	1.1476
30.0	1.1824	1.1777	1.1705	1.1600	1.1491
35.0	1.1840	1.1787	1.1720	1.1615	1.1507
40.0	1.1854	1.1794	1.1734	1.1627	1.1522
45.0	1.1867	1.1798	1.1750	1.1642	1.1540
50.0	1.1880	1.1801	1.1763	1.1652	1.1556

[1] Standard uncertainties (u) are: $u(T)$= 0.007 K, $u_r(p)$= 0.01, $u_r(\rho)$= 7·10^{-4} g.cm^{-3}

Table S9. Experimental data of density as a function of pressure and temperature for the system composed of ChCl and 1,3 propanediol (1:2.3)[1].

	ρ (g.cm^{-3})				
Pressure (MPa)	**T (K)**				
	293.15	**298.15**	**313.15**	**333.15**	**353.15**
1.0	1.0804	1.0752	1.0674	1.0561	1.0454
5.0	1.0819	1.0782	1.0692	1.0577	1.0472
10.0	1.0838	1.0801	1.0713	1.0597	1.0494
15.0	1.0856	1.0819	1.0733	1.0616	1.0516
20.0	1.0874	1.0837	1.0752	1.0636	1.0534
25.0	1.0889	1.0853	1.0770	1.0653	1.0555
30.0	1.0902	1.0871	1.0787	1.0671	1.0574
35.0	1.0915	1.0887	1.0802	1.0687	1.0592
40.0	1.0930	1.0900	1.0818	1.0705	1.0610
45.0	1.0945	1.0914	1.0834	1.0721	1.0626
50.0	1.0959	1.0931	1.0849	1.0737	1.0642

[1] Standard uncertainties (u) are: $u(T)$= 0.007 K, $u_r(p)$= 0.01, $u_r(\rho)$= 7·10^{-4} g.cm^{-3}

Table S10. Experimental data of density as a function of pressure and temperature for the system composed of ChCl and glycolic acid (1:1.2)[1].

	ρ (g.cm^{-3})				
Pressure (MPa)	**T (K)**				
	293.15	**298.15**	**313.15**	**333.15**	**353.15**
1.0	1.2254	1.2230	1.2139	1.2023	1.1888
5.0	1.2298	1.2268	1.2167	1.2030	1.1910
10.0	1.2320	1.2288	1.2188	1.2049	1.1933
15.0	1.2337	1.2303	1.2205	1.2067	1.1955
20.0	1.2352	1.2317	1.2220	1.2085	1.1975
25.0	1.2367	1.2329	1.2237	1.2102	1.1995
30.0	1.2381	1.2343	1.2253	1.2118	1.2014
35.0	1.2396	1.2355	1.2267	1.2131	1.2033
40.0	1.2409	1.2369	1.2281	1.2140	1.2048
45.0	1.2422	1.2381	1.2294	1.2150	1.2063
50.0	1.2436	1.2394	1.2307	1.2156	1.2079

[1] Standard uncertainties (u) are: $u(T)$= 0.007 K, $u_r(p)$= 0.01, $u_r(\rho)$= 7·10^{-4} g.cm^{-3}

Table S11. Temperature and density ranges at 1 bar for each HBA and HBD investigated to use the individual approach.

Component	Temperature range (K)	Density range (mol/m³)	N_p	AARD% in ρ	Ref.
Choline Chloride	293.15 – 353.15	7681.34 – 7884.03	13	0.01	Francisco et al. 2013[1]
1,3 propanediol	293.15 – 318.15	13631.75 – 13839.39	6	0.01	Zhang et al. 2020[2]
Glycolic acid	293.15 – 373.15	15401.43 – 16028.63	17	0.03	Crespo et al. 2018[3]

References

(1) Francisco, M.; González, A. S. B.; García De Dios, S. L.; Weggemans, W.; Kroon, M. C. Comparison of a Low Transition Temperature Mixture (LTTM) Formed by Lactic Acid and Choline Chloride with Choline Lactate Ionic Liquid and the Choline Chloride Salt: Physical Properties and Vapour-Liquid Equilibria of Mixtures Containing Water and Ethanol. *RSC Adv.* 2013, *3*, 23553–23561. https://doi.org/10.1039/c3ra40303c.

(2) Zhang, R.; Yue, X.; Li, B.; Yang, J.; Wu, Z.; Zhang, J. Dynamic Viscosity, Density and Surface Tension of 1,3-Propanediol (1) + 1,2-Propanediamine (2) Binary System at T = (293.15 to 318.15) K and Atmosphere Pressure. *J. Mol. Liq.* 2020, *299* (78), 1–10. https://doi.org/10.1016/j.molliq.2019.112213.

(3) Crespo, E. A.; Silva, L. P.; Martins, M. A. R.; Bülow, M.; Ferreira, O.; Sadowski, G.; Held, C.; Pinho, S. P.; Coutinho, J. A. P. The Role of Polyfunctionality in the Formation of [Ch]Cl-Carboxylic Acid-Based Deep Eutectic Solvents. *Ind. Eng. Chem. Res.* 2018, *57* (32), 11195–11209. https://doi.org/10.1021/acs.iecr.8b01249.

CAPÍTULO 7

Phase behavior and thermodynamic modeling of Deep eutectic solvents and carbon dioxide at high pressures

(Artigo em fase de correção e submissão)

Fernanda Paludetto Pelaquim[a], Klebson Santos[b,c], Irede Angela Lucini Dalmolin[d], Elton Franceschi [b,c], Gustavo Rodrigues Borges [b,c], Claudio Dariva [b,c], Mariana Conceição da Costa[a5*].

[a] School of Chemical Engineering, University of Campinas – UNICAMP, Avenida Albert Einstein 500, ZIP Code 13083-852, Campinas, SP, Brazil

b Center for Studies on Colloidal Systems (NUESC) – Institute of Technology and Research (ITP), Av. Murilo Dantas, 300, Aracaju, SE, ZIP Code 49032-490, Brazil

[c] Tiradentes University (UNIT), Postgraduate Program in Process Engineering (PEP), Av. Murilo Dantas, 300, Aracaju, SE, ZIP Code 49032-490, Brazil

[c] Academic Department of Engineering, Universidade Tecnológica Federal do Paraná (UTFPR), Linha Santa Bárbara, ZIP Code 85601-970, Francisco Beltrão, PR, Brazil

5 [*] Corresponding author.

E-mail address: mcdcosta@unicamp.br (M.C. Costa)

phone number: +551935213962.

Abstract

The global climate has witnessed severe changes in the last two decades, mainly due to greenhouse gases released into the atmosphere. CO_2 is the main greenhouse gas that contributes to global warming and climate change, therefore finding an effective method to avoid the release of large amounts of CO_2 into the atmosphere has been the objective of many research centers. The main CO_2 capture system is absorption which uses a regenerable liquid solvent such as monoethanolamine (MEA), diethanolamine (DEA) or Selexol process. However, these compounds have the potential to degrade resulting in equipment corrosion and the generation of volatile compounds. On that basis, it is important to find other solvents, a more viable alternative, for example, the Deep Eutectic Solvents (DESs), that have been used in numerous fields due to their high thermal stability, low vapor pressure, inexpensiveness, and non-toxicity. The capture of CO_2 by DESs has been extensively studied at atmospheric pressure. Information on phase equilibria at high pressures of DESs+CO_2 is essential for many chemical processes and also to fill a gap in the literature. The seek of this study, was to measure the CO_2 solubility in six DESs (ChCl:ethylene glycol, ChCl:1,3 propanediol, ChCl:glycerol, ChCl:glycolic acid, ChCl:lactic acid, and ChCl:malonic acid) at 298.15, 303.15, 318.15 and 333.15 K. The CO_2 solubility increases with the pressure raise and decreases with the temperature raise. The absorbed CO_2 in all DESs was not higher than 0.20 mol CO_2/mol DES, probably due to its high viscosity and small mass transfer, and a better result was reached using ChCl and malonic acid DES.

1. Introduction

In the last few years, Deep Eutectic Solvents (DESs) became suitable candidates to act in several applications in chemical industries due to their great potential as a solvent, especially in green chemistry[1,2]. The interest in such components is due to their high thermal stability, wide liquid range, low vapor pressure, and volatility. Moreover, they are usually tunable solvents, inexpensive, non-toxic and non-flammable, biodegradable, and easy to prepare since require any purification steps[3,4]. Consequently, the production costs and the environmental effects are reduced, achieving the objectives of green engineering, i.e., safety, maximum efficiency, and minimum ecological and health impacts at all stages[5].

DESs are a mixture of two or more components composed of a hydrogen bond acceptor (HBA) and a hydrogen bond donor (HBD) in which the eutectic point temperature is below the temperature of an ideal liquid mixture, forming a homogenous liquid phase[6]. They have been used in numerous fields as polymerization[7], biomass processing[8,9], biocatalysis[10], extraction[11–13], denitrification[14], battery technology[15–17], synthesis of nano-particles[18–20]. However, one of the most interesting applications is the absorption of gases, especially carbon dioxide (CO_2)[4].

The dependence on nonrenewable fossil resources since the industrial revolution resulted in a constant increase in global energy[21]. Therefore, hydrocarbons and, mainly CO_2 produced by incomplete combustion in the industry have led to worldwide climate change events with a negative impact on the planet's ecosystems and environment such as the increase of 0.8 °C in the global temperature[22]. The atmospheric concentration of CO_2 has been increasing drastically, hitting 415 ppm in October 2022[23], and is expected to reach 900 ppm by 2050[21], making the prevention

and control of CO_2 absorption urgent. Postponing this issue promotes and favors climate change.

Carbon capture and storage (CCS) is the main technology used to reduce CO_2 emissions which are expected to lead to a 24% reduction of total emissions by 2060[24]. Transportation, compression, and storage are the established and technologically available steps, however, the capture step which accounts for almost two-thirds of the total CCS costs is an obstacle[2]. The idea of capturing CO_2 is to obtain an extremely concentrated CO_2 stream and separated it from gas mixtures such as flue gas released from power plants. Absorption in a solvent, use of a membrane to selectively separate CO_2, adsorption into solid surfaces, and cryogenic distillation of flue gases are examples of the used methods to capture CO_2[25].

Although the high energy requirements for solvent regeneration impact costs, CO_2 absorption is the most widely used and mature full-scale technology to capture the gas[2,25]. The chemical fluids used in this process are usually alkanolamines (monoethanolamine (MEA), diethanolamine (DEA), N-methyldiethanolamine (MDEA), and trimethylethanolamine) which chemically remove CO_2 efficiently but present several drawbacks as thermal degradation, high volatility, toxicity and regeneration temperature, equipment corrosion, pollution and energy-intensive consumption[26–28]. Concerning physical solvents, Selexol is a mature technology that uses the physical absorbent of Dimethyl Ethers of Polyethylene Glycol (DEPG), presents low vapor pressure, chemical and thermal stability, non-corrosive and non-toxic nature. However, its high viscosity enhanced the pumping cost.

Therefore, the development and application of new efficient, low-cost, and sustainable solvents are needed, such as DESs. Li et al. (2008) were the first authors

to determine the CO_2 solubility in DESs at high pressures. They investigated the DES composed of choline chloride (ChCl) and urea at three molar ratios, different temperatures, and pressure ranges and found that all variables influence solubility[29]. After that, several authors investigated the solubility of CO_2 in other DESs, considering different combinations of HBAs and HBDs[21,28,30–36], reaching 73 studied DESs according to Haghbakhsh et al. (2021)[4]. Although the number of DESs investigated has been high, it is not meaningful compared to the number of DESs discovered so far, which exceeds 300. In addition, there is also a limitation in the temperature and pressure ranges studied in the published works, which along with the restricted number of DESs studied becomes a gap in the study of CO_2 solubility.

This study comes to expand the literature on CO_2 solubility in DESs at high pressures. Hence, the CO_2 solubility measurements in six DESs were performed using a high-pressure variable-volume view cell at four temperatures of 298.15, 303.15, 318.15, and 333.15 K and pressures ranging from 0.1 to 26 MPa. The selected DESs were composed of ChCl as the HBA and ethylene glycol, 1,3 propanediol, glycerol, glycolic acid, lactic acid, and malonic acid as the HBDs. In addition, Henry's constant values and standard Gibbs free energies of dissolution were calculated at the studied pressures and temperatures.

2. Experimental Section

2.1. Materials

Carbon dioxide (mass fraction purity 0.999 in the liquid phase) was supplied by White Martins S.A. (Brazil). Choline Chloride (ChCl) with purity higher than 98.5%, 1,3 propanediol (purity ≥ 98%), lactic acid (purity ≥ 99.5%), and malonic acid (purity ≥ 99%) were purchased from Sigma Aldrich. Ethylene glycol (purity ≥ 99.5%) was

purchased from Merck, glycerol (purity ≥ 99%) from Anidrol, and glycolic acid (purity ≥ 99.7%) from Acros. All components were dried at room temperature and under vacuum for 72 h before the DESs preparation and placed at room temperature in a desiccator. All details of the components are presented in Table 1.

Table 1. Chemical structures, CAS number, and melting properties of the components used in this work.

Component	CAS Number	Molar weight (g.mol-1)	T_m(K)	$\Delta_m H$ (kJ.mol-1)
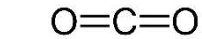 Carbon Dioxide	124-38-9	44.01		
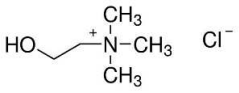 Choline Chloride	67-48-1	139.62	597[44]	4.30[44]
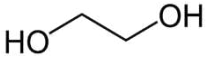 Ethylene Glycol	107-21-1	62.07	256.60[45]	9.50[45]
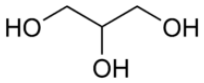 Glycerol	56-81-5	92.09	293[46]	18.28[46]
 1.3 propanediol	504-63-2	76.09	249[46]	11.40[46]
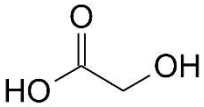 Glycolic Acid	79-14-1	76.05	351.30[47]	19.30[47]
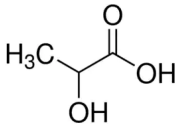 Lactic Acid	50-21-5	90.08	289.90[48]	11.34[48]
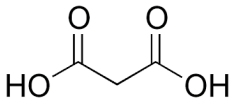 Malonic Acid	141-82-2	104.06	407.50[49]	23.10[49]

2.2. Preparation of Deep Eutectic Solvents

DESs were prepared at their eutectic composition and have proven to be a Deep Eutectic Solvent in previous works[50,51]. ChCl was selected as the hydrogen bond acceptor (HBA), and three polyalcohols and three carboxylic acids were chosen as the

hydrogen bond donors (HBDs). Table 2 shows the molar ratios used for the prepared DESs.

According to the required molar ratio, known quantities of each component were weighed using an analytical scale with a precision of $\pm 2 \times 10^{-4} g$ (Shimadzu AUY220, Japan) for a total mass of 100 g. The mixture was placed into a 250 ml Erlenmeyer flask, and then into a glycerin bath with reciprocal stirring at 333.15 K for 120 min, or until a clear, homogeneous liquid is formed. The formed DESs were transferred to amber flasks and kept at room temperature in a desiccator for minimal water absorption. This procedure was conducted following the methodology of heating combined with stirring proposed by Abbott et al. (2003) [52].

As DESs are usually hygroscopic systems, the water content of each investigated mixture was measured using a Metrohm 831 Karl Fischer coulometer, with the Hydranal-Coulomat AG analyzer from Riedel-de Haën.

Table 2. Molar ratio (x_2) of the ChCl(1)-based DESs prepared for use in the measurements of CO_2 solubilities at high pressures.

DES			Molar ratio (x_2)	Average of water content (%)
HBA (1)	HBD (2)	System	Solubility	
ChCl	Ethylene Glycol	ChCl:EG	0.67	0.75
ChCl	Glycerol	ChCl:GLY	0.60	0.80
ChCl	1,3 propanediol	ChCl:PD	0.70	0.89
ChCl	Glycolic Acid	ChCl:GLY AC	0.55	3.58
ChCl	Lactic Acid	ChCl:LAT AC	0.50	1.09
ChCl	Malonic Acid	ChCl:MAL AC	0.50	1.23

2.3. Phase equilibrium apparatus and procedure

The experimental data determination of CO_2 solubility in DESs was done using a high-pressure variable-volume view cell[53–56], a widely employed and reliable method.

The experimental apparatus (Figure 1) contains an ethanol container, which is the pressurization fluid (1), and a high-pressure syringe pump (ISCO 260L, Lincoln, USA) (2) that guides the fluid into the cell. The device is also equipped with a CO_2 gas cylinder (3) and another high-pressure syringe pump (4) in charge of filling the front of the cell along with the DES. To ensure that CO_2 is liquid, a thermostatic bath (TECNA, model TE-184) (5) controlled the pump fluid temperature.

An absolute pressure transducer with a precision of ±0.03 MPa (Smar LD 301) (6) measures the system pressure, and the phase transitions occur in a high-pressure variable-volume view cell (7), with a total capacity of $2.7 \times 10^{-5}\ m^3$. The transitions are observed by two sapphire windows (8 and 9). To feed the mixture components and determine the cell temperature, removable connections (10) and a PT-100 temperature indicator (11) are inserted in the cell. The pressure control inside the cell is carried out by a mobile piston (12). The temperature inside the cell is controlled by a cooling system formed by a metal jacket in which ethylene glycol is recirculated through a thermostatic bath (14) at the desired temperature.

To ensure equipment safety, several valves are installed: to flush and relieve the system (16), to stop the flow in the gas line (17 and 18), and a check valve (19) to guarantee that at high pressures no gas returns to the cylinder.

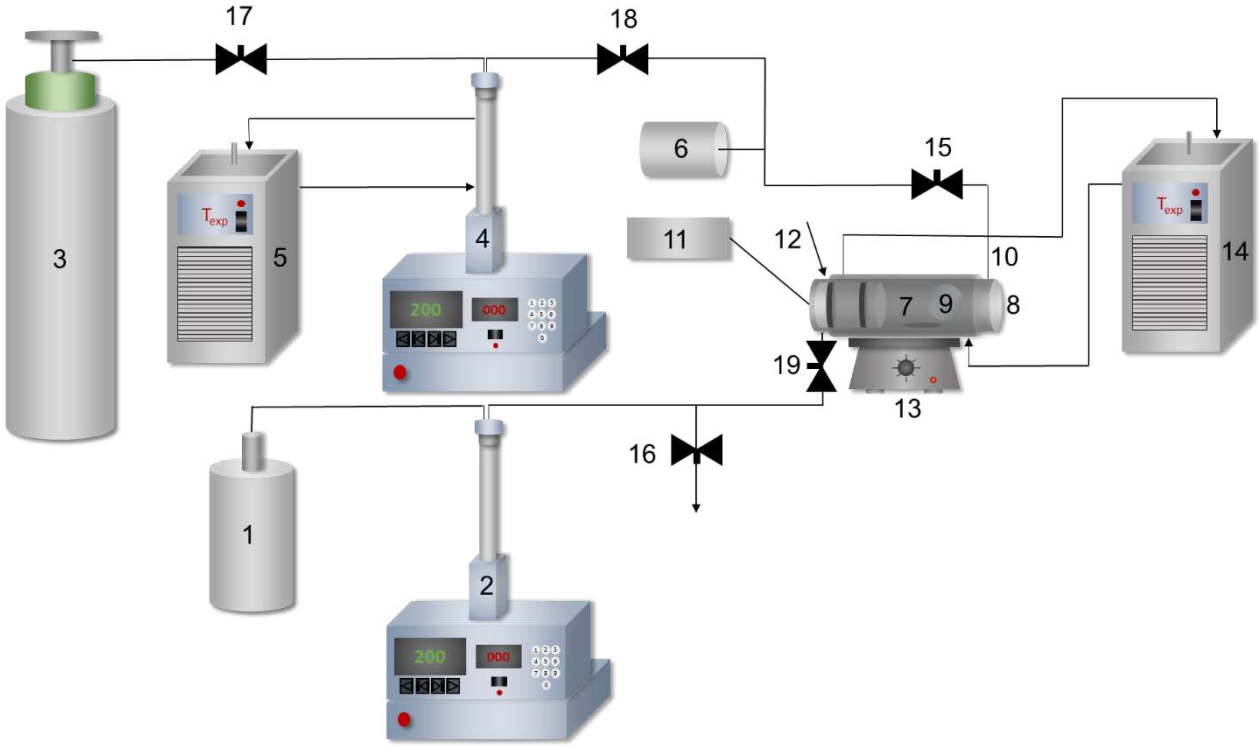

Figure 1. Schematic diagram of the experimental apparatus for phase equilibrium at high pressures. (1) ethanol container; (2 and 4) syringe pumps; (3) gas cylinder; (5 and 14) thermostatic baths; (6) absolute pressure transducer; (7) high-pressure variable-volume view cell; (8 and 9) sapphire windows; (10) removable connections; (11) PT-100 temperature indicator; (12) movable piston; (13) stir plate; (15 and 16) needle valves; (17 and 18) sphere valves; (19) check valve.

To determine the phase equilibrium between the DESs and CO_2, the experiment was done isothermally with the aid of two syringe pumps. The first pump contained the CO_2 that was inserted together with the DESs into the front of the cell, and the second pump was filled with ethanol to feed the bottom of the cell. The use of two pumps was necessary since some transitions were found at pressures lower than the vapor pressure of CO_2, which would increase the pump's effort, and does not occur with ethanol, since it is liquid.

Initially, the desired CO_2 compositions were chosen and a known amount of the less volatile component, namely DES, was placed in the front connection of the cell.

To confirm the absence of atmospheric air inside the cell, an atmosphere exchange was done by injecting CO_2 and eliminating the atmospheric air by slightly opening the feed connection. The pressure was then set at 10 MPa and the temperature at 278.15 K, when these conditions were reached the required volume of CO_2 was slowly added to the cell. The solvent volume was calculated based on the difference in the internal volume of the pump, the density at the desired conditions was obtained using the Hankinson-Brobst-Thomson (HBT) method and based on this information the solvent mass was determined[57].

Finally, for data acquisition, the system was submitted to the desired temperature, and the cell pressure was increased by injecting ethanol at the back of the piston, supported by the syringe pump, until a single liquid phase was observed. The mixture was then homogenized for at least 4 hours through continuous stirring to guarantee the existence of only one phase. After that, the pressure was slowly and isothermally reduced (0.3 to 0.5 MPa/min) until the formation of two phases, i.e., a transition pressure is determined at a given temperature. This procedure was done in triplicate for each temperature and overall composition.

3. Thermodynamic modeling

3.1. Henry's law constant

Henry's law can represent the physical solubility of very dilute concentrations of dissolved gases in liquid solvents. The quantity of the dissolved gas in a liquid is proportional to its fugacity in the gas phase. Henry's law constant (H_x) can be quantitatively obtained using the solubility experimental data according to Equation 1[58].

$$H_x(P,T) = \frac{f_2^{liq}(P,T,x_2)}{x_2} \quad (1)$$

where $H_x(P,T)$ is Henry's law constant based on the molar ratio; $f_2^{liq}(P,T,x_2)$ is the fugacity of CO_2 in the liquid phase, i.e., the DES, at the equilibrium pressure (P) and temperature (T); and x_2 is the molar ratio of CO_2 in the liquid phase.

In the vapor-liquid equilibrium, the fugacity of CO_2 in the liquid phase should be equal to the CO_2 fugacity in the gas phase as follow:

$$f_2^{liq}(P,T,x_2) = f_2^{vap}(P,T,y_2) = y_2 P\phi_2(P,T,y_2) \quad (2)$$

in which $f_2^{vap}(P,T,y_2)$ is the fugacity of CO_2 in the vapor phase; $y_2$is the molar ratio of CO_2 in the vapor phase; and $\phi_2(P,T,y_2)$ is the fugacity coefficient of CO_2 in the vapor phase.

It is well-known that the vapor pressure of DESs at the studied temperature is very small compared with the CO_2 equilibrium partial pressure and can be neglected[59]. Moreover, it was assumed that the vapor phase has only carbon dioxide and is approximately equal to unity. The fugacity coefficient of CO_2 can be calculated using the third term of the virial equation, so H_x is expressed according to Equation 3:

$$H_x(P,T) = \frac{f_2^{liq}(P,T,x_2)}{x_2} = \frac{P\phi_2(P,T,y_2)}{x_2} \cong \frac{P\phi_2(P,T)}{x_2} \quad (3)$$

It was also possible to determine the Gibbs energy ($\Delta_{dis}G$) according to the correlation below, in which $P^0 = 0.1$ MPa:

$$\Delta_{dis}G = RTln\left(\frac{H(T,P)}{P^0}\right) \quad (4)$$

4. Results and Discussion

4.1. CO_2 solubility in DESs

The CO_2 experimental solubility data in six DESs were measured at 298.15, 303.15, 318.15, and 333.15 K under pressures varying from 0.1 to 26 MPa. Only one

molar ratio of each DES was chosen, respecting their eutectic composition. Each data point was repeated three times, however, due to the nature of the experimental apparatus, repeating the exact molar ratio is not possible. Since each data point was collected separately and a trend was observed, the accuracy of the data is strongly reliable. All experimental data are depicted in Figure 2 and presented in Tables 3 – 8.

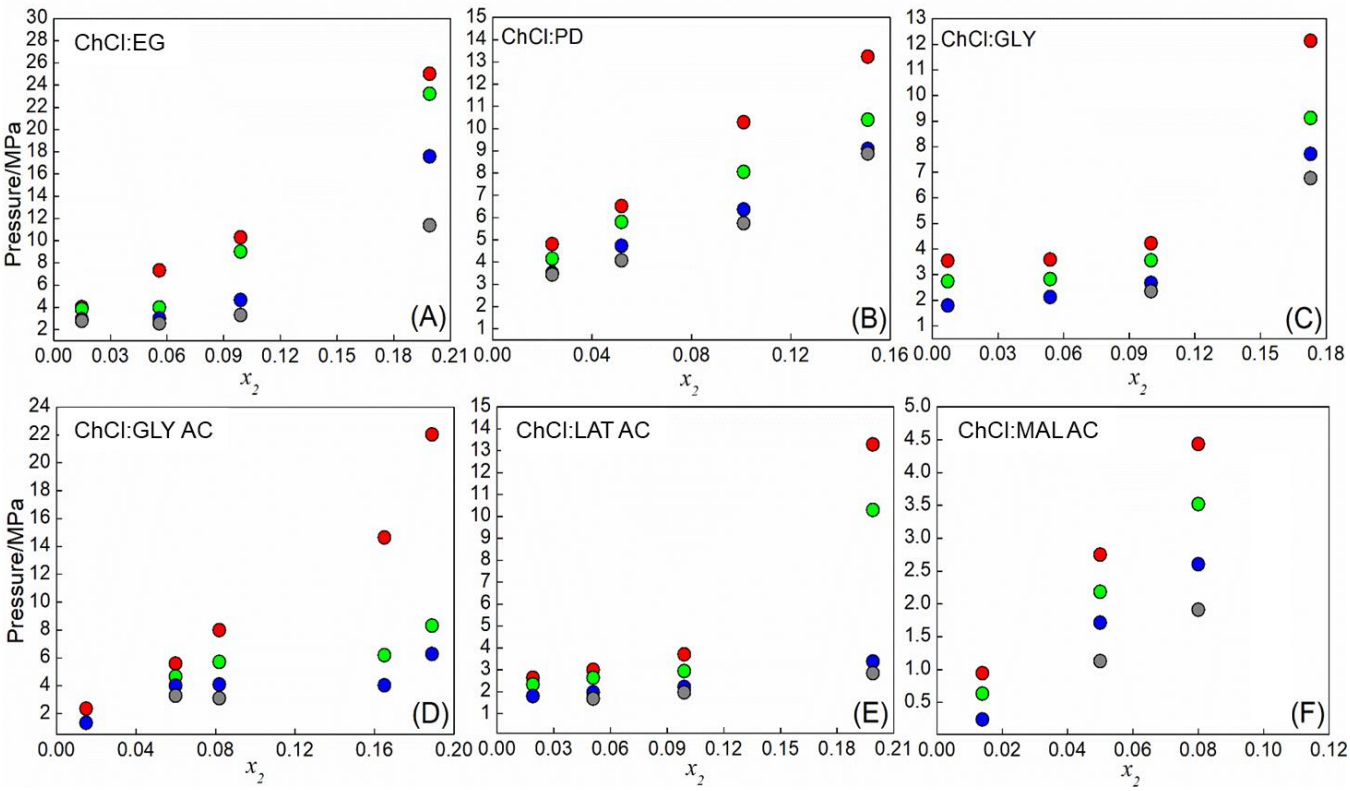

Figure 2. Solubility isotherms of CO_2 (2) in (A) ChCl:EG (1); (B) ChCl:PD (1); (C) ChCl:GLY (1); (D) ChCl:GLY AC (1); (E) ChCl:LAT AC (1); (F) ChCl:MAL AC (1). The symbols represent (●) 298.15 K; (●) 303.15 K; (●) 318.15 K; (●) 333.15 K.

The solubility of CO_2 in all six DESs tends to increase with pressure raise and decrease with temperature raise, thus higher solubilities are obtained at high pressures and low temperatures. This trend was expected and also similar to several works reported in the literature[2,21,25,60]. Regarding the temperature, the solubility decreases probably due to a decrease in the intermolecular interactions forces, resulting in a

higher rate of escape from the solution[21]. Besides, at higher temperatures, the gas desorption is favored, which raises the CO_2 desorbed and reduces de CO_2 absorbed[24].

It is possible to observe in Figure 2 that all DESs absorbed small quantities of CO_2, with a maximum of 0.20 mol CO_2/mol DES. At values higher than these, two phases coexist even after five hours of homogenization. This is probably due to the high viscosity of the DESs, which hinders the mass transfer inside the high-pressure variable-volume view cell and the strong HBA and HBD intermolecular hydrogen bonds lead to lower CO_2 solubility. In addition, several solid-liquid phase diagrams of DESs, including those in this study, exhibit near-ideal behavior, leading to a strong interaction between the components, i.e., a small free volume, promoting low solubilities of CO_2. One can see that in Tables 5 – 8 at 298.15 K, for some CO_2 compositions, the transition pressure was not observed due to the high viscosity and weak homogenization.

Leron et al. (2013)[61] also measured the CO_2 solubility in ChCl:ETGLY at 1:2 molar ratio, but the results differ from this work, and the DES water content was not reported by the authors. DESs are usually hygroscopic, and the effect of the water content on CO_2 solubility varies based on the DES molar ratio (HBA:HBD). The water can act as an anti-solvent and significantly decrease the solubility or can lead to a reduction of the DESs viscosity, increasing the solubility[60]. In the case of ChCl:ETGLY, researchers found that the increase in the water content reduces CO_2 solubility[62]. Therefore, the DES prepared by Leron et al. (2013) possibly presented a smaller content of water than the DES used in this work.

Table 3. Isothermal vapor-liquid equilibrium (VLE-BP) of ChCl:EG (1) + CO_2 (2) system in four temperatures*.

298.15 K	303.15 K	318.15 K	333.15 K

P (MPa)	x_2	P (MPa)	x_2	P (MPa)	x_2	P (MPa)	x_2
2.76	0.02	2.94	0.02	3.84	0.02	4.03	0.02
2.54	0.06	3.01	0.06	3.96	0.06	7.31	0.06
3.29	0.10	4.66	0.10	9.02	0.10	10.29	0.10
11.38	0.20	17.58	0.20	23.21	0.20	25.02	0.20

*V – vapour phase, L – liquid phase, E –equilibrium, BP – bubble point

Table 4. Isothermal vapor-liquid equilibrium (VLE-BP) of ChCl:PD (1) + CO_2 (2) system in four temperatures*.

298.15 K		303.15 K		318.15 K		333.15 K	
P (MPa)	x_2	**P (MPa)**	x_2	**P (MPa)**	x_2	**P (MPa)**	x_2
3.43	0.02	3.50	0.02	4.15	0.02	4.80	0.02
4.07	0.05	4.73	0.05	5.79	0.05	6.51	0.05
5.75	0.10	6.37	0.10	8.05	0.10	10.28	0.10
8.88	0.15	9.08	0.15	10.40	0.15	13.23	0.15

*V – vapour phase, L – liquid phase, E –equilibrium, BP – bubble point

Table 5. Isothermal vapor-liquid equilibrium (VLE-BP) of ChCl:GLY (1) + CO_2 (2) system in four temperatures.

298.15 K		303.15 K		318.15 K		333.15 K	
P (MPa)	x_2	**P (MPa)**	x_2	**P (MPa)**	x_2	**P (MPa)**	x_2
	0.01	1.80	0.01	2.74	0.01	3.54	0.01
	0.05	2.12	0.05	2.82	0.05	3.58	0.05
2.35	0.10	2.67	0.10	3.56	0.10	4.22	0.10
6.77	0.17	7.72	0.17	9.11	0.17	12.13	0.17

*V – vapour phase, L – liquid phase, E –equilibrium, BP – bubble point

Table 6. Isothermal vapor-liquid equilibrium (VLE-BP) of ChCl:GLY AC (1) + CO_2 (2) system in four temperatures.

298.15 K		303.15 K		318.15 K		333.15 K	
P (MPa)	x_2	**P (MPa)**	x_2	**P (MPa)**	x_2	**P (MPa)**	x_2
	0.02	1.33	0.02		0.02	2.36	0.02
3.28	0.06	3.99	0.06	4.67	0.06	5.57	0.06
3.11	0.08	4.10	0.08	5.70	0.08	7.98	0.08
	0.16	4.02	0.16	6.19	0.16	14.63	0.16
	0.19	6.26	0.19	8.30	0.19	22.03	0.19

*V – vapour phase, L – liquid phase, E –equilibrium, BP – bubble point

Table 7. Isothermal vapor-liquid equilibrium (VLE-BP) of ChCl:LAT AC (1) + CO_2 (2) system in four temperatures.

298.15 K		303.15 K		318.15 K		333.15 K	
P (MPa)	x_2	**P (MPa)**	x_2	**P (MPa)**	x_2	**P (MPa)**	x_2

	0.02	1.80	0.02	2.33	0.02	2.62	0.02
1.67	0.05	1.97	0.05	2.62	0.05	2.99	0.05
1.97	0.10	2.21	0.10	2.93	0.10	3.70	0.10
2.84	0.20	3.38	0.20	10.28	0.20	13.28	0.20

*V – vapour phase, L – liquid phase, E –equilibrium, BP – bubble point

Table 8. Isothermal vapor-liquid equilibrium (VLE-BP) of ChCl:MAL (1) + CO_2 (2) system in four temperatures.

298.15 K		**303.15 K**		**318.15 K**		**333.15 K**	
P (MPa)	x_2	**P (MPa)**	x_2	**P (MPa)**	x_2	**P (MPa)**	x_2
	0.01	0.24	0.01	0.63	0.01	0.94	0.01
1.13	0.05	1.71	0.05	2.18	0.05	2.75	0.05
1.91	0.08	2.60	0.08	3.52	0.08	4.43	0.08
0.42	0.10	1.52	0.10	2.07	0.10	3.69	0.10

*V – vapour phase, L – liquid phase, E –equilibrium, BP – bubble point

A comparison between the results of this work with those of Haghtalab and Ghahremani (2015)[63] can be seen in Figure 3. In their work, the CO_2 solubility in N-methyldiethanolaminen (MDEA) + 2-amino-2-methyl-1-propanol (AMP) + piperazine (PZ) was measured in a high-pressure cell in a composition of (25+10+15) wt% at several temperatures and up to 4 MPa. Alkanolamines as MDEA are commonly used to remove gas contaminants, PZ acts as a chemical activator and AMP is a steric amine which is the hindered form of MEA, both enhancing the CO_2 absorption rates[63]. It is possible to observe that the CO_2 solubility in the six DESs is lower than the CO_2 solubility reported in the literature. The different absorption mechanisms are the reason for such a difference in alkanolamines solution both chemisorption and physisorption act, whereas in the studied DESs CO_2 is only physically absorbed[64].

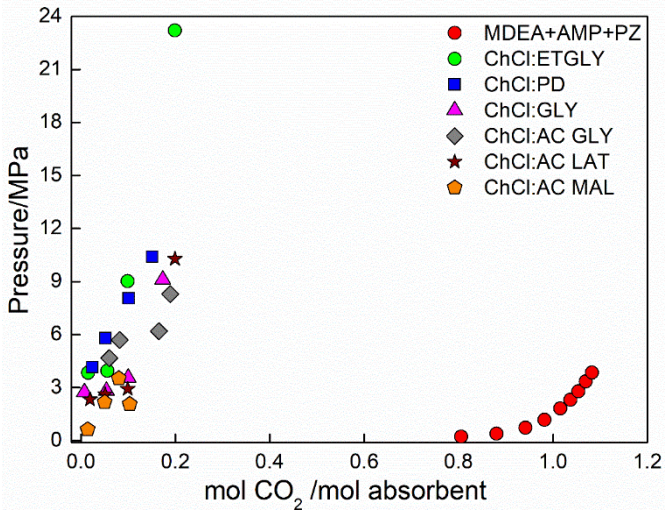

Figure 3. Comparison between CO_2 solubility in the six DESs studied in this work at 318.15 K and in MDEA+AMP+PZ (25+10+15) wt%[63] at 313.15 K.

Another interesting comparison can be made between the own studied DESs, comparing those DES in which alcohol compounds are HBDs with those in which carboxylic acids are HBDs (Figure 4) as ChCl is the HBA for all solvents. One can observe in Figure 4(A) that the DESs are arranged in decreasing order in terms of their CO_2 solubility as follows: ChCl:GLY > ChCl:PD ≅ ChCl:ETGLY. A possible explanation is related to the excess molar volume of each DES: the higher the value of excess molar volume, the higher the solubility of CO_2 as shown in Table 9. The increase in the alkyl chain length, i.e., the enhancement in the free volume in ChCl:GLY also improves the CO_2 absorption capacity. Similarly, in Figure 4(B) the descending order in terms of CO_2 solubility in carboxylic acid-based DES was ChCl:AC MAL > ChCl:AC LAT > ChCl:AC GLY. In this case, the increase in the alkyl chain length (from glycolic acid to lactic and malonic acid) enhanced the CO_2 solubility.

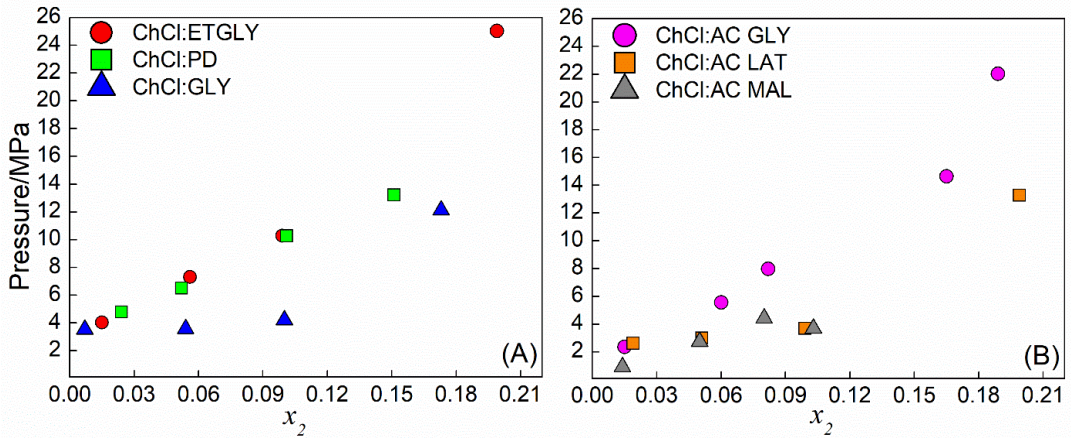

Figure 4. Comparison between the CO_2 solubility of the studied DESs (A) containing alcohol as HBDs and (B) containing carboxylic acids as HBDs.

Table 9. Excess molar volume of the studied DESs in this work.

DESs	Excess Molar volume ($cm^3.mol^{-1}$)
ChCl:ETGLY	-0.73
ChCl:GLY	-1.62
ChCl:PD	-0.66

It is also important to compare the influence of DESs precursors (HBA and/or HBDs) on CO_2 solubility to understand if there is any benefit in using DESs. For that, it was used Global Phase Equilibrium Calculations (GPEC), a computer program that allows the calculation of phase diagrams and other thermodynamic plots for binary systems using equations of state[65,66]. The calculation results are presented in Table 10 and Figures 5 and 6 show a comparison between the experimental data of CO_2 solubility in ChCl:GLY and ChCl:AC GLY DESs, and the predicted CO_2 solubility in GLY and AC GLY using Peng-Robinson EoS. Moreover, the binary interaction parameter (k_{ij}) was assumed to be equal to zero and the data were analyzed at 318.15 K and 333.15 K. It is possible to observe that in both cases and temperatures, the predicted CO_2 solubility in the HBDs is higher than the experimental CO_2 solubility in their respective DESs. The difference between the solubilities increases at higher temperatures, for example, the pressure difference in the CO_2 solubility between

ChCl:GLY and GLY at 0.06 CO_2 molar ratio and 318.15 and 333.15 K are 2.90 MPa and 3.33 MPa, respectively. This also occurs for ChCl:AC GLY and AC GLY when the CO_2 molar ratio is increased.

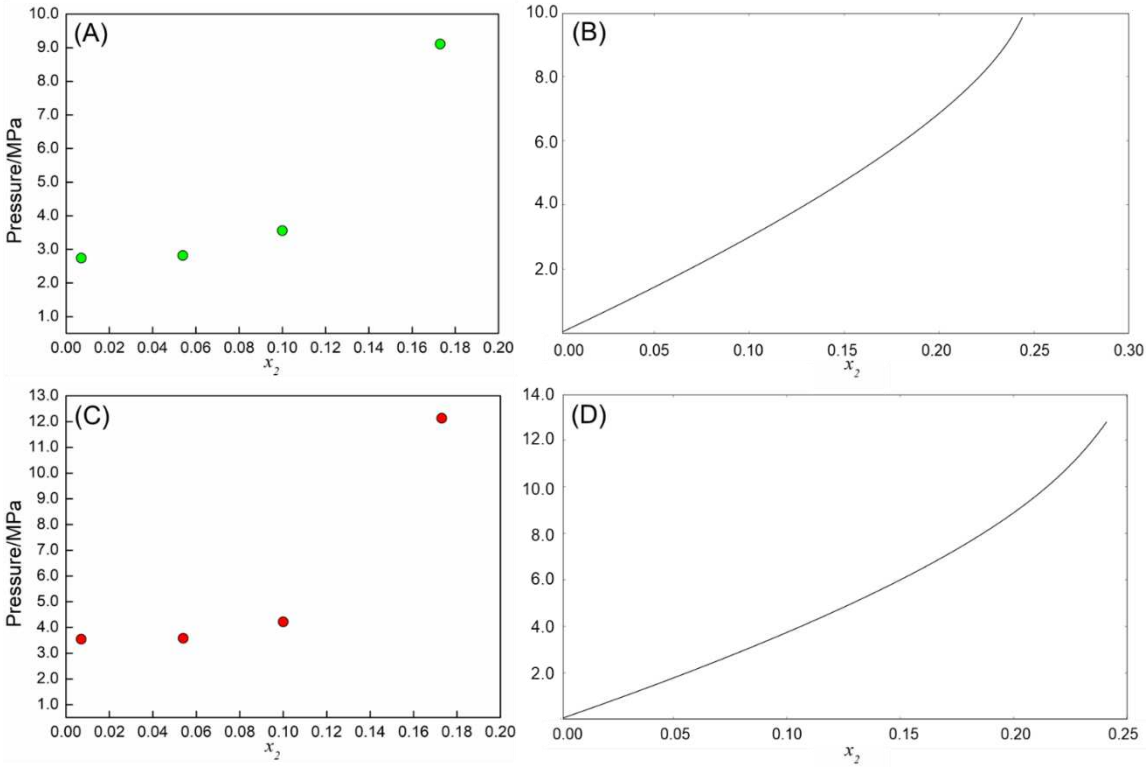

Figure 5. CO_2 solubility in (A) ChCl:GLY at 318.15 K; (B) GLY at 318.15 K; (C) ChCl:GLY at 333.15 K; (D) GLY at 333.15 K. The symbols represent the experimental data of this work, and the lines represent the predicted data using Peng-Robinson considering $k_{ij} = 0$ though GPEC software.

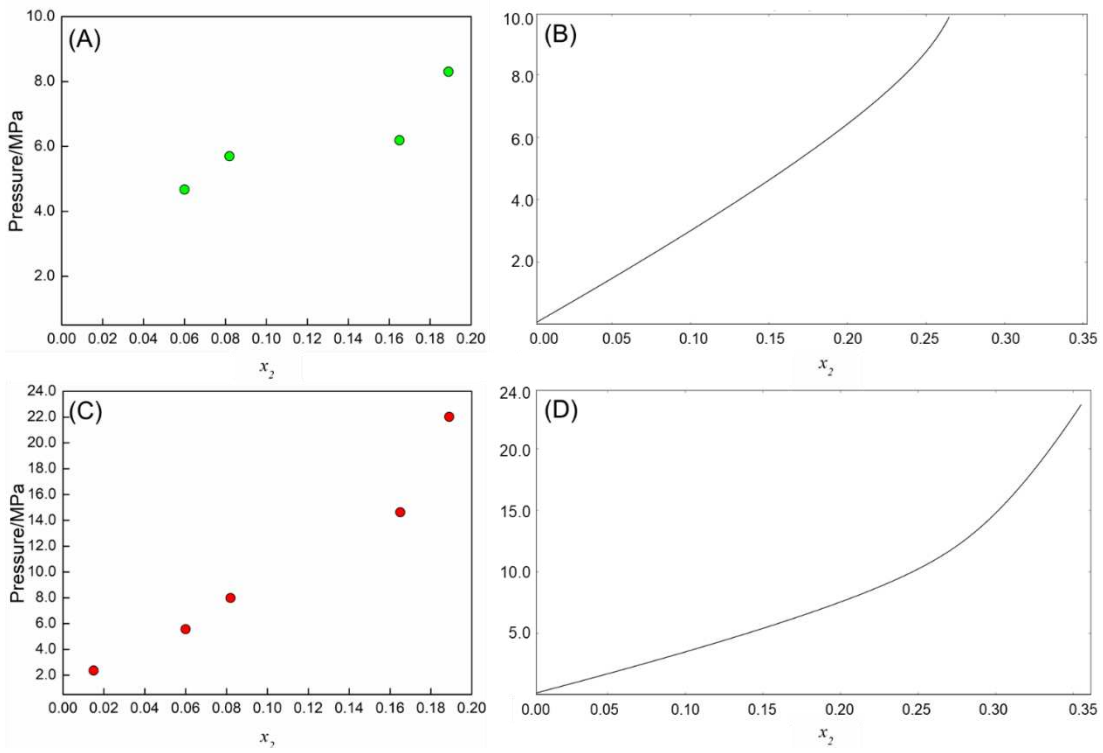

Figure 6. CO_2 solubility in (A) ChCl:AC GLY at 318.15 K; (B) AC GLY at 318.15 K; (C) ChCl:AC GLY at 333.15 K; (D) AC GLY at 333.15 K. The symbols represent the experimental data of this work, and the lines represent the predicted data using Peng-Robinson EoS considering $k_{ij} = 0$ though GPEC software.

A study conducted by Alizadeh, Esser and Kirchner (2021)[67] analyzed the interaction between CO_2 and ChCl:ETGLY using *ab initio* molecular dynamic simulations (AIMD) under two pressure levels to better understand the CO_2 absorption in DES. They found a strong anion (Cl^-) and HBD effect and a minor cation (Ch^+) effect on CO_2 absorption. It was expected cooperation between the anion and HBD, however, competition between them was indicated. This should be the reason why CO_2 solubility in pure HBD compounds is always higher than in DESs as shown in Table 10 and Figures 5 and 6.

Table 10. Comparison between the experimental data of CO_2 solubility in the two DESs determined in this work and the CO_2 solubility in the HBDs of the studied DESs obtained through GPEC software using Peng-Robinson EoS and considering $k_{ij} = 0$.

x_{CO2}	ChCl:GLY + CO_2 (MPa)		GLY + CO_2 (MPa)		x_{CO2}	ChCl:AC GLY + CO_2 (MPa)		AC GLY + CO_2 (MPa)	
	318.00 K	333.18 K	318.00 K	333.18 K		318.08 K	333.43 K	318.08 K	333.43 K
0.01	2.74	3.54	0.25	0.38	0.02	-	2.36	0.43	0.57
0.05	2.82	3.58	1.48	1.79	0.06	4.67	5.57	1.77	2.24
0.10	3.56	4.22	2.95	3.79	0.08	5.70	7.98	2.42	2.90
0.17	9.11	12.13	5.52	7.08	0.16	6.19	14.63	5.14	6.01
-	-	-	-	-	0.19	8.30	22.03	6.30	7.20

4.2. Thermodynamic properties

Henry's law constant and Gibbs energy are important parameters to understand the gas solubility in a solvent. These properties were calculated and are shown in Table 11. Since solubility and Henry's law constant are inversely proportional, it was expected that the constants increased with temperature raise for all DESs and decreased with pressure raise.

Also, the standard Gibbs energies were calculated, and their positive values indicate a nonspontaneous process of the CO_2 solubility in all studied DESs. By the temperature increase, one can observe that the positive values of $\Delta_{dis}G$ becomes higher, moving the process to a more nonspontaneous state, due to the low capacity of DES to absorb CO_2 at high temperatures[36].

Table 11. Calculated values of Henry's law constant and change in Gibbs energy of CO_2 – DESs.

CO_2 – DES	Temperature (K)	Pressure (MPa)	$H_x(P,T)$ (MPa)	$\Delta_{dis}G$ (kJ.mol^{-1})
ChCl:ETGLY	333.15	4.03	97.30	19.08
		7.31	20.68	14.78
		10.29	7.77	12.07
		25.02	0.23	23.03
	318.15	3.84	79.43	17.66
		3.96	21.15	14.16
		9.02	5.83	10.75
		23.21	0.10	-0.35
	303.15	2.94	66.06	16.38
		3.01	17.65	13.05
		4.66	8.40	11.17
		17.58	0.13	71.13
	298.15	2.76	61.72	15.94
		2.54	16.60	12.68
		3.29	9.03	11.17
		11.38	0.63	45.79
ChCl:PD	333.15	4.80	51.42	17.30
		6.51	19.85	14.67
		10.28	5.55	11.13
		13.23	2.08	8.41
	318.15	4.15	41.82	15.97
		5.79	15.37	13.32
		8.05	5.08	10.39
		10.40	1.96	7.87
	303.15	3.50	34.19	14.72
		4.73	12.80	12.24
		6.37	4.50	9.61
		9.08	1.40	6.65
	298.15	3.43	31.36	14.28
		4.07	12.943	12.08
		5.75	4.483	9.44
		8.88	1.162	6.09
ChCl:GLY	333.15	12.13	0.65	5.20
		4.22	8.29	12.24
		3.58	16.69	14.18

		3.54	129.28	19.85
		9.11	0.74	5.27
	318.15	3.56	6.71	11.12
		2.82	13.92	13.05
		2.74	108.32	18.47
		7.72	0.74	5.27
	303.15	2.67	6.71	11.12
		2.12	13.92	13.05
		1.80	108.32	18.47
	298.15	6.77	0.61	4.46
		2.35	5.53	9.95
		22.03	0.18	16.87
		14.63	1.22	6.94
	333.15	11.73	4.24	10.39
		7.98	9.39	12.59
		5.57	18.17	14.42
		2.36	78.84	18.49
		8.51	4.72	10.19
		8.30	2.33	8.33
	318.15	6.19	4.20	9.89
		5.70	9.26	11.98
ChCl:AC GLY		4.67	14.93	13.24
		6.26	2.28	7.88
		4.34	7.61	10.93
		4.10	8.65	11.25
	303.15	4.02	4.37	9.52
		3.99	12.06	12.09
		1.33	50.19	15.68
		3.82	7.46	10.69
	298.15	3.28	12.17	11.91
		3.11	9.13	11.19
		2.62	59.98	17.73
	333.15	2.99	22.66	15.03
		3.70	11.53	13.16
ChCl:AC LAT		13.28	0.98	6.32
		2.33	50.36	16.47
	318.15	2.62	18.89	13.87
		2.93	9.66	12.10

		10.28	1.02	6.14
		1.80	41.23	15.19
	303.15	1.97	15.53	12.73
		2.21	8.03	11.07
		3.38	3.56	9.01
		1.67	14.33	12.31
	298.15	1.97	7.50	10.71
		2.84	3.50	8.82
		0.94	48.47	17.14
	333.15	2.75	21.20	14.84
		3.69	9.97	12.75
		4.43	11.93	13.25
		0.63	34.57	15.44
	318.15	2.07	8.45	11.72
		2.18	17.50	13.65
ChCl:AC MAL		3.52	10.07	12.19
		0.24	15.02	12.64
	303.15	1.52	6.85	10.66
		1.71	14.44	12.54
		2.60	8.76	11.28
		0.42	3.27	8.66
	298.15	1.13	12.31	11.95
		1.91	8.55	11.04

5. Conclusions

In this work, the CO_2 solubility in six DESs (ChCl:ETGLY, ChCl:PD, ChCl:GLY, ChCl:AC GLY, ChCl:AC LAT, and ChCl:AC MAL) was determined at 298.15, 303.15, 318.15 and 333.15 K to enhance the literature on the thermophysical properties of DESs. Henry's law constants and the standard Gibbs energy were calculated.

In all cases, the CO_2 solubility increases with the pressure raise and decreases with temperature raise as expected, obtaining higher solubilities at high pressures and low temperatures. Henry's law constants agree with these results, with higher values at higher temperatures and small values at higher pressures.

The absorbed amount of CO_2 in all DESs was small, and not higher than 0.20 mol CO_2/mol DES, probably due to its high viscosity which hinders the mass transfer and the quasi-ideal behavior of solid-liquid phase diagrams of DESs. Comparing the experimental results with those from the literature on CO_2 solubility in more common solvents, the absorption capacity is up to 1.5 times smaller.

A comparison between the experimental CO_2 solubility in ChCl:GLY and ChCl:AC GLY and predicted CO_2 solubility in their pure HBDs shows that the solubility in the precursors is higher than in their DESs.

The CO_2 solubility in alcohol-based DESs was arranged as follows: ChCl:GLY > ChCl:PD ≅ ChCl: ETGLY because of the excess molar volume values, since the higher the value, the higher the solubility, and due to the higher alkyl chain length in ChCl:GLY. Whereas the CO_2 solubility in carboxylic acid-based DESs was organized as ChCl:AC MAL > ChCl:AC LAT > ChCl:AC GLY because of the alkyl chain length increase.

Acknowledgments

The authors would like to thank the São Paulo Research Foundation (FAPESP – 2018/19198-9 and 2014/21252-0), Coordination for the Improvement of Higher Education Personnel - Brasil (CAPES) – Finance Code 001, the National Council for Scientific and Technological Development (CNPq – 306666/2020-0), and the Fund for the Support of Education, Research and Extension (FAEPEX/ UNICAMP) for the financial support. The authors also thank the Human Resources Program of the National Agency of Petroleum, Natural Gas and Biofuels (PRH-ANP); and the Espaço da Escrita – Pró-Reitoria de Pesquisa - UNICAMP – for the language services provided.

References

(1) Smith, E. L.; Abbott, A. P.; Ryder, K. S. Deep Eutectic Solvents (DESs) and Their Applications. *Chem. Rev.* **2014**, *114* (21), 11060–11082. https://doi.org/10.1021/cr300162p.

(2) Zubeir, L. F.; Van Osch, D. J. G. P.; Rocha, M. A. A.; Banat, F.; Kroon, M. C. Carbon Dioxide Solubilities in Decanoic Acid-Based Hydrophobic Deep Eutectic Solvents. *J. Chem. Eng. Data* **2018**, *63*, 913–919. https://doi.org/10.1021/acs.jced.7b00534.

(3) Hansen, B. B.; Spittle, S.; Chen, B.; Poe, D.; Zhang, Y.; Klein, J. M.; Horton, A.; Adhikari, L.; Zelovich, T.; Doherty, B. W.; Gurkan, B.; Maginn, E. J.; Ragauskas, A.; Dadmun, M.; Zawodzinski, T. A.; Baker, G. A.; Tuckerman, M. E.; Savinell, R. F.; Sangoro, J. R. Deep Eutectic Solvents: A Review of Fundamentals and Applications. *Chem. Rev.* **2021**, *121* (3), 1232–1285. https://doi.org/10.1021/acs.chemrev.0c00385.

(4) Haghbakhsh, R.; Keshtkar, M.; Shariati, A.; Raeissi, S. Experimental Investigation of Carbon Dioxide Solubility in the Deep Eutectic Solvent (1 ChCl + 3 Triethylene Glycol) and Modeling by the CPA EoS. *J. Mol. Liq.* **2021**, *330*, 1–12. https://doi.org/10.1016/j.molliq.2021.115647.

(5) Mulvihill, M. J.; Beach, E. S.; Zimmerman, J. B.; Anastas, P. T. Green Chemistry and Green Engineering: A Framework for Sustainable Technology Development. *Annu. Rev. Environ. Resour.* **2011**, *36* (1), 271–293. https://doi.org/10.1146/annurev-environ-032009-095500.

(6) MartinsM., M. A. R.; Pinho, S. P.; Coutinho, J. A. P. Insights into the Nature of Eutectic and Deep Eutectic Mixtures. *J. Solution Chem.* **2018**, 1–21. https://doi.org/10.1007/s10953-018-0793-1.

(7) Mota-Morales, J. D.; Gutiérrez, M. C.; Ferrer, M. L.; Sanchez, I. C.; Elizalde-Peña, E. A.; Pojman, J. A.; Monte, F. Del; Luna-Bárcenas, G. Deep Eutectic Solvents as Both Active Fillers and Monomers for Frontal Polymerization. *J. Polym. Sci. Part A Polym. Chem.* **2013**, *51* (8), 1767–1773. https://doi.org/10.1002/pola.26555.

(8) Loow, Y.-L.; Wu, T. Y.; Yang, G. H.; Ang, L. Y.; New, E. K.; Siow, L. F.; Md. Jahim, J.; Mohammad, A. W.; Teoh, W. H. Deep Eutectic Solvent and Inorganic Salt Pretreatment of Lignocellulosic Biomass for Improving Xylose Recovery. *Bioresour. Technol.* **2018**, *249*, 818–825. https://doi.org/10.1016/j.biortech.2017.07.165.

(9) Loow, Y.-L.; New, E. K.; Yang, G. H.; Ang, L. Y.; Foo, L. Y. W.; Wu, T. Y. Potential Use of Deep Eutectic Solvents to Facilitate Lignocellulosic Biomass Utilization and Conversion. *Cellulose* **2017**, *24* (9), 3591–3618. https://doi.org/10.1007/s10570-017-1358-y.

(10) Yang, T.-X.; Zhao, L.-Q.; Wang, J.; Song, G.-L.; Liu, H.-M.; Cheng, H.; Yang, Z. Improving Whole-Cell Biocatalysis by Addition of Deep Eutectic Solvents and Natural Deep Eutectic Solvents. *ACS Sustain. Chem. Eng.* **2017**, *5* (7), 5713–5722. https://doi.org/10.1021/acssuschemeng.7b00285.

(11) Warrag, S. E. E.; Darwish, A. S.; Adeyemi, I. A.; Hadj-Kali, M. K.; Kroon, M. C.; AlNashef, I. M. Extraction of Pyridine from N-Alkane Mixtures Using Methyltriphenylphosphonium Bromide-Based Deep Eutectic Solvents as Extractive Denitrogenation Agents. *Fluid Phase Equilib.* **2020**, *517*, 112622. https://doi.org/10.1016/j.fluid.2020.112622.

(12) Jiao, T.; Qin, X.; Zhang, H.; Zhang, W.; Zhang, Y.; Liang, P. Separation of Phenol and Pyridine from Coal Tar via Liquid–Liquid Extraction Using Deep Eutectic Solvents. *Chem. Eng. Res. Des.* **2019**, *145*, 112–121.

https://doi.org/10.1016/j.cherd.2019.03.006.

(13) Wojeicchowski, J. P.; Marques, C.; Igarashi-Mafra, L.; Coutinho, J. A. P.; Mafra, M. R. Extraction of Phenolic Compounds from Rosemary Using Choline Chloride – Based Deep Eutectic Solvents. *Sep. Purif. Technol.* **2021**, *258*, 1–8. https://doi.org/10.1016/j.seppur.2020.117975.

(14) Rogošić, M.; Krišto, A.; Kučan, K. Z. DEEP EUTECTIC SOLVENTS BASED ON BETAINE AND PROPYLENE GLYCOL AS POTENTIAL DENITRIFICATION AGENTS: A LIQUID-LIQUID EQUILIBRIUM STUDY. *Brazilian J. Chem. Eng.* **2019**, *36* (4), 1703–1716. https://doi.org/10.1590/0104-6632.20190364s20190049.

(15) Li, T.; Xiong, Y.; Yan, X.; Hu, T.; Jing, S.; Wang, Z.; Ge, X. Closed-Loop Cobalt Recycling from Spent Lithium-Ion Batteries Based on a Deep Eutectic Solvent (DES) with Easy Solvent Recovery. *J. Energy Chem.* **2022**, *72*, 532–538. https://doi.org/10.1016/j.jechem.2022.05.008.

(16) Li, B.; Li, Q.; Wang, Q.; Yan, X.; Shi, M.; Wu, C. Deep Eutectic Solvent for Spent Lithium-Ion Battery Recycling: Comparison with Inorganic Acid Leaching. *Phys. Chem. Chem. Phys.* **2022**, *24* (32), 19029–19051. https://doi.org/10.1039/D1CP05968H.

(17) Lu, B.; Du, R.; Wang, G.; Wang, Y.; Dong, S.; Zhou, D.; Wang, S.; Li, C. High-Efficiency Leaching of Valuable Metals from Waste Li-Ion Batteries Using Deep Eutectic Solvents. *Environ. Res.* **2022**, *212*, 113286. https://doi.org/10.1016/j.envres.2022.113286.

(18) Dong, J.-Y.; Lin, C.-H.; Hsu, Y.-J.; Lu, S.-Y.; Wong, D. S.-H. Single-Crystalline Mesoporous ZnO Nanosheets Prepared with a Green Antisolvent Method Exhibiting Excellent Photocatalytic Efficiencies. *CrystEngComm* **2012**, *14* (14), 4732. https://doi.org/10.1039/c2ce06739k.

(19) Mohammadpour, Z.; Abdollahi, S. H.; Safavi, A. Sugar-Based Natural Deep Eutectic Mixtures as Green Intercalating Solvents for High-Yield Preparation of Stable MoS 2 Nanosheets: Application to Electrocatalysis of Hydrogen Evolution Reaction. *ACS Appl. Energy Mater.* **2018**, *1* (11), 5896–5906. https://doi.org/10.1021/acsaem.8b00838.

(20) Adhikari, L.; Larm, N. E.; Baker, G. A. Argentous Deep Eutectic Solvent Approach for Scaling Up the Production of Colloidal Silver Nanocrystals. *ACS Sustain. Chem. Eng.* **2019**, *7* (13), 11036–11043. https://doi.org/10.1021/acssuschemeng.9b01777.

(21) Pishro, K. A.; Murshid, G.; Mjalli, F. S.; Naser, J. Carbon Dioxide Solubility in Amine-Based Deep Eutectic Solvents: Experimental and Theoretical Investigation. *J. Mol. Liq.* **2021**, *325*, 115133. https://doi.org/10.1016/j.molliq.2020.115133.

(22) Sosa, F. H. B.; Costa, M. C.; Silvestre, A. J. D.; Costa Lopes, A. M. Deep Eutectic Solvents for Sustainable Separation Processes. *Sustain. Sep. Eng.* **2022**, *2*, 605–652. https://doi.org/10.1002/9781119740117.ch17.

(23) Scripps Institution of Oceanography. The Keeling Curve https://scripps.ucsd.edu/programs/keelingcurve/ (accessed Oct 6, 2022).

(24) Aravena, C.; Lee, D.; Park, J.; Yoo, Y. Characteristics of Deep Eutectic Solvents for CO2 Capture with Hydro Effects for Improvement of Mass Transfer. *J. Ind. Eng. Chem.* **2022**, *111*, 337–345. https://doi.org/10.1016/j.jiec.2022.04.015.

(25) Mirza, N. R.; Nicholas, N. J.; Wu, Y.; Mumford, K. A.; Kentish, S. E.; Stevens, G. W. Experiments and Thermodynamic Modeling of the Solubility of Carbon Dioxide in Three Different Deep Eutectic Solvents (DESs). *J. Chem. Eng. Data* **2015**, *60*, 3246–3252. https://doi.org/10.1021/acs.jced.5b00492.

(26) Taib, M. M.; Murugesan, T. Solubilities of CO2 in Aqueous Solutions of Ionic Liquids (ILs) and Monoethanolamine (MEA) at Pressures from 100 to 1600kPa. *Chem. Eng. J.* **2012**, *181–182*, 56–62. https://doi.org/10.1016/j.cej.2011.09.048.

(27) Garg, S.; Shariff, A. M.; Shaikh, M. S.; Lal, B.; Aftab, A.; Faiqa, N. VLE of CO 2 in Aqueous Potassium Salt of L-Phenylalanine: Experimental Data and Modeling Using Modified Kent-Eisenberg Model. *J. Nat. Gas Sci. Eng.* **2016**, *34*, 864–872. https://doi.org/10.1016/j.jngse.2016.07.047.

(28) Rabhi, F.; Mutelet, F.; Sifaoui, H. Solubility of Carbon Dioxide in Carboxylic Acid-Based Deep Eutectic Solvents. *J. Chem. Eng. Data* **2021**, *66*, 702–711. https://doi.org/10.1021/acs.jced.0c00844.

(29) Li, X.; Hou, M.; Han, B.; Wang, X.; Zou, L. Solubility of CO2 in a Choline Chloride + Urea Eutectic Mixture. *J. Chem. Eng. Data* **2008**, *53* (2), 548–550. https://doi.org/10.1021/je700638u.

(30) Qin, H.; Song, Z.; Cheng, H.; Deng, L.; Qi, Z. Physical Absorption of Carbon Dioxide in Imidazole-PTSA Based Deep Eutectic Solvents. *J. Mol. Liq.* **2021**, *326*, 1–7. https://doi.org/10.1016/j.molliq.2021.115292.

(31) Al-Bodour, A.; Alomari, N.; Gutiérrez, A.; Aparicio, S.; Atilhan, M. High-Pressure Carbon Dioxide Solubility in Terpene Based Deep Eutectic Solvents. *J. Environ. Chem. Eng.* **2022**, *10* (5), 108237. https://doi.org/10.1016/j.jece.2022.108237.

(32) Liu, X.; Ao, Q.; Shi, S.; Li, S. CO2capture by Alcohol Ammonia Based Deep Eutectic Solvents with Different Water Content. *Mater. Res. Express* **2022**, *9* (1). https://doi.org/10.1088/2053-1591/ac47c6.

(33) Sarmad, S.; Nikjoo, D.; Mikkola, J. P. Amine Functionalized Deep Eutectic Solvent for CO2 Capture: Measurements and Modeling. *J. Mol. Liq.* **2020**, *309*,

113159. https://doi.org/10.1016/j.molliq.2020.113159.

(34) Haider, M. B.; Jha, D.; Kumar, R.; Marriyappan Sivagnanam, B. Ternary Hydrophobic Deep Eutectic Solvents for Carbon Dioxide Absorption. *Int. J. Greenh. Gas Control* **2020**, *92* (September 2019), 102839. https://doi.org/10.1016/j.ijggc.2019.102839.

(35) Siani, G.; Tiecco, M.; Di Profio, P.; Guernelli, S.; Fontana, A.; Ciulla, M.; Canale, V. Physical Absorption of CO2 in Betaine/Carboxylic Acid-Based Natural Deep Eutectic Solvents. *J. Mol. Liq.* **2020**, *315*, 1–7. https://doi.org/10.1016/j.molliq.2020.113708.

(36) Haghbakhsh, R.; Keshtkar, M.; Shariati, A.; Raeissi, S. A Comprehensive Experimental and Modeling Study on CO2 Solubilities in the Deep Eutectic Solvent Based on Choline Chloride and Butane-1,2-Diol. *Fluid Phase Equilib.* **2022**, *561* (March), 113535. https://doi.org/10.1016/j.fluid.2022.113535.

(37) Haider, M. B.; Kumar, R. Solubility of CO2 and CH4 in Sterically Hindered Amine-Based Deep Eutectic Solvents. *Sep. Purif. Technol.* **2020**, *248*, 117055. https://doi.org/10.1016/j.seppur.2020.117055.

(38) Ali, E.; Hadj-Kali, M. K.; Mulyono, S.; Alnashef, I.; Fakeeha, A.; Mjalli, F.; Hayyan, A. Solubility of CO2 in Deep Eutectic Solvents: Experiments and Modelling Using the Peng-Robinson Equation of State. *Chem. Eng. Res. Des.* **2014**, *92* (10), 1898–1906. https://doi.org/10.1016/j.cherd.2014.02.004.

(39) Haider, M. B.; Jha, D.; Marriyappan Sivagnanam, B.; Kumar, R. Thermodynamic and Kinetic Studies of CO2 Capture by Glycol and Amine-Based Deep Eutectic Solvents. *J. Chem. Eng. Data* **2018**, *63*, 2671–2680. https://doi.org/10.1021/acs.jced.8b00015.

(40) Zubeir, L. F.; Held, C.; Sadowski, G.; Kroon, M. C. PC-SAFT Modeling of CO2 Solubilities in Deep Eutectic Solvents. *J. Phys. Chem. B* **2016**, *120*, 2300–2310. https://doi.org/10.1021/acs.jpcb.5b07888.

(41) Dietz, C. H. J. T.; van Osch, D. J. G. P.; Kroon, M. C.; Sadowski, G.; van Sint Annaland, M.; Gallucci, F.; Zubeir, L. F.; Held, C. PC-SAFT Modeling of CO2 Solubilities in Hydrophobic Deep Eutectic Solvents. *Fluid Phase Equilib.* **2017**, *448*, 94–98. https://doi.org/10.1016/j.fluid.2017.03.028.

(42) Pelaquim, F. P.; Bitencourt, R. G.; Neto, A. M. B.; Dalmolin, I. A. L.; da Costa, M. C. Carbon Dioxide Solubility in Deep Eutectic Solvents: Modelling Using Cubic Plus Association and Peng-Robinson Equations of State. *Process Saf. Environ. Prot.* **2022**, *163*, 14–26. https://doi.org/10.1016/j.psep.2022.04.075.

(43) Haghbakhsh, R.; Raeissi, S. Modeling the Phase Behavior of Carbon Dioxide Solubility in Deep Eutectic Solvents with the Cubic Plus Association Equation of State. *J. Chem. Eng. Data* **2018**, *63* (4), 897–906. https://doi.org/10.1021/acs.jced.7b00472.

(44) Fernandez, L.; Silva, L. P.; Martins, M. A. R.; Ferreira, O.; Ortega, J.; Pinho, S. P.; Coutinho, J. A. P. Indirect Assessment of the Fusion Properties of Choline Chloride from Solid-Liquid Equilibria Data. *Fluid Phase Equilib.* **2017**, *448*, 9–14. https://doi.org/10.1016/j.fluid.2017.03.015.

(45) Daubert, T. E.; Sibul, H. M.; Stebbins, C. C.; Danner, R. P.; Rowley, R. L.; Adams, M. E.; Wilding, W. V; Marshall, T. L. *Physical and Thermodynamic Properties of Pure Chemicals: DIPPR: Data Compilation: Core + Supplements 1−10*; Taylor & Francis, 2000.

(46) Jabrane, S.; Létoffé, J. .; Claudy, P. Study of the Thermal Behaviour of 1,3-

Propanediol and Its Aqueous Solutions. *Thermochim. Acta* **1998**, *311* (1–2), 121–127. https://doi.org/10.1016/S0040-6031(97)00416-4.

(47) Emel'yanenko, V. N.; Verevkin, S. P.; Stepurko, E. N.; Roganov, G. N.; Georgieva, M. K. Thermodynamic Properties of Glycolic Acid and Glycolide. *Russ. J. Phys. Chem. A* **2010**, *84* (8), 1301–1308. https://doi.org/10.1134/S0036024410080054.

(48) Domalski, E. S.; Hearing, E. D. Heat Capacities and Entropies of Organic Compounds in the Condensed Phase. Volume III. *J. Phys. Chem. Ref. Data* **1996**, *25* (1), 1–525. https://doi.org/10.1063/1.555985.

(49) Hansen, A. R.; Beyer, K. D. Experimentally Determined Thermochemical Properties of the Malonic Acid/Water System: Implications for Atmospheric Aerosols. *J. Phys. Chem. A* **2004**, *108* (16), 3457–3466. https://doi.org/10.1021/jp0376166.

(50) Crespo, E. A.; Silva, L. P.; Martins, M. A. R.; Bülow, M.; Ferreira, O.; Sadowski, G.; Held, C.; Pinho, S. P.; Coutinho, J. A. P. The Role of Polyfunctionality in the Formation of [Ch]Cl-Carboxylic Acid-Based Deep Eutectic Solvents. *Ind. Eng. Chem. Res.* **2018**, *57* (32), 11195–11209. https://doi.org/10.1021/acs.iecr.8b01249.

(51) Silva, L. P.; Martins, M. A. R.; Conceição, J. H. F.; Pinho, S. P.; Coutinho, J. A. P. Eutectic Mixtures Based on Polyalcohols as Sustainable Solvents: Screening and Characterization. *ACS Sustain. Chem. Eng.* **2020**, *8*, 15317–15326. https://doi.org/10.1021/acssuschemeng.0c05518.

(52) Abbott, A. P.; Capper, G.; Davies, D. L.; Rasheed, R. K.; Tambyrajah, V. Novel Solvent Properties of Choline Chloride / Urea Mixtures. *R. Soc. Chem.* **2003**, 70–71. https://doi.org/10.1039/B210714G.

(53) Santos, N. G. O.; Rebelatto, E. A.; Mayer, D. A.; Lanza, M.; Vladimir Oliveira, J.

High-Pressure Phase Behavior of the Quaternary System (Carbon Dioxide + Dichloromethane + E–caprolactone + Poly(E–caprolactone): Experimental Data and PC-SAFT Modeling. *Fluid Phase Equilib.* **2022**, *554*, 113306. https://doi.org/10.1016/j.fluid.2021.113306.

(54) Favareto, R.; de Araujo, P. C. C.; Bezerra, I. D.; Zanette, A. F.; Arce, P. F.; Ferreira-Pinto, L.; Cardozo-Filho, L. Experimental Data and Thermodynamics Modeling (PC-SAFT EoS) of the {CO2 + Chloroform + PHBV} System at High Pressures. *J. Supercrit. Fluids* **2021**, *170*, 105140. https://doi.org/10.1016/j.supflu.2020.105140.

(55) Vogelpohl, C.; Brandenbusch, C.; Sadowski, G. High-Pressure Gas Solubility in Multicomponent Solvent Systems for Hydroformylation. Part I: Carbon Monoxide Solubility. *J. Supercrit. Fluids* **2013**, *81*, 23–32. https://doi.org/10.1016/j.supflu.2013.04.006.

(56) Charin, R. M.; Corazza, M. L.; Ndiaye, P. M.; Mazutti, M. A.; Oliveira, J. V. Phase Equilibrium Data and Thermodynamic Modeling of the System Propane+NMP+methanol at High Pressures. *J. Supercrit. Fluids* **2010**, *55* (1), 23–31. https://doi.org/10.1016/j.supflu.2010.08.017.

(57) Thomson, G. H.; Brobst, K. R.; Hankinson, R. W. An Improved Correlation for Densities of Compressed Liquids and Liquid Mixtures. *AIChE J.* **1982**, *28* (4), 671–676. https://doi.org/10.1002/aic.690280420.

(58) Prausnitz, J. M.; Lichtenthaler, R. N.; de Azevedo, E. G. *Molecular Thermodynamics of Fluid-Phase Equilibria*, 3rd ed.; Prentice Hall: Nova Jersey, 1999. https://doi.org/10.1016/0021-9614(70)90078-9.

(59) Shahbaz, K.; Mjalli, F. S.; Vakili-Nezhaad, G.; AlNashef, I. M.; Asadov, A.; Farid,

M. M. Thermogravimetric Measurement of Deep Eutectic Solvents Vapor Pressure. *J. Mol. Liq.* **2016**, *222*, 61–66. https://doi.org/10.1016/j.molliq.2016.06.106.

(60) Aboshatta, M.; Magueijo, V. A Comprehensive Study of Co2 Absorption and Desorption by Choline-Chloride/Levulinic-Acid-Based Deep Eutectic Solvents. *Molecules* **2021**, *26* (18). https://doi.org/10.3390/molecules26185595.

(61) Leron, R. B.; Li, M. H. Solubility of Carbon Dioxide in a Choline Chloride-Ethylene Glycol Based Deep Eutectic Solvent. *Thermochim. Acta* **2013**, *551*, 14–19. https://doi.org/10.1016/j.tca.2012.09.041.

(62) Harifi-Mood, A. R.; Mohammadpour, F.; Boczkaj, G. Solvent Dependency of Carbon Dioxide Henry's Constant in Aqueous Solutions of Choline Chloride-Ethylene Glycol Based Deep Eutectic Solvent. *J. Mol. Liq.* **2020**, *319*, 114173. https://doi.org/10.1016/j.molliq.2020.114173.

(63) Haghtalab, A.; Ghahremani, E. The Solubility Measurement and Modeling of CO2 in Aqueous Solution of N-Methyldiethanolaminen+2-Amino-2-Methyl-1-Propanol+piperazine at High Pressures. *Fluid Phase Equilib.* **2015**, *400*, 62–75. https://doi.org/10.1016/j.fluid.2015.04.016.

(64) Chen, Y.; Ai, N.; Li, G.; Shan, H.; Cui, Y.; Deng, D. Solubilities of Carbon Dioxide in Eutectic Mixtures of Choline Chloride and Dihydric Alcohols. *J. Chem. Eng. Data* **2014**, *59*, 1247–1253. https://doi.org/10.1021/je400884v.

(65) Cismondi, M.; Michelsen, M. L. Global Phase Equilibrium Calculations: Critical Lines, Critical End Points and Liquid–Liquid–Vapour Equilibrium in Binary Mixtures. *J. Supercrit. Fluids* **2007**, *39* (3), 287–295. https://doi.org/10.1016/j.supflu.2006.03.011.

(66) Cismondi, M.; Michelsen, M. Automated Calculation of Complete Pxy and Txy Diagrams for Binary Systems. *Fluid Phase Equilib.* **2007**, *259* (2), 228–234.

https://doi.org/10.1016/j.fluid.2007.07.019.

(67) Alizadeh, V.; Esser, L.; Kirchner, B. How Is CO2absorbed into a Deep Eutectic Solvent? *J. Chem. Phys.* **2021**, *154* (9). https://doi.org/10.1063/5.0038093.

CAPÍTULO 8

CONCLUSÕES GERAIS

1. Conlusões Gerais

A presente tese contribuiu com a modelagem de dados da literatura relacionados a solubilidade de CO_2 e outros gases em mais de 15 ESs, utilizando as equações de estado Peng-Robinson e CPA, e também o *software* COSMO-RS. Além disso, dados de equilíbrio sólido-líquido a altas pressões, densidade a altas pressões e dados de solubilidade de CO_2 em seis ESs foram estudados utilizando uma célula de alta pressão de volume variável, com dados inéditos para a literatura.

Inicialmente, foi possível observer que as equações de estado Peng-Robinson e CPA conseguem descrever de maneira adequada o comportamento do CO_2 nos ESs, com desvios menores que 20% para a CPA e menores que 11% para a Peng-Robinson, quando otimizados os parâmetros de interação binária (k_{ij}). Além disso, é importante ressaltar que a abordagem do componente individual para os ESs apresenta melhores resultados, uma vez que esses solventes são considerados uma mistura e não um novo componente. A modelagem termodinâmica de dados de solubilidade de gases leves em ESs é de extrema importância, pois com as informações obtidas através da modelagem seria possível prever quais os melhores absorventes, uma vez que a quantidade de ESs existentes é muito grande. Entretanto, esses dados e a investigação de mais equações de estado ainda são escassos na literatura fazendo com que a predição para qualquer sistema entre gás e ES não seja possível.

O COSMO-RS é outro modelo que pode predizer a solubilidade de gases em ESs, entretanto não possui resultados tão acurados quanto as equações de estado, uma vez que ele não utiliza nenhum parâmetro e é uma ferramenta totalmente preditiva. Em altas pressões, o COSMO-RS também apresenta maiores desvios pois ele calcula apenas os coeficientes de atividade independentemente da pressão. Apesar disso, ele apresentou desvios médios absolutos menores que 0,21, podendo ser considerado um modelo mais qualitativo do que quantitativo, ou seja, pode ser usado uma pré-seleção dos melhores DESs que podem absorver os gases leves a fim de economizar tempo e custos, que é ainda pouco visto pela literatura.

Já experimentalmente, os diagramas de fase sólido-líquido dos solventes eutéticos são de grande importância para a determinação das melhores condições desses solventes e também para definir se ele é de fato um ES. Nesse trabalho, foram

determinados os diagramas sólido-líquido de seis ESs (ChCl + etilenoglicol, + glicerol, + 1,3 propanodiol, + ácido glicólico, + ácido lático e + ácido malônico) em altas pressões pela primeira vez na literatura. Todos os sistemas apresentaram o mesmo comportamento observado à pressão atmosférica, ou seja, um único ponto eutético, com a composição eutética não alterando com o aumento da pressão. O aumento da temperatura de fusão é relativamente pequeno entre as pressões 6 - 25 MPa, mas grande entre 0,1 - 6 MPa uma vez que o aumento da pressão leva as misturas a estados de menor volume, fazendo com que a energia para a transição de fases seja mais elevada, bem como a temperatura de fusão.

A densidade é outra propriedade importante para os ESs. Em pressão atmosférica ela já foi amplamente estudada, porém, novamente em alta pressão poucos dados são encontrados na literatura. Nesta tese também foi determinada a densidade de 4 ESs (ChCl + etilenoglicol, + glicerol, + 1,3 propanodiol, e + ácido glicólico) em pressões entre 1 – 50 MPa e temperaturas entre 298,15 e 353,15 K. Obsevou-se que a densidade diminui com o aumento da temperatura e aumenta com o aumento da pressão, conforme esperado. Além disso, a equação Tammann-Tait modificada e a equação CPA foram utilizadas para correlacionar os dados experimentais. A primeira forneceu uma boa correlação apresentando AADs% menores do que 0,45%. A CPA mostrou desvios não superiores a 0,50%. Em comparação, a Tammann-Tait modificada apresentou melhores previsões, como esperado, uma vez que ela tem uma natureza preditiva e menos parâmetros.

Por fim, a solubilidade do CO_2 em seis DESs (ChCl + etilenoglicol, + glicerol, + 1,3 propanodiol, + ácido glicólico, + ácido lático e + ácido malônico) foi determinada em 298,15, 303,15, 318,15 e 333,15 K para enriquecer a literatura sobre as propriedades termofísicas dos DESs. Em todos os casos, a solubilidade do CO_2 aumenta com o aumento da pressão e diminui com o aumento da temperatura como esperado. As constantes da lei de Henry concordam com estes resultados, com valores mais elevados em temperaturas mais elevadas e com valores menores em maiores pressões. Além disso, a quantidade absorvida de CO_2 em todos os DESs foi pequena, e não superior a 0,20 mol CO_2/mol DES, provavelmente devido à sua elevada viscosidade, o que dificulta a transferência de massa. Comparando os

resultados experimentais com os da literatura relativos à solubilidade de CO_2 em solventes mais comuns, a capacidade de absorção é até 1,5 vezes inferior.

A determinação de dados experimentais do equilíbrio sólido-líquido e a densidade de ESs a altas pressões é de extrema importância para a literatura de modo a enriquece-la com mais propriedades termofísicas desses solventes, ainda não existentes, além de auxiliar na escolha dos melhores solventes na utilização de processos. A determinação de dados experimentais e a modelagem termodinâmica da solubilidade de CO_2 em ESs a altas pressões também preenche uma lacuna na literatura, e foi estudada de modo a tentar encontrar uma alternativa ambientavelmente amigável aos solventes orgânicos tradicionalmente utilizados na captura de CO_2 na CCS. Infelizmente, para os ESs estudados nessa tese, foi possível observar que eles não absorvem de maneira mais eficiente que os solventes comuns, não os tornando interessante para o fim pretendido. Entretanto, se faz necessário estudar diferentes tipos e famílias de ESs, como os hidrofóbicos, que já se mostraram mais eficientes, para que novas alternativas sejam encontradas.

2. Sugestões para trabalhos futuros

A partir da discussão deste trabalho é possível concluir que ainda existe uma diversidade muito grande de ESs a serem estudados através do equilíbrio sólido-líquido e da densidade tanto a pressão atmosférica quanto a altas pressões, além de diversas outras propriedades termofísicas. Esses estudos enriqueceriam o conhecimento sobre os sistemas contendo ESs e otimizariam diversos processos.

Com relação a solubilidade de gases leves em ESs, há a necessidade de determinar essa propriedade em outros tipos de ES, como por exemplo, os hidrofóbicos e hidrofílicos, a fim de verificar se há algum grupo de família que os ESs possam ser bons absorventes. Adicionado a isso, há uma lacuna na literatura com relação aos gases estudados, uma vez que a maioria dos estudos se concentram no CO_2, então seria interessante o estudo da solubilidade em outros gases, como o metano, etano, sulfeto de hidrogênio, nitrogênio e hidrogênio. E posteriormente, aplicá-los em maior escala.

Além disso, é preciso avaliar mais modelos termodinâmicos e equações de estado que consigam modelar os dados de solubilidade e também de densidade a altas pressões, para que se torne possível sem a necessidade de dados experimentais predizer quais seriam os melhores absorventes para a captura de gases.

3. Referência bibliográfica geral

2030 climate & energy framework [WWW Document], n.d. URL https://ec.europa.eu/clima/policies/strategies/2030_en (accessed 5.19.21).

A. Al-Bodour, N. Alomari, A. Gutiérrez, S. Aparicio, M. Atilhan, High-pressure carbon dioxide solubility in terpene based deep eutectic solvents, Journal of Environmental Chemical Engineering. 10 (2022) 108237. https://doi.org/10.1016/j.jece.2022.108237.

A. Hayyan, F.S. Mjalli, I.M. AlNashef, Y.M. Al-Wahaibi, T. Al-Wahaibi, M.A. Hashim, Glucose-based deep eutectic solvents: Physical properties, Journal of Molecular Liquids. 178 (2013) 137–141. https://doi.org/10.1016/j.molliq.2012.11.025.

A. Kamgar, S. Mohsenpour, F. Esmaeilzadeh, Solubility prediction of CO2, CH4, H2, CO and N2 in Choline Chloride/Urea as a eutectic solvent using NRTL and COSMO-RS models, J Mol Liq. 247 (2017) 70–74. https://doi.org/10.1016/j.molliq.2017.09.101.

A. Klamt, Conductor-like screening model for real solvents: A new approach to the quantitative calculation of solvation phenomena, Journal of Physical Chemistry. 99 (1995) 2224–2235. https://doi.org/10.1021/j100007a062.

A. Klamt, V. Jonas, T. Bürger, J.C.W. Lohrenz, Refinement and Parametrization of COSMO-RS, J Phys Chem A. 102 (1998) 5074–5085. https://doi.org/10.1021/jp980017s.

A. Paiva, R. Craveiro, I. Aroso, M. Martins, R.L. Reis, A.R.C. Duarte, Natural deep eutectic solvents - Solvents for the 21st century, ACS Sustain Chem Eng. 2 (2014) 1063–1071. https://doi.org/10.1021/sc500096j.

A. Yadav, S. Pandey, Densities and viscosities of (choline chloride + urea) deep eutectic solvent and its aqueous mixtures in the temperature range 293.15 K to 363.15 K, Journal of Chemical and Engineering Data. 59 (2014) 2221–2229. https://doi.org/10.1021/je5001796.

A. Yadav, S. Trivedi, R. Rai, S. Pandey, Densities and dynamic viscosities of (choline chloride+glycerol) deep eutectic solvent and its aqueous mixtures in the temperature range (283.15-363.15)K, Fluid Phase Equilibria. 367 (2014) 135–142. https://doi.org/10.1016/j.fluid.2014.01.028.

A.C. Kouakou, K. Le Mapihan, J. Pauly, Solid–liquid equilibria under high pressure of pure fatty acid methyl esters, Fuel. 109 (2013) 297–302. https://doi.org/10.1016/j.fuel.2013.01.036.

A.P. Abbott, D. Boothby, G. Capper, D.L. Davies, R.K. Rasheed, Deep Eutectic Solvents formed between choline chloride and carboxylic acids: Versatile alternatives to ionic liquids, Journal of the American Chemical Society. 126 (2004) 9142–9147. https://doi.org/10.1021/ja048266j.

A.R. Hansen, K.D. Beyer, Experimentally Determined Thermochemical Properties of the Malonic Acid/Water System: Implications for Atmospheric Aerosols, The Journal of Physical Chemistry A. 108 (2004) 3457–3466. https://doi.org/10.1021/jp0376166.

Aaron, D., Tsouris, C., 2005. Separation of CO2 from flue gas: A review. Sep. Sci. Technol. 40, 321–348. https://doi.org/10.1081/SS-200042244

ABBOTT, A. P. et al. Novel solvent properties of choline chloride / urea mixtures. The Royal Society of Chemistry, v. 1, p. 70–71, 2003.

Abdelkareem, M.A., El Haj Assad, M., Sayed, E.T., Soudan, B., 2018. Recent progress in the use of renewable energy sources to power water desalination plants. Desalination 435, 97–113. https://doi.org/10.1016/j.desal.2017.11.018

Abdul Halim, H.N., Shariff, A.M., Tan, L.S., Bustam, M.A., 2015. Mass transfer performance of CO2 absorption from natural gas using monoethanolamine (MEA) in high pressure operations. Ind. Eng. Chem. Res. 54, 1675–1680. https://doi.org/10.1021/ie504024m

Aboshatta, M.; Magueijo, V. A Comprehensive Study of Co2 Absorption and Desorption by Choline-Chloride/Levulinic-Acid-Based Deep Eutectic Solvents. Molecules 2021, 26 (18). https://doi.org/10.3390/molecules26185595.

Adhikari, L.; Larm, N. E.; Baker, G. A. Argentous Deep Eutectic Solvent Approach for Scaling Up the Production of Colloidal Silver Nanocrystals. ACS Sustain. Chem. Eng. 2019, 7 (13), 11036–11043. https://doi.org/10.1021/acssuschemeng.9b01777.

Aghaie, M.; Zendehboudi, S. Estimation of CO2 Solubility in Ionic Liquids Using Connectionist Tools Based on Thermodynamic and Structural Characteristics. Fuel 2020, 279, 1–11.

Akbari, M., Valeh-e-Sheyda, P., 2019. CO2 equilibrium solubility in and physical properties for monoethanolamine glycinate at low pressures. Process Saf. Environ. Prot. 132, 116–125. https://doi.org/10.1016/j.psep.2019.10.003

Al-Bodour, A.; Alomari, N.; Gutiérrez, A.; Aparicio, S.; Atilhan, M. High-Pressure Carbon Dioxide Solubility in Terpene Based Deep Eutectic Solvents. J. Environ. Chem. Eng. 2022, 10 (5), 108237. https://doi.org/10.1016/j.jece.2022.108237.

ALDAWSARI, J. N. et al. Polyethylene glycol-based deep eutectic solvents as a novel agent for natural gas sweetening. PLoS ONE, v. 15, p. 1–22, 2020. Disponível em: <http://dx.doi.org/10.1371/journal.pone.0239493>.

ALI, E. et al. Solubility of CO2 in deep eutectic solvents: Experiments and modelling using the Peng-Robinson equation of state. Chemical Engineering Research and Design, v. 92, n. 10, p. 1898–1906, 2014.

Alioui, O.; Benguerba, Y.; Alnashef, I. M. Investigation of the CO2-Solubility in Deep Eutectic Solvents Using COSMO-RS and Molecular Dynamics Methods. J. Mol. Liq. 2020, 307, 1–9.

Alizadeh, V.; Esser, L.; Kirchner, B. How Is CO2absorbed into a Deep Eutectic Solvent? J. Chem. Phys. 2021, 154 (9). https://doi.org/10.1063/5.0038093.

Alkhatib, I. I. I.; Ferreira, M. L.; Alba, C. G.; Bahamon, D.; Llovell, F.; Pereiro, A. B.; Araújo, J. M. M.; Abu-Zahra, M. R. M.; Vega, L. F. Screening of Ionic Liquids and Deep Eutectic Solvents for Physical CO2 Absorption by Soft-SAFT Using Key Performance Indicators. J. Chem. Eng. Data 2020, 65, 5844–5861.

Altamash, T.; Amhamed, A. I.; Aparicio, S.; Atilhan, M. Combined Experimental and Theoretical Study on High Pressure Methane Solubility in Natural Deep Eutectic Solvents. Ind. Eng. Chem. Res. 2019, 58, 8097–8111.

Althuluth, M.; Kroon, M. C.; Peters, C. J. High Pressure Solubility of Methane in the Ionic Liquid 1-Hexyl-3-Methylimidazolium Tricyanomethanide. J. Supercrit. Fluids 2017, 128, 145–148.

Anderson, J. L.; Dixon, J. K.; Brennecke, J. F. Solubility of CO2, CH4, C2H6, C2H4, O2, and N2 in 1-Hexyl-3-Methylpyridinium Bis(Trifluoromethylsulfonyl)Imide: Comparison to Other Ionic Liquids. Acc. Chem. Res. 2007, 40, 1208–1216.

Ansarypur, G., Bayareh, M., Jahangiri, A., 2022. Experimental investigation and thermodynamic modeling of CO2 absorption by a chemical solution. J. Therm. Anal. Calorim. 147, 1689–1697. https://doi.org/10.1007/s10973-021-10554-3

Anthony, J. L.; Maginn, E. J.; Brennecke, J. F. Gas Solubilities in 1-n-Butyl-3-Methylimidazolium Hexafluorophosphate. Am. Chem. Soc. 2002, 818, 260–269.

Aravena, C.; Lee, D.; Park, J.; Yoo, Y. Characteristics of Deep Eutectic Solvents for CO2 Capture with Hydro Effects for Improvement of Mass Transfer. J. Ind. Eng. Chem. 2022, 111, 337–345. https://doi.org/10.1016/j.jiec.2022.04.015.

Aroonwilas, A., Veawab, A., 2004. Characterization and Comparison of the CO 2 Absorption Performance into Single and Blended Alkanolamines in a Packed Column. Ind. Eng. Chem. Res. 43, 2228–2237. https://doi.org/10.1021/ie0306067

Awwad, A.M., Al-Dujaili, A.H., Salman, H.E., 2002. Relative permittivities, densities, and refractive indices of the binary mixtures of sulfolane with ethylene glycol, diethylene glycol, and poly(ethylene glycol) at 303.15 K. J. Chem. Eng. Data 47, 421–424. https://doi.org/10.1021/je010259c

Ayittey, F. K.; Saptoro, A.; Kumar, P.; Wong, M. K. Energy-Saving Process Configurations for Monoethanolamine-Based CO2 Capture System. Asia-Pacific J. Chem. Eng. 2020, No. February, 1–15.

B. Ahmed, Q. Wu, J.G. et Al., Degumming of Hemp Fibers Using Combined Microwave Energy and Deep Eutectic Solvent Treatment, Research Square. (2022) 1–25. https://doi.org/https://doi.org/10.21203/rs.3.rs-1094469/v1.

B. Hashemi, F. Shiri, F. Svec, L. Nováková, Green solvents and approaches recently applied for extraction of natural bioactive compounds, Trends in Analytical Chemistry. 157 (2022) 1–10. https://doi.org/10.1016/j.trac.2022.116732.

B. Li, Q. Li, Q. Wang, X. Yan, M. Shi, C. Wu, Deep eutectic solvent for spent lithium-ion battery recycling: comparison with inorganic acid leaching, Physical Chemistry Chemical Physics. 24 (2022) 19029–19051. https://doi.org/10.1039/D1CP05968H.

B. Lu, R. Du, G. Wang, Y. Wang, S. Dong, D. Zhou, S. Wang, C. Li, High-efficiency leaching of valuable metals from waste Li-ion batteries using deep eutectic solvents, Environmental Research. 212 (2022) 113286.

https://doi.org/10.1016/j.envres.2022.113286.

B. Nowosielski, M. Jamrógiewicz, J. Łuczak, M. Śmiechowski, D. Warmińska, Experimental and predicted physicochemical properties of monopropanolamine-based deep eutectic solvents, Journal of Molecular Liquids. 309 (2020) 113110. https://doi.org/10.1016/j.molliq.2020.113110.

B. Singh, H. Lobo, G. Shankarling, Selective N-Alkylation of Aromatic Primary Amines Catalyzed by Bio-catalyst or Deep Eutectic Solvent, Catal Letters. 141 (2011) 178–182. https://doi.org/10.1007/s10562-010-0479-9.

B. Tang, K.H. Row, Recent developments in deep eutectic solvents in chemical sciences, Monatsh Chem. 144 (2013) 1427–1454. https://doi.org/10.1007/s00706-013-1050-3.

Bates, E. D.; Mayton, R. D.; Ntai, I.; Davis, J. H. CO2 Capture by a Task-Specific Ionic Liquid. J. Am. Chem. Soc. 2002, 124 (6), 926–927.

Ben-Mansour, R., Habib, M.A., Bamidele, O.E., Basha, M., Qasem, N.A.A., Peedikakkal, A., Laoui, T., Ali, M., 2016. Carbon capture by physical adsorption: Materials, experimental investigations and numerical modeling and simulations - A review. Appl. Energy 161, 225–255. https://doi.org/10.1016/j.apenergy.2015.10.011

BHOWN, A. S.; FREEMAN, B. C. Analysis and status of post-combustion carbon dioxide capture technologies. Environmental Science and Technology, v. 45, p. 8624–8632, 2011.

C. Florindo, F.S. Oliveira, L.P.N. Rebelo, A.M. Fernandes, I.M. Marrucho, Insights into the Synthesis and Properties of Deep Eutectic Solvents Based on Cholinium Chloride and Carboxylic Acids, ACS Sustainable Chemistry & Engineering. 2 (2014) 2416–2425. https://doi.org/10.1021/sc500439w.

C. Steffen, K. Thomas, U. Huniar, A. Hellweg, O. Rubner, A. Schroer, TmoleX-A graphical user interface for TURBOMOLE, J Comput Chem. 31 (2010) 2967–2970. https://doi.org/10.1002/jcc.21576.

C.A. Marques, A.A.S.C. Machado, Environmental Sustainability: implications and limitations to Green Chemistry, Found Chem. 16 (2014) 125–147. https://doi.org/10.1007/s10698-013-9189-x.

C.J. Clarke, W.C. Tu, O. Levers, A. Bröhl, J.P. Hallett, Green and Sustainable Solvents in Chemical Processes, Chemical Reviews. 118 (2018) 747–800. https://doi.org/10.1021/acs.chemrev.7b00571.

Chao, C., Deng, Y., Dewil, R., Baeyens, J., Fan, X., 2021. Post-combustion carbon capture. Renew. Sustain. Energy Rev. 138, 110490. https://doi.org/10.1016/j.rser.2020.110490

Charin, R. M.; Corazza, M. L.; Ndiaye, P. M.; Mazutti, M. A.; Oliveira, J. V. Phase Equilibrium Data and Thermodynamic Modeling of the System Propane+NMP+methanol at High Pressures. J. Supercrit. Fluids 2010, 55 (1), 23–31. https://doi.org/10.1016/j.supflu.2010.08.017.

Chen, Y.; Ai, N.; Li, G.; Shan, H.; Cui, Y.; Deng, D. Solubilities of Carbon Dioxide in Eutectic Mixtures of Choline Chloride and Dihydric Alcohols. J. Chem. Eng. Data 2014, 59, 1247–1253.

Chen, Y.; Jiang, B.; Dou, H.; Zhang, L.; Tantai, X.; Sun, Y. Highly Efficient and Reversible Capture of Low Partial Pressure SO2 by Functional Deep Eutectic Solvents. Energy & Fuels 2018, 32, 10737–10744.

Cichowska-Kopczyńska, I., Warmińska, D., Nowosielski, B., 2021. Solubility of carbon dioxide in deep eutectic solvents based on 3-amino-1-propanol and tetraalkylammonium salts at low pressure. Materials (Basel). 14, 1–14. https://doi.org/10.3390/ma14030594

Cismondi, M.; Michelsen, M. Automated Calculation of Complete Pxy and Txy Diagrams for Binary Systems. Fluid Phase Equilib. 2007, 259 (2), 228–234. https://doi.org/10.1016/j.fluid.2007.07.019.

Cismondi, M.; Michelsen, M. L. Global Phase Equilibrium Calculations: Critical Lines, Critical End Points and Liquid–Liquid–Vapour Equilibrium in Binary Mixtures. J. Supercrit. Fluids 2007, 39 (3), 287–295. https://doi.org/10.1016/j.supflu.2006.03.011.

Cole, P.J., 1960. The Density of Solid Phenol. J. Chem. Eng. Data 5, 367. https://doi.org/10.1021/je60007a036

Concentration of CO2 https://scripps.ucsd.edu/programs/keelingcurve/ (2020) (accessed Oct 14, 2020).

COSMOTHERM, B. Reference manual. [s.l: s.n.].

COSMOTHERM, B. Release 2021. [s.l: s.n.]. Disponível em: <http://www.3ds.com>.

CRESPO, E. A. et al. Characterization and Modeling of the Liquid Phase of Deep Eutectic Solvents Based on Fatty Acids/Alcohols and Choline Chloride. Industrial & Engineering Chemistry Research, v. 56, n. 42, p. 12192–12202, 2017. Disponível em: <http://pubs.acs.org/doi/abs/10.1021/acs.iecr.7b02382>.

CRESPO, E. A. et al. The Role of Polyfunctionality in the Formation of [Ch]Cl-Carboxylic Acid-Based Deep Eutectic Solvents. Industrial and Engineering Chemistry Research, v. 57, n. 32, p. 11195–11209, 2018.

Crespo, E.A., Costa, J.M.L., Palma, A.M., Soares, B., Martín, M.C., Segovia, J.J., Carvalho, P.J., Coutinho, J.A.P., 2019. Thermodynamic characterization of deep eutectic solvents at high pressures. Fluid Phase Equilib. 500, 1–13. https://doi.org/10.1016/j.fluid.2019.112249

D. Borjan, D. Cör, M. Knez Marevci, I. Grčar, Ž. Knez, Phase Equilibrium Data of Tetrabutylurea, Tetramethylurea, and Tetramethylthiourea/Carbon Dioxide at Pressures up to 200 bar at 313.15 and 333.15 K, Journal of Chemical & Engineering Data. (2022). https://doi.org/10.1021/acs.jced.2c00079.

D. Carriazo, M.C. Serrano, M.C. Gutiérrez, M.L. Ferrer, F. del Monte, Deep-eutectic solvents playing multiple roles in the synthesis of polymers and related materials, Chem Soc Rev. 41 (2012) 4996. https://doi.org/10.1039/c2cs15353j.

D. Deng, Y. Jiang, X. Liu, Z. Zhang, N. Ai, Investigation of solubilities of carbon dioxide in five levulinic acid-based deep eutectic solvents and their thermodynamic properties, Journal of Chemical Thermodynamics. 103 (2016) 212–217. https://doi.org/10.1016/j.jct.2016.08.015.

D. Lee, W. Go, J. Oh, J. Lee, I. Jo, K.S. Kim, Y. Seo, Thermodynamic inhibition effects of an ionic liquid (choline chloride), a naturally derived substance (urea), and their mixture (deep eutectic solvent) on CH4 hydrates, Chemical Engineering Journal. 399 (2020) 125830. https://doi.org/10.1016/j.cej.2020.125830.

D. Yang, M. Hou, H. Ning, J. Zhang, J. Ma, G. Yang, B. Han, Efficient SO2 absorption by renewable choline chloride–glycerol deep eutectic solvents, Green Chemistry. 15

(2013) 2261–2265. https://doi.org/10.1039/c3gc40815a.

D.A. Lashof, D.R. Ahuja, Relative contributions of greenhouse gas emissions to global warming, Nature. 344 (1990) 529–531. https://doi.org/10.1038/344529a0.

D.O. Abranches, L.P. Silva, M.A.R. Martins, L. Fernandez, S.P. Pinho, J.A.P. Coutinho, Can cholinium chloride form eutectic solvents with organic chloride-based salts?, Fluid Phase Equilibria. 493 (2019) 120–126. https://doi.org/10.1016/j.fluid.2019.04.019.

D.O. Abranches, L.P. Silva, M.A.R. Martins, S.P. Pinho, J.A.P. Coutinho, Understanding the Formation of Deep Eutectic Solvents: Betaine as a Universal Hydrogen Bond Acceptor, ChemSusChem. 13 (2020) 4916–4921. https://doi.org/10.1002/cssc.202001331.

DAI, Y. et al. Natural deep eutectic solvents as new potential media for green technology. Analytica Chimica Acta, v. 766, p. 61–68, 2013. Disponível em: <http://dx.doi.org/10.1016/j.aca.2012.12.019>.

DALMOLIN, I. A. L. Uso de sementes de uva, um resíduo da agroindústria vinícula, empregando tecnologias supercríticas. 2013. Universidade Estadual de Campinas, 2013.

Daubert, T. E.; Sibul, H. M.; Stebbins, C. C.; Danner, R. P.; Rowley, R. L.; Adams, M. E.; Wilding, W. V; Marshall, T. L. Physical and Thermodynamic Properties of Pure Chemicals: DIPPR: Data Compilation: Core + Supplements 1−10; Taylor & Francis, 2000.

DAVIS, S. J.; CALDEIRA, K.; MATTHEWS, H. D. Future CO2 Emissions and Climate Change from Existing Energy Infrastructure. Science, v. 329, n. 5997, p. 1330–1333, 10 set. 2010. Disponível em: <https://www.science.org/doi/10.1126/science.1188566>.

Dawson, R. M. C. .; Elliott, D. C. .; Elliott, W. H. .; Jones, K. M. Data for Biochemical Research; Oxford University Press: Oxford, 1986.

Deng, D., Jiang, Y., Liu, X., Zhang, Z., Ai, N., 2016. Investigation of solubilities of carbon dioxide in five levulinic acid-based deep eutectic solvents and their thermodynamic properties. J. Chem. Thermodyn. 103, 212–217.

https://doi.org/10.1016/j.jct.2016.08.015

Deng, D.; Han, G.; Jiang, Y. Investigation of a Deep Eutectic Solvent Formed by Levulinic Acid with Quaternary Ammonium Salt as an Efficient SO2 Absorbent. New J. Chem. 2015, 39, 8158–8164.

DIEDENHOFEN, M.; KLAMT, A. COSMO-RS as a tool for property prediction of IL mixtures—A review. Fluid Phase Equilibria, v. 294, n. 1–2, p. 31–38, jul. 2010. Disponível em: <https://linkinghub.elsevier.com/retrieve/pii/S0378381210000695>.

Dietz, C. H. J. T.; van Osch, D. J. G. P.; Kroon, M. C.; Sadowski, G.; van Sint Annaland, M.; Gallucci, F.; Zubeir, L. F.; Held, C. PC-SAFT Modeling of CO2 Solubilities in Hydrophobic Deep Eutectic Solvents. Fluid Phase Equilib. 2017, 448, 94–98. https://doi.org/10.1016/j.fluid.2017.03.028.

Domalski, E. S.; Hearing, E. D. Heat Capacities and Entropies of Organic Compounds in the Condensed Phase. Volume III. J. Phys. Chem. Ref. Data 1996, 25 (1), 1–525. https://doi.org/10.1063/1.555985.

Dong, J.-Y.; Lin, C.-H.; Hsu, Y.-J.; Lu, S.-Y.; Wong, D. S.-H. Single-Crystalline Mesoporous ZnO Nanosheets Prepared with a Green Antisolvent Method Exhibiting Excellent Photocatalytic Efficiencies. CrystEngComm 2012, 14 (14), 4732. https://doi.org/10.1039/c2ce06739k.

E.A. Crespo, J.M.L. Costa, A.M. Palma, B. Soares, M.C. Martín, J.J. Segovia, P.J. Carvalho, J.A.P. Coutinho, Thermodynamic characterization of deep eutectic solvents at high pressures, Fluid Phase Equilib. 500 (2019) 1–13. https://doi.org/10.1016/j.fluid.2019.112249.

E.A. Crespo, L.P. Silva, J.O. Lloret, P.J. Carvalho, L.F. Vega, F. Llovell, J.A.P. Coutinho, A methodology to parameterize SAFT-type equations of state for solid precursors of deep eutectic solvents: The example of cholinium chloride, Physical Chemistry Chemical Physics. 21 (2019) 15046–15061. https://doi.org/10.1039/c9cp02548k.

E.A. Crespo, L.P. Silva, M.A.R. Martins, L. Fernandez, J. Ortega, O. Ferreira, G. Sadowski, C. Held, S.P. Pinho, J.A.P. Coutinho, Characterization and Modeling of the Liquid Phase of Deep Eutectic Solvents Based on Fatty Acids/Alcohols and Choline

Chloride, Ind Eng Chem Res. 56 (2017) 12192–12202. https://doi.org/10.1021/acs.iecr.7b02382.

E.L. Smith, A.P. Abbott, K.S. Ryder, Deep Eutectic Solvents (DESs) and Their Applications, Chem Rev. 114 (2014) 11060–11082. https://doi.org/10.1021/cr300162p.

E.S. Domalski, E.D. Hearing, Heat Capacities and Entropies of Organic Compounds in the Condensed Phase. Volume III, Journal of Physical and Chemical Reference Data. 25 (1996) 1–525. https://doi.org/10.1063/1.555985.

ELLIOT, R. J.; SURESH, S. J.; DONOHUE, M. D. A Simple Equation of State for Nonspherical and Associating Molecules. Industrial and Engineering Chemistry Research, v. 29, p. 1476–1485, 1990.

Elsaid, K., Kamil, M., Sayed, E.T., Abdelkareem, M.A., Wilberforce, T., Olabi, A., 2020. Environmental impact of desalination technologies: A review. Sci. Total Environ. 748, 1–19. https://doi.org/10.1016/j.scitotenv.2020.141528

Emel'yanenko, V. N.; Verevkin, S. P.; Stepurko, E. N.; Roganov, G. N.; Georgieva, M. K. Thermodynamic Properties of Glycolic Acid and Glycolide. Russ. J. Phys. Chem. A 2010, 84 (8), 1301–1308. https://doi.org/10.1134/S0036024410080054.

F. Eckert, A. Klamt, Fast solvent screening via quantum chemistry: COSMO-RS approach, AIChE Journal. 48 (2002) 369–385. https://doi.org/10.1002/aic.690480220.

F. Gabriele, M. Chiarini, R. Germani, M. Tiecco, N. Spreti, Effect of water addition on choline chloride/glycol deep eutectic solvents: Characterization of their structural and physicochemical properties, Journal of Molecular Liquids. 291 (2019) 111301. https://doi.org/10.1016/j.molliq.2019.111301.

F. Liu, W. Chen, J. Mi, J.Y. Zhang, X. Kan, F.Y. Zhong, K. Huang, A.M. Zheng, L. Jiang, Thermodynamic and molecular insights into the absorption of H2S, CO2 , and CH4 in choline chloride plus urea mixtures, AIChE Journal. 65 (2019) 1–10. https://doi.org/10.1002/aic.16574.

F. Luo, X. Liu, S. Chen, Y. Song, X. Yi, C. Xue, L. Sun, J. Li, Comprehensive Evaluation of a Deep Eutectic Solvent Based CO2Capture Process through Experiment and Simulation, ACS Sustain Chem Eng. 9 (2021) 10250–10265.

https://doi.org/10.1021/acssuschemeng.1c02722.

F. Petrakopoulou, G. Tsatsaronis, Can Carbon Dioxide Capture and Storage from Power Plants Reduce the Environmental Impact of Electricity Generation?, Energy & Fuels. 28 (2014) 5327–5338. https://doi.org/10.1021/ef500925h.

F. Rabhi, F. Mutelet, H. Sifaoui, Solubility of Carbon Dioxide in Carboxylic Acid-Based Deep Eutectic Solvents, J Chem Eng Data. 66 (2021) 702–711. https://doi.org/10.1021/acs.jced.0c00844.

F.H.B. Sosa, D.O. Abranches, A.M. da Costa Lopes, J.A.P. Coutinho, M.C. da Costa, Kraft Lignin Solubility and Its Chemical Modification in Deep Eutectic Solvents, ACS Sustainable Chemistry & Engineering. 8 (2020) 18577–18589. https://doi.org/10.1021/acssuschemeng.0c06655.

F.O. Farias, F.H.B. Sosa, L. Igarashi-Mafra, J.A.P. Coutinho, M.R. Mafra, Study of the pseudo-ternary aqueous two-phase systems of deep eutectic solvent (choline chloride:sugars) + K2HPO4 + water, Fluid Phase Equilib. 448 (2017) 143–151. https://doi.org/10.1016/j.fluid.2017.05.018.

F.P. Pelaquim, A.M. Barbosa Neto, I.A.L. Dalmolin, M.C. da Costa, Gas Solubility Using Deep Eutectic Solvents: Review and Analysis, Ind Eng Chem Res. (2021) acs.iecr.1c00947. https://doi.org/10.1021/acs.iecr.1c00947.

F.P. Pelaquim, R.G. Bitencourt, A.M.B. Neto, I.A.L. Dalmolin, M.C. da Costa, Carbon dioxide solubility in Deep Eutectic Solvents: Modelling using Cubic Plus Association and Peng-Robinson equations of state, Process Safety and Environmental Protection. 163 (2022) 14–26. https://doi.org/10.1016/j.psep.2022.04.075.

F.S. Mjalli, G. Murshid, S. Al-Zakwani, A. Hayyan, Monoethanolamine-based deep eutectic solvents, their synthesis and characterization, Fluid Phase Equilibria. 448 (2017) 30–40. https://doi.org/10.1016/j.fluid.2017.03.008.

Favareto, R.; de Araujo, P. C. C.; Bezerra, I. D.; Zanette, A. F.; Arce, P. F.; Ferreira-Pinto, L.; Cardozo-Filho, L. Experimental Data and Thermodynamics Modeling (PC-SAFT EoS) of the {CO2 + Chloroform + PHBV} System at High Pressures. J. Supercrit. Fluids 2021, 170, 105140. https://doi.org/10.1016/j.supflu.2020.105140.

Feng, Z.; Jing-Wen, M.; Zheng, Z.; You-Ting, W.; Zhi-Bing, Z. Study on the Absorption

of Carbon Dioxide in High Concentrated MDEA and ILs Solutions. Chem. Eng. J. 2012, 181–182, 222–228.

Fernandez, L.; Silva, L. P.; Martins, M. A. R.; Ferreira, O.; Ortega, J.; Pinho, S. P.; Coutinho, J. A. P. Indirect Assessment of the Fusion Properties of Choline Chloride from Solid-Liquid Equilibria Data. Fluid Phase Equilib. 2017, 448, 9–14. https://doi.org/10.1016/j.fluid.2017.03.015.

FOLAS, G. K. et al. Application of the cubic-plus-association equation of state to mixtures with polar chemicals and high pressures. Industrial and Engineering Chemistry Research, v. 45, p. 1516–1526, 2006.

Francisco, M., González, A.S.B., García De Dios, S.L., Weggemans, W., Kroon, M.C., 2013. Comparison of a low transition temperature mixture (LTTM) formed by lactic acid and choline chloride with choline lactate ionic liquid and the choline chloride salt: Physical properties and vapour-liquid equilibria of mixtures containing water and ethanol. RSC Adv. 3, 23553–23561. https://doi.org/10.1039/c3ra40303c

FREDRIKSEN, S. B.; JENS, K.-J. Oxidative Degradation of Aqueous Amine Solutions of MEA, AMP, MDEA, Pz: A Review. Energy Procedia, v. 37, p. 1770–1777, 2013. Disponível em: <https://linkinghub.elsevier.com/retrieve/pii/S1876610213002968>.

G. Ansarypur, M. Bayareh, A. Jahangiri, Experimental investigation and thermodynamic modeling of CO2 absorption by a chemical solution, J Therm Anal Calorim. 147 (2022) 1689–1697. https://doi.org/10.1007/s10973-021-10554-3.

G. Cui, J. Liu, S. Lyu, H. Wang, Z. Li, J. Wang, Efficient and reversible SO2 Absorption by environmentally friendly task-specific deep eutectic solvents of PPZBr + Gly, ACS Sustain Chem Eng. 7 (2019) 14236–14246. https://doi.org/10.1021/acssuschemeng.9b03245.

G. García, S. Aparicio, R. Ullah, M. Atilhan, Deep Eutectic Solvents: Physicochemical Properties and Gas Separation Applications, Energy & Fuels. 29 (2015) 2616–2644. https://doi.org/10.1021/ef5028873.

G. Li, D. Deng, Y. Chen, H. Shan, N. Ai, Solubilities and thermodynamic properties of CO2 in choline-chloride based deep eutectic solvents, J Chem Thermodyn. 75 (2014) 58–62. https://doi.org/10.1016/j.jct.2014.04.012.

G. Luderer, V. Bosetti, M. Jakob, M. Leimbach, J.C. Steckel, H. Waisman, O. Edenhofer, The economics of decarbonizing the energy system—results and insights from the RECIPE model intercomparison, Clim Change. 114 (2012) 9–37. https://doi.org/10.1007/s10584-011-0105-x.

G. Moradi, M. Rahimi, S. Zinadini, M. Shamsipur, N. Babajani, Natural deep eutectic solvent modified nanofiltration membranes with superior antifouling properties for pharmaceutical wastewater treatment, Chemical Engineering Journal. 448 (2022) 137704. https://doi.org/10.1016/j.cej.2022.137704.

G. Siani, M. Tiecco, P. Di Profio, S. Guernelli, A. Fontana, M. Ciulla, V. Canale, Physical absorption of CO2 in betaine/carboxylic acid-based Natural Deep Eutectic Solvents, J Mol Liq. 315 (2020) 1–7. https://doi.org/10.1016/j.molliq.2020.113708.

Garg, S.; Shariff, A. M.; Shaikh, M. S.; Lal, B.; Aftab, A.; Faiqa, N. VLE of CO 2 in Aqueous Potassium Salt of L-Phenylalanine: Experimental Data and Modeling Using Modified Kent-Eisenberg Model. J. Nat. Gas Sci. Eng. 2016, 34, 864–872. https://doi.org/10.1016/j.jngse.2016.07.047.

Ghaedi, H., Zhao, M., Clough, P.T., Anthony, E.J., Fennell, P.S., 2020. High CO2 absorption in new amine based-transition-temperature mixtures (deep eutectic analogues) and reporting thermal stability, viscosity and surface tension: Response surface methodology (RSM). J. Mol. Liq. 316, 1–11. https://doi.org/10.1016/j.molliq.2020.113863

GORKE, J. T.; SRIENC, F.; KAZLAUSKAS, R. J. Deep Eutectic Solvents for Candida antarctica Lipase B-Catalyzed Reactions. In: Ionic Liquid Applications: Pharmaceuticals, Therapeutics, and Biotechnology. Washington, D.C: American Chemical Society, 2010.

Gross, J., Sadowski, G., 2001. Perturbed-chain SAFT: An equation of state based on a perturbation theory for chain molecules. Ind. Eng. Chem. Res. 40, 1244–1260. https://doi.org/10.1021/ie0003887

Gu, Y., Hou, Y., Ren, S., Sun, Y., Wu, W., 2020. Hydrophobic Functional Deep Eutectic Solvents Used for Efficient and Reversible Capture of CO2. ACS Omega 5, 6809–6816. https://doi.org/10.1021/acsomega.0c00150

Guo, W., Hou, Y., Ren, S., Tian, S., Wu, W., 2013. Formation of deep eutectic solvents by phenols and choline chloride and their physical properties. J. Chem. Eng. Data 58, 866–872. https://doi.org/10.1021/je300997v

Gurkan, B. E.; Fuente, J. C. De; Mindrup, E. M.; Ficke, L. E.; Goodrich, B. F.; Price, E. A.; Schneider, W. F.; Brennecke, J. F. Equimolar CO2 Absorption by Anion-Functionalized Ionic Liquids. J. Am. Chem. Soc. 2010, 132, 2116–2117.

H. Cheng, C. Liu, J. Zhang, L. Chen, B. Zhang, Z. Qi, Screening deep eutectic solvents for extractive desulfurization of fuel based on COSMO-RS model, Chemical Engineering and Processing - Process Intensification. 125 (2018) 246–252. https://doi.org/10.1016/j.cep.2018.02.006.

H. Cheng, Z. Qi, Applications of deep eutectic solvents for hard-to-separate liquid systems, Sep Purif Technol. 274 (2021) 119027. https://doi.org/10.1016/j.seppur.2021.119027.

H. Ghaedi, M. Ayoub, S. Sufian, A.M. Shariff, S.M. Hailegiorgis, S.N. Khan, CO2 capture with the help of Phosphonium-based deep eutectic solvents, J Mol Liq. 243 (2017) 564–571. https://doi.org/10.1016/j.molliq.2017.08.046.

H. Huang, Q. Tang, G. Lin, C. Yu, H. Wang, Z. Li, High-efficiency and recyclable ramie cellulose fiber degumming enabled by deep eutectic solvent, Industrial Crops and Products. 171 (2021) 113879. https://doi.org/10.1016/j.indcrop.2021.113879.

H. Huang, Q. Tang, G. Lin, Y. Liu, J. Yu, B. Ding, Z. Li, Anthraquinone-assisted deep eutectic solvent degumming of ramie fibers: Evaluation of fiber properties and degumming performance, Industrial Crops and Products. 185 (2022) 115115. https://doi.org/10.1016/j.indcrop.2022.115115.

H. Qin, Z. Song, H. Cheng, L. Deng, Z. Qi, Physical absorption of carbon dioxide in imidazole-PTSA based deep eutectic solvents, J Mol Liq. 326 (2021) 1–7. https://doi.org/10.1016/j.molliq.2021.115292.

H. Srinivasan, P.S. Dubey, V.K. Sharma, R. Biswas, S. Mitra, R. Mukhopadhyay, Molecular dynamics of acetamide based ionic deep eutectic solvents, in: AIP Conf. Proc. 1942, 2018: p. 110032. https://doi.org/10.1063/1.5029015.

H. Suo, Z. Peng, Z. Guo, C. Wu, J. Liu, L. Wang, J. Xiao, X. Li, Deep eutectic solvent-

based ultrasonic-assisted extraction of phenolic compounds from different potato genotypes: Comparison of free and bound phenolic profiles and antioxidant activity, Food Chemistry. 388 (2022) 133058. https://doi.org/10.1016/j.foodchem.2022.133058.

H. Yu, Z. Xue, R. Shi, F. Zhou, T. Mu, Lignin dissolution and lignocellulose pretreatment by carboxylic acid based deep eutectic solvents, Industrial Crops and Products. 184 (2022) 115049. https://doi.org/10.1016/j.indcrop.2022.115049.

H.S. Salehi, R. Hens, O.A. Moultos, T.J.H. Vlugt, Computation of gas solubilities in choline chloride urea and choline chloride ethylene glycol deep eutectic solvents using Monte Carlo simulations, J Mol Liq. 316 (2020) 1–10. https://doi.org/10.1016/j.molliq.2020.113729.

H.-Zhen. SU, J.-Mei. YIN, Q.-Shan. LIU, C.-Ping. LI, Properties of Four Deep Eutectic Solvents: Density, Electrical Conductivity, Dynamic Viscosity and Refractive Index, Acta Physico-Chimica Sinica. 31 (2015) 1468–1473. https://doi.org/10.3866/PKU.WHXB201506111.

HAGHBAKHSH, R. et al. Experimental investigation of carbon dioxide solubility in the deep eutectic solvent (1 ChCl + 3 triethylene glycol) and modeling by the CPA EoS. Journal of Molecular Liquids, v. 330, p. 1–12, 2021. Disponível em: <https://doi.org/10.1016/j.molliq.2021.115647>.

Haghbakhsh, R., Raeissi, S., 2017. Modeling the Phase Behavior of Carbon Dioxide Solubility in Deep Eutectic Solvents with the Cubic Plus Association Equation of State. J. Chem. Eng. Data 63, 897–906. https://doi.org/10.1021/acs.jced.7b00472

Haghbakhsh, R.; Keshtkar, M.; Shariati, A.; Raeissi, S. A Comprehensive Experimental and Modeling Study on CO2 Solubilities in the Deep Eutectic Solvent Based on Choline Chloride and Butane-1,2-Diol. Fluid Phase Equilib. 2022, 561 (March), 113535. https://doi.org/10.1016/j.fluid.2022.113535.

Haghtalab, A.; Ghahremani, E. The Solubility Measurement and Modeling of CO2 in Aqueous Solution of N-Methyldiethanolaminen+2-Amino-2-Methyl-1-Propanol+piperazine at High Pressures. Fluid Phase Equilib. 2015, 400, 62–75. https://doi.org/10.1016/j.fluid.2015.04.016.

HAIDER, M. B. et al. Ternary hydrophobic deep eutectic solvents for carbon dioxide

absorption. International Journal of Greenhouse Gas Control, v. 92, n. September 2019, p. 102839, 2020. Disponível em: <https://doi.org/10.1016/j.ijggc.2019.102839>.

HAIDER, M. B. et al. Thermodynamic and Kinetic Studies of CO2 Capture by Glycol and Amine-Based Deep Eutectic Solvents. Journal of Chemical and Engineering Data, v. 63, p. 2671–2680, 2018.

Haider, M. B.; Jha, D.; Marriyappan Sivagnanam, B.; Kumar, R. Modelling and Simulation of CO2 Removal from Shale Gas Using Deep Eutectic Solvents. J. Environ. Chem. Eng. 2019, 7, 1–9.

Haider, M. B.; Kumar, R. Solubility of CO2 and CH4 in Sterically Hindered Amine-Based Deep Eutectic Solvents. Sep. Purif. Technol. 2020, 248, 117055. https://doi.org/10.1016/j.seppur.2020.117055.

Haider, M.B., Maheshwari, P., Kumar, R., 2021. CO2 capture from flue gas using phosphonium based deep eutectic solvents: Modeling and simulation approach. J. Environ. Chem. Eng. 9, 106727. https://doi.org/10.1016/j.jece.2021.106727

Hansen, A. R.; Beyer, K. D. Experimentally Determined Thermochemical Properties of the Malonic Acid/Water System: Implications for Atmospheric Aerosols. J. Phys. Chem. A 2004, 108 (16), 3457–3466. https://doi.org/10.1021/jp0376166.

Hansen, B. B.; Spittle, S.; Chen, B.; Poe, D.; Zhang, Y.; Klein, J. M.; Horton, A.; Adhikari, L.; Zelovich, T.; Doherty, B. W.; Gurkan, B.; Maginn, E. J.; Ragauskas, A.; Dadmun, M.; Zawodzinski, T. A.; Baker, G. A.; Tuckerman, M. E.; Savinell, R. F.; Sangoro, J. R. Deep Eutectic Solvents: A Review of Fundamentals and Applications. Chem. Rev. 2021, 121 (3), 1232–1285. https://doi.org/10.1021/acs.chemrev.0c00385.

Harifi-Mood, A. R.; Mohammadpour, F.; Boczkaj, G. Solvent Dependency of Carbon Dioxide Henry's Constant in Aqueous Solutions of Choline Chloride-Ethylene Glycol Based Deep Eutectic Solvent. J. Mol. Liq. 2020, 319, 114173. https://doi.org/10.1016/j.molliq.2020.114173.

Hartono, A.; Ahmad, R.; Usman, M.; Asif, N.; Svendsen, H. F. Solubility of CO2 in 0.1M, 1M and 3M of 2-Amino-2-Methyl-1-Propanol (AMP) from 313 to 393K and Model Representation Using the ENRTL Framework. Fluid Phase Equilib. 2020, 511, 1–53.

Hester, R.E., Harrison, R.M., 2010. Carbon Capture: Sequestration and Storage. The

Royal Society of Chemistry, Cambridge.

Hirshfeld, F. L. Bonded-Atom Fragments for Describing Molecular Charge Densities. Theor. Chim. Acta 1977, 44, 129–138.

Hodgman, C. .; Lange, N. Handbook of Chemistry and Physics; Chemical Rubber Publishing Company: Cleveland, 1951.

I. Bahadur, T.M. Letcher, S. Singh, G.G. Redhi, P. Venkatesu, D. Ramjugernath, Excess molar volumes of binary mixtures (an ionic liquid+water): A review, J Chem Thermodyn. 82 (2015) 34–46. https://doi.org/10.1016/j.jct.2014.10.003.

IEA. Global Energy & CO2 Status Report 2019; Paris, 2019.

IEA. Global Energy and CO2 Emissions in 2020; Paris, 2020.

International Energy Agency, Global Energy Review: CO2 Emissions in 2021 Global emissions rebound sharply to highest ever level, 2022.

INTERNATIONAL ENERGY AGENCY. Global Energy Review: CO2 Emissions in 2021 Global emissions rebound sharply to highest ever levelIEA. [s.l: s.n.]. Disponível em: <https://iea.blob.core.windows.net/assets/c3086240-732b-4f6a-89d7-db01be018f5e/GlobalEnergyReviewCO2Emissionsin2021.pdf>.

IPCC, 2005. IPCC special report on carbon dioxide capture and storage. Prepared by working group III of the Intergovernmental Panel on Climate Change.

IPCC, 2018. Global warming of 1,5 °C an IPCC Special Report on the Impacts of Global Warming of 1.5 °C above Pre-industrial Levels and Related Global Greenhouse Gas Emission Pathways, in the Context of Strengthening the Global Response to the Threat of Climate Change.

J. Liu, X. Li, K. Ho Row, Development of deep eutectic solvents for sustainable chemistry, Journal of Molecular Liquids. 362 (2022) 119654. https://doi.org/10.1016/j.molliq.2022.119654.

J. Wang, H. Cheng, Z. Song, L. Chen, L. Deng, Z. Qi, Carbon Dioxide Solubility in Phosphonium-Based Deep Eutectic Solvents: An Experimental and Molecular Dynamics Study, Industrial and Engineering Chemistry Research. 58 (2019) 17514–17523. https://doi.org/10.1021/acs.iecr.9b03740.

J. Wang, Z. Song, L. Chen, T. Xu, L. Deng, Z. Qi, Prediction of CO2 solubility in deep eutectic solvents using random forest model based on COSMO-RS-derived descriptors, Green Chemical Engineering. 2 (2021) 431–440. https://doi.org/10.1016/j.gce.2021.08.002.

J. Zhu, H. Shao, L. Feng, Y. Lu, H. Meng, C. Li, Absorptive separation of HCl gas by choline chloride-based deep eutectic solvents, J Mol Liq. 341 (2021) 116928. https://doi.org/10.1016/j.molliq.2021.116928.

J.B. Ott, J.R.E.X. Goates, J.D. Lamb, Solid-liquid phase equilibria in water-I- ethylene glycol, Journal of Chemical Thermodynamics. 4 (1972) 123–126.

J.G. Lynam, N. Kumar, M.J. Wong, Deep eutectic solvents' ability to solubilize lignin, cellulose, and hemicellulose; thermal stability; and density, Bioresource Technology. 238 (2017) 684–689. https://doi.org/10.1016/j.biortech.2017.04.079.

J.H. Dymond, R. Malhotra, The Tait equation: 100 years on, Int J Thermophys. 9 (1988) 941–951. https://doi.org/10.1007/BF01133262.

Jabrane, S.; Létoffé, J. .; Claudy, P. Study of the Thermal Behaviour of 1,3-Propanediol and Its Aqueous Solutions. Thermochim. Acta 1998, 311 (1–2), 121–127. https://doi.org/10.1016/S0040-6031(97)00416-4.

Jacquemin, J.; Costa Gomes, M. F.; Husson, P.; Majer, V. Solubility of Carbon Dioxide, Ethane, Methane, Oxygen, Nitrogen, Hydrogen, Argon, and Carbon Monoxide in 1-Butyl-3-Methylimidazolium Tetrafluoroborate between Temperatures 283 K and 343 K and at Pressures Close to Atmospheric. J. Chem. Thermodyn. 2006, 38, 490–502.

Jacquemin, J.; Husson, P.; Majer, V.; Gomes, M. F. C. Low-Pressure Solubilities and Thermodynamics of Solvation of Eight Gases in 1-Butyl-3-Methylimidazolium Hexafluorophosphate. Fluid Phase Equilib. 2006, 240, 87–95.

Jacquemin, J.; Husson, P.; Padua, A. A. H.; Majer, V. Density and Viscosity of Several Pure and Water-Saturated Ionic Liquids. Green Chem. 2006, 8, 172–180.

Ji, Y.; Hou, Y.; Ren, S.; Yao, C.; Wu, W. Phase Equilibria of High Pressure CO2 and Deep Eutectic Solvents Formed by Quaternary Ammonium Salts and Phenol. Fluid Phase Equilib. 2016, 429, 14–20.

Jiang, J.; Ye, B.; Liu, J. Research on the Peak of CO2 Emissions in the Developing World: Current Progress and Future Prospect. Appl. Energy 2019, 235, 186–203.

Jiao, T.; Qin, X.; Zhang, H.; Zhang, W.; Zhang, Y.; Liang, P. Separation of Phenol and Pyridine from Coal Tar via Liquid–Liquid Extraction Using Deep Eutectic Solvents. Chem. Eng. Res. Des. 2019, 145, 112–121. https://doi.org/10.1016/j.cherd.2019.03.006.

Joback, K. G.; Reid, R. C. Estimation of Pure-Component Properties from Group-Contributions. Chem. Eng. Commun. 1987, 57, 233–243.

Joshi, M., Hawkins, E., Sutton, R., Lowe, J., Frame, D., 2011. Projections of when temperature change will exceed 2°C above pre-industrial levels. Nat. Clim. Chang. 1, 407–412. https://doi.org/10.1038/nclimate1261

K. Kumar, S. Keshri, A. Bharti, S. Kumar, S. Mogurampelly, Solubility of Gases in Choline Chloride-Based Deep Eutectic Solvents from Molecular Dynamics Simulation, Ind Eng Chem Res. 61 (2022) 4659–4671. https://doi.org/10.1021/acs.iecr.1c04923.

K. Paduszyński, An overview of the performance of the COSMO-RS approach in predicting the activity coefficients of molecular solutes in ionic liquids and derived properties at infinite dilution, Physical Chemistry Chemical Physics. 19 (2017) 11835–11850. https://doi.org/10.1039/C7CP00226B.

K. Shahbaz, F.S. Mjalli, M.A. Hashim, I.M. AlNashef, Prediction of deep eutectic solvents densities at different temperatures, Thermochimica Acta. 515 (2011) 67–72. https://doi.org/10.1016/j.tca.2010.12.022.

K. Shahbaz, Farouq.S. Mjalli, M.A. Hashim, Inas.M. ALNashef, Using Deep Eutectic Solvents for the Removal of Glycerol from Palm Oil-Based Biodiesel, Journal of Applied Sciences. 10 (2010) 3349–3354. https://doi.org/10.3923/jas.2010.3349.3354.

K.A. Kurnia, S.P. Pinho, J.A.P. Coutinho, Evaluation of the Conductor-like Screening Model for Real Solvents for the Prediction of the Water Activity Coefficient at Infinite Dilution in Ionic Liquids, Ind Eng Chem Res. 53 (2014) 12466–12475. https://doi.org/10.1021/ie5021415.

K.R. Siongco, R.B. Leron, M.-H. Li, Densities, refractive indices, and viscosities of N,N-diethylethanol ammonium chloride–glycerol or –ethylene glycol deep eutectic solvents

and their aqueous solutions, The Journal of Chemical Thermodynamics. 65 (2013) 65–72. https://doi.org/10.1016/j.jct.2013.05.041.

Kamgar, A.; Mohsenpour, S.; Esmaeilzadeh, F. Solubility Prediction of CO2, CH4, H2, CO and N2 in Choline Chloride/Urea as a Eutectic Solvent Using NRTL and COSMO-RS Models. J. Mol. Liq. 2017, 247, 70–74.

Keyes, D. B. Handbook of Chemistry and Physics. Twelfth Edition (Hodgman, Charles D.; Lange, Norbert A.). J. Chem. Educ. 1928, 5, 241.

KLAMT, A. Conductor-like screening model for real solvents: A new approach to the quantitative calculation of solvation phenomena. Journal of Physical Chemistry, v. 99, n. 7, p. 2224–2235, 1995.

KLAMT, A. COSMO-RS From Quantum Chemistry to Fluid Phase Thermodynamics and Drug Design. 1st Editio ed. [s.l.] Elsevier Science, 2005.

KONTOGEORGIS, G. M. et al. An Equation of State for Associating Fluids. Industrial and Engineering Chemistry Research, v. 35, p. 4310–4318, 1996.

KONTOGEORGIS, G. M. et al. Multicomponent phase equilibrium calculations for water–methanol–alkane mixtures. Fluid Phase Equilibria, v. 158–160, p. 201–209, jun. 1999. Disponível em: <https://linkinghub.elsevier.com/retrieve/pii/S0378381299000606>.

Kontogeorgis, G.M., Folas, G.K., 2009. Thermodynamic Models for Industrial Applications: From Classical and Advanced Mixing Rules to Association Theories, Thermodynamic Models for Industrial Applications: From Classical and Advanced Mixing Rules to Association Theories. https://doi.org/10.1002/9780470747537

Krishnan, A., Gopinath, K.P., Vo, D.V.N., Malolan, R., Nagarajan, V.M., Arun, J., 2020. Ionic liquids, deep eutectic solvents and liquid polymers as green solvents in carbon capture technologies: a review. Environ. Chem. Lett. 18, 2031–2054. https://doi.org/10.1007/s10311-020-01057-y

Kumar, P. P.; Paramashivappa, R.; Vithayathil, P. J.; Rao, P. V. S.; Rao, A. S. Process for Isolation of Cardanol from Technical Cashew (Anacardium Occidentale l.) Nut Shell Liquid. J. Agric. Food Chem. 2002, 50, 4705–4708.

L. Fernandez, L.P. Silva, M.A.R. Martins, O. Ferreira, J. Ortega, S.P. Pinho, J.A.P. Coutinho, Indirect assessment of the fusion properties of choline chloride from solid-liquid equilibria data, Fluid Phase Equilibria. 448 (2017) 9–14. https://doi.org/10.1016/j.fluid.2017.03.015.

L. Moity, M. Durand, A. Benazzouz, C. Pierlot, V. Molinier, J.M. Aubry, Panorama of sustainable solvents using the COSMO-RS approach, Green Chemistry. 14 (2012) 1132–1145. https://doi.org/10.1039/c2gc16515e.

L. V. Yelash, T. Kraska, Closed-Loops of liquid-liquid immiscibility in binary mixtures of equal sized molecules predicted with a simple theoretical equation of state, Berichte Der Bunsengesellschaft Für Physikalische Chemie. 102 (1998) 213–223. https://doi.org/10.1002/bbpc.19981020212.

L.P. Silva, L. Fernandez, J.H.F. Conceição, M.A.R. Martins, A. Sosa, J. Ortega, S.P. Pinho, J.A.P. Coutinho, Design and Characterization of Sugar-Based Deep Eutectic Solvents Using Conductor-like Screening Model for Real Solvents, ACS Sustainable Chemistry & Engineering. 6 (2018) 10724–10734. https://doi.org/10.1021/acssuschemeng.8b02042.

L.P. Silva, M.A.R. Martins, D.O. Abranches, S.P. Pinho, J.A.P. Coutinho, Solid-liquid phase behavior of eutectic solvents containing sugar alcohols, Journal of Molecular Liquids. 337 (2021) 116392. https://doi.org/10.1016/j.molliq.2021.116392.

L.P. Silva, M.A.R. Martins, J.H.F. Conceição, S.P. Pinho, J.A.P. Coutinho, Eutectic Mixtures Based on Polyalcohols as Sustainable Solvents: Screening and Characterization, ACS Sustain Chem Eng. 8 (2020) 15317–15326. https://doi.org/10.1021/acssuschemeng.0c05518.

LANZA, M. Comportamento de Fases dos Óleos de Oliva, Soja e Mamona em n-Butano e Propano a Alta Pressão. 2004. URI-Campus de Erechim, Erechim/RS, 2004.

Leron, R. B.; Caparanga, A.; Li, M. H. Carbon Dioxide Solubility in a Deep Eutectic Solvent Based on Choline Chloride and Urea at T = 303.15-343.15K and Moderate Pressures. J. Taiwan Inst. Chem. Eng. 2013, 44, 879–885.

Leron, R. B.; Li, M. H. Solubility of Carbon Dioxide in a Choline Chloride-Ethylene Glycol Based Deep Eutectic Solvent. Thermochim. Acta 2013, 551, 14–19.

https://doi.org/10.1016/j.tca.2012.09.041.

Leron, R. B.; Li, M. H. Solubility of Carbon Dioxide in a Eutectic Mixture of Choline Chloride and Glycerol at Moderate Pressures. J. Chem. Thermodyn. 2013, 57, 131–136.

Leron, R.B., Li, M.H., 2012. High-pressure volumetric properties of choline chloride-ethylene glycol based deep eutectic solvent and its mixtures with water. Thermochim. Acta 546, 54–60. https://doi.org/10.1016/j.tca.2012.07.024

Leron, R.B., Soriano, A.N., Li, M.H., 2012. Densities and refractive indices of the deep eutectic solvents (choline chloride+ethylene glycol or glycerol) and their aqueous mixtures at the temperature ranging from 298.15 to 333.15K. J. Taiwan Inst. Chem. Eng. 43, 551–557. https://doi.org/10.1016/j.jtice.2012.01.007

Leung, D.Y.C., Caramanna, G., Maroto-Valer, M.M., 2014. An overview of current status of carbon dioxide capture and storage technologies. Renew. Sustain. Energy Rev. 39, 426–443. https://doi.org/10.1016/j.rser.2014.07.093

Li, B.; Li, Q.; Wang, Q.; Yan, X.; Shi, M.; Wu, C. Deep Eutectic Solvent for Spent Lithium-Ion Battery Recycling: Comparison with Inorganic Acid Leaching. Phys. Chem. Chem. Phys. 2022, 24 (32), 19029–19051. https://doi.org/10.1039/D1CP05968H.

Li, F., Hemmati, A., Rashidi, H., 2020. Industrial CO2 absorption into methyldiethanolamine/piperazine in place of monoethanolamine in the absorption column. Process Saf. Environ. Prot. 142, 83–91. https://doi.org/10.1016/j.psep.2020.06.006

Li, G., Deng, D., Chen, Y., Shan, H., Ai, N., 2014. Solubilities and thermodynamic properties of CO2 in choline-chloride based deep eutectic solvents. J. Chem. Thermodyn. 75, 58–62. https://doi.org/10.1016/j.jct.2014.04.012

Li, T.; Xiong, Y.; Yan, X.; Hu, T.; Jing, S.; Wang, Z.; Ge, X. Closed-Loop Cobalt Recycling from Spent Lithium-Ion Batteries Based on a Deep Eutectic Solvent (DES) with Easy Solvent Recovery. J. Energy Chem. 2022, 72, 532–538. https://doi.org/10.1016/j.jechem.2022.05.008.

Li, X.; Hou, M.; Han, B.; Wang, X.; Zou, L. Solubility of CO2 in a Choline Chloride + Urea Eutectic Mixture. J. Chem. Eng. Data 2008, 53 (2), 548–550.

https://doi.org/10.1021/je700638u.

Li, X.; Kersten, S. R. A.; Schuur, B. Extraction of Guaiacol from Model Pyrolytic Sugar Stream with Ionic Liquids. Ind. Eng. Chem. Res. 2016, 55, 4703–4710.

Li, Y.; Huang, W.; Zheng, D.; Mi, Y.; Dong, L. Solubilities of CO2 Capture Absorbents 2-Ethoxyethyl Ether, 2-Butoxyethyl Acetate and 2-(2-Ethoxyethoxy)Ethyl Acetate. Fluid Phase Equilib. 2014, 370, 1–7.

Lin, C. M.; Leron, R. B.; Caparanga, A. R.; Li, M. H. Henry's Constant of Carbon Dioxide-Aqueous Deep Eutectic Solvent (Choline Chloride/Ethylene Glycol, Choline Chloride/Glycerol, Choline Chloride/Malonic Acid) Systems. J. Chem. Thermodyn. 2014, 68, 216–220.

Liu, F.; Chen, W.; Mi, J.; Zhang, J. Y.; Kan, X.; Zhong, F. Y.; Huang, K.; Zheng, A. M.; Jiang, L. Thermodynamic and Molecular Insights into the Absorption of H2S, CO2 , and CH4 in Choline Chloride plus Urea Mixtures. AIChE J. 2019, 65, 1–10.

Liu, X., Ao, Q., Shi, S., Li, S., 2022. CO2capture by alcohol ammonia based deep eutectic solvents with different water content. Mater. Res. Express 9. https://doi.org/10.1088/2053-1591/ac47c6

Liu, X.; Gao, B.; Deng, D. SO2 Absorption/Desorption Performance of Renewable Phenol-Based Deep Eutectic Solvents. Sep. Sci. Technol. 2018, 53, 2150–2158.

Liu, X.; Gao, B.; Jiang, Y.; Ai, N.; Deng, D. Solubilities and Thermodynamic Properties of Carbon Dioxide in Guaiacol-Based Deep Eutectic Solvents. J. Chem. Eng. Data 2017, 62, 1448–1455.

Loow, Y.-L.; New, E. K.; Yang, G. H.; Ang, L. Y.; Foo, L. Y. W.; Wu, T. Y. Potential Use of Deep Eutectic Solvents to Facilitate Lignocellulosic Biomass Utilization and Conversion. Cellulose 2017, 24 (9), 3591–3618. https://doi.org/10.1007/s10570-017-1358-y.

Loow, Y.-L.; Wu, T. Y.; Yang, G. H.; Ang, L. Y.; New, E. K.; Siow, L. F.; Md. Jahim, J.; Mohammad, A. W.; Teoh, W. H. Deep Eutectic Solvent and Inorganic Salt Pretreatment of Lignocellulosic Biomass for Improving Xylose Recovery. Bioresour. Technol. 2018, 249, 818–825. https://doi.org/10.1016/j.biortech.2017.07.165.

Lu, B.; Du, R.; Wang, G.; Wang, Y.; Dong, S.; Zhou, D.; Wang, S.; Li, C. High-Efficiency Leaching of Valuable Metals from Waste Li-Ion Batteries Using Deep Eutectic Solvents. Environ. Res. 2022, 212, 113286. https://doi.org/10.1016/j.envres.2022.113286.

Lu, M.; Han, G.; Jiang, Y.; Zhang, X.; Deng, D.; Ai, N. Solubilities of Carbon Dioxide in the Eutectic Mixture of Levulinic Acid (or Furfuryl Alcohol) and Choline Chloride. J. Chem. Thermodyn. 2015, 88, 72–77.

Luo, X. Y.; Fan, X.; Shi, G. L.; Li, H. R.; Wang, C. M. Decreasing the Viscosity in CO2 Capture by Amino-Functionalized Ionic Liquids through the Formation of Intramolecular Hydrogen Bond. J. Phys. Chem. B 2016, 120, 2807–2813.

Luo, X.; Guo, Y.; Ding, F.; Zhao, H.; Cui, G.; Li, H.; Wang, C. Significant Improvements in CO2 Capture by Pyridine-Containing Anion-Functionalized Ionic Liquids through Multiple-Site Cooperative Interactions. Angew. Chemie - Int. Ed. 2014, 53, 7053–7057.

Lydersen, A. L. Estimation of Critical Properties of Organic Compounds by the Method of Group Contibutions; Madison, 1955.

M. Diedenhofen, A. Klamt, COSMO-RS as a tool for property prediction of IL mixtures—A review, Fluid Phase Equilib. 294 (2010) 31–38. https://doi.org/10.1016/j.fluid.2010.02.002.

M. Faggian, S. Sut, B. Perissutti, V. Baldan, I. Grabnar, S. Dall'Acqua, Natural Deep Eutectic Solvents (NADES) as a Tool for Bioavailability Improvement: Pharmacokinetics of Rutin Dissolved in Proline/Glycine after Oral Administration in Rats: Possible Application in Nutraceuticals, Molecules. 21 (2016) 1531. https://doi.org/10.3390/molecules21111531.

M. Hayyan, T. Aissaoui, M.A. Hashim, M.A. AlSaadi, A. Hayyan, Triethylene glycol based deep eutectic solvents and their physical properties, Journal of the Taiwan Institute of Chemical Engineers. 50 (2015) 24–30. https://doi.org/10.1016/j.jtice.2015.03.001.

M. Höök, X. Tang, Depletion of fossil fuels and anthropogenic climate change—A review, Energy Policy. 52 (2013) 797–809. https://doi.org/10.1016/j.enpol.2012.10.046.

M. Lu, G. Han, Y. Jiang, X. Zhang, D. Deng, N. Ai, Solubilities of carbon dioxide in the eutectic mixture of levulinic acid (or furfuryl alcohol) and choline chloride, J Chem Thermodyn. 88 (2015) 72–77. https://doi.org/10.1016/j.jct.2015.04.021.

M. Ramdin, S.P. Balaji, J.M. Vicent-Luna, J.J. Gutiérrez-Sevillano, S. Calero, T.W. De Loos, T.J.H. Vlugt, Solubility of the precombustion gases CO2, CH4, CO, H2, N2, and H2S in the ionic liquid [bmim][Tf2N] from Monte Carlo simulations, Journal of Physical Chemistry C. 118 (2014) 23599–23604. https://doi.org/10.1021/jp5080434.

M. Wang, C. Li, M. Zhou, Z. Xia, Y. Huang, Natural deep eutectic solvent assisted synthesis and applications of chiral carbon dots, Green Chemistry. (2022). https://doi.org/10.1039/D2GC01949C.

M. Xu, H. Dou, F. Peng, N. Yang, X. Xiao, X. Tantai, Y. Sun, B. Jiang, L. Zhang, Ultra-stable copper decorated deep eutectic solvent based supported liquid membranes for olefin/paraffin separation: In-depth study of carrier stability, Journal of Membrane Science. 659 (2022) 120775. https://doi.org/10.1016/j.memsci.2022.120775.

M. Yang, T. Narita, Y. Tanaka, T. Sotani, S. Matsuo, Solid–liquid phase equilibria in binary (1-octanol + n-alkane) mixtures under high-pressure, Fluid Phase Equilibria. 204 (2003) 55–64. https://doi.org/10.1016/S0378-3812(02)00203-0.

M.A. Sedghamiz, S. Raeissi, Physical properties of deep eutectic solvents formed by the sodium halide salts and ethylene glycol, and their mixtures with water, Journal of Molecular Liquids. 269 (2018) 694–702. https://doi.org/10.1016/j.molliq.2018.08.045.

M.B. Taysun, E. Sert, F.S. Atalay, Physical properties of benzyl tri-methyl ammonium chloride based deep eutectic solvents and employment as catalyst, Journal of Molecular Liquids. 223 (2016) 845–852. https://doi.org/10.1016/j.molliq.2016.07.148.

M.J. Pratas, M.B. Oliveira, M.J. Pastoriza-Gallego, A.J. Queimada, M.M. Piñeiro, J.A.P. Coutinho, High-pressure biodiesel density: Experimental measurements, correlation, and cubic-plus-association equation of state (CPA EoS) modeling, Energy and Fuels. 25 (2011) 3806–3814. https://doi.org/10.1021/ef200807m.

M.K. Alomar, M. Hayyan, M.A. Alsaadi, S. Akib, A. Hayyan, M.A. Hashim, Glycerol-based deep eutectic solvents: Physical properties, Journal of Molecular Liquids. 215 (2016) 98–103. https://doi.org/10.1016/j.molliq.2015.11.032.

Malik, A.; Dhattarwal, H. S.; Kashyap, H. K. Distinct Solvation Structures of CO2and SO2 in Reline and Ethaline Deep Eutectic Solvents Revealed by AIMD Simulations. J. Phys. Chem. B 2021, 125, 1852–1860.

Martins, M. A. R.; Sharma, G.; Pinho, S. P.; Gardas, R. L.; Coutinho, J. A. P.; Carvalho, P. J. Selection and Characterization of Non-Ideal Ionic Liquids Mixtures to Be Used in CO2 Capture. Fluid Phase Equilib. 2020, 518, 1–13.

Maximo, G.J., Carareto, N.D.D., Costa, M.C., 2019. Thermodynamics of Phase Equilibria in Food Engineering, 1st ed, Thermodynamics of Phase Equilibria in Food Enhineering. Elsevier. https://doi.org/10.1016/C2016-0-01686-8

Mirza, N. R.; Nicholas, N. J.; Wu, Y.; Mumford, K. A.; Kentish, S. E.; Stevens, G. W. Experiments and Thermodynamic Modeling of the Solubility of Carbon Dioxide in Three Different Deep Eutectic Solvents (DESs). J. Chem. Eng. Data 2015, 60, 3246–3252. https://doi.org/10.1021/acs.jced.5b00492.

Mohamed, H.O., Obaid, M., Sayed, E.T., Abdelkareem, M.A., Park, M., Liu, Y., Kim, H.Y., Barakat, N.A.M., 2017. Graphite Sheets as High-Performance Low-Cost Anodes for Microbial Fuel Cells Using Real Food Wastewater. Chem. Eng. Technol. 40, 2243–2250. https://doi.org/10.1002/ceat.201700058

Mohammadpour, Z.; Abdollahi, S. H.; Safavi, A. Sugar-Based Natural Deep Eutectic Mixtures as Green Intercalating Solvents for High-Yield Preparation of Stable MoS 2 Nanosheets: Application to Electrocatalysis of Hydrogen Evolution Reaction. ACS Appl. Energy Mater. 2018, 1 (11), 5896–5906. https://doi.org/10.1021/acsaem.8b00838.

Mota-Morales, J. D.; Gutiérrez, M. C.; Ferrer, M. L.; Sanchez, I. C.; Elizalde-Peña, E. A.; Pojman, J. A.; Monte, F. Del; Luna-Bárcenas, G. Deep Eutectic Solvents as Both Active Fillers and Monomers for Frontal Polymerization. J. Polym. Sci. Part A Polym. Chem. 2013, 51 (8), 1767–1773. https://doi.org/10.1002/pola.26555.

Mulvihill, M. J.; Beach, E. S.; Zimmerman, J. B.; Anastas, P. T. Green Chemistry and Green Engineering: A Framework for Sustainable Technology Development. Annu. Rev. Environ. Resour. 2011, 36 (1), 271–293. https://doi.org/10.1146/annurev-environ-032009-095500.

N. Ramzan, M. Rizwan, M. Zaman, M. Adnan, A. Ullah, A. Gungor, U. Shakeel, A. ul Haq, Pre-combustion carbon dioxide capture: A thermo-economic comparison for dual-stage Selexol process and combined Sulfinol-Selexol process, Int J Energy Res. (2022). https://doi.org/10.1002/er.8674.

N. Xia, L. Xiong, S. Bi, F. Qian, P. Wang, Development of biocompatible DES/NADES as co-solvents for efficient biosynthesis of chiral alcohols, Bioprocess and Biosystems Engineering. 43 (2020) 1987–1997. https://doi.org/10.1007/s00449-020-02387-5.

N.D. Dorighello Carareto, M.C. Costa, A.J.A. Meirelles, J. Pauly, High Pressure Solid-Liquid Equilibrium of Fatty Alcohols Binary Systems from 1-Dodecanol, 1-Tetradecanol, 1-Hexadecanol, and 1-Octadecanol, Journal of Chemical and Engineering Data. 60 (2015) 2966–2973. https://doi.org/10.1021/acs.jced.5b00330.

N.D.D. Carareto, M.C. Costa, A.J.A. Meirelles, J. Pauly, High pressure solid-liquid equilibrium of fatty acid ethyl esters binary systems, Fluid Phase Equilibria. 382 (2014) 158–163. https://doi.org/10.1016/j.fluid.2014.09.007.

N.F. Gajardo-Parra, M.J. Lubben, J.M. Winnert, Á. Leiva, J.F. Brennecke, R.I. Canales, Physicochemical properties of choline chloride-based deep eutectic solvents and excess properties of their pseudo-binary mixtures with 1-butanol, The Journal of Chemical Thermodynamics. 133 (2019) 272–284. https://doi.org/10.1016/j.jct.2019.02.010.

N.G.O. Santos, E.A. Rebelatto, D.A. Mayer, M. Lanza, J. Vladimir Oliveira, High-pressure phase behavior of the quaternary system (carbon dioxide + dichloromethane + ε–caprolactone + poly(ε–caprolactone): Experimental data and PC-SAFT modeling, Fluid Phase Equilibria. 554 (2022) 113306. https://doi.org/10.1016/j.fluid.2021.113306.

NDIAYE, P. M. Equilíbrio de Fases de Óleos Vegetais e de Biodiesel em CO2, Propano e n- Butano. 2004. Universidade Federal do Rio de Janeiro, Escola de Química, Rio de Janeiro/RJ, 2004.

No Title, (n.d.). https://doi.org/https://doi.org/10.1016/j.rser.2012.10.020.

Nozaeim, A. A.; Tavasoli, A.; Mortaheb, H. R.; Mafi, M. CO2 Absorption/Desorption in Aqueous DEEA/MDEA and Their Hybrid Solutions with Sulfolane. J. Nat. Gas Sci. Eng. 2020, 76, 1–10.

O. Zannou, H. Pashazadeh, C.M. Galanakis, A.S. Alamri, I. Koca, Carboxylic acid-based deep eutectic solvents combined with innovative extraction techniques for greener extraction of phenolic compounds from sumac (Rhus coriaria L.), Journal of Applied Research on Medicinal and Aromatic Plants. 30 (2022) 100380. https://doi.org/10.1016/j.jarmap.2022.100380.

O.G. Sas, G.R. Ivaniš, M.L. Kijevčanin, B. González, A. Domínguez, I.R. Radović, High pressure densities and derived thermodynamic properties of deep eutectic solvents with menthol and saturated fatty acids, Journal of Chemical Thermodynamics. 162 (2021) 1–10. https://doi.org/10.1016/j.jct.2021.106578.

O.V. Junior, L. Ferreira-Pinto, V.F. Cabral, W.M. Giufrida, L. Cardozo-Filho, Experimental Measurements of the {CO 2 (1) + Acetone (2) + Ivermectin (3)} System at High Pressure, Journal of Chemical & Engineering Data. 64 (2019) 3786–3792. https://doi.org/10.1021/acs.jced.9b00072.

Oliveira, M.B., Queimada, A.J., Kontogeorgis, G.M., Coutinho, J.A.P., 2011. Evaluation of the CO2 behavior in binary mixtures with alkanes, alcohols, acids and esters using the Cubic-Plus-Association Equation of State. J. Supercrit. Fluids 55, 876–892. https://doi.org/10.1016/j.supflu.2010.09.036

P. Anastas, N. Eghbali, Green Chemistry: Principles and Practice, Chem. Soc. Rev. 39 (2010) 301–312. https://doi.org/10.1039/B918763B.

P. Zhang, W. Xiong, M. Shi, Z. Tu, X. Hu, X. Zhang, Y. Wu, Natural deep eutectic solvent-based gels with multi-site interaction mechanism for selective membrane separation of SO2 from N2 and CO2, Chemical Engineering Journal. 438 (2022) 135626. https://doi.org/10.1016/j.cej.2022.135626.

P.V.A. Pontes, E.A. Crespo, M.A.R. Martins, L.P. Silva, C.M.S.S. Neves, G.J. Maximo, M.D. Hubinger, E.A.C. Batista, S.P. Pinho, J.A.P. Coutinho, G. Sadowski, C. Held, Measurement and PC-SAFT modeling of solid-liquid equilibrium of deep eutectic solvents of quaternary ammonium chlorides and carboxylic acids, Fluid Phase Equilib. 448 (2017) 69–80. https://doi.org/10.1016/j.fluid.2017.04.007.

Pachauri, R.K., Allen, M.R., Barros, V.R., Broome, J., Cramer, W., Christ, R., Church, J.A., Clarke, L., Dahe, Q., Dasgupta, P., Dubash, N.K., Edenhofer, O., Elgizouli, I.,

Field, C.B., Forster, P., Friedlingstein, P., Fuglestvedt, J, J.P., 2014. Climate Change 2014: Synthesis Report. Contribution of Working Groups I, II and III to the Fifth Assessment Report of the Intergovernmental Panel on Climate Change. Geneva, Switzerland.

Pandey, D.; Mondal, M. K. Equilibrium CO2 Solubility in the Aqueous Mixture of MAE and AEEA: Experimental Study and Development of Modified Thermodynamic Model. Fluid Phase Equilib. 2020, 522, 1–11.

Pelaquim, F. P.; Bitencourt, R. G.; Neto, A. M. B.; Dalmolin, I. A. L.; da Costa, M. C. Carbon Dioxide Solubility in Deep Eutectic Solvents: Modelling Using Cubic Plus Association and Peng-Robinson Equations of State. Process Saf. Environ. Prot. 2022, 163, 14–26. https://doi.org/10.1016/j.psep.2022.04.075.

Pelaquim, F.P., Barbosa Neto, A.M., Dalmolin, I.A.L., Costa, M.C. da, 2021. Gas Solubility Using Deep Eutectic Solvents: Review and Analysis. Ind. Eng. Chem. Res. acs.iecr.1c00947. https://doi.org/10.1021/acs.iecr.1c00947

PENG, D. Y.; ROBINSON, D. B. A New Two-Constant Equation of State. Industrial and Engineering Chemistry Fundamentals, v. 15, p. 59–64, 1976.

PENG, D. Y.; ROBINSON, D. B. The Characterization of the Heptanes and Heavier Fractions for the GPA Peng-Robinson Programs. [s.l.] Gas Processors Association, 1978.

Pires, J. C. M.; Martins, F. G.; Alvim-Ferraz, M. C. M.; Simões, M. Recent Developments on Carbon Capture and Storage: An Overview. Chem. Eng. Res. Des. 2011, 89, 1446–1460.

PISHRO, K. A. et al. Carbon dioxide solubility in amine-based deep eutectic solvents: Experimental and theoretical investigation. Journal of Molecular Liquids, v. 325, p. 115133, 2021. Disponível em: <https://doi.org/10.1016/j.molliq.2020.115133>.

Prausnitz, J. M.; Lichtenthaler, R. N.; de Azevedo, E. G. Molecular Thermodynamics of Fluid-Phase Equilibria, 3rd ed.; Prentice Hall: Nova Jersey, 1999. https://doi.org/10.1016/0021-9614(70)90078-9.

Q. Yu, F. Wang, Y. Jian, V.M. Chernyshev, Y. Zhang, Z. Wang, Z. Yuan, X. Chen, Extraction of flavonoids from Glycyrrhiza residues using deep eutectic solvents and its

molecular mechanism, Journal of Molecular Liquids. 363 (2022) 119848. https://doi.org/10.1016/j.molliq.2022.119848.

Q. Zhang, K. De Oliveira Vigier, S. Royer, F. Jérôme, Deep eutectic solvents: Syntheses, properties and applications, Chem Soc Rev. 41 (2012) 7108–7146. https://doi.org/10.1039/c2cs35178a.

Qin, H., Song, Z., Cheng, H., Deng, L., Qi, Z., 2021. Physical absorption of carbon dioxide in imidazole-PTSA based deep eutectic solvents. J. Mol. Liq. 326, 1–7. https://doi.org/10.1016/j.molliq.2021.115292

R. S. Mulliken. Electronic Population Analysis on LCAO-MO Molecular Wave Functions. I. J. Chem. Phys 1955, 23, 1833–1840.

R. Yusof, E. Abdulmalek, K. Sirat, M. Rahman, Tetrabutylammonium Bromide (TBABr)-Based Deep Eutectic Solvents (DESs) and Their Physical Properties, Molecules. 19 (2014) 8011–8026. https://doi.org/10.3390/molecules19068011.

R. Zhao, D. Pei, P. Yu, J. Wei, N. Wang, D. Di, Y. Liu, Aqueous two-phase systems based on deep eutectic solvents and their application in green separation processes, J Sep Sci. 43 (2020) 348–359. https://doi.org/10.1002/jssc.201900991.

R.C. Wilhoit, Daniel. Shiao, Thermochemistry of Biologically Important Compounds. Heats of Combustion of Solid Organic Acids., Journal of Chemical & Engineering Data. 9 (1964) 595–599. https://doi.org/10.1021/je60023a038.

R.J. Hemley, Effects of High Pressure on Molecules, Annual Review of Physical Chemistry. 5 (2000) 763–800.

R.K. Ibrahim, M. Hayyan, M.A. AlSaadi, S. Ibrahim, A. Hayyan, M.A. Hashim, Physical properties of ethylene glycol-based deep eutectic solvents, Journal of Molecular Liquids. 276 (2019) 794–800. https://doi.org/10.1016/j.molliq.2018.12.032.

R.M. Dias, M.C. da Costa, Y.P. Jimenez, Perspectives of Using DES-Based Systems for Solid–Liquid and Liquid–Liquid Extraction of Metals from E-Waste, Minerals. 12 (2022) 1–20. https://doi.org/10.3390/min12060710.

Rabaia, M.K.H., Abdelkareem, M.A., Sayed, E.T., Elsaid, K., Chae, K.J., Wilberforce, T., Olabi, A.G., 2021. Environmental impacts of solar energy systems: A review. Sci.

Total Environ. 754, 1–19. https://doi.org/10.1016/j.scitotenv.2020.141989

Rabhi, F.; Mutelet, F.; Sifaoui, H. Solubility of Carbon Dioxide in Carboxylic Acid-Based Deep Eutectic Solvents. J. Chem. Eng. Data 2021, 66, 702–711. https://doi.org/10.1021/acs.jced.0c00844.

RABHI, F.; MUTELET, F.; SIFAOUI, H. Solubility of Carbon Dioxide in Carboxylic Acid-Based Deep Eutectic Solvents. Journal of Chemical and Engineering Data, v. 66, p. 702–711, 2021.

Ramdin, M.; Balaji, S. P.; Vicent-Luna, J. M.; Gutiérrez-Sevillano, J. J.; Calero, S.; De Loos, T. W.; Vlugt, T. J. H. Solubility of the Precombustion Gases CO2, CH4, CO, H2, N2, and H2S in the Ionic Liquid [Bmim][Tf2N] from Monte Carlo Simulations. J. Phys. Chem. C 2014, 118, 23599–23604.

Ramdin, M.; De Loos, T. W.; Vlugt, T. J. H. State-of-the-Art of CO 2 Capture with Ionic Liquids. Ind. Eng. Chem. Res. 2012, 51 (24), 8149–8177.

RAMZAN, N. et al. Pre-combustion carbon dioxide capture: A thermo-economic comparison for dual-stage Selexol process and combined Sulfinol-Selexol process. International Journal of Energy Research, 2022.

Renon, H., Prausnitz, J.M., 1968. Local compositions in thermodynamic excess functions for liquid mixtures. AIChE J. 14, 135–144. https://doi.org/10.1002/aic.690140124

Ribeiro, B. D.; Florindo, C.; Iff, L. C.; Coelho, M. A. Z.; Marrucho, I. M. Menthol-Based Eutectic Mixtures: Hydrophobic Low Viscosity Solvents. ACS Sustain. Chem. Eng. 2015, 3, 2469–2477.

ROCHELLE, G. T. Thermal degradation of amines for CO2 capture. Current Opinion in Chemical Engineering, v. 1, p. 183–190, 2012. Disponível em: <http://dx.doi.org/10.1016/j.coche.2012.02.004>.

Rogošić, M.; Krišto, A.; Kučan, K. Z. DEEP EUTECTIC SOLVENTS BASED ON BETAINE AND PROPYLENE GLYCOL AS POTENTIAL DENITRIFICATION AGENTS: A LIQUID-LIQUID EQUILIBRIUM STUDY. Brazilian J. Chem. Eng. 2019, 36 (4), 1703–1716. https://doi.org/10.1590/0104-6632.20190364s20190049.

S. Benabid, Y. Benguerba, I.M. AlNashef, N. Haddaoui, Theoretical study of physicochemical properties of selected ammonium salt-based deep eutectic solvents, Journal of Molecular Liquids. 285 (2019) 38–46. https://doi.org/10.1016/j.molliq.2019.04.052.

S. Cherukuvada, A. Nangia, Eutectics as improved pharmaceutical materials: design, properties and characterization, Chem. Commun. 50 (2014) 906–923. https://doi.org/10.1039/C3CC47521B.

S. Deniz, A.E. Ünlü, S. Takaç, Ultrasound-assisted natural deep eutectic solvent extraction of phenolic compounds from apple pomace, Separation Science and Technology. (2022) 1–12. https://doi.org/10.1080/01496395.2022.2112603.

S. Jabrane, J.M. Létoffé, P. Claudy, Study of the thermal behaviour of 1,3-propanediol and its aqueous solutions, Thermochimica Acta. 311 (1998) 121–127. https://doi.org/10.1016/S0040-6031(97)00416-4.

S. Sun, Y. Niu, Q. Xu, Z. Sun, X. Wei, Efficient SO2 absorptions by four kinds of deep eutectic solvents based on choline chloride, Ind Eng Chem Res. 54 (2015) 8019–8024. https://doi.org/10.1021/acs.iecr.5b01789.

S.P. Ijardar, Deep eutectic solvents composed of tetrabutylammonium bromide and PEG: Density, speed of sound and viscosity as a function of temperature, The Journal of Chemical Thermodynamics. 140 (2020) 105897. https://doi.org/10.1016/j.jct.2019.105897.

Salehi, H. S.; Hens, R.; Moultos, O. A.; Vlugt, T. J. H. Computation of Gas Solubilities in Choline Chloride Urea and Choline Chloride Ethylene Glycol Deep Eutectic Solvents Using Monte Carlo Simulations. J. Mol. Liq. 2020, 316, 1–10.

Salleh, Z.; Wazeer, I.; Mulyono, S.; El-blidi, L.; Hashim, M. A.; Hadj-Kali, M. K. Efficient Removal of Benzene from Cyclohexane-Benzene Mixtures Using Deep Eutectic Solvents – COSMO-RS Screening and Experimental Validation. J. Chem. Thermodyn. 2017, 104, 33–44.

Santos, N. G. O.; Rebelatto, E. A.; Mayer, D. A.; Lanza, M.; Vladimir Oliveira, J. High-Pressure Phase Behavior of the Quaternary System (Carbon Dioxide + Dichloromethane + E–caprolactone + Poly(E–caprolactone): Experimental Data and

PC-SAFT Modeling. Fluid Phase Equilib. 2022, 554, 113306. https://doi.org/10.1016/j.fluid.2021.113306.

Sarmad, S., Mikkola, J.P., Ji, X., 2017. Carbon Dioxide Capture with Ionic Liquids and Deep Eutectic Solvents: A New Generation of Sorbents. ChemSusChem 10, 324–352. https://doi.org/10.1002/cssc.201600987

Sarmad, S., Nikjoo, D., Mikkola, J.P., 2020. Amine functionalized deep eutectic solvent for CO2 capture: Measurements and modeling. J. Mol. Liq. 309, 1–11. https://doi.org/10.1016/j.molliq.2020.113159

Schaeffer, N.; Martins, M. A. R.; Neves, C. M. S. S.; Pinho, S. P.; Coutinho, J. A. P. Sustainable Hydrophobic Terpene-Based Eutectic Solvents for the Extraction and Separation of Metals. Chem. Commun. 2018, 54, 8104–8107.

Schmelz, W.J., Hochman, G., Miller, K.G., 2020. Total cost of carbon capture and storage implemented at a regional scale: northeastern and midwestern United States. Interface Focus 10, 1–15. https://doi.org/10.1098/rsfs.2019.0065

Scripps Institution of Oceanography. The Keeling Curve https://scripps.ucsd.edu/programs/keelingcurve/ (accessed Oct 6, 2022).

SHAHBAZ, K. et al. Prediction of deep eutectic solvents densities at different temperatures. Thermochimica Acta, v. 515, n. 1–2, p. 67–72, 2011. Disponível em: <http://dx.doi.org/10.1016/j.tca.2010.12.022>.

Shahbaz, K.; Baroutian, S.; Mjalli, F. S.; Hashim, M. A.; Alnashef, I. M. Densities of Ammonium and Phosphonium Based Deep Eutectic Solvents: Prediction Using Artificial Intelligence and Group Contribution Techniques. Thermochim. Acta 2012, 527, 59–66.

Shahbaz, K.; Mjalli, F. S.; Vakili-Nezhaad, G.; AlNashef, I. M.; Asadov, A.; Farid, M. M. Thermogravimetric Measurement of Deep Eutectic Solvents Vapor Pressure. J. Mol. Liq. 2016, 222, 61–66. https://doi.org/10.1016/j.molliq.2016.06.106.

Shukla, S. K.; Mikkola, J. P. Intermolecular Interactions upon Carbon Dioxide Capture in Deep-Eutectic Solvents. Phys. Chem. Chem. Phys. 2018, 20, 24591–24601.

Shunji, K.; Xizhou, S.; Wenze, Y. Investigation of CO2 Desorption Kinetics in MDEA

and MDEA+DEA Rich Amine Solutions with Thermo-Gravimetric Analysis Method. Int. J. Greenh. Gas Control 2020, 95, 1–10.

Siani, G.; Tiecco, M.; Di Profio, P.; Guernelli, S.; Fontana, A.; Ciulla, M.; Canale, V. Physical Absorption of CO2 in Betaine/Carboxylic Acid-Based Natural Deep Eutectic Solvents. J. Mol. Liq. 2020, 315, 1–7. https://doi.org/10.1016/j.molliq.2020.113708.

Silva, L. P.; Martins, M. A. R.; Conceição, J. H. F.; Pinho, S. P.; Coutinho, J. A. P. Eutectic Mixtures Based on Polyalcohols as Sustainable Solvents: Screening and Characterization. ACS Sustain. Chem. Eng. 2020, 8, 15317–15326. https://doi.org/10.1021/acssuschemeng.0c05518.

Skylogianni, E.; Perinu, C.; Cervantes Gameros, B. Y.; Knuutila, H. K. Carbon Dioxide Solubility in Mixtures of Methyldiethanolamine with Monoethylene Glycol, Monoethylene Glycol–Water, Water and Triethylene Glycol. J. Chem. Thermodyn. 2020, 151, 1–10.

Sohaib, Q.; Vadillo, J. M.; Gómez-Coma, L.; Albo, J.; Druon-Bocquet, S.; Irabien, A.; Sanchez-Marcano, J. CO2 Capture with Room Temperature Ionic Liquids; Coupled Absorption/Desorption and Single Module Absorption in Membrane Contactor. Chem. Eng. Sci. 2020, 223, 1–11.

Song, Z., Song, Z., Hu, X., Wu, H., Mei, M., Linke, S., Zhou, T., Zhou, T., Qi, Z., Sundmacher, K., Sundmacher, K., 2020. Systematic Screening of Deep Eutectic Solvents as Sustainable Separation Media Exemplified by the CO2 Capture Process. ACS Sustain. Chem. Eng. 8, 8741–8751. https://doi.org/10.1021/acssuschemeng.0c02490

Soriano, A. N.; Doma, B. T.; Li, M. H. Solubility of Carbon Dioxide in 1-Ethyl-3-Methylimidazolium Tetrafluoroborate. J. Chem. Eng. Data 2008, 53, 2550–2555.

Sosa, F. H. B.; Costa, M. C.; Silvestre, A. J. D.; Costa Lopes, A. M. Deep Eutectic Solvents for Sustainable Separation Processes. Sustain. Sep. Eng. 2022, 2, 605–652. https://doi.org/10.1002/9781119740117.ch17.

STEFFEN, C. et al. TmoleX-A graphical user interface for TURBOMOLE. Journal of Computational Chemistry, v. 31, p. 2967–2970, 19 ago. 2010. Disponível em: <https://onlinelibrary.wiley.com/doi/10.1002/jcc.21576>.

Stevanovic, S.; Costa Gomes, M. F. Solubility of Carbon Dioxide, Nitrous Oxide, Ethane, and Nitrogen in 1-Butyl-1-Methylpyrrolidinium and Trihexyl(Tetradecyl)Phosphonium Tris(Pentafluoroethyl)Trifluorophosphate (EFAP) Ionic Liquids. J. Chem. Thermodyn. 2013, 59, 65–71.

Sultan, T., Zabiri, H., Shahbaz, M., Maulud, A.S., 2021. Performance Evaluation of the Fast Model Predictive Control Scheme on a CO2 Capture Plant through Absorption/Stripping System. Process Saf. Environ. Prot. 157, 218–236. https://doi.org/10.1016/j.psep.2021.11.018

Sun, C.; Wang, S.; Zhou, S.; Chen, C. SO2 Effect on Monoethanolamine Oxidative Degradation in CO2 Capture Process. Int. J. Greenh. Gas Control 2014, 23, 98–104.

Sun, S.; Niu, Y.; Xu, Q.; Sun, Z.; Wei, X. Efficient SO2 Absorptions by Four Kinds of Deep Eutectic Solvents Based on Choline Chloride. Ind. Eng. Chem. Res. 2015, 54, 8019–8024.

T.E. Daubert, H.M. Sibul, C.C. Stebbins, R.P. Danner, R.L. Rowley, M.E. Adams, W. V Wilding, T.L. Marshall, Physical and Thermodynamic Properties of Pure Chemicals: DIPPR: Data Compilation: Core + Supplements 1−10, Taylor & Francis, 2000.

Taib, M. M.; Murugesan, T. Solubilities of CO2 in Aqueous Solutions of Ionic Liquids (ILs) and Monoethanolamine (MEA) at Pressures from 100 to 1600kPa. Chem. Eng. J. 2012, 181–182, 56–62. https://doi.org/10.1016/j.cej.2011.09.048.

Tapia, J.F.D., Lee, J.Y., Ooi, R.E.H., Foo, D.C.Y., Tan, R.R., 2016. Planning and scheduling of CO2 capture, utilization and storage (CCUS) operations as a strip packing problem. Process Saf. Environ. Prot. 104, 358–372. https://doi.org/10.1016/j.psep.2016.09.013

The 2030 Agenda for sustainable development, 2016. https://doi.org/10.1201/b20466-7.

THOMSON, G. H.; BROBST, K. R.; HANKINSON, R. W. An improved correlation for densities of compressed liquids and liquid mixtures. AIChE Journal, v. 28, n. 4, p. 671–676, 1982.

TSIVINTZELIS, I. et al. Modeling phase equilibria for acid gas mixtures using the CPA equation of state. Part II: Binary mixtures with CO2. Fluid Phase Equilibria, v. 306, p.

38–56, 2011. Disponível em: <http://dx.doi.org/10.1016/j.fluid.2011.02.006>.

Twu, C.H., 1986. Generalized method for predicting viscosities of petroleum fractions. AIChE J. 32, 2091–2094. https://doi.org/10.1002/aic.690321221

Ullah, R.; Atilhan, M.; Anaya, B.; Khraisheh, M.; García, G.; Elkhattat, A.; Tariq, M.; Aparicio, S. A Detailed Study of Cholinium Chloride and Levulinic Acid Deep Eutectic Solvent System for CO2capture via Experimental and Molecular Simulation Approaches. Phys. Chem. Chem. Phys. 2015, 17, 20941–20960.

V. Sivabalan, N. Hasnor, B. Lal, Z. Kassim, A.S. Maulud, Tetraethylammoniumacetate and tetraethylammonium bromide-based deep eutectic solvents as thermodynamic CO2 gas hydrate inhibitors, Applied Sciences (Switzerland). 10 (2020). https://doi.org/10.3390/app10196794.

V.N. Emel'yanenko, S.P. Verevkin, E.N. Stepurko, G.N. Roganov, M.K. Georgieva, Thermodynamic properties of glycolic acid and glycolide, Russian Journal of Physical Chemistry A. 84 (2010) 1301–1308. https://doi.org/10.1134/S0036024410080054.

VALDERRAMA, J. O.; ROBLES, P. A. Critical properties, normal boiling temperature, and acentric factor of another 200 ionic liquids. Industrial and Engineering Chemistry Research, v. 46, p. 1338–1344, 2007.

VALENCIA-MARQUEZ, D.; FLORES-TLACUAHUAC, A.; VASQUEZ-MEDRANO, R. An optimization approach for CO2 capture using ionic liquids. Journal of Cleaner Production, v. 168, p. 1652–1667, dez. 2017. Disponível em: <https://linkinghub.elsevier.com/retrieve/pii/S0959652616319035>.

Van Osch, D. J. G. P.; Parmentier, D.; Dietz, C. H. J. T.; Van Den Bruinhorst, A.; Tuinier, R.; Kroon, M. C. Removal of Alkali and Transition Metal Ions from Water with Hydrophobic Deep Eutectic Solvents. Chem. Commun. 2016, 52, 11987–11990.

Van Osch, D. J. G. P.; Zubeir, L. F.; Van Den Bruinhorst, A.; Rocha, M. A. A.; Kroon, M. C. Hydrophobic Deep Eutectic Solvents as Water-Immiscible Extractants. Green Chem. 2015, 17, 4518–4521.

Vogelpohl, C.; Brandenbusch, C.; Sadowski, G. High-Pressure Gas Solubility in Multicomponent Solvent Systems for Hydroformylation. Part I: Carbon Monoxide Solubility. J. Supercrit. Fluids 2013, 81, 23–32.

https://doi.org/10.1016/j.supflu.2013.04.006.

VOUTSAS, E. C.; YAKOUMIS, I. V.; TASSIOS, D. P. Prediction of phase equilibria in water/alcohol/alkane systems. Fluid Phase Equilibria, v. 158–160, p. 151–163, jun. 1999. Disponível em: <https://linkinghub.elsevier.com/retrieve/pii/S0378381299001314>.

W. Guo, Y. Hou, S. Ren, S. Tian, W. Wu, Formation of deep eutectic solvents by phenols and choline chloride and their physical properties, Journal of Chemical and Engineering Data. 58 (2013) 866–872. https://doi.org/10.1021/je300997v.

W.R. Giacomin Junior, C.A. Capeletto, F.A.P. Voll, M.L. Corazza, Phase Equilibrium Measurements and Thermodynamic Modeling of the Systems (CO 2 + Ethyl Levulinate) and (CO 2 + Levulinic Acid), Journal of Chemical & Engineering Data. 64 (2019) 2011–2017. https://doi.org/10.1021/acs.jced.8b01023.

Wang, J., Cheng, H., Song, Z., Chen, L., Deng, L., Qi, Z., 2019. Carbon Dioxide Solubility in Phosphonium-Based Deep Eutectic Solvents: An Experimental and Molecular Dynamics Study. Ind. Eng. Chem. Res. 58, 17514–17523. https://doi.org/10.1021/acs.iecr.9b03740

Warrag, S. E. E.; Darwish, A. S.; Adeyemi, I. A.; Hadj-Kali, M. K.; Kroon, M. C.; AlNashef, I. M. Extraction of Pyridine from N-Alkane Mixtures Using Methyltriphenylphosphonium Bromide-Based Deep Eutectic Solvents as Extractive Denitrogenation Agents. Fluid Phase Equilib. 2020, 517, 112622. https://doi.org/10.1016/j.fluid.2020.112622.

Wilberforce, T., Olabi, A.G., Sayed, E.T., Elsaid, K., Abdelkareem, M.A., 2021. Progress in carbon capture technologies. Sci. Total Environ. 761, 1–11. https://doi.org/10.1016/j.scitotenv.2020.143203

Wojeicchowski, J. P.; Marques, C.; Igarashi-Mafra, L.; Coutinho, J. A. P.; Mafra, M. R. Extraction of Phenolic Compounds from Rosemary Using Choline Chloride – Based Deep Eutectic Solvents. Sep. Purif. Technol. 2021, 258, 1–8. https://doi.org/10.1016/j.seppur.2020.117975.

Wood, E. Data for Biochemical Research (Third Edition). Biochem. Educ. 1987, 15, 97.

X. Meng, K. Ballerat-Busserolles, P. Husson, J.-M. Andanson, Impact of water on the melting temperature of urea + choline chloride deep eutectic solvent, New J. Chem. 40 (2016) 4492–4499. https://doi.org/10.1039/C5NJ02677F.

Y. Chen, N. Ai, G. Li, H. Shan, Y. Cui, D. Deng, Solubilities of Carbon Dioxide in Eutectic Mixtures of Choline Chloride and Dihydric Alcohols, J Chem Eng Data. 59 (2014) 1247–1253. https://doi.org/10.1021/je400884v.

Y. Ji, Y. Hou, S. Ren, C. Yao, W. Wu, Phase equilibria of high pressure CO2 and deep eutectic solvents formed by quaternary ammonium salts and phenol, Fluid Phase Equilib. 429 (2016) 14–20. https://doi.org/10.1016/j.fluid.2016.08.020.

Y. Liao, S. Gong, G. Wang, T. Wu, X. Meng, Q. Huang, Y. Su, F. Wu, R.M. Kelly, A Novel Ternary Deep Eutectic Solvent for Efficient Recovery of Critical Metals from Spent Lithium-Ion Batteries Under Mild Conditions, SSRN Electronic Journal. (2022). https://doi.org/10.2139/ssrn.4124040.

Y. Liu, H. Yu, Y. Sun, S. Zeng, X. Zhang, Y. Nie, S. Zhang, X. Ji, Screening Deep Eutectic Solvents for CO2 Capture With COSMO-RS, Front Chem. 8 (2020) 1–11. https://doi.org/10.3389/fchem.2020.00082.

Y. Liu, Z. Dai, Z. Zhang, S. Zeng, F. Li, X. Zhang, Y. Nie, L. Zhang, S. Zhang, X. Ji, Ionic liquids/deep eutectic solvents for CO2 capture: Reviewing and evaluating, Green Energy and Environment. 6 (2021) 314–328. https://doi.org/10.1016/j.gee.2020.11.024.

Y. Wang, L. Zhao, A. Otto, M. Robinius, D. Stolten, A Review of Post-combustion CO2 Capture Technologies from Coal-fired Power Plants, Energy Procedia. 114 (2017) 650–665. https://doi.org/10.1016/j.egypro.2017.03.1209.

Yadav, A., Pandey, S., 2014. Densities and viscosities of (choline chloride + urea) deep eutectic solvent and its aqueous mixtures in the temperature range 293.15 K to 363.15 K. J. Chem. Eng. Data 59, 2221–2229. https://doi.org/10.1021/je5001796

Yang, D.; Hou, M.; Ning, H.; Zhang, J.; Ma, J.; Yang, G.; Han, B. Efficient SO2 Absorption by Renewable Choline Chloride–Glycerol Deep Eutectic Solvents. Green Chem. 2013, 15, 2261–2265.

Yang, T.-X.; Zhao, L.-Q.; Wang, J.; Song, G.-L.; Liu, H.-M.; Cheng, H.; Yang, Z.

Improving Whole-Cell Biocatalysis by Addition of Deep Eutectic Solvents and Natural Deep Eutectic Solvents. ACS Sustain. Chem. Eng. 2017, 5 (7), 5713–5722. https://doi.org/10.1021/acssuschemeng.7b00285.

Yim, J. H.; Oh, B. K.; Lim, J. S. Solubility Measurement and Correlation of CO2in Bis(Pentafluoroethylsulfonyl)Imide ([BETI]) Anion-Based Ionic Liquids: [EMIM][BETI], [BMIM][BETI], [HMIM][BETI]. J. Chem. Eng. Data 2020, 65, 4378–4386.

Z. Maugeri, P. Domínguez de María, Novel choline-chloride-based deep-eutectic-solvents with renewable hydrogen bond donors: levulinic acid and sugar-based polyols, RSC Adv. 2 (2012) 421–425. https://doi.org/10.1039/C1RA00630D.

Z. Wang, M. Cheng, J. Bu, L. Cheng, J. Ru, Y. Hua, D. Wang, Understanding the electrochemical behavior of Sn(II) in choline chloride-ethylene glycol deep eutectic solvent for tin powders preparation, Advanced Powder Technology. 33 (2022) 103670. https://doi.org/10.1016/j.apt.2022.103670.

Zhang, S.; Chen, Y.; Ren, R. X. F.; Zhang, Y.; Zhang, J.; Zhang, X. Solubility of CO2 in Sulfonate Ionic Liquids at High Pressure. J. Chem. Eng. Data 2005, 50, 230–233.

Zhang, Y.; Ji, X.; Lu, X. Choline-Based Deep Eutectic Solvents for CO2 Separation: Review and Thermodynamic Analysis. Renew. Sustain. Energy Rev. 2018, 97, 436–455.

Zhang, Z., Pan, S., Li, H., Cai, J., Ghani, A., John, E., Manovic, V., 2020. Recent advances in carbon dioxide utilization. Renew. Sustain. Energy Rev. 125, 1–17. https://doi.org/10.1016/j.rser.2020.109799

Zubeir, L. F.; Held, C.; Sadowski, G.; Kroon, M. C. PC-SAFT Modeling of CO2 Solubilities in Deep Eutectic Solvents. J. Phys. Chem. B 2016, 120, 2300–2310. https://doi.org/10.1021/acs.jpcb.5b07888.

Zubeir, L. F.; Lacroix, M. H. M.; Kroon, M. C. Low Transition Temperature Mixtures as Innovative and Sustainable CO2 Capture Solvents. J. Phys. Chem. B 2014, 118 (49), 14429–14441.

Zubeir, L. F.; Romanos, G. E.; Weggemans, W. M. A.; Iliev, B.; Schubert, T. J. S.; Kroon, M. C. Solubility and Diffusivity of CO2 in the Ionic Liquid 1-Butyl-3-Methylimidazolium Tricyanomethanide within a Large Pressure Range (0.01 MPa to

10 MPa). J. Chem. Eng. Data 2015, 60, 1544–1562.

Zubeir, L. F.; Van Osch, D. J. G. P.; Rocha, M. A. A.; Banat, F.; Kroon, M. C. Carbon Dioxide Solubilities in Decanoic Acid-Based Hydrophobic Deep Eutectic Solvents. J. Chem. Eng. Data 2018, 63, 913–919. https://doi.org/10.1021/acs.jced.7b00534.